STATE OF CALIFORNIA DEPARTMENT OF TRANSPORTATION

TECHNICAL REPORT DOCUMENTATION PAGE

TR0003 (REV. 10/98)

1. REPORT NUMBER	2. GOVERNMENT ASSOCIATION NUMBER	3. RECIPIENT'S CATALOG NUMBER
CA18-2343		

4. TITLE AND SUBTITLE	5. REPORT DATE
Reusable Instrumented Test Pile Phase 2	April, 2018
	6. PERFORMING ORGANIZATION CODE
7. AUTHOR(S)	8. PERFORMING ORGANIZATION REPORT NO.
Jason T. DeJong[1]	N/A
9. PERFORMING ORGANIZATION NAME AND ADDRESS	10. WORK UNIT NUMBER
[1]Professor Department of Civil and Environmental Engineering University of California One Shields Ave Davis, CA 95616	11. CONTRACT OR GRANT NUMBER Technical Agreement #65A0481
12. SPONSORING AGENCY AND ADDRESS	13. TYPE OF REPORT AND PERIOD COVERED
California Department of Transportation Division of Research, Innovation & System Information, MS-83 1120 N Street Sacramento, CA 95814	Final Report 14. SPONSORING AGENCY CODE

15. SUPPLEMENTAL NOTES

This report documents the further development of the Reusable Instrumented Test Pile (RTP) during Phase II. During this development phase the RTP evolved to become a specific configuration of the instrumented Becker Penetration Test, which is a simplified configuration for use as a dynamic penetrometer. The functioning components of the equipment and the data analysis platform is similar, and for this reason the chapters include information on both components.

16. ABSTRACT

The performance and constructability of pile foundations in coarse granular soils contains significant uncertainty due to challenges in site characterization and uncertainty in pile prediction methods. The Reusable Test Pile idea was conceived as a large diameter instrumented test pile that could be deployed during the site investigation phase of a project where a deep foundation design and or coarse grained soils were expected. Static and dynamic data obtained by the RTP during this phase was envisioned to be useful to designers and contractors for assessing soil properties, pile drivability, and pile performance (capacity, displacement). This report contains four journal papers and a M.S.C.E. thesis that describe the equipment design, data collected, and data processing and interpretation as it applies to evaluating penetration resistance, soil properties, pile driving dynamics, and static pile loading behavior. This includes an initial formulation for static pile capacity estimation based on RTP data and considerations for dynamic pile modeling.

17. KEY WORDS	18. DISTRIBUTION STATEMENT	
Gravels, coarse grained soils, site characterization, pile capacity, pile drivability, pile design, driven piles	No restrictions. This document is available to the public through the National Technical Information Service, Springfield, VA 22161	
19. SECURITY CLASSIFICATION (of this report)	20. NUMBER OF PAGES	21. PRICE
Unclassified	236 Pages	

Reproduction of completed page authorized

DISCLAIMER STATEMENT

This document is disseminated in the interest of information exchange. The contents of this report reflect the views of the authors who are responsible for the facts and accuracy of the data presented herein. The contents do not necessarily reflect the official views or policies of the State of California or the Federal Highway Administration. This publication does not constitute a standard, specification or regulation. This report does not constitute an endorsement by the Department of any product described herein.

For individuals with sensory disabilities, this document is available in Braille, large print, audiocassette, or compact disk. To obtain a copy of this document in one of these alternate formats, please contact: the Division of Research and Innovation, MS-83, California Department of Transportation, P.O. Box 942873, Sacramento, CA 94273-0001.

Division of Research & Innovation

Reusable Instrumented Test Pile for Improved Pile Design in Granular Soils –Phase II

DRSI Research Task No. 1233,
DRSI Project No. P656,
Contract No. 65A0264

TABLE OF CONTENTS

CHAPTER 1 **1**

Instrumented Becker Penetration Test I: Equipment, Operation, and Performance

CHAPTER 2 **37**

Instrumented Becker Penetration Test. II: iBPT-SPT Correlation for Characterization and Liquefaction Assessment of Gravelly Soils

CHAPTER 3 **71**

Use of Reusable Test Pile for Pile Design as Informed by Full Scale Pile Load Tests

CHAPTER 4 **146**

Pile Driving Mechanics at the Base as Informed by Direct Measurements

CHAPTER 5 **190**

Prediction, Performance, and Uncertainty in Dynamic Load Testing and Signal Matching Applications as Informed by Direct Measurements from an Instrumented Becker Penetration Test

CHAPTER 1

Instrumented Becker Penetration Test
I: Equipment, Operation, and Performance

Jason T. DeJong, M.ASCE[1], Mason Ghafghazi, M.ASCE[2], Alexander P. Sturm, S.M.ASCE[3], Daniel W. Wilson, M.ASCE[4], Joel den Dulk[5], Richard J. Armstrong[6], Adam Perez[7], Craig A. Davis, M.ASCE[8]

[1] Professor, Department of Civil & Environmental Engineering, University of California at Davis, One Shields Ave., Davis, CA 95616, +1 (530) 754 – 8995, jdejong@ucdavis.edu

[2] Assistant Professor, Department of Civil Engineering, University of Toronto, 35 St. George St., Toronto, ON M5S 1A4, +1 (416) 978 – 5972, mason.ghafghazi@utoronto.ca

[3] Graduate Student, Department of Civil & Environmental Engineering, University of California at Davis, One Shields Ave., Davis, CA 95616, +1 (650) 580 – 2729, apsturm@ucdavis.edu

[4] Associate Director, Center for Geotechnical Modeling, University of California at Davis, One Shields Ave., Davis, CA 95616, Phone: +1 (530) 754 – 9761, dxwilson@ucdavis.edu

[5] Mechanical Engineer, 533 Antioch Dr., Davis, CA 95616, machnerd@yahoo.com

[6] Assistant Professor, Department of Civil Engineering, Sacramento State University, CSU Sacramento 6000 J St., Sacramento, CA 95819, +1 (916) 278 – 6812, Richard.Armstrong@csus.edu

[7] Design Geotechnical Engineering Group Manager, Los Angeles Department of Water and Power, 111 N. Hope Street, Room 1368, Los Angeles, CA 90012, +1 (213) 367 – 0262, Adam.Perez@ladwp.com

[8] Trunk Line Design Manager, Los Angeles Department of Water and Power, 111 N. Hope Street, Room 1356, Los Angeles, CA 90012, +1 (213) 367 – 0769, Craig.Davis@ladwp.com

Paper Reference:

DeJong, J.T., Ghafghazi, M., Sturm, A.P., Wilson, D.W., den Dulk, J., Armstrong, R.J., Perez, A., and Davis, C.A. "Instrumented Becker Penetration Test, I: Equipment, Operation, and Performance", *ASCE J. Geotechnical and Geoenvironmental Engineering*, 2017, https://doi.org/10.1061/(ASCE)GT.1943-5606.0001717

ABSTRACT

The Becker Penetration Test (BPT) is a widely used tool for characterizing gravelly soils, especially for liquefaction assessment. Interpretation of BPT data is complicated by the energy transferred from the hammer to the drill string being variable and by the shaft resistance that develops along the drill string generally increasing with penetration depth. Existing interpretation methods that utilize above-ground measurements to interpret BPT measurements have had limited success in accurately separating the shaft and tip resistance. Therefore, penetration resistance with depth cannot be reliably predicted.

An instrumented Becker Penetration Test (iBPT), that measures acceleration and force directly behind the driving shoe in order to compute the energy delivered to the driving tip, was developed and integrated into the standard closed-ended Becker drill system. The equipment and data acquisition system are described in this paper. The analysis procedure used to compute energy normalized blow count values and produce continuous penetration resistance profiles are outlined. The energy normalized blow count profiles generated are shown to be independent of penetration depth, pre-drilling depth, shaft resistance magnitude, and hammer operating conditions. In particular, the efficacy of a residual energy based normalization scheme is demonstrated. Finally, a discussion regarding energy measurements, locked-in stress at the drill string tip, and the use of the pull-back and re-drive procedure is presented.

INTRODUCTION

The use of in-situ penetration tests, namely the standard penetration test (SPT) and cone penetration test (CPT), has become the standard of practice for characterizing the liquefaction potential of cohesionless soils, largely because adequate sampling in these soils is prohibitively

difficult. Assessing the characteristics of gravelly soils using either SPT or CPT poses difficulties due to large particle size – to – penetrometer diameter ratios (Daniel et al., 2004). In the case of the SPT, gravel particles can clog or block the split-spoon sampler resulting in limited recovery and/or unrepresentative blow counts. Depending on the abundance of large particles during cone penetration, gravel particles can either completely block the advancement of the cone, or cause a misalignment in the rods.

The BPT was widely adopted for liquefaction assessment after the 1983 Borah Peak, Idaho, earthquake (Harder and Seed, 1986), where extensive liquefaction was observed in gravelly soils. The large diameter of the BPT device was particularly applicable in these coarse materials, where it provided more repeatable results and fewer occurrences of refusals compared to smaller scale split-spoon penetrometers (e.g. SPT).

Becker drilling was developed in Canada in the late 1950's for oil explorations at gravel sites (Sy and Campanella, 1994). It consists of driving a hollow, steel drill string into the ground using a double-acting diesel hammer. The double-acting hammer is faster due to the additional reaction force provided by compressing air in the bounce chamber above the ram. The BPT can be performed open- or closed-ended using one of three different drill string diameters (140 mm [5 1/2 in], 168 mm [6 5/8 in], and 230 mm [9 in]). Disturbed bulk samples can be obtained during open-ended drilling by transporting soil cuttings up the hollow drill string to the ground surface using compressed air that is delivered to the tip via the casing annulus. For characterization of penetration resistance, a closed-ended tip is used and the measured blows per foot (0.3 m) is correlated to soil strength.

Despite having obvious benefits over other in-situ testing devices in gravelly soils, a fundamental challenge exists when using the BPT for determining penetration resistances for

liquefaction assessment. Unlike the SPT, performed through an over-bored open hole, shaft resistance accumulates as the Becker drill string is advanced into the ground. The shaft resistance contributes to the number of blows required for penetration, leading to the measured penetration resistance not directly reflecting the soil resistance beneath the drill string tip. Efforts to eliminate shaft resistance by using an oversized driving shoe have produced inconsistent results due to material caving (Wightman et al., 1993). Additionally, the utilization of drilling mud to reduce shaft resistance has proven impractical (Sy and Lum, 1997).

Harder and Seed (1986) standardized the BPT by recommending a standard equipment configuration: a 168 mm (6 5/8 in) diameter drill string with a closed-ended, eight tooth, crowd-out bit driven with an AP-1000 drill rig. They proposed a method that uses the bounce chamber pressure to indirectly account for the energy transferred to the penetrometer. Harder and Seed (1986) proposed an empirical correlation for estimating equivalent SPT blow count values from the bounce chamber pressure normalized BPT blow count values. Although this method provided the basis for standardization of the BPT equipment and of the procedures, the method does not reliably estimate equivalent SPT blow count values since it does not account for the accumulated shaft resistance.

Sy and Campanella (1994) proposed a more theoretically rigorous method to estimate the energy transmitted to the drill string and account for the influence of shaft resistance in estimation of the tip penetration resistance. The energy transmitted to the top of the drill string is directly measured using pile driving analysis (PDA) equipment and used in a two stage wave equation analysis process (Rausche et al., 1972). CAPWAP analyses are first used to estimate the shaft resistance followed by WEAP (Wave Equation Analysis for Pile Driving) analyses which are used to correct the blow count values to what would have been recorded had no shaft resistance been

present. They proposed a set of BPT-SPT correlations that depend on the estimated static shaft resistance. The method presented by Sy and Campanella (1994) made significant advances in measuring the energy transmitted to the drill string and understanding the mechanisms affecting the BPT results. However, limited validation, uncertainty in the wave equation analyses since it produces a non-unique solution, and the compound effects of the underlying assumptions have led to inconsistent results.

Applying the two BPT interpretation methods (Harder and Seed, 1986; Sy and Campanella, 1994) often produces significant differences in the estimated equivalent SPT N_{60} values. The Harder and Seed method will produce different values for a given depth when different amounts of shaft resistance exist in two adjacent soundings. The Sy and Campanella method will produce different equivalent N_{60} values when different practitioners use the same measured acceleration-force data set due to differences in how the CAPWAP (CAse Pile Wave Analysis Program) analyses are performed. For a given project it is not possible to know which, if either, of these methods correctly estimate equivalent SPT N_{60} values. The inaccuracy in these methods has become an acute challenge in liquefaction assessment for gravelly soil deposits at depth and where softer soils underlie stiffer soils (e.g. foundation strata beneath dams). In these latter cases the shaft resistance absorbs the majority of the energy delivered by the hammer; thus, the above methods cannot accurately characterize these soft layers since they do not reliably measure, or correct for, the shaft resistance.

This paper describes the development, integration, and validation of a new instrumented Becker Penetration Test (iBPT) system that is fully integrated with the standard closed-ended Becker drill string. Most importantly, the iBPT system measures the acceleration and force 0.5 m (1.5 ft) behind the drill string tip in order to compute the energy arriving at this point. Hereinafter

it is stated that these measurements and the subsequently calculated energy occur 'at the tip' as it is not practically possible to mount the gages directly on, or closer to, the BPT drill string tip. The difference in energy delivered to the tip and measurement gage location was assumed to be negligible. Computing the energy based on direct measurements at the drill string tip eliminates the effect of shaft resistance on normalized blow count values. Herein the iBPT equipment design and data acquisition system are described. The processes for analysis and integration of the collected data to produce continuous, energy-normalized blow count profiles, are outlined. The repeatability of normalized blow count profiles produced is assessed and the robustness of the energy normalization scheme for calculation of the normalized blow count values is established. The ability of the method to produce consistent results with variable shaft resistance (or pre-drilling) is documented. Finally, a discussion regarding energy measurements, locked-in stress at the drill string tip, and use of the pull-back and re-drive procedure is presented.

iBPT SYSTEM

The instrumented Becker Penetration Test (iBPT) is a site investigation tool that measures the energy normalized penetration resistance of soil beneath the drill string tip. The equipment design goal of the iBPT was to obtain direct measurements of acceleration and force at the drill string tip using robust, reliable, low maintenance equipment with commercial-level performance. Advances in sensor technology and the availability of robust, smaller, and faster data acquisition systems at reasonable cost have only recently made the iBPT, that is presented herein, possible.

The instrumented Becker Penetration Test (iBPT) equipment consists of 0.6 m (2 ft) long, 168 mm (6 5/8 in) diameter, pipe sections (hereinafter referred to as iBPT sections) which are added to the drill string as shown in Figure 1a and b. Two instrumented sections, one located

directly behind the drill string tip (hereafter referred to as the 'tip' location) and a second located above ground directly below the hammer (hereafter referred to as the 'head' location), were used in iBPT development and are used in standard operation. Therefore, measurements from this setup are presented herein. However, only the tip instrumented section is essential for calculation of the iBPT energy normalized tip resistance. Data collected at the drill string tip is processed by a small, robust, in-pipe data acquisition module that digitally transmits the data to an above-ground host. A parallel conventional field data acquisition system (Figure 1c) collects data from the iBPT head unit and other above above-ground sensors (bounce chamber pressure, string potentiometers). The overall operation of the iBPT system occurs in a small, mobile trailer.

Four strain transducers are mounted inside the iBPT sections, equidistant around the circumference, to measure axial strain. Two diametrically opposite strain transducers are wired in pairs, yielding two average measurements of axial strain to minimize sensitivity to bending. Two accelerometers are mounted coincidently with two of the four strain transducers, producing two measurements of pipe motion. The transducers are secured to the inside of the iBPT pipe sections with two bolts using special tools to ensure axial alignment with no preloading. The strain transducers have an accuracy of ±2% and can measure up to 2,000 micro-strain. The piezo-resistive critically damped accelerometers have an accuracy of ±1%, a capacity of 2,000 g, and a natural frequency above 10 kHz. Thermistors enable measurement of temperature change in the iBPT section near the sensors. Extensive laboratory and field testing was performed to ensure reliability and robustness of the measurements. All sensors conform to, or exceed, ASTM D4633 (2010) and D4945 (2012) standards on energy measurement for dynamic penetrometers and dynamic testing of deep foundations.

A computer module is installed inside the iBPT section at the tip for data acquisition. A shock absorption system limits the impact acceleration experienced by the electronics to 50 g, a reduction from the ~1,500 g typically experienced by the iBPT sections. The data acquisition provides excitation (power) to the sensors, receives the analog signals, gains (magnifies) the signals, conditions the signals with a low pass filter, and digitizes the signals at 14.4 kHz per channel before transmitting them via a Controller Area Network (CAN) bus to the above-ground host. To ensure the entire dynamic wave is captured, the operator specifies the recorded signal duration. The 14.4 kHz sampling frequency enables recorded measurement signal frequencies of up to 7.2 kHz (Nyquist frequency). Extensive testing with higher sampling frequencies confirmed that the 14.4 kHz sampling frequency fully captures Becker hammer dynamic impacts (which have typical frequency contents less than 2 kHz).

The two accelerometers and four strain gage transducers located within the head section (directly below the Becker hammer) are individually connected to the above-ground data acquisition unit in the trailer. This enables more efficient operation of the in-pipe data acquisition module in the head section and allows for independent recording of all four strain gages to monitor pipe bending.

In addition, a 6.35 m (20.8 ft) string potentiometer is connected to a collar mounted on the drill string head to measure displacement per blow and to track the depth during driving. The hammer bounce chamber pressure is continuously measured using a 3.4 MPa (500 psi) pressure transducer. The bounce chamber pressure and string potentiometer data are utilized by the data acquisition system to automatically log the number of blows per foot.

The iBPT system can also collect force and displacement data during static pull-back (tension pull-out) tests to measure the static shaft resistance versus displacement curve. Two short

stroke (0.32 m, 12.5 in), high accuracy string potentiometers, mounted to an isolated reference frame, monitor the pull-back displacement. The amount of force required for pull-back is recorded using the head section strain gages that are also used for dynamic measurements. Force-displacement curves are produced in real time to determine when the maximum static resistance is reached.

The equipment is fully integrated within the standard (168 mm, 6 5/8 in) closed-ended Becker system and comprised of modular components that enable reliable operation and rapid repairs for deployment on industry projects. Individual segments of the downhole communication cable are installed inside each 1.5 or 3 m (5 or 10 ft) Becker pipe at the beginning of a field program and connections are made and broken as pipe sections are added and removed, respectively, during driving and removal of pipe sections. The level of operational efficiency and reliability are critical to the success of iBPT investigations, as the high cost of drilling does not allow for extensive delays.

MEASUREMENTS AND DATA PROCESSING

The strain and acceleration values measured at the tip and in the head unit are processed to generate energy normalized blow count values. Driving forces are calculated from the strain gage measurements with the cross-sectional area (A) and Young's modulus (E_s) of the iBPT sections. A baseline correction is applied to the dynamic force measurements by referencing a 'quiet time' (flat-line signature) prior to the impact arrival. At the drill string tip, the baseline reading includes a locked-in residual force (F_R) which is due to the generation of an upwards force caused by the elastic rebound of the soil below the tip (discussed in detail in the Discussion section); the locked-in residual force is balanced by an opposing resultant downward force along the shaft. A

temperature correction is also applied to correct for the strain that is induced by the differential thermal expansion of the steel pipe and aluminum strain gages as the gages are heated by the shaft friction during driving.

A baseline correction is performed on accelerations by referencing a quiet time prior to the impact arrival. The measured acceleration time histories are integrated to produce velocity time histories. Often a minute post impact residual velocity is calculated after integration of accelerations. This residual velocity is an artifact of the accelerometer measurements recorded during each impact (which was confirmed through the supplemental lab testing). To correct this post-impact residual velocity to zero, a baseline is fit through the recorded data during the post-impact quiet time. A half cosine baseline shift function is applied during the impact to generate a smooth baseline correction between the zero pre- and post-impact velocities.

Conventionally, the velocity is multiplied by the impedance of the section ($Z = E_sA/c$) and plotted alongside force in dynamic pile analyses (e.g. Rausche et al., 1972), as shown in Figure 2, for both head and tip sections. E_s is the Young's Modulus of the steel, A is the cross sectional area of the drill string, and c is the wave velocity ($c = \sqrt{E_s/\rho}$). The time required for the wave to travel to the bottom of the drill string and back ($2L/c$) is also indicated as dashed lines in the figure. The wave measured at the head arrived at the tip with a delay of L/c. As expected, exact force-velocity proportionality was not observed at the head section between 0 L/c and 2 L/c after the hammer impact, due to the reflection waves caused by shaft resistance and impedance contrasts due to pipe joints (closest joint located 0.3 m from measurement location) and drill-string non-uniformities (i.e. welded joints along drill pipe and threaded connections between drill pipes). It is noted that this condition is different than in conventional pile driving where proportionality is expected at the

beginning of pile impact (approximately 0 L/c); this is because a substantial pile length below the measurement location is in the air (and has no shaft friction) when pile driving begins.

Displacements are calculated by integrating velocity time histories. Representative displacement time histories for both the head and the tip section are shown in Figure 2. The residual displacements calculated at the head and tip sections were similar due to the very stiff Becker drill-string. The computed displacements also matched the measured values obtained with the above-ground string potentiometer. The agreement between measured displacements determined using different approaches provided additional confidence in the quality of the measurements.

ENERGY CALCULATION AND NORMALIZING BLOW COUNTS

The number of blows per foot of penetration, or measured blow count value, N_B, are calculated by using the depth measured by the string potentiometer and the continuous bounce chamber pressure data. The number of peaks in bounce chamber pressure that occur in each foot of driving are reported as the blow count value.

The amount of energy delivered by the hammer (E), defined in a normalized manner consistent with how the SPT hammer energy is defined (and the energy hammer ratio as is conventional for pile driving), is calculated by integrating the measured force (F) multiplied by velocity (V) over the impact time (t). The energy is expressed as a percentage of the rated (theoretical) ICE 180 hammer energy (11.0 kJ),

$$E\ (\%) = \frac{\int F(t)V(t)dt}{11.0\ kJ} \qquad [1]$$

At the tip, the force includes both the dynamic and the static locked-in forces. The energy time history for both the head and tip sections are also plotted in Figure 2. The energy reached a peak value E_{max} (or ENTHRU) before reducing to a residual value E_{res} (or E_{fnl} in pile driving). The

reduction in the amount of energy after the peak was caused by elastic rebound within the drill string and within the soil below the tip; E_{res} represents the energy delivered to the soil below the tip. The difference between the peak and residual energy is typically more pronounced at the head section due to the elastic rebound within the drill string. Therefore, as addressed further in the Discussion section, E_{res} was mechanistically more appropriate than E_{max} (ENTHRU) for normalizing the residual, or permanent, displacements.

The difference between the amount of energy delivered to the tip and head can be attributed to the amount of energy absorbed by shaft resistance. The ratio of the residual energy at the tip to the residual energy at the head, defined as the delivered energy ratio ($ER_{T/H}$), quantifies the energy absorbed by shaft friction.

$$ER_{T/H} = \frac{E_{res,Tip}}{E_{res,Head}} \quad [2]$$

Higher $ER_{T/H}$ values indicate that more energy was transmitted to the tip (i.e. less energy was lost to shaft resistance), and vice versa.

The energy normalized blow count, N_{B30}, is computed by normalizing the measured blow count values, N_B, to 30% reference energy (Sy and Campanella, 1994) using E_{res} at the tip section:

$$N_{B30} = N_B \frac{E_{res,Tip}}{30} \quad [3]$$

In this equation, $E_{res,Tip}$ is the amount of residual energy at the drill string tip, as averaged over each foot of driving. The energy normalized blow count value, N_{B30}, is the main output of the iBPT system and represents penetration resistance; it is analogous to the N_{60} value for SPT. It is noted that N_{B30} defined here is different from that defined by Sy and Campanella (1994), who used the maximum energy measured at the head ($E_{max,Head}$ or ENTHRU) instead of the residual energy measured at the tip $E_{res,Tip}$ in Equation 3.

EXAMPLE iBPT OUTPUT

An example set of results from the iBPT system is presented in Figure 3. The raw blow count (N_B) profile in Figure 3a contains large variations with depth, which reflect the stratigraphic depositional variations at the site. The residual energy (E_{res}) profiles, presented in Figure 3b, show the hammer energy delivered to the drill string at the head ($E_{res,Head}$) as well as the remaining energy that is transmitted to the tip ($E_{res,Tip}$). The E_{res} at the head ranged from 20% to 45% throughout the sounding, and is similar to the 30% energy used as reference. In contrast, the E_{res} delivered to the tip generally decreases with depth, as shaft friction accumulates, eventually decreasing to values less than 5%.

There is a steady decay of the energy ratio, $ER_{T/H}$, due to an increase in shaft resistance with penetration depth as shown in Figure 3c. Shaft resistance can accumulate rapidly with depth, resulting in $ER_{T/H}$ values of less than 5% after only 10 m (33 ft) of driving (as observed in some compacted embankments). Alternatively, shaft resistance can accumulate more slowly, resulting in $ER_{T/H}$ values near 40% after 30.5 m (100 ft) of driving (Figure 3c). When soft layers are encountered (e.g. at 18 m (60 ft) depth in Figure 3c), the energy delivered to the tip can be further reduced as the soil below the tip is less stiff than the soil acting along the shaft. This observed reduction is a crucial reason why direct measurements at the drill string tip are important for detection of weak layers at depth.

The energy normalized blow count (N_{B30}) profile, as shown in Figure 3d, is the main output of the iBPT system. The N_{B30} values can be correlated with other penetration test results (e.g. SPT N_{60} as presented in the companion manuscript Ghafghazi et al. 2017) for site characterization. The continuous profile with depth enables detection of thin, weaker layers. The ability of the iBPT to produce reliable results in a wide range of soil types makes it a valuable investigation tool for sites where the presence of gravelly and cobbly soils limits the application of other penetration tests.

FIELD TESTING

Four extensive field programs have been completed to date. These programs have provided data across a wide range of soil and drilling conditions. The first site, the Headworks West Reservoir, is founded on alluvial deposits from the original alignment of the Los Angeles River, as such there is in significant vertical and horizontal variability in the subsurface. Sixteen iBPT soundings (406 linear m, 1,332 linear ft total) were performed with penetration depths ranging between 12 and 38 m (40 and 125 ft). Gravelly and cobbly materials were frequently encountered in all soundings. The blow count values were generally high with occasional low penetration resistance zones. The variable site conditions provided an opportunity for testing the robustness of the equipment and for developing an understanding of the range and quality of the iBPT measurements.

The second site, the new alignment for North Haiwee Dam, is located along the southeastern edge of the Sierra Nevada mountain range in Eastern California. The predominately calm hydro-geologic, depositional environment created a relatively uniform soil profile in both the vertical and lateral directions. Soils at the site consisted of silty sand and clean sand deposits with occasional gravelly lenses. Ten soundings (248 linear m, 813 linear ft) were performed with penetration depths ranging between 18 and 29 m (60 and 95 ft). The site homogeneity was conducive to perform side-by-side soundings (spaced ~3 m apart) to investigate the performance of the iBPT system.

The third site, the Stone Canyon Dam, is located within a narrow canyon in the city of Los Angeles. The arroyo, alluvial foundation beneath the dam is comprised of highly interlayered and intermixed low plasticity clays and sands with frequent gravel-sized, slate fragments. There is

significant variability in the alluvium; however, the man-made, embankment dam units are relatively homogeneous. Eight soundings (166 linear m, 546 linear ft) were performed with penetration depths reaching 51 m (168 ft). The compacted dam materials, which generated significant shaft friction, required pre-drilling with a 190 mm (7 ½ in) oversized bit before the Becker penetrometer could reach the underlying alluvium of concern. The pre-drilling sequence and homogeneity of the man-made dam units enabled assessment of the influence of varying shaft resistance on iBPT measurements.

The fourth site, Bouquet Canyon Dam, is located near the city of Palmdale, California. The alluvial foundation beneath the dam is comprised of an upper, sandy, alluvium and a lower, gravelly, alluvium which is underlain by highly weathered bedrock. The investigation, performed for liquefaction assessment of the foundation and toe materials of the existing dam, consisted of eight borings (100 linear m (330 linear ft) in total; boring depths from 12 m (39 ft) to 46 m (150 ft)) either performed directly from the ground surface or after 20 to 35 m (65 to 115 ft) of pre-drilling through the embankment to reach the alluvium.

iBPT OPERATION

The iBPT equipment and procedures have been refined through the field work completed to date. The iBPT system was designed for operation with any conventional Becker drill rig; no modification is necessary. The maximum achievable depth is controlled by drivability; depths of over 50 m have been achieved to date. Use of the iBPT system with the Becker system slows productivity time by about 15%. Nonetheless, in loose soils typically of concern for liquefaction analysis 30+ m (100+ ft) of driving per day is typical. Post processing and reporting of data have been automated with software to allow for reporting efficiency that is comparable to more

traditional techniques, despite the significantly larger dataset collected. The instrumentation inside the iBPT pipe sections prevents immediate post sounding grouting during retraction; therefore, the entire drill string must be removed before grouting can commence.

iBPT PERFORMANCE VALIDATION

The iBPT was operated in the field and side-by-side soundings were performed to evaluate the repeatability of N_{B30} values, the effect of shaft resistance on N_{B30} values, and the applicability of the linear energy normalization used to calculate N_{B30} values.

Repeatability of N_{B30}

The repeatability of iBPT N_{B30} measurements was confirmed by performing two soundings, spaced 3 m (10 ft) apart at the relatively uniform North Haiwee Dam site. Based on the results, presented in Figure 4, the raw blow count values and amount of energy delivered to the tip were consistent between the two soundings. After energy normalization, the resulting N_{B30} profiles were practically identical. The level of repeatability between these iBPT profiles is comparable to that observed in CPT data from the same site and better than that observed in SPT data.

Effect of Shaft Resistance on N_{B30}

iBPT N_{B30} values were confirmed to be independent of the amount of shaft resistance by comparing the results from two soundings that were predrilled to different depths in order to obtain data in penetration through the same alluvium with different magnitudes of shaft resistance. The adjacent soundings, performed at the Stone Canyon Dam site at 3 m (10 ft) spacing, are presented in Figure 5. In these soundings the pre-drilling depths were staggered, with the first being predrilled to a depth of 23 m (75.5 ft) while the other was predrilled to a depth of 27 m (88.6 ft).

This resulted in significantly different amounts of shaft resistance at certain depth intervals (e.g. 23.5 to 32 m, 76 to 105 ft and 27 to 33 m, 89 to 109 ft).

Different amounts of energy were delivered to the tip in the two soundings due to the difference in the amount of shaft resistance (Figure 5b). For example, in sounding 'iBPT C' in Figure 5b at about 32 m (105 ft), less than 2% energy is delivered to the tip. At the same depth in sounding 'iBPT D' about 13% energy was delivered to the tip. However, when energy normalization was applied (per Eq. 3), the computed N_{B30} values from the two soundings were practically identical.

Energy Normalization of N_{B30}

The energy normalization (Eq. 3) is based on the assumption that the number of hammer blows required to advance the penetrometer is inversely proportional to the average energy that is transferred to the soil by each blow. The normalization is fundamentally based on the proportionality between the amount of plastic work that is input to the system and the amount of plastic deformations that are incurred in the soil. Energy normalization, for all dynamic penetration tests, are commonly based on the same assumption (e.g. Schmertmann and Palacios, 1979).

The energy normalization proportionality was confirmed for the iBPT system, and is exemplified herein by using multiple pairs of adjacent soundings (3 m, 10 ft spacing) at the North Haiwee Dam (Figure 6) and Headworks West Reservoir (4.5 m, 15 ft spacing) sites. In each pair of soundings, one sounding was performed using 'high' hammer energy and the second was performed using 'low' energy. The Becker hammer energy is controlled by the fuel throttle controls; high energy consisted of full-throttle with the turbo charger operating, while low energy consisted of operation at ¼ to ½ of full-throttle and no turbo charger operating (in general the hammer operated close to ¼ throttle after a new drill string was added before being gradually

increased to ½ throttle). Based on the pair of example soundings in Figure 6, differences in raw blow counts (N_B, Figure 6a) and residual energies measured at the tip ($E_{res,Tip}$, Figure 6b), resulting from the differenced in energy input by the hammer throttle settings, coalesce into nearly identical N_{B30} profiles (Figure 6c). The differences in N_{B30} values between a depth of 2 and 5 m (7 to 16 ft) resulted from the heterogeneity of the randomly placed fill.

The measurements from the aforementioned tests are summarized in Figure 7 where the raw (per foot) blow counts from the higher energy sounding were divided by the corresponding lower energy sounding, resulting in ratios less than unity on the vertical axis. The associated average per foot energies measured at the tip ($E_{res,Tip}$) during the lower energy sounding were divided by those from the higher energy sounding, again resulting in ratios less than unity on the horizontal axis. A sample calculation is presented in Figure 7a for reference. Ideally, energy normalization and homogeneous soil deposits would result in the data aligning with the 1:1 line. The data presented generally align with the 1:1 line (Figure 7b), confirming that energy normalization according to Eq. 2 will result in near identical N_{B30} profiles, in identical strata, independent of the amount of hammer energy applied.

The data closer to the origin in Figure 7b represent the highest difference between the energies arriving at the tip in adjacent soundings and are thus most relevant toward supporting the linearity of energy normalization. The data plotted in the upper right corner of Figure 7b, represent repeatability of the drilling operation since similar blow counts were achieved in the same strata when similar energies arrived at the tip. Additional data, presented from Figure 5, where differences in shaft resistance led to different energies delivered at the tip, plot closer to the origin and provide additional support for the energy normalization methodology. The largest spread in

Figure 7b is clustered in the upper right corner, at ratios greater than about 0.6. These data (open circles) are from the sounding that were presented in Figure 4.

The data presented close to the origin in Figure 7b represent energy normalization by a factor as large as ten with $E_{res,Tip}$ values as low as 2%. There is a small bias at such extremes because driving at lower energy is less efficient than driving at high energies due to the greater plastic work loss in the larger number of unload-reload loops. Nevertheless, based on the data, negligible bias was observed for all practical purposes. The potential for such bias is minimized when the energy was measured at the tip compared to head measurements which were also influenced by the shaft resistance and the associated non-linearity.

DISCUSSION

Above-ground energy measurements have been routinely used for normalizing blow counts obtained from dynamic penetration tests. A similar approach was adopted for the iBPT system with additional considerations and improvements discussed in this section. First, the contribution of the locked-in residual force on the energy measurement at the tip is discussed. Then, the importance of using the residual energy, instead of the maximum energy, for energy normalization of blow counts is highlighted. Finally, the merits of pull-back and re-drive procedures, commonly used in Becker penetration testing, are elaborated.

Locked-in Residual Force at the Tip

A locked-in, compressive, residual force (F_R) develops at the drill string tip due to the opposing downward resultant force along the drill string caused by the elastic soil rebound at the end of hammer blows. The drill string weight also contributes to the locked-in residual force. The locked-in residual force gradually develops with driving; it typically increases with depth and is

proportional to the soil stiffness below the tip. The locked-in residual force contributes to the amount of work done on the soil during each hammer blow; therefore, it is included in the energy calculation presented in Equation 1. Schmertmann and Palacios (1979) identified a similar effect caused by the weight of rods for SPT energy calculations.

The contribution of the locked-in residual force to the residual energy at the tip ($E_{res,Tip}$) is the product of the residual force and the residual displacement for each hammer impact. The locked-in residual force can exceed 200 kN, which can contribute up to 5% energy to the residual energy measured at the tip, depending on the displacement caused by a given hammer impact. The contribution of the locked-in residual force to the residual energy at the tip is more pronounced when less energy is delivered to the tip by the hammer. For example, in Figure 5b between the depths of 30.5 and 32 m (100 and 105 ft), up to two thirds of the residual energy reported at the tip is associated with the work done on the soil by the locked-in residual force. The near perfect match obtained between N_{B30} values (Figure 5c) was only possible after measuring and including the contribution of the locked-in residual force to the energy measured at the tip.

Energy Calculation

Energy measurement in dynamic penetration tests has been guided by developments in the SPT. Research into the amount of energy that a hammer system can deliver to a drill string was initiated by the realization that driving energy significantly affects the measured blow count. Kovacs (1979) monitored the hammer velocity immediately before the impact and developed guidelines for the effects of hammer configuration and drop height on the measured blow counts. Schmertmann and Palacios (1979) developed a strain gage based system for measuring the force, and thus the energy delivered to the drill string. Both approaches targeted measuring the maximum energy delivered to the drill string because the residual energy, transferred at the end of the impact,

could not be reliably measured at the time. Schmertmann and Palacios (1979) used force-velocity proportionality during the first *2L/c* time interval to compute the energy available to advance the sampler into the ground. The approach, commonly known as the F^2 method, uses Equation 4 to calculate the energy. An assumption that the drill string connections do not cause any reflections is also included.

$$EF2 = \frac{c}{AE_s} \int F(t)^2 dt \qquad [4]$$

The rationale for imposing a cutoff at *2L/c* was that arrival of the tension wave at that time ends the contact between the hammer and the drill rods; therefore, no significant energy is transferred to the sampler after that point in time.

Sy and Campanella (1991) measured the energy delivered to the SPT drill rods without assuming force-velocity proportionality by utilizing a set of accelerometers in the instrumentation. Sy and Campanella (1991) showed that the uniform rod assumption was not valid because reflection waves, produced by the rod connections, cause an error in the amount of energy computed by the F^2 method. Subsequent research (e.g. Daniel et al., 2005) has also shown that the hammer-rod contact can be lost before time *2L/c* and additional impacts can occur at later times, further advancing the sampler. In the Sy and Campanella (1991) approach, the energy (*EFV*) is calculated by integrating the product of the force and velocity over the entire impact time.

$$EFV = \int F(t)V(t)dt \qquad [5]$$

In order to normalize SPT blow counts to a reference energy, Schmertmann and Palacios (1979) adopted the Housel (1965) definition of *ENTHRU* which is defined as the maximum energy transferred through the pile hammer-cushion-anvil system and delivered to the drill string. Using *ENTHRU* was practically appealing as the peak energy was computed based on the first *2L/c* after the impact. Advances in energy measurement techniques (e.g. piezo-resistive accelerometers) have

allowed for better measurement of the complete energy time history over the entire duration of the impact. However, *ENTHRU* has remained the de facto index for SPT energy normalization.

In the iBPT method the measured residual energy at the tip is used to normalize penetration values rather than the maximum energy (*ENTHRU*). The residual energy (the energy transferred to the soil after reflections have attenuated) is a more appropriate index for normalizing blow counts from penetration tests. Blow counts are associated with the permanent (plastic) deformations induced in soil by each hammer impact. For example, the displacements shown previously in Figure 2 exhibit peak values which reduce to the residual values following the impact. This reflects the elastic rebound occurring in both the soil and the drill string during driving. The residual energy represents the amount of energy used to permanently advance the penetrometer and is consistent with the associated plastic deformation.

Utilizing the residual energy to compute energy normalizing blow counts is an improvement in the fundamental assumptions of penetration testing. The difference between the traditional peak energy (*ENTHRU*) and the proposed residual energy is less pronounced in the iBPT tip measurements, as compared to the above-ground measurements, but the difference can still be significant. SPT energy normalization which utilizes *ENTHRU*, as opposed to the residual energy, may result in biased blow count values especially for long rods which will experience more elastic rebound. This bias is likely embedded in the corrections for rod length and overburden stress applied during SPT N_{60} calculation.

Pull-back and Re-drive

A pull-back and re-drive procedure has been implemented in practice, on occasion, in an attempt to quantify the shaft resistance which accumulated during driving of the BPT. When this procedure is utilized, driving is ceased and the drill string is pulled back approximately 1 m (3 ft)

before being re-driven through the open cavity, past the depth at which the pull-back was initiated. The hypothesis underlying this procedure is that the blow count values at the beginning of the re-drive, through the open cavity, can be attributed solely to shaft resistance. Hence, the blow count values measured while driving through virgin material can be corrected for the effect of shaft resistance through subtraction of blow counts measured during re-drive. An additional perceived benefit of the procedure is a potential reduction in the shaft resistance after the re-drive, enabling penetration to greater depths.

The iBPT system provides data to evaluate the validity of the hypotheses underlying the pull-back and re-drive procedure by directly measuring the energy dissipated by shaft friction. The energy dissipated by shaft resistance, $E_{res,Shaft}$, is the difference between the energy delivered to the top of the drill string, $E_{res,Head}$, and the energy arriving at the tip, $E_{res,Tip}$. Raw blow counts can be normalized using $E_{res,Shaft}$ to calculate the blows that can be hypothetically attributed to shaft resistance, $N_{B30,Shaft}$. If the hypothesis underlying the pull-back and re-drive procedure was true, $N_{B30,Head}$ at the start of a re-drive ($N_{B30,Head,Redrive}$) should be approximately equal to $N_{B30,Shaft}$ during the original drive. Typical measurements obtained from pull-back and re-drive procedures are presented in Figures 8a and 8b. Figure 8b shows that $N_{B30,Head,Redrive}$ values are significantly less than $N_{B30,Shaft}$ values. Multiple pull-out and re-drive tests, such as those shown in Figure 8, were performed in the field and the data are summarized in Figure 9a. The data consistently shows that $N_{B30,Shaft}$ values that were obtained during virgin driving are significantly greater than $N_{B30,Head}$ obtained during re-drive. Based on the difference, a correction based on re-drive blow count value cannot be expected to capture the effect of shaft resistance on energy measurements made only at the drill string head. The use of pull-back and re-drives to correct for the influence of shaft resistance has been shown to significantly underestimate the blow counts attributed to shaft

resistance, resulting in overestimating the penetration resistance of the soil under the tip of the drill string.

Finally, the potential for pull-back and re-drives to reduce shaft resistance in subsequent driving was investigated using the delivered energy ratio ($ER_{T/H}$). If the pull-back and re-drive procedure resulted in a significant reduction in shaft resistance more energy would reach the tip, thus $ER_{T/H}$ would increase. In Figure 8c the delivered energy ratio at the end of the re-drive (i.e. 12.5 to 13 m) is very similar to that before the pull-back. The near equivalency between the delivered energy ratios before and after the pull-back suggests that shaft resistance was not significantly reduced and driving below the pull-back depth was generally unaffected. Similar data collected during the field exploration program are summarized in Figure 9b and confirm that the results from Figure 8c are typical of a general trend.

CONCLUSIONS

The development and validation of the iBPT system, driven by observations that conventional in-situ tests (SPT and CPT) often cannot produce reliable penetration resistance measurements in gravelly soils, has led to the following observations and conclusions:

- The large diameter alternative, the Becker Penetration Test, is influenced by shaft resistance. Interpretation methods that only use above-ground measurements cannot produce consistent and reliable results.
- The instrumented Becker Penetration Test (iBPT) eliminates the shaft resistance issue through direct measurement of acceleration and force at the drill string tip, enabling calculation of the energy delivered to the soil below the tip of the closed-ended Becker drill string.

- The energy measured at the tip is used to normalize the Becker blow counts, enabling characterization of a wide range of soils including those with significant gravel content. The measurements have a high degree of repeatability and reliably by accounting for variations in delivered energy at the tip due to either variation in equipment or shaft resistance accumulation.
- The iBPT provides a continuous normalized blow count profile (N_{B30}) that accounts for wide variations of delivered energy to the tip, including the common scenario of characterizing thin, weak layers below harder natural layers and/or man-made embankments.
- The equipment is fully integrated within the industry standard closed-ended Becker testing system. The iBPT system operates with a closed ended tip, which must be retracted before hole grounding can begin. It has been successfully used in a variety of sites, driving conditions, and penetration depths.

The companion paper (Ghafghazi et al., 2017) presents the development of a correlation between iBPT N_{B30} and SPT N_{60} values that enables the penetration resistance of gravelly soils to be characterized with a parameter commonly used in geotechnical engineering practice for liquefaction assessment (e.g. Idriss and Boulanger, 2008).

ACKNOWLEDGEMENTS

The authors appreciate the funding and support provided by the Division of Safety of Dams (DSOD) of the California Department of Water Resources (David Gutierrez), the Los Angeles Department of Water and Power (Jianping Wu), and the California Department of Transportation (Caltrans, Tom Shantz). The support of Bill Sluis, Daret Kehlet, Jon Pearson, Chase Temple, Kevin Kuei, and Chris Krage of the Department of Civil and Environmental Engineering at the University of California Davis is also greatly appreciated. The technical contributions of John

Lemke of Geodaq in developing the downhole data acquisition module is acknowledged. In addition, the collaboration with AMEC Foster Wheeler (Marty Hudson and Alek Harounian), AECOM (Wolfgang Roth and S. Nesarajah), GeoPentech (Jon Barneich, Andrew Dinsick and Doug Wahl), and Great West Drilling (Jim Benson) is appreciated.

REFERENCES

ASTM D4633-10 (2010). "Standard test method for energy measurement for dynamic penetrometers." ASTM International, West Conshohocken, PA, USA.

ASTM D4945-12 (2012). "Standard test method for high-strain dynamic testing of deep foundations." ASTM International, West Conshohocken, PA, USA.

Daniel, C.R., Howie, J.A., Campanella, R.G., and Sy, A. (2004). "Characterization of SPT grain size effects in gravels." 2nd Int. Conf. Site Characterization (ISC'2). Porto, Portugal.

Daniel, C.R., Howie, J.A., Jackson, R.S., and Walker, B. (2005). "Review of Standard Penetration Test Short Rod Corrections." J. Geotech. Geoen. Eng., ASCE, 131(4), 489-497.

Ghafghazi, M., DeJong, J.T., Sturm, A.P., and Temple, C.E. (2017). "Instrumented Becker Penetration Test II: iBPT- SPT Correlation for Liquefaction Assessment in Gravelly Soils." Under review.

Harder, L.F.Jr., and Seed, H.B. (1986). "Determination of penetration resistance for coarse-grained soils using the Becker Hammer Drill." College of Engineering, University of California, Berkeley, Report No. UCB/EERC-86/06. May 1986.

Housel, W. (1965). "Michigan study of pile driving hammers." J. soil mech. and found. div., ASCE 91(SM5), 37-64.

Idriss, I.M., and Boulanger, R.W. (2008). "Soil Liquefaction during Earthquakes." Oakland, California. Earthquake Engineering Research Institute.

Kovacs, W.D. (1979). "Velocity measurement of free-fall SPT hammer." J. Geotech. Eng. Div., ASCE, 105(1), 1-10.

McVay, M.C., Alvarez, V., Zhang, L., Perez ,A., and Gibson, A. (2002). "Estimating driven pile capacities during construction." University of Florida report (4910450460312) to FDOT.

Odebrecht, E., Schnaid, F., Rocha, M.M., and Bernardes, G.P. (2005). "Energy Efficiency for Standard Penetration Tests." J. Geotech. Geoenv. Eng., ASCE, 131(10), 1252-1263.

Rausche, F., Moses, F., and Goble, G. (1972). "Soil resistance predictions from pile dynamics." J. Soil Mech. Found. Div., ASCE, 98(SM9), 917-937.

Schmertmann, J.H., and Palacios, A. (1979). "Energy dynamics of SPT." J. Geotech. Eng. Div., 105(8), 909-926.

Sy, A. and Campanella, R.G. (1991). "An alternative method of measuring SPT energy." Proc. 2nd Int. Conf. Recent Advances in Geotechnical Earthquake Engineering and Soil Dynamics, St Louis, MO, 499–505.

Sy, A. and Campanella, R.G. (1994). "Becker and standard penetration tests (BPT-SPT) correlations with consideration of casing friction." Can. Geotech. J., 31(3), 343-356.

Sy, A., and Lum, K.K.Y. (1997). "Correlations of mud-injection Becker and standard penetration tests." Can. Geotech. J., 34(1), 139–144.

Wightman, A., Yan, L., and Diggle, D.A. (1993). "Improvements to the Becker Penetration Test for Estimation of SPT Resistance in Gravelly Soils." Proc. 46th Can. Geotech. Conf., Saskatoon, SK, September 27-29, 379-388.

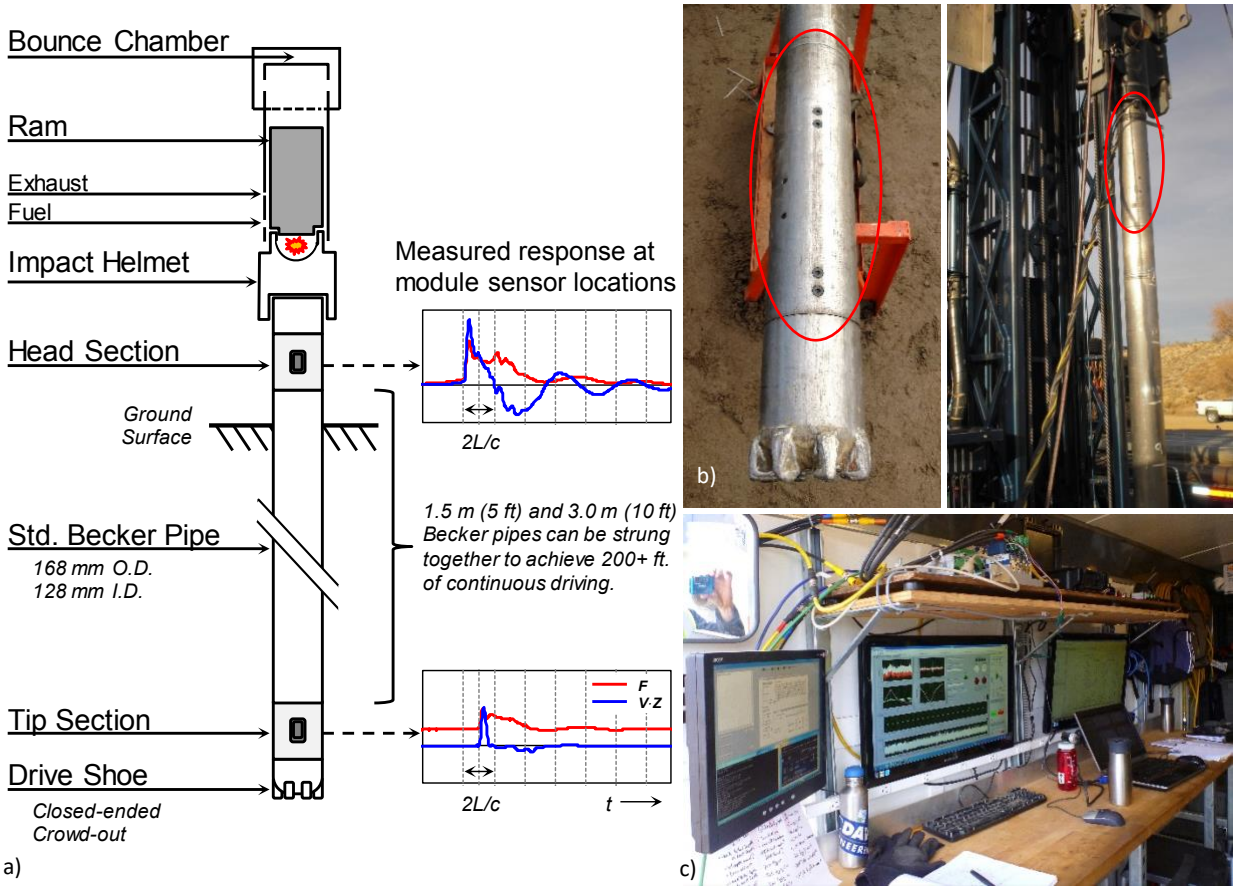

Fig. 1. iBPT system: a) Schematic iBPT system and Becker hammer; b) Tip and head modules; c) Field control unit.

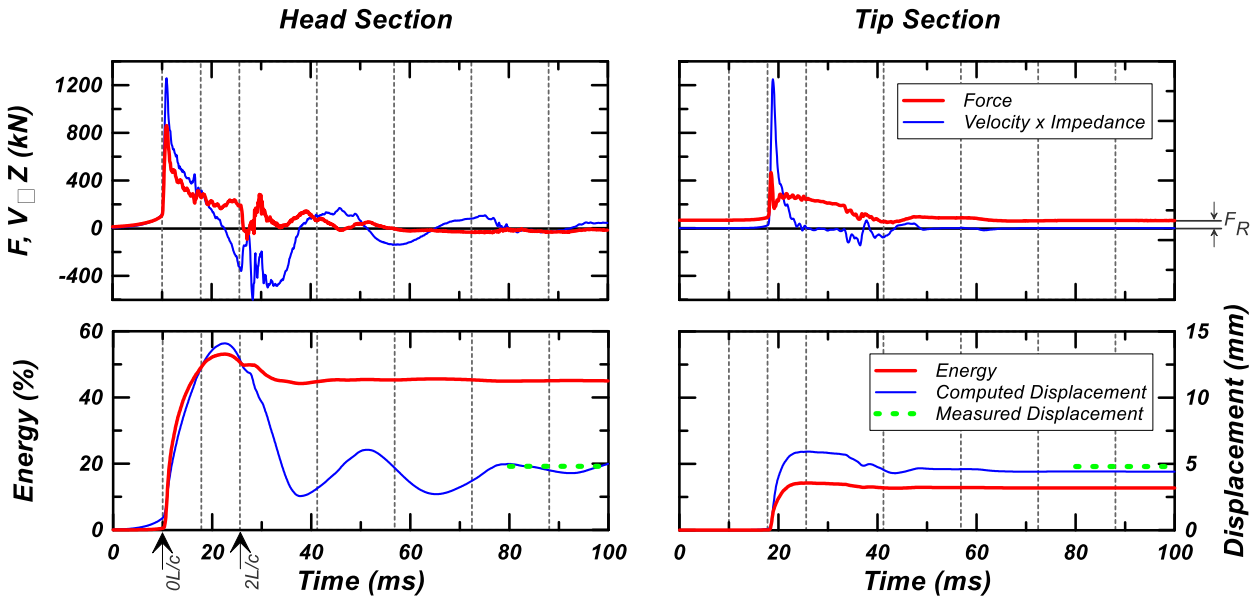

Fig. 2. iBPT measurements of force, velocity (multiplied by impedance), displacements and energies at head (above ground) and tip sections from impact at 37.5 m (122.5 ft) depth in relatively dense soil; data from Stone Canyon Dam.

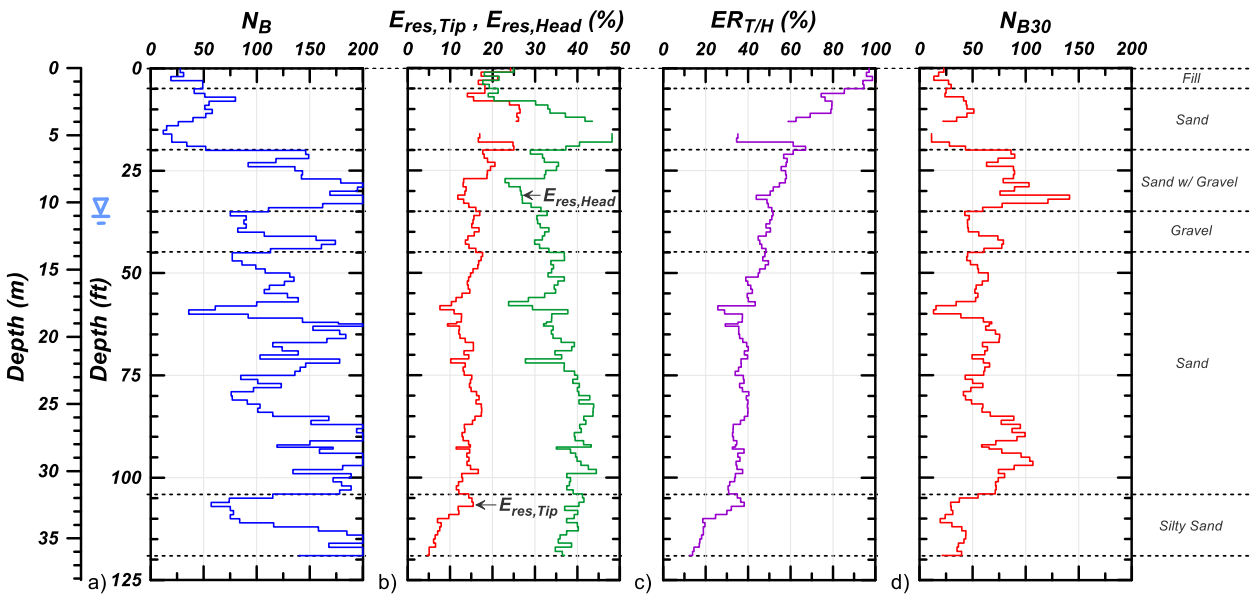

Fig. 3. iBPT output profile: a) Automatically recorded raw blow counts; b) Average residual energies measured at head and tip sections; c) Delivered energy ratio $ER_{T/H}$; d) Blow counts normalized based on energy measured at tip; data from Headworks West Reservoir.

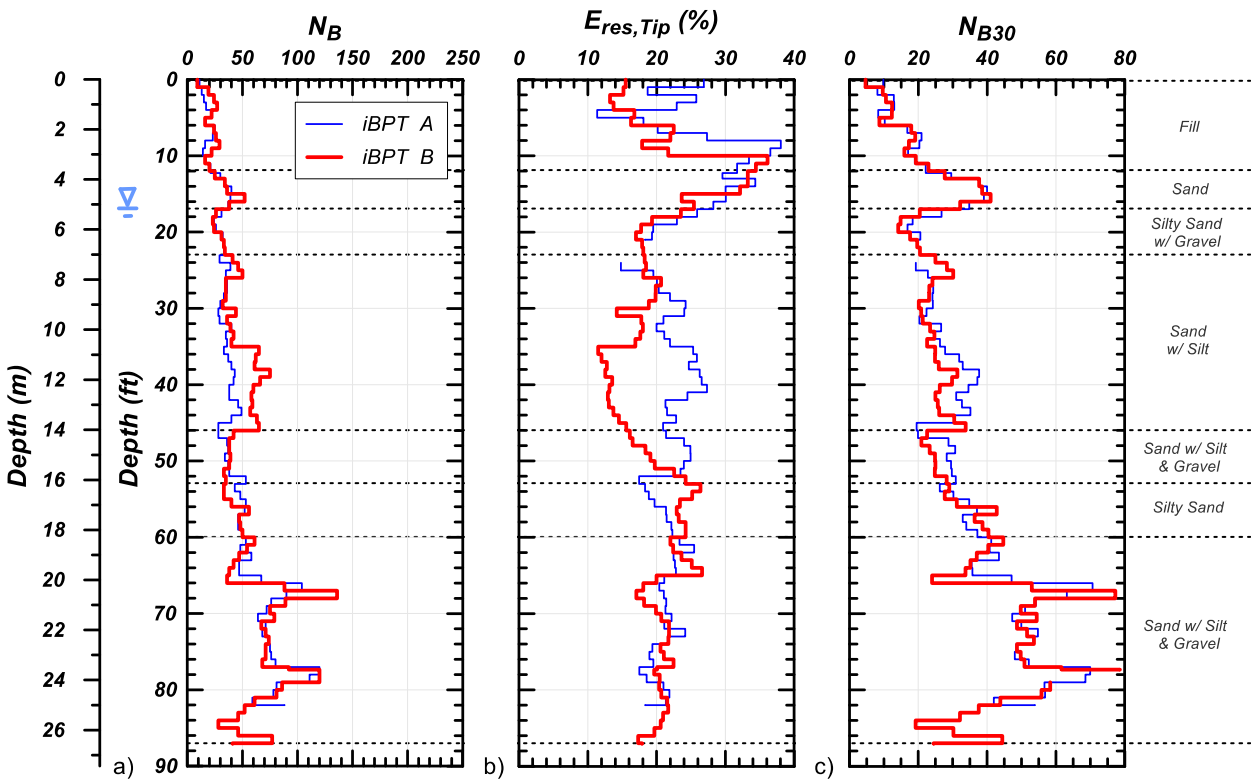

Fig. 4. Repeatability of iBPT results in adjacent soundings: a) Raw blow counts; b) Average residual energy measured at tip; c) Blow counts normalized based on energy measured at tip; data from North Haiwee Dam.

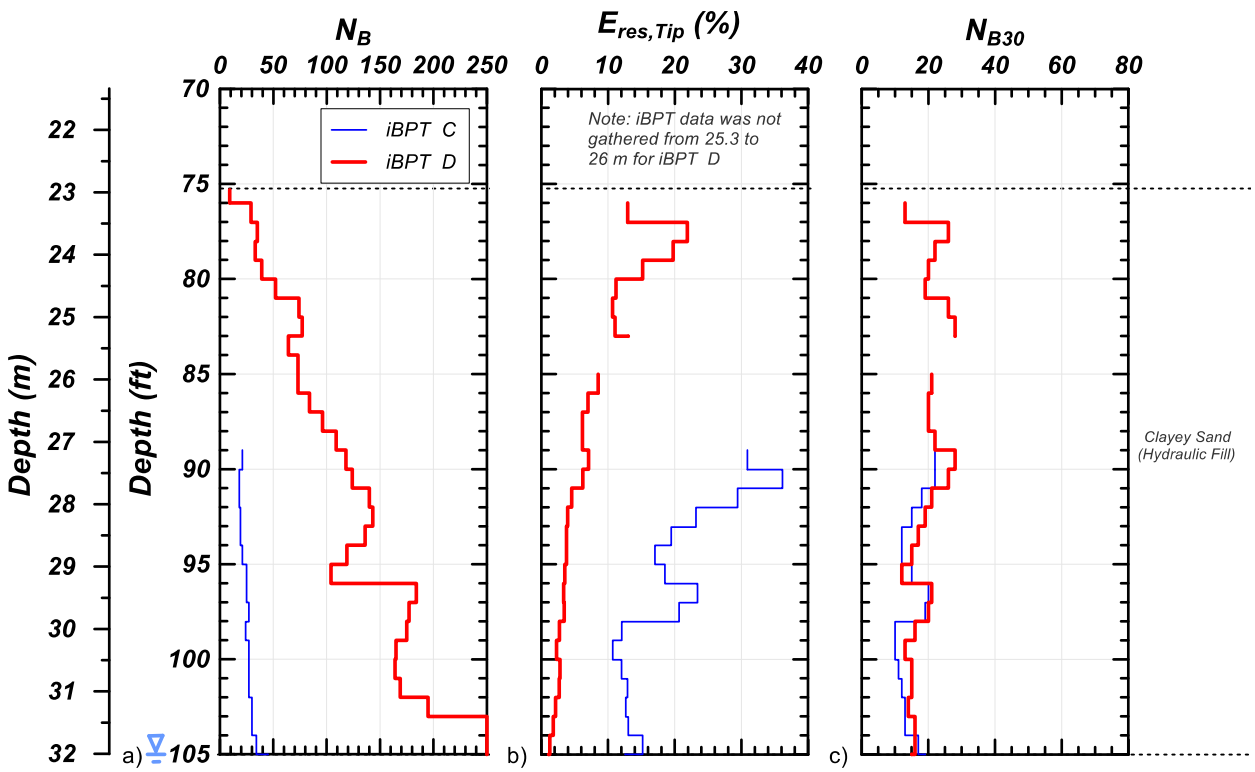

Fig. 5. Effect of shaft resistance on iBPT results in adjacent soundings: a) Raw blow counts; b) Average residual energy measured at tip; c) Blow counts normalized based on energy measured at tip; data from Stone Canyon Dam.

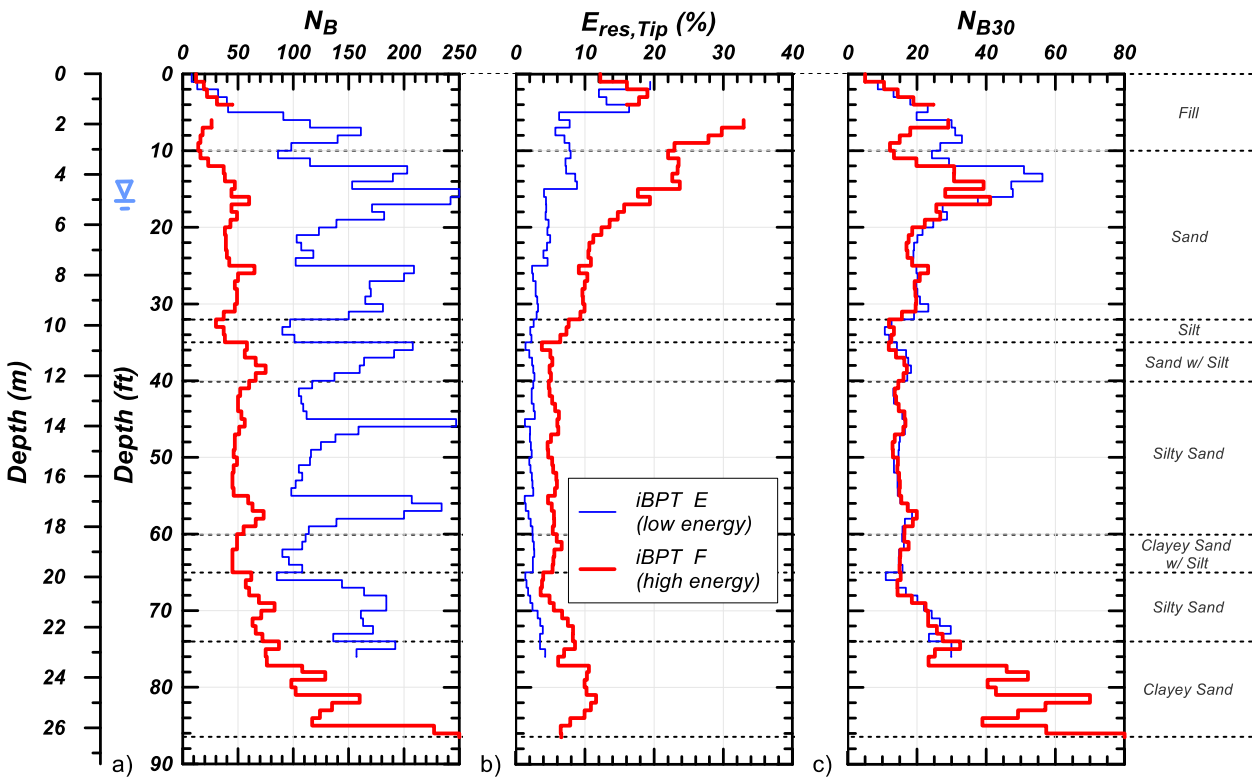

Fig. 6. Linearity of the iBPT results in adjacent soundings: a) Raw blow counts; b) Average residual energy measured at the tip; c) Blow counts normalized based on energy measured at the tip; data from North Haiwee Dam.

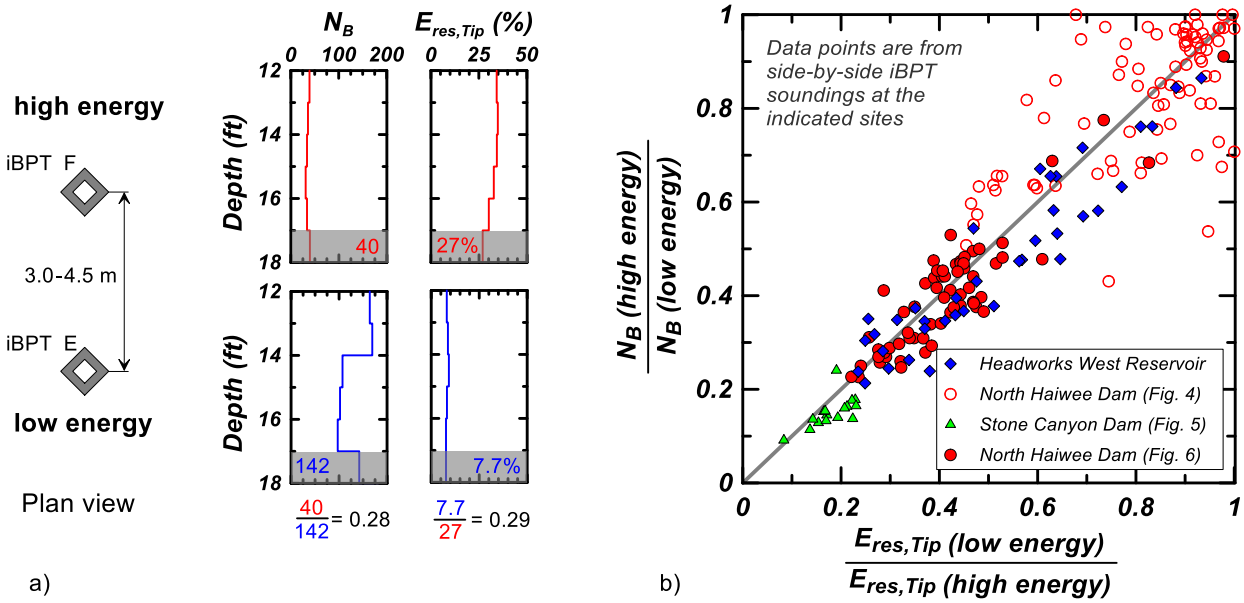

Fig. 7. Linearity of the energy normalization of blow counts with residual energy measured at tip. a) Schematic soundings layout and calculation of energy and blow count ratios; b) Equivalency of ratios of tip energy and raw blow counts in adjacent soundings; data from three sites.

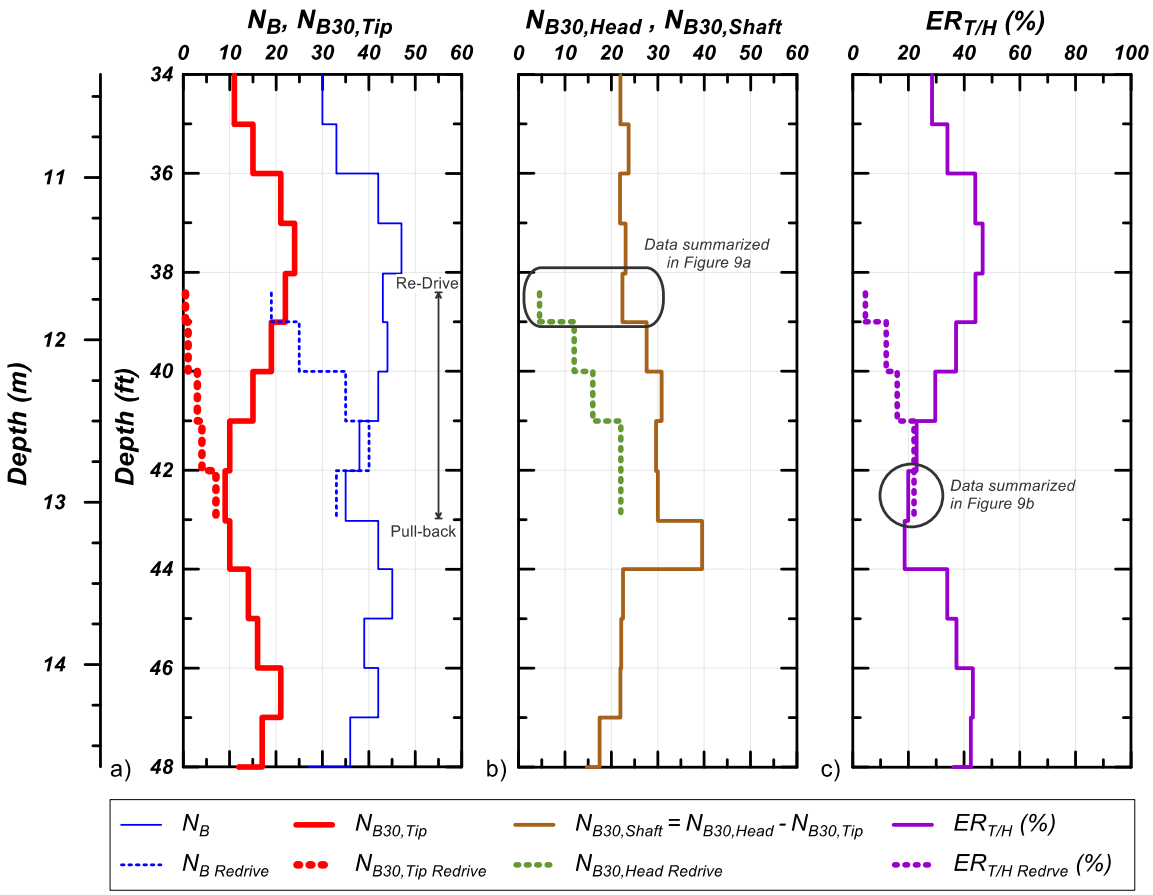

Fig. 8. Typical measurements during redrives: a) Raw and energy normalized blow counts during virgin driving and redrive; b) Energy normalized blow counts attributed to shaft resistance during virgin driving and redrive blow counts normalized based on energy measured at head; c) Delivered energy ratios during virgin driving and redrive; data from North Haiwee Dam.

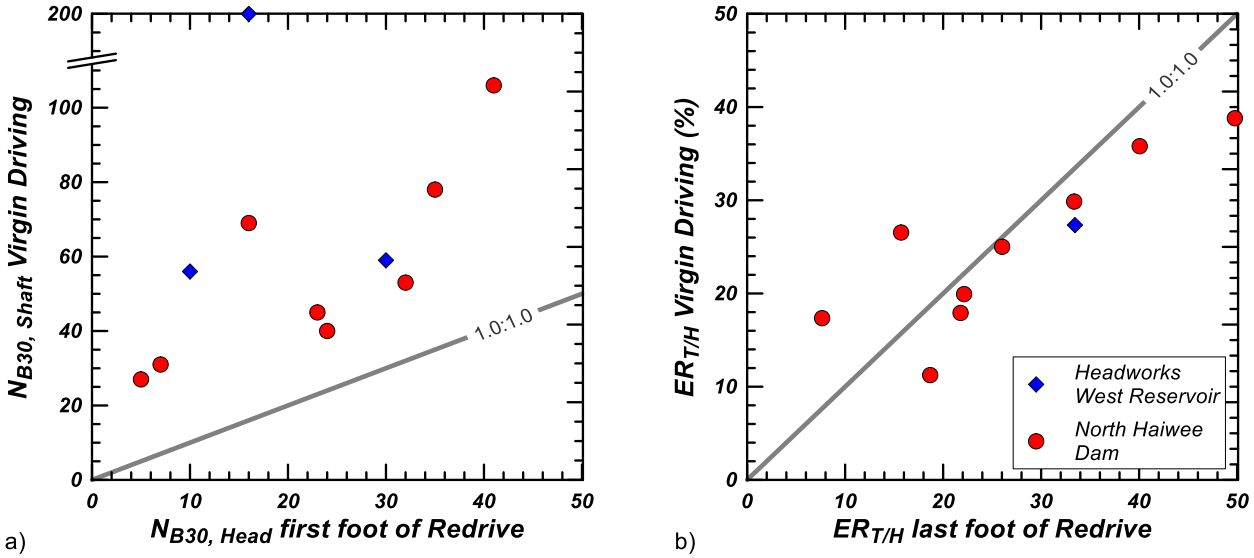

Fig. 9. Summary of measurements during redrives from two sites: a) Energy normalized blow counts attributed to shaft resistance during virgin driving and redrive blow counts normalized based on energy measured at head at the beginning of redrive; b) Delivered energy ratios during virgin driving and the end of redrive.

CHAPTER 2

Instrumented Becker Penetration Test. II: iBPT-SPT Correlation for Characterization and Liquefaction Assessment of Gravelly Soils

Mason Ghafghazi, M.ASCE[1], Jason T. DeJong, M.ASCE[2], Alexander P. Sturm, S.M.ASCE[3], and Charles E. Temple[4]

[1] Assistant Professor, Department of Civil Engineering, University of Toronto, 35 St. George St., Toronto, ON M5S 1A4, mason.ghafghazi@utoronto.ca

[2] Professor, Department of Civil & Environmental Engineering, University of California at Davis, One Shields Ave., Davis, CA 95616, jdejong@ucdavis.edu

[3] Graduate Student, Department of Civil & Environmental Engineering, University of California at Davis, One Shields Ave., Davis, CA 95616, apsturm@ucdavis.edu

[4] Former Graduate Student, Senior Engineer, US Army Corps of Engineers, 1325 J Street, Sacramento, California, 95814, cetemple@ucdavis.edu

Paper Reference:

Ghafghazi M, DeJong JT, Sturm AP, Temple CE. "Instrumented Becker Penetration Test, II: iBPT- SPT correlation for liquefaction assessment in gravelly soils", *ASCE J. Geotechnical and Geoenvironmental Engineering*, 2017, https://doi.org/10.1061/(ASCE)GT.1943-5606.0001718

ABSTRACT

The Becker Penetration Test (BPT) is a widely used tool for the characterization of gravelly soils, especially liquefaction assessment. An instrumented Becker Penetration Test (iBPT) was developed and integrated into the standard, closed-ended Becker drill string. The iBPT produces a continuous profile of energy normalized blow count values, N_{B30}, which are computed using the acceleration and strain measurements recorded directly behind the driving shoe. The N_{B30} profile is repeatable and unaffected by hammer driving energy or accumulated shaft resistance. This paper presents the correlation between iBPT N_{B30} and SPT N_{60} values which is necessary for performing liquefaction assessment in gravelly soils. In developing this correlation, field variability was addressed by comparing median iBPT N_{B30} and Standard Penetration Test (SPT) N_{60} values from adjacent soundings over geologically consistent depth intervals. A framework was also developed to assess, and, when appropriate, correct for gravel influence on measured SPT blow count (N) values. This framework utilizes SPT blows-per-inch as well as physical evidence from SPT and adjacent Sonic samples. The correlation between iBPT N_{B30} and SPT N_{60} is shown to be a constant value of 1.8 and independent of soil type or penetration resistance magnitude.

INTRODUCTION

Penetration tests, namely the Standard Penetration Test (SPT) and Cone Penetration Test (CPT), have become the standard for characterizing the liquefaction potential of cohesionless soils. Assessing the characteristics of gravelly soils poses additional difficulties due to the large particle to probe diameter ratio (e.g. Daniel et al., 2004). In the case of the SPT, gravel particles can clog or block the split-spoon sampler, resulting in limited recovery and/or unrepresentative blow counts. Depending on the abundance of large particles during the CPT, gravel particles can either

block the advancement of the cone, cause a misalignment in the rods, and/or adversely influence the measurements.

In order to obtain a representative penetration measurement in gravelly soils, current practice will often (1) use SPT blows-per-inch to detect and correct for the influence of large particles and/or (2) conduct large diameter in-situ testing such as the Becker Penetration Test (BPT). If the BPT is utilized, then equivalent energy normalized SPT blow count (N_{60}) values must be estimated using empirically developed correlations. The large diameter (168 mm, 6 5/8 in) of the BPT is particularly applicable in these coarse materials, where it provides more repeatable results and fewer occurrences of refusal compared to smaller scale split-spoon penetrometers (e.g. SPT). Other site investigation tools are occasionally used to characterize gravelly soils (i.e. large penetration tests (e.g. California Modified Sampler, North American Large Penetration Test, etc. (Daniel et al. 2004) and the Chinese Dynamic Penetration Test (Cao et al., 2013)). However, these tools are only slightly larger than CPT and SPT and therefore influenced by large particles in a similar manner.

The first correlation between BPT and SPT *N* values by Becker Drills Inc. from the 1970s proposed a correlation factor of 1.0 based on data collected from side-by-side soundings at a number of sites around British Columbia, Canada (Harder and Seed, 1986). The use of the correlation became questionable after the effects of driving energy on both SPT and BPT were recognized. Harder and Seed (1986) proposed a correlation between SPT N_{60} and BPT blow count values corrected to a constant hammer combustion condition, N_{BC}. Sy and Campanella (1994) developed a set of correlations between energy normalized BPT blow count values, N_{B30}, and SPT N_{60} values. The correlations of Sy and Campanella (1994) are dependent on the amount of

estimated static shaft resistance along the drill string, calculated using signal matching and wave equation analysis techniques.

The equivalent SPT N_{60} estimated by both Harder and Seed (1986) and Sy and Campanella (1994) are limited in accuracy and reliability due to the inherent limitations in how the contribution of shaft resistance is accounted for in the overall penetration resistance measured by the BPT. The limitations stem from their underlying assumptions and the datasets used to develop the correlations. Harder and Seed (1986) did not directly account for the influence of shaft resistance on the measured blow counts. The equivalent N_{60} values produced by the method underestimated at low shaft resistance values and overestimated at high shaft resistance values. The Sy and Campanella (1994) method utilized a more rigorous approach to correct for the contribution of shaft resistance by using wave matching techniques (CAPWAP) to estimate the total static shaft resistance developed along the drill string. However, the shortcomings of wave matching techniques in modelling the drill string response from individual hammer impacts, non-uniqueness of the wave matching solutions in separating drill string shaft and tip contributions, the deficiency of static shaft resistance as a proxy for energy loss, and the limited field data used to develop the correlation have resulted in inconsistent results. The estimated N_{60} values from Sy and Campanella (1994) are generally overestimated at low shaft resistance and erratic at medium to high shaft resistance.

Sy and Lum (1997) presented a modified, mudded BPT, using reduced diameter drill strings and drilling mud circulated behind the driving shoe, in an effort to reduce or eliminate shaft resistance. The mudded BPT was shown to eliminate the shaft resistance, but its application has remained limited to research explorations because of the difficulties associated with circulating mud with the BPT in pervious, gravelly soils.

The instrumented Becker Penetration Test (iBPT) provides a solution to the problem of shaft resistance in Becker Penetration Test. The iBPT equipment (DeJong et al., 2017) measures the acceleration and strain directly behind the drill string tip in order to calculate the energy delivered to the soil beneath the tip from individual hammer blows. iBPT blow count values per 0.3 m (1 ft) of penetration, N_B, are normalized by the residual energy delivered to the tip:

$$N_{B30} = N_B \frac{E_{res,Tip}}{30\ (\%)} \qquad [1]$$

where $E_{res,Tip}$ is the residual energy transferred to the instrumented section above the drill string tip at the end of each blow, expressed as a percentage of the rated ICE 180 hammer energy (11 kJ), and normalized to a reference 30% hammer energy efficiency (similar to 60% for SPT N_{60}).

DeJong et al. (2017) demonstrated that the iBPT system provides repeatable, reliable N_{B30} profiles that are unaffected by the input hammer energy, accumulated shaft resistance, and other driving conditions. The iBPT is fully integrated with standard Becker drilling equipment and can be performed as deep as Becker driving is possible. The robust and reliable N_{B30} measurements obtained with the iBPT system provide the opportunity to develop a more reliable correlation to compute equivalent SPT N_{60} values.

The development of the correlation between iBPT N_{B30} and SPT N_{60} values is described in this paper. The correlation uses data from four, extensive, field exploration programs including SPT, iBPT, and Sonic soundings. The materials from the four sites encompass those soils commonly encountered in practice and range from low plasticity clays, silts, and sands to gravelly sands. Most of the materials were of alluvial origin; however, man-made, compacted and hydraulically-placed fills as well as residual soils were also encountered. In order to develop a reliable correlation, the first step was to ensure that the SPT N_{60} values used were of high quality. This resulted in the development of a framework to assess the quality of SPT data obtained in

gravelly soils, and includes a systematic approach for quality evaluation and, when appropriate, blow count value correction. Next, the extent of spatial variability that typically exists in gravelly alluvia was evaluated and a consistent, geology-informed, methodology was used to handle the effects of spatial variability on the final correlation. A linear correlation was developed to convert iBPT N_{B30} values to equivalent SPT N_{60} values. This paper demonstrates that the correlation is independent of soil type and therefore applicable to all soils that may be encountered when characterizing sites with gravels.

FIELD MEASUREMENTS AND TEST SITES

The iBPT system was deployed at four project sites. The 42 iBPT soundings (915 linear meters) provided data in a wide range of ground and drilling conditions. Data were obtained in residual and alluvial deposits as well as man-made compacted and hydraulically placed fills. A variety of soil types were encountered including mixtures of clays, silts, sands, gravelly sands and sandy gravels. Collectively, the particle size ranged from small cobbles to clays, the plasticity ranged from 0 to about 27, the percent gravel ranged from 0% to 50%, and the percent fines ranged from 0% to 90%. Driving was performed from the ground surface and from various depths below grade (after pre-drilling) to avoid refusal stemming from high shaft friction when penetrating through the compacted dam embankment.

All testing was performed in clusters where one (or occasionally two) iBPT soundings were performed at a distance of 2 to 4 m (6 to 14 ft) from SPT and Sonic soundings. CPT soundings were also performed in many cases (at similar spacing), which provided additional data on stratigraphic layering and field variability. The positioning and spacing between the soundings was determined considering the depositional environment (i.e. aligning borings parallel to historic

stream flow to enhance cross-correlation), the zone of influence of the different tests, the test sequence, and site access. Table 1 contains a summary of the tests performed at each site.

SPT data were obtained through rotary wash drilling at all sites. The procedures recommended by Idriss and Boulanger (2008) were used to correct measured N values to N_{60} values. Individual energy measurements, obtained per the procedures recommended in ASTM D4633-10, were used for energy normalization in two SPT borings at each site. For SPT borings where direct energy measurements were not available, the average energy of the hammer measured on the same site was used, with the short rod correction applied when appropriate. The SPT samplers used at two of the sites had no inside clearance, while the SPT samplers used at the other two sites had clearance for liners with no liners installed. The liner correction recommended by Idriss and Boulanger (2008) was applied to the latter.

A summary of the four sites is presented here with additional details provided in DeJong et al. (2017). The first site, Headworks West Reservoir, is founded on alluvial gravelly and cobbly deposits from the original alignment of the Los Angeles River. The second site, the new alignment for North Haiwee Dam, is located in a predominately calm hydro-geologic depositional environment and comprised of silty sand and clean sand deposits with occasional gravel lenses. The third site, Stone Canyon Dam, is located within a narrow canyon and underlain by arroyo-alluvial foundation comprised of highly interlayered and intermixed low plasticity clays and sands with frequent gravel-sized, slate fragments. There is significant variability in the alluvium; however, the man-made, dam embankment units are relatively homogeneous and comprised of clayey silts and silty clays. The fourth site, Bouquet Canyon Dam, consists of a dam founded on an upper, sandy, alluvium and a lower, gravelly, alluvium which is underlain by highly weathered, schist bedrock.

DEVELOPMENT OF iBPT-SPT CORRELATION

Geotechnical design and analysis in general, and liquefaction assessment procedures in particular, often use SPT N_{60} as a proxy for the soil strength and denseness since sampling and laboratory characterization of cohesionless soils is impractical. The prevalence of SPT N_{60} data in sands has led to the development of numerous methodologies for estimating liquefaction susceptibility from SPT N_{60} values. iBPT N_{B30} values provide reliable penetration resistances in gravelly soils (DeJong et al, 2017); however, there are no direct methods to estimate liquefaction susceptibility from iBPT N_{B30} values. As such, iBPT N_{B30} values need to be converted to equivalent SPT N_{60} values in order to predict the liquefaction susceptibility of gravelly soils. This approach assumes that the SPT-based liquefaction triggering correlations, developed for sand, are applicable to sandy soils with gravels and to gravelly soils.

The correlation was developed by comparing 915 linear meters of iBPT N_{B30} values and 349 SPT N_{60} values obtained in 42 pairs of adjacent soundings/borings across four project sites. The following steps were taken:

- All SPTs were screened for gravel influence through a conservative framework (described in detail below) with consideration of additional information from adjacent Sonic soundings. SPT blow counts which were determined to be adversely influenced by the presence of gravel particles were excluded from the correlation database.
- SPT N_{60} values were computed using Idriss and Boulanger (2008).
- iBPT N_{B30} values were computed using DeJong et al. (2017).
- SPT N_{60} and iBPT N_{B30} measurements were binned over geologically consistent depth intervals that had comparable penetration resistance trends and soil types. This was

done in an effort to handle the spatial variability between two adjacent soundings, spaced about 3 m (9.8 ft) apart, in alluvial deposits.

- Median values of the binned SPT N_{60} and iBPT N_{B30} values were compared to develop the correlation.

Screening for Gravel Influence on SPT

The presence of large particles (gravels and larger) can increase SPT blow counts (Rollins et al., 1998). Large particles may get trapped below the driving shoe, temporarily increasing the blow counts until they are pushed out of the way, moved into the sampler, or broken apart by subsequent hammer blows. Large particles may also clog the sampler, changing the penetration mechanism from open-ended to closed-ended (full displacement).

The occurrence and consequence of encountering large particles during an SPT test is dependent on the soil gradation, the soil density, the particle shape and hardness, and where along the SPT penetration length of 0.45 m (18 in) the large particles are encountered, among other factors. It is difficult to detect and quantify the gravel influence on SPT *N* values with a high level of certainty. It is, however, possible to identify circumstances where gravel influence is more likely, and develop a simplified framework to screen and, when possible, correct, the SPT *N* values for gravel influence.

A rigorous and conservative framework to evaluate the potential for gravel influence on SPT *N* values was developed. The framework was designed to conservatively separate SPT N_{60} values into high (HQ) and low quality (LQ) categories. HQ data represent measurements where information indicated that little or no gravel influence occurred and LQ data represent measurements where the possibility of significant gravel influence could not be ruled out.

The developed framework evaluates the potential influence of gravel using per-inch SPT blow counts (Figure 1) as well as any physical evidence. The physical evidence includes gradation of the samples retrieved in the split-spoon sampler and Sonic cores, photographs of the sample retrieved in the split-spoon sampler and Sonic cores, sample recovery, and field logs. When possible soil gradations from Sonic core samples should be considered as the SPT split-spoon sample can scalp large particles resulting in an under-estimation of the gravel content. This is evident in the ranges of gradations observed in gravelly soils from SPT (ID= 35 mm or 1 3/8 inch) and Sonic core (ID= 102 mm or 4 inch) samples from two sites (Figure 2). Sonic cores are not immune to scalping, but the larger diameter results in a more accurate (closer to in-situ) gradations.

Gravels often cause an increase in per-inch blows over a few inches of penetration (e.g. Figures 1b and 1c.ii). These "spike" features in the blows per-inch profile can be corrected by manually removing the "spike" feature from the per-inch blow count trend, as illustrated in Figures 1b and 1c. On the other hand, greater judgment is needed when a steady rise or consistently high values are observed (e.g. Figure 1c.i). When there are multiple changes in the blows per-inch profile (e.g. Figure 1d.i), or in cases of refusal (less than about 15 inch sampler penetration out of the standard 18 inch), the measurements are considered unreliable.

Every SPT test is assigned one of five different quality indices as defined in the following rubric:

I – No sign of gravel influence in per-inch blow counts. No signs of influential gravels in the physical evidence from SPT *and* Sonic testing.

II – No sign of gravel influence in per-inch blow counts. Sign(s) of influential gravels in physical evidence from SPT *and/or* Sonic testing.

III – Sign(s) of gravel influence in per-inch blow count which were considered acceptable, or were reliably corrected. No sign of influential gravels in physical evidence from SPT *and* Sonic testing.

IV – Sign(s) of gravel influence in per-inch blow counts which were considered acceptable, or were reliably corrected. Sign(s) of influential gravels in physical evidence from SPT *and/or* Sonic testing.

V – Sign(s) of gravel influence in per-inch blow counts which cannot be reliably corrected. Sign(s) of influential gravels in physical evidence from SPT *and/or* Sonic testing.

The implication of indices I and II is that gravels were deemed not present in the vicinity of the SPT sampler (I), or the sampler did not encounter the gravel particles (II). Index III, which is seldom observed, accounts for cases where dense sand seams are encountered. Index IV pertains to cases where the presence of gravel is virtually certain, but its adverse influence on the blow count may be negligible, or eliminated by applying a reliable correction. Index V pertains to the cases where the presence of gravel is certain and its effects cannot be reliably corrected. Table 2 summarizes the five indices for assessing gravel influence on SPT results.

The intention behind the screening framework is to consider the blows-per-inch and physical evidence separately, and then combine them to make a final decision based on the index definitions. In some cases, the two factors may corroborate to better explain how large particles influenced the blow counts. One example is when a gravel particle is located within the sampler close to the penetration depth where a blow count 'spike' is observed. Another example is when *N* values are consistently high and the recovery is small, or the length of sample recovered is similar to the penetration distance up to the depth where a high blow zone begins. In other cases,

physical evidence and per-inch blow counts may not necessarily align. The indices are specifically worded to methodically categorize various possibilities and facilitate the decision-making process.

After an Index (I – V) is assigned to each *N* value the data are separated into high quality (HQ) and low quality (LQ) categories. HQ data represent measurements where little or no gravel influence was expected and is defined as data with indices of I to III. LQ data represent measurements where the possibility of significant gravel influence could not be ruled out and is defined as data with indices of IV and V. In addition to this criteria, all samples with more than 20% grave present in the spilt-spoon sampler were removed. This additional step of data omission was developed considering guidance from Idriss and Boulanger (2008), including a 'rule-of-thumb' 15-20% gravel threshold. This additional 20% gravel present in the SPT spilt-spoon sampler cutoff was applied as a further objective and conservative criteria after applying the gravel screening framework presented above to ensure that the data selected for use in the correlation development was free from gravel influence. As detailed below, subsequent evaluation verified that this additional level of screening (20% threshold) was conservative resulting in many HQ SPT data being excluded. Appendix A details how this SPT screening framework may be applied more broadly for general site investigations to evaluate the influence of gravel on SPT data.

The screening framework described above was applied to each SPT sample from the four sites in order to assess gravel influence on SPT *N* values. Only the SPTs identified as HQ were included in developing the iBPT-SPT correlation. The majority of these were obtained in soils that did not contain gravel (Index I). The remainder of the database was comprised of SPT N_{60} values obtained in soils where the presence of the gravel was determined to have not adversely influenced the SPT (Indices II and III, with less than 20% gravel).

Field Variability

The differences between the two measurements (i.e. iBPT N_{B30} and SPT N_{60}) obtained in adjacent soundings can be attributed to a combination of differences between the tests as well as field variability. In order to distinguish between the contributions of these two factors, and quantify the extent of field variability, results from identical tests performed in adjacent soundings can be compared. Figure 3 presents measurements made in the same horizons from four pairs of CPT soundings (spacing between pairs of soundings being 4.6 m (15 ft)) and from four pairs of iBPT soundings (spacing between pairs of soundings being between 2.8 and 4.0 m (9 to 13 ft)) from the North Haiwee Dam site. The CPT tip resistance, q_t, is widely recognized as the most repeatable in-situ penetration resistance measurement (e.g. Kulhawy and Trautmann, 1996). The per-foot average q_t values from pairs of CPT soundings are plotted in Figure 3a, and have a log-normal coefficient of variation (COV) of 0.40. iBPT N_{B30} values from adjacent soundings are plotted in Figure 3b, and have a log-normal COV of 0.37. The field variability bands from CPT and iBPT measurements are similar, which demonstrates that the iBPT N_{B30} measurement is as repeatable as the CPT q_t measurement. More importantly, ±40% variability bands reflect the range that can generally be expected when the comparing the results from adjacent soundings (3 to 4.5 m distance) in an alluvial deposit.

The same range of variability, about ±40%, is therefore expected in the correlation between iBPT N_{B30} and SPT N_{60} values as its development is based on the comparison of data from two adjacent borings/soundings. Further, the SPT is a less repeatable method compared to other in-situ penetration tests (e.g. Kulhawy and Trautmann 1996, Rogers 2006), and is therefore the likely source of additional scatter in the correlation.

Binning of Data for Correlation Development

The comparison of representative, median penetration resistance values obtained by two different methods (e.g. iBPT N_{B30} and SPT N_{60} values) over geologically consistent depth intervals enables evaluation of the relation between penetration resistances between the two methods. The basis for this approach is founded in the recognition that the soils encountered in two adjacent soundings at a specific horizon may not have been deposited simultaneously due to the spatial variability of the alluvial depositional processes. However, similar soils will be deposited over a larger depth interval when the depositional environment is consistent over time; these geologically consistent depth intervals can be binned and the median values from these intervals used as representative values.

The application of this binning approach using iBPT N_{B30} and SPT N_{60} data for the correlation developed is illustrated in Figure 4. The consistency of the iBPT N_{B30} and SPT N_{60} signatures were considered in selection of intervals for binning. For example, in each of the two bins at depths of 3.5 to 6.5 m (11 to 21 ft), and 8 to 13.5 m (26 to 44 ft), iBPT N_{B30} and SPT N_{60} trends are similar, and distinctly different from other intervals. The SPT and Sonic logs, grain size distributions, and photos are also compared within each potential bin to confirm that the interval generally consists of one material type. In general, there was consistency between the materials encountered in the iBPT, Sonic, and SPT soundings from a single cluster and this binning approach associated statistically similar materials in most cases.

For the correlation development the bins which include mainly high quality SPT data were classified as high quality (HQ) and those with low quality SPTs were classified as low quality (LQ) and were excluded from the correlation development. Transitional depth intervals or those without enough data were not assigned to a bin and were omitted from correlation development.

iBPT N_{B30} - SPT N_{60} Correlation

A linear correlation

$$N_{60} = 1.8\ N_{B30} \qquad [2]$$

exists between median SPT N_{60} and iBPT N_{B30} values from high quality (HQ) bins with a log-normal COV of 0.35. Figure 5 presents the median data pairs for the 122 HQ bins developed, with the symbol diameter representing the amount of data in each bin. These 122 bins are based on 349 individual HQ SPT measurements with an adjacent, continuous iBPT N_{B30} profile (Table 1). No clear bias is evident amongst the data from the four different sites, and the extent of variability was similar to that present at the test sites, as indicated by the ±40% variability bands in the figure.

The use of median bin values was effective at capturing the correlation between SPT N_{60} and iBPT N_{B30} values in the spatially variable, alluvial deposits. The effect of the binning procedure is evident in Figure 6 where bars that represent the range of SPT N_{60} and iBPT N_{B30} values present in each bin is plotted (Note that iBPT data was obtained every 0.3 m while SPT data was obtained every 0.75 or 1.5 m). The largest error bars are observed at Headworks West Reservoir which is the most geologically variable site in the database. The binning approach presented above appears to adequately curb the variability in more variable sites to the same level observed in Figure 3.

No material dependence is observed in the correlation. This is evident in Figure 7 where the data have been presented based on the dominant soil type present in each defined bin. The data are presented on log-log scale in Figure 7b for better visibility across their entire data range.

The correlation factor is constant across the full range of penetration resistances measured. To assess the sensitivity of the correlation factor, the cumulative distribution of the ratio of SPT N_{60} to iBPT N_{B30} median values are plotted in Figure 8. The correlation factor of 1.8 represents the median (50th percentile) value in the cumulative plot. SPT N_{60} values less than 40 ($N_{B30} < 23$) are specifically important to liquefaction assessment. If only data bins within this range of data are

included in the cumulative plot, a nearly identical cumulative distribution curve is obtained. This supports the 1.8 correlation factor to the range of N_{60} values included in correlation development. A cumulative distribution curve is also plotted for the database after all bins with gravelly soils were excluded. The nearly identical curve supports the inclusion of the SPT N_{60} values which were corrected for gravel influence.

The bins that were defined as LQ based on the SPT N_{60} measured are plotted on top of the high quality data in Figure 9. As expected, a significant portion of the LQ data lie above the field variability bands, which is consistent with the expectation that the presence of gravel typically increases measured SPT N_{60} values. A significant number of the LQ data also plot within the ±40% variability bands of the correlation, suggesting that the presence of gravel had little or no influence on median N_{60} values of these LQ bins, which confirms that the screening criteria applied to the SPT data was conservative.

The correlation produces very good agreement between the iBPT equivalent N_{60} profiles and those directly measured by the SPT in adjacent soundings. Figure 10 shows four iBPT equivalent N_{60} profiles, one from each site. The agreement between the N_{60} values from iBPT and SPT is evident. Also evident is the improved resolution of the subsurface stratigraphic provided by the continuous profile of iBPT equivalent N_{60} values. The iBPT based profile provides a representative N_{60} value for every foot of penetration, whereas SPT measurements are typically performed at 1.5 m (5 ft) vertical increments. This increased resolution improves detection of the transitions between layers, the presence of weak layers, and the vertical uniformity within individual layers. The plots in Figure 10 and these observations are representative and consistent in the profiles of the 42 SPT borings and adjacent iBPT soundings pairs examined to date.

CONCLUSIONS

The instrumented Becker Penetration Test (iBPT) provides a continuous, normalized blow count profile (N_{B30}). The measurements allow for a high degree of repeatability and reliability by the directly measuring, and correction for, the magnitude of energy delivered to the drill string tip. The iBPT enables characterization of a wide range of soils, including clayey, silty, sandy, and clean gravels, as well as gravelly soils (DeJong et al, 2017). Analysis of SPT and Sonic data, in combination with the iBPT data has led to the following observations and conclusions:

- A systematic framework for the assessment of gravel influence and, when applicable, correction for its effects on SPT *N* measurements was developed. This method is based examination of the SPT blows-per-inch trend as well as physical information from SPT and Sonic samples of the soil penetrated. The method was applied in development of the iBPT – SPT correlation and was demonstrated to be an effective, conservative approach for selecting SPT measurements that were not affected by gravel. A less conservative version of this framework can be used for evaluation of the influence of gravel on SPT data as described in Appendix A.
- The spatial variability in alluvial deposits was shown to be significant, and relatively consistent across the project sites. In general, identical measurements obtained in two soundings performed at ~3m spacing had approximately ±40% variability. This level of variability is due to the alluvial depositional process itself, and therefore should be expected when two measurements are compared at a similar spacing.
- A data binning approach was proposed to systematically handle the spatial variability of alluvial deposits. Bins were defined where vertical intervals of SPT N_{60} and iBPT N_{B30} values

as well as encountered soil types were consistent. The median SPT N_{60} and iBPT N_{B30} values were used to represent the bin characteristics.

- A linear correlation with an empirical factor of 1.8 was developed to estimated equivalent SPT N_{60} from iBPT N_{B30} values. This correlation was evaluated and shown to be robust across all four project sites, applicable in the soils tested, and stable across the range of penetration resistances measured. Further, no bias with respect to measurement depth or soil saturation (above or below the water table) was evident. The bin data used to develop the correlation contained about ±40% variability; this is attributed to spatial variability of alluvial deposits, as opposed to a systematic difference between the iBPT N_{B30} and SPT N_{60} measurements.
- Representative profiles of the 42 SPT borings and adjacent iBPT soundings pairs examined show that the correlation produces very good agreement between the iBPT equivalent N_{60} values and those directly measured by the SPT in adjacent soundings. In addition, the vertical continuity (relative to SPT measurements obtained every 1.5 m) in the stratigraphic profile produced by the iBPT improves the characterization and assessment of transitions between layers, and detection of critical, weak zones.

Appendix A. Practical SPT Screening Framework

When only SPT measurements are available (e.g. early in a site investigation) a practical screening framework for evaluating gravel influence may prove useful to guide the selection of subsequent site investigation tools (e.g. whether iBPT may be appropriate). As such, insights gained from the large iBPT dataset have been used to develop a practical framework for SPT screening.

The practical framework uses blows-per-inch SPT data as well as physical evidence from SPT, and if available Sonic soundings. A flowchart detailing the proposed practical SPT screening

framework is presented in Figure 11. The framework uses the indexing scheme defined in Table 2. Indices I to III are considered uninfluenced by gravel, and index V is considered influenced by gravel to the extent that a reliable correction cannot be applied. The SPT samples classified with an index IV are considered free of gravel influence if their gravel content is less than 20%.

In this practical SPT screening framework, the 20% gravel content threshold is used as an inclusion criterion for index IV samples as opposed to an exclusion criterion all samples, as is proposed in the conservative screening framework. This subtle change places more emphasis on the assigned indices and allows those samples which are influenced by gravel, but the influence is believed to be negligible or adequately corrected, to be used for characterization.

The practical framework may admit a number of the SPT measurements dismissed by the conservative framework used to develop the iBPT correlation. In Figure 10, those SPTs which were considered LQ, based on the conservative screening framework, but are considered unlikely to be influenced by gravel, based on the practical framework, are circumscribed by open circles. It is evident that most of the SPTs now pass the criteria, and all of those SPTs which pass agree with the iBPT profile. As expected, the SPTs which are still considered LQ (e.g. Figure 10.d at 10.5 m (35 ft) depth) have N_{60} values that are greater than the iBPT profile.

The application of this practical framework for screening of SPT values on a project without a companion iBPT profile does not provide a site-specific definitive confirmation of the SPT data quality. As such, this practical framework is appropriate for initial screening of SPT data to determine if there is sufficient gravel present such that the SPT data quality may be questionable and further testing may be warranted. In all cases the decision to use SPT data or perform more advanced testing depends on the project value, the societal consequences of failure, and the influence of the uncertainty in the (equivalent) SPT value on the predicted system performance.

ACKNOWLEDGEMENTS

The authors appreciated the funding and support provided by the Division of Safety of Dams (DSOD) of the California Department of Water Resources (David Gutierrez and Richard Armstrong), the Los Angeles Department of Water and Power (Craig Davis and Adam Perez), and the California Department of Transportation (Caltrans, Tom Shantz). In addition, the support and collaboration of AMEC (Marty Hudson and Alek Harounian), AECOM (Wolfgang Roth and S. Nesarajah), GeoPentech (Jon Barneich, Andrew Dinsick and Doug Wahl), and Great West Drilling (Jim Benson) is appreciated.

REFERENCES

ASTM D2487-10 (2011), Standard Practice for Classification of Soils for Engineering Purposes (Unified Soil Classification System). ASTM International, West Conshohocken, PA, USA.

ASTM D4633-10 (2010). Standard test method for energy measurement for dynamic penetrometers. ASTM International, West Conshohocken, PA, USA.

Cao Z., Youd L.T., Yuan, X. (2013). Chinese Dynamic Penetration Test for Liquefaction Evaluation in Gravelly Soils. Journal of Geotechnical and Geoenvironmental Engineering, ASCE, 139(8): 1312-1333.

Daniel C.R., Howie J.A., Campanella R.G., and Sy A. (2004). Characterization of SPT grain size effects in gravels. Second International Conference on Site Characterization (ISC'2). Porto, Portugal.

DeJong J.T., Ghafghazi M., Sturm A.P., Wilson D.W., den Dulk J., Armstrong R.J., Perez A., and Davis C.A. (2017). Instrumented Becker Penetration Test I: Equipment, Operation,

and Performance. Under review.

Harder L.F.Jr., and Seed H.B. (1986). Determination of penetration resistance for coarse-grained soils using the Becker Hammer Drill. College of Engineering, University of California, Berkeley. Report No. UCB/EERC-86/06. May 1986.

Idriss I.M., and Boulanger R.W. (2008). Soil Liquefaction during Earthquakes. Earthquake Engineering Research Institute publication No. MNO-12. ISBN #978-1-932884-36-4.

Kulhawy F., and Trautman C.H. (1996). Estimation of insitu test uncertainty. Uncertainty in the Geologic Environment: From Theory to Practice, Proceeding of Uncertainty '96, ASCE Geotechnical Special Publication No. 58.

Rogers J.D. (2006). Subsurface Exploration Using the Standard Penetration Test and the Cone Penetrometer Test. Environmental and Engineering Geoscience, 12(2): 161-179.

Rollins K.M., Diehl N.B., and Weaver T.J. (1998). Implications of Vs - BPT $(N_1)_{60}$ Correlations for Liquefaction Assessment in Gravels. Geotechnical Earthquake Engineering and Soil Dynamics III, 1:506-507.

Sy A. and Campanella R.G. (1994). Becker and standard penetration tests (BPT-SPT) correlations with consideration of casing friction. Canadian Geotechnical Journal, 31(3): 343-356.

Sy, A., and Lum, K.K.Y. (1997). Correlations of mud-injection Becker and standard penetration tests. Canadian Geotechnical Journal, 34(1): 139-144.

Table 1. Summary of field testing used for developing iBPT - SPT correlation.

Project	*Number of Soundings*	*Total Linear Footage (m/ft)*	*Complimentary Drilling*	*High/Low Quality SPTs*	*High/Low Quality Bins*
Headworks West Reservoir	*16*	*400/1300*	*SPT, Sonic*	*94/103*	*25/28*
North Haiwee Dam	*10*	*250/800*	*SPT, CPT, Sonic*	*93/10*	*45/5*
Stone Canyon Dam	*8*	*165/550*	*SPT, CPT, Sonic*	*120/57*	*36/18*
Bouquet Canyon Dam	*8*	*100/330*	*SPT, CPT, Sonic*	*42/40*	*16/17*
Total	*42*	*915/2980*		*349/210*	*122/68*

Table 2. Rubric developed for assigning gravel influence indices to SPT data.

Index	*Per-Inch SPT Blow Counts*		*Physical Evidence**	
	Is there a sign of Gravel Influence?	*Can a reliable correction be applied?*	*Are gravels present based on the physical evidence from SPT (and/or Sonic)?*	*Is the gravel present influential gravel**?*
I	*No*	-	*No* *Yes*	- *No*
II	*No*	-	*Yes*	*Yes*
III	*Yes*	*Yes*	*Yes* *No*	*No* -
IV	*Yes*	*Yes*	*Yes*	*Yes*
V	*Yes*	*No*	*Yes*	*Yes*

** Physical Evidence refers to soil gradations, sample photos and field logs from SPT split spoon samples and/or Sonic cores in the vicinity of the SPT sample.*

*** Influential gravel is one of sufficient size and abundance to have plausibly affected SPT penetration measurement.*

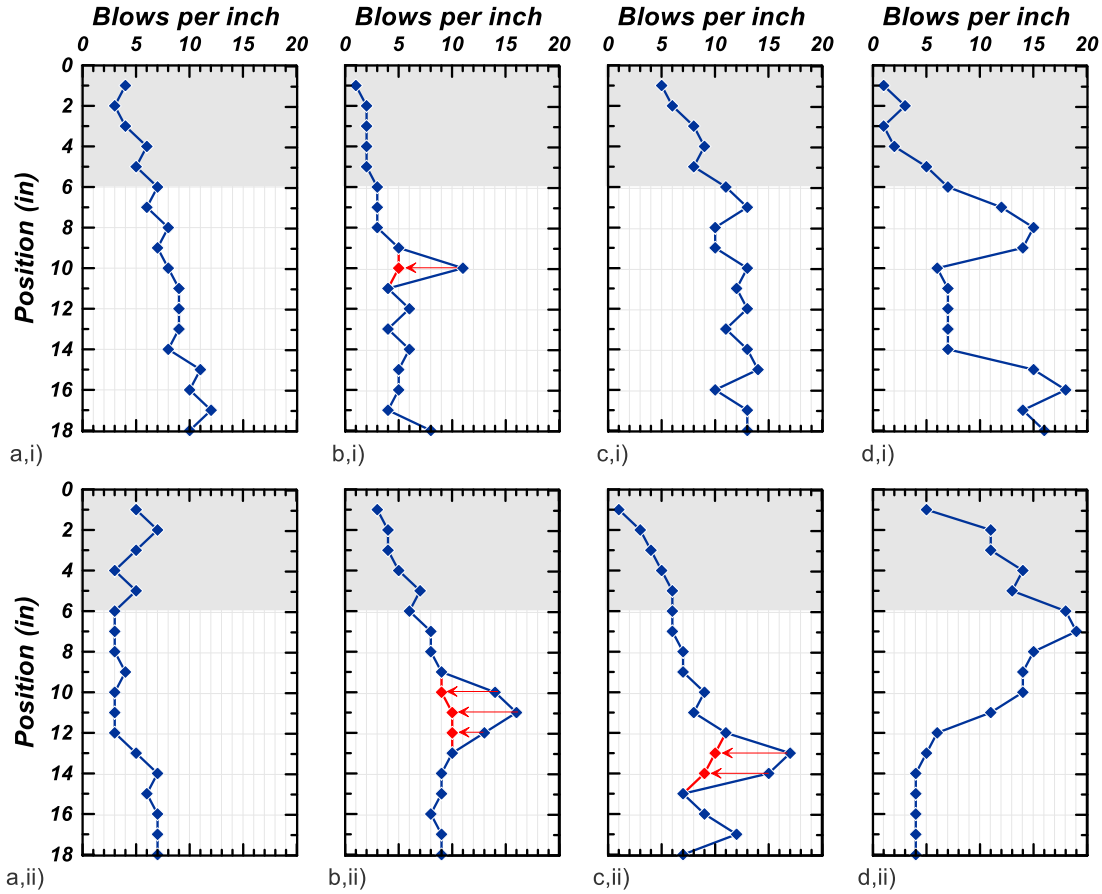

Fig. 1. Per-inch SPT blow counts used to evaluate gravel influence; a) No influence (indices I and II); b) Potential influence with reliable correction (index III); c) Influence with reasonable trend or reliable correction (index IV); d) Influence, not correctable (index V).

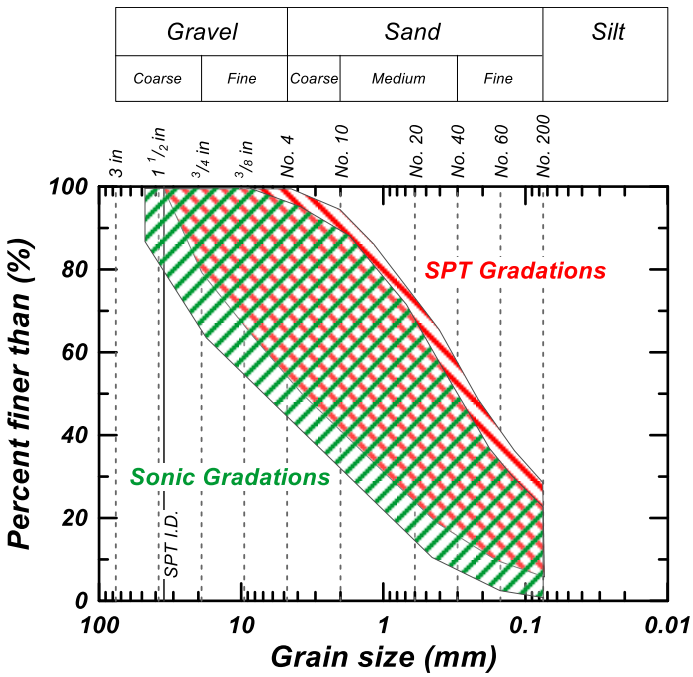

Fig. 2. Effect of scalping on grain size distribution curves (ASTM D2487, 2011) of SPT samples; comparison to grain size distribution curves of Sonic cores; data from the Headworks West Reservoir.

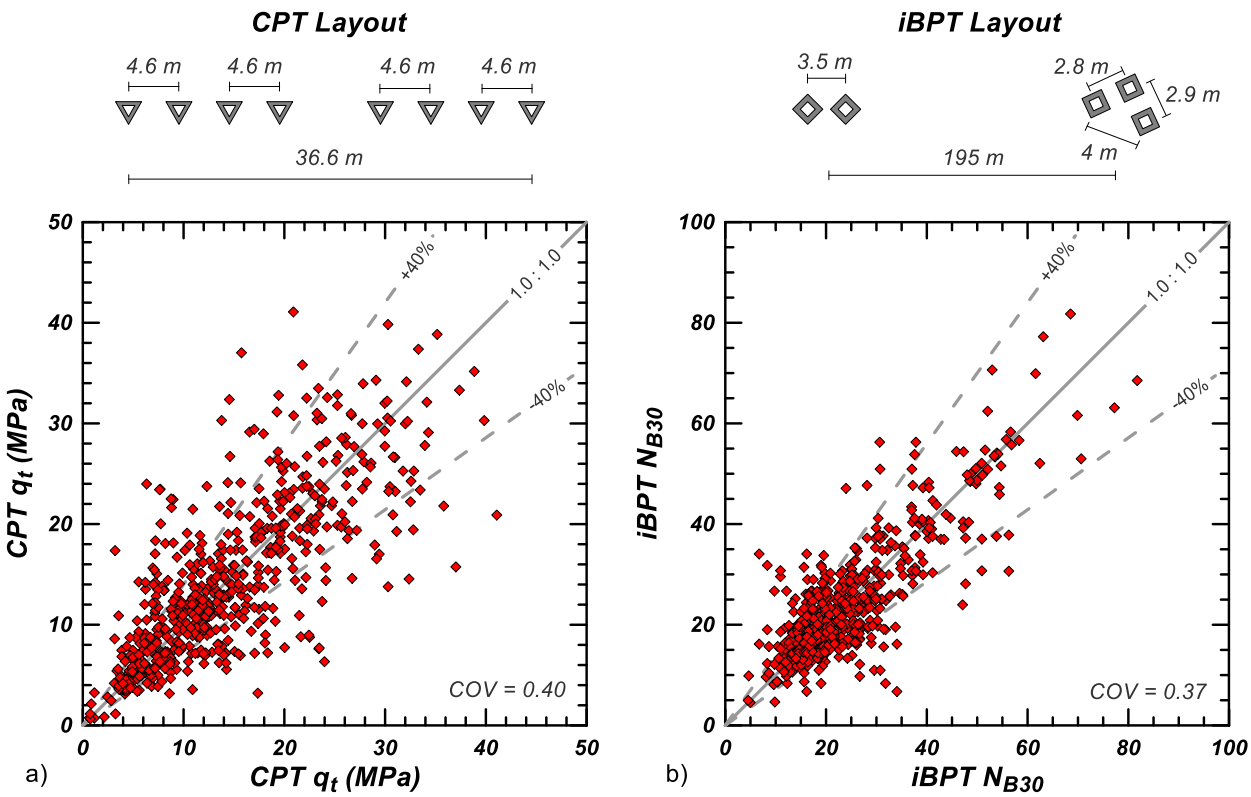

Fig. 3. Field variability in adjacent soundings at North Haiwee Dam; a) Comparison of adjacent CPT tip resistances (q_t) averaged per foot of penetration b) Comparison of adjacent iBPT N_{B30} values per foot of penetration.

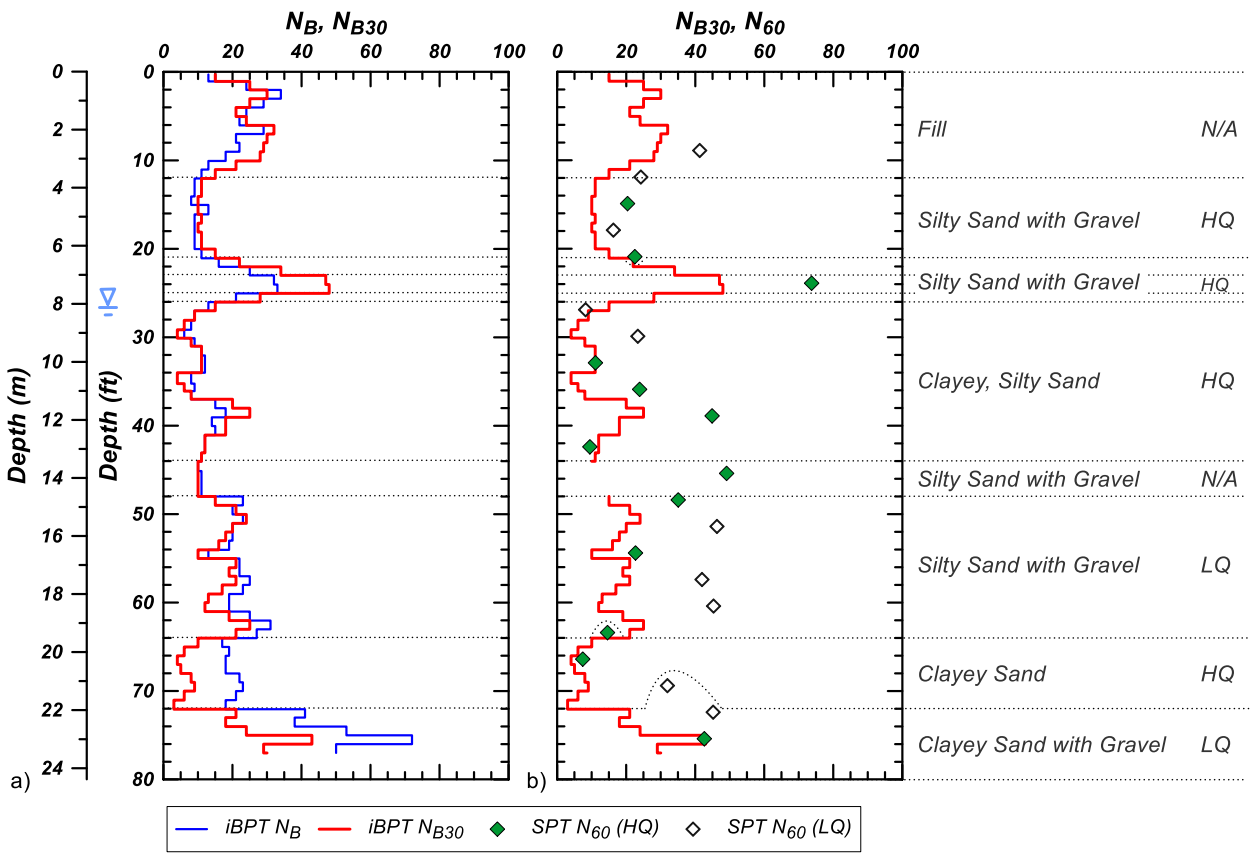

Fig. 4. Example profile from the Stone Canyon Dam; a) iBPT raw blow counts N_B, normalized blow counts based on tip measurements N_{B30}; b) High and low quality SPT N_{60} and iBPT N_{B30}, and depth intervals and material types identified for binning.

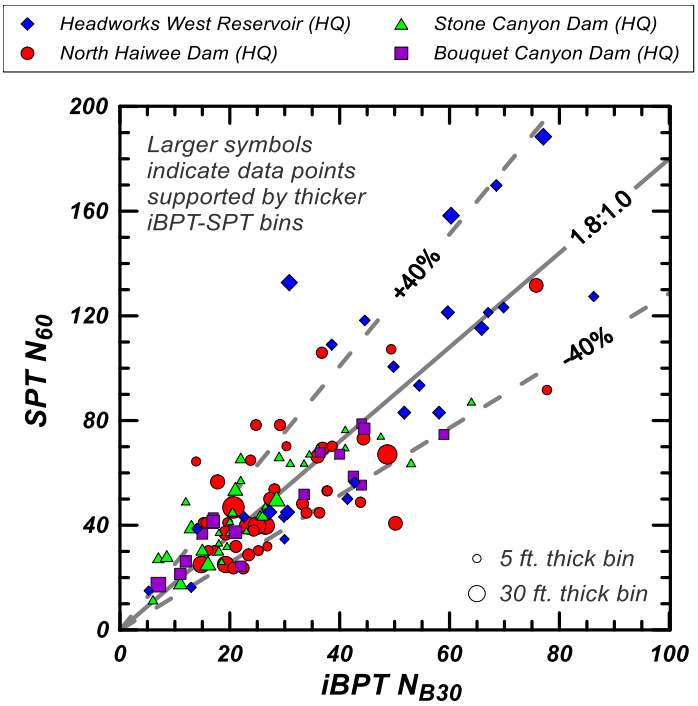

Fig. 5. Correlation between medians of iBPT N_{B30} from tip measurements, and SPT N_{60}; high quality (HQ) data from four sites.

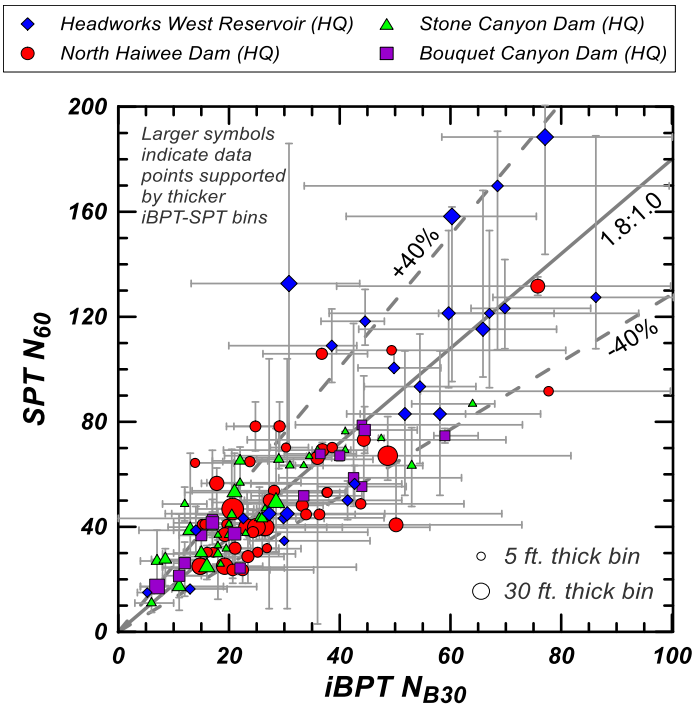

Fig. 6. Range of data included in bins used to develop correlation between medians of iBPT N_{B30} from tip measurements, and SPT N_{60}; High quality (HQ) data from four sites.

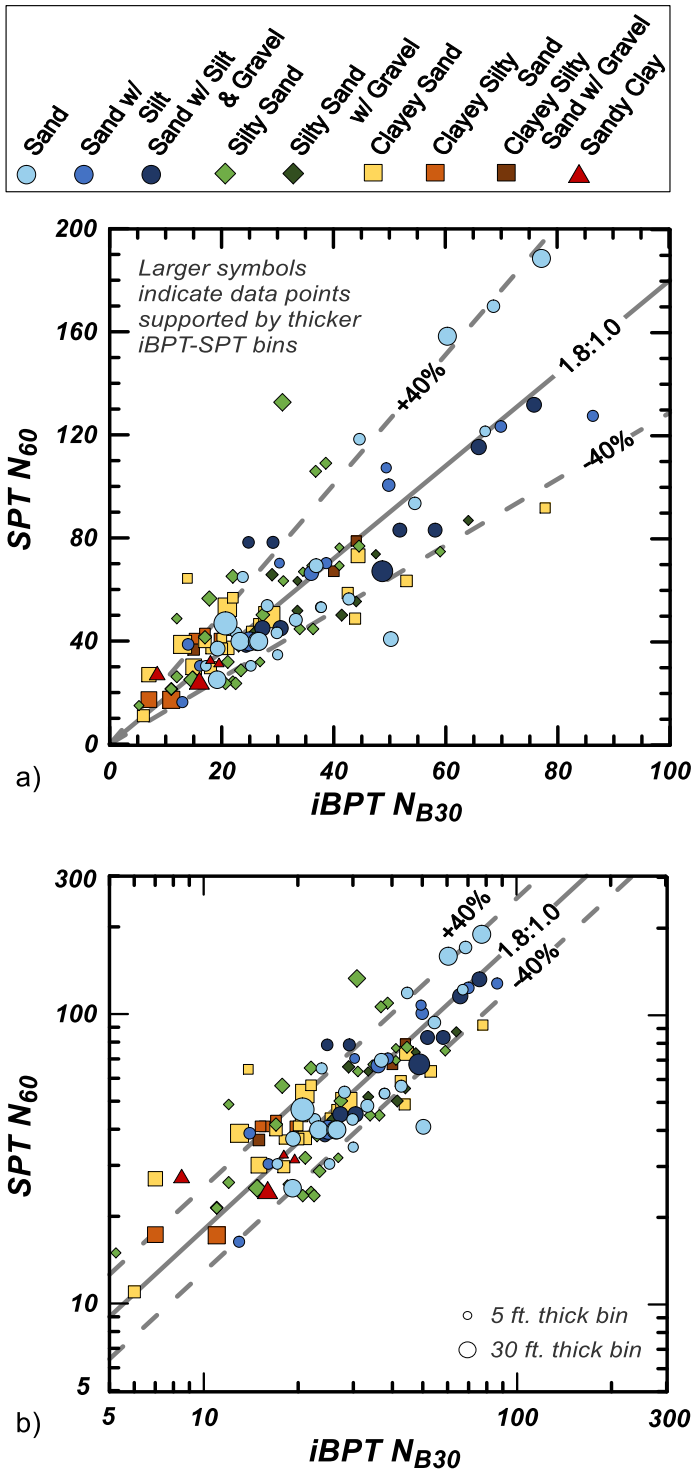

Fig. 7. High quality (HQ) bins used to develop correlation between medians of iBPT N_{B30} from tip measurements, and SPT N_{60}; material types identified; data from four sites. a) Linear axes; b) Logarithmic axes.

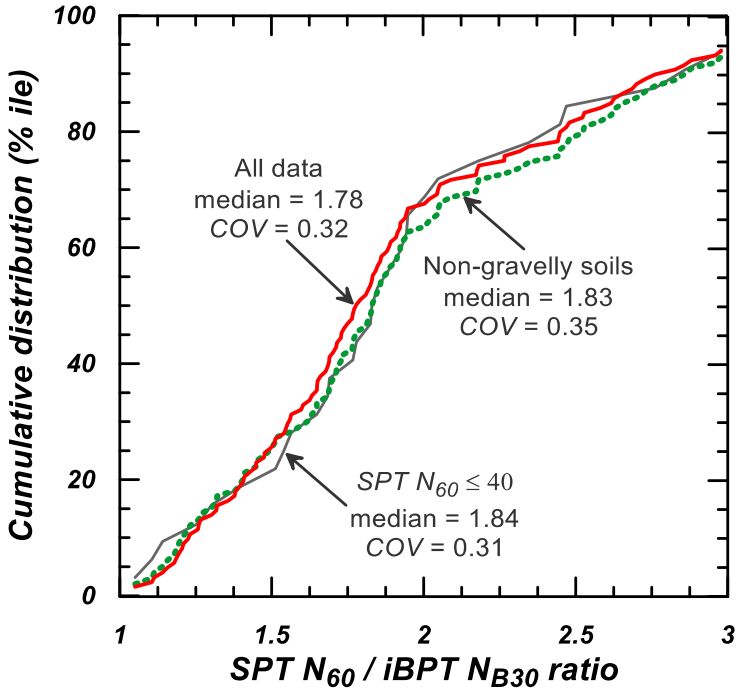

Fig. 8. Cumulative distribution of iBPT-SPT correlation factor from high quality (HQ) bins.

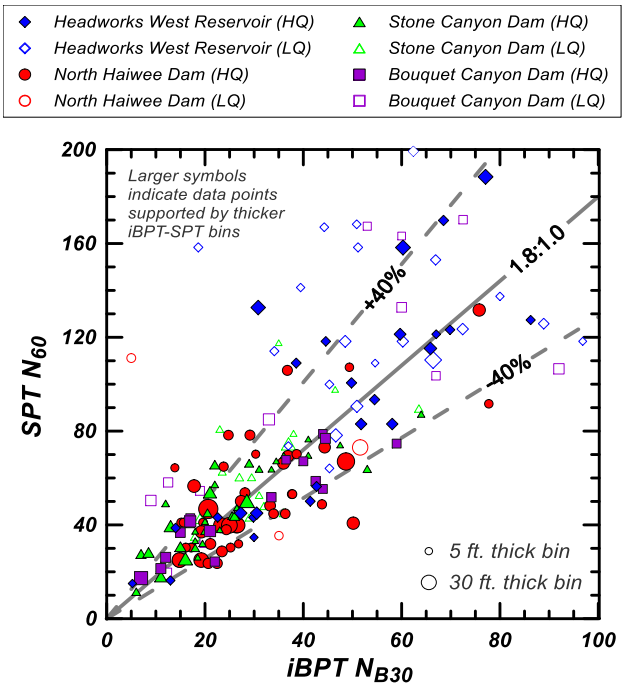

Fig. 9. Correlation between medians of iBPT N_{B30} from tip measurements, and SPT N_{60}; low quality (LQ) and high quality (HQ) data from four sites.

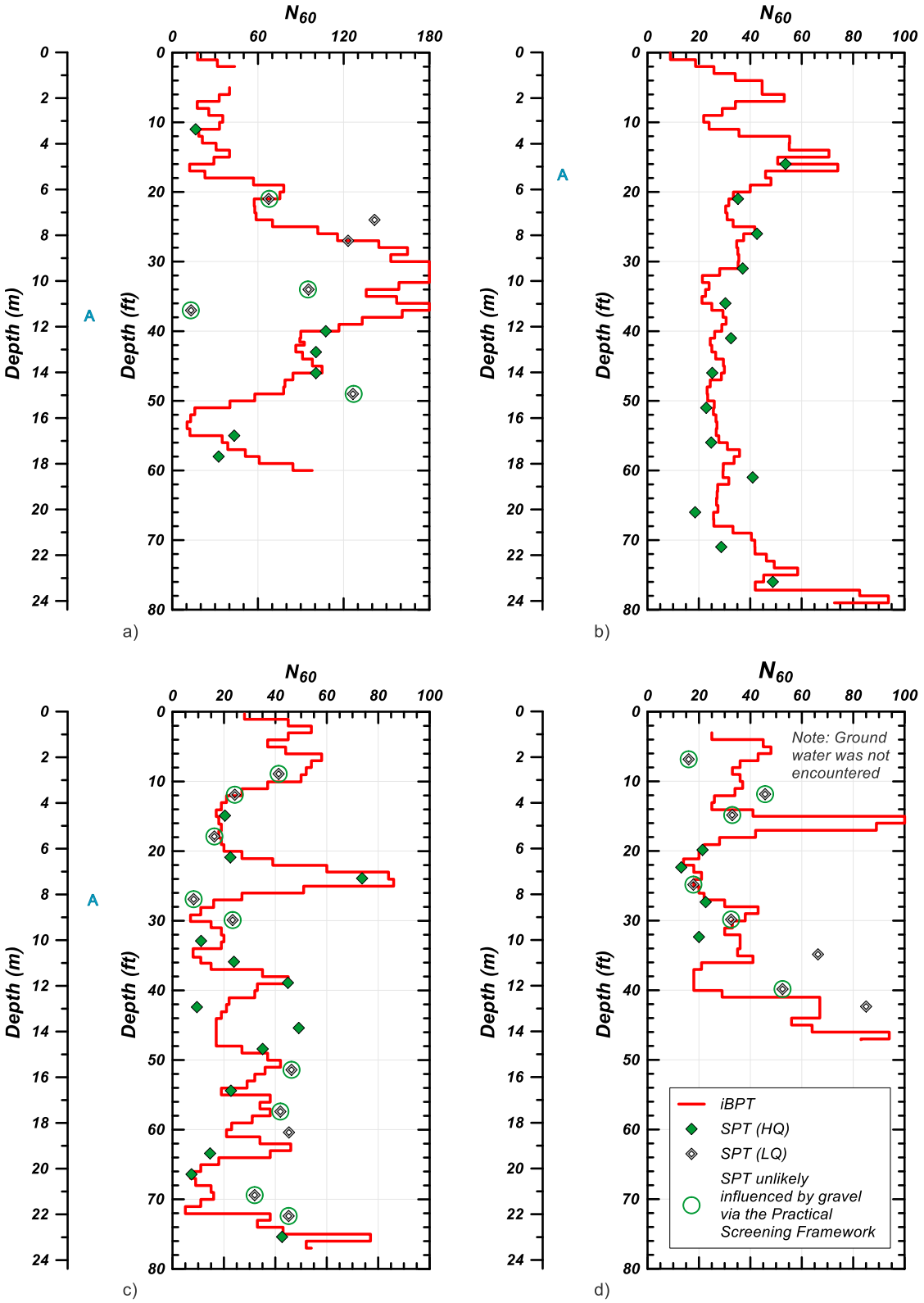

Fig. 10. Equivalent iBPT comparison to SPT N_{60}: a) Example from Headworks West Reservoir; b) Example from North Haiwee Dam; c) Example from Stone Canyon Dam (see Figure 4); d) Example from Bouquet Canyon Dam.

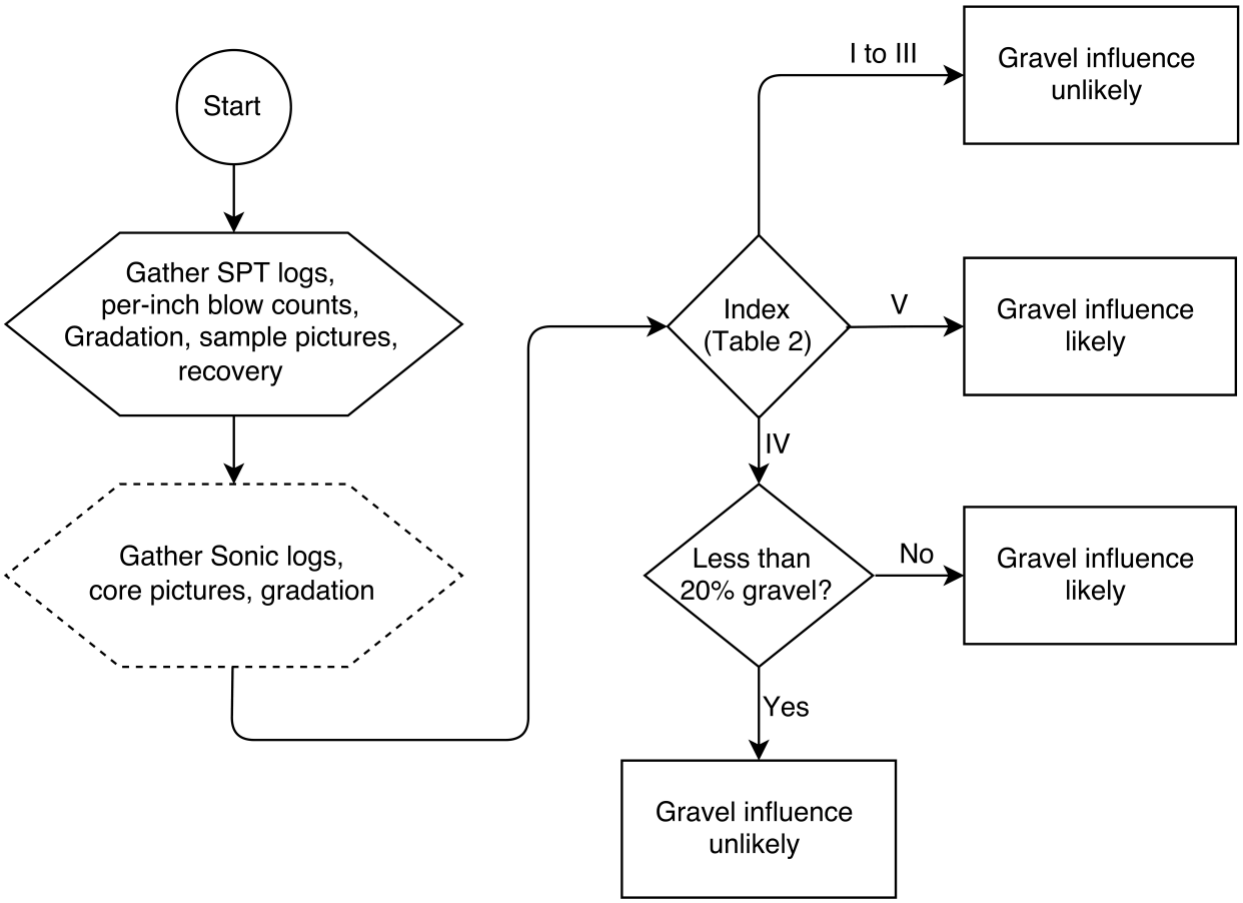

Fig. 11. Flowchart for practical screening framework for gravel influence on SPT.

CHAPTER 3

Use of Reusable Test Pile for Pile Design as Informed by Full Scale Pile Load Tests

A. Max Rossiter[1] and Jason T. DeJong[2]

[1] Former Graduate Student, Department of Civil & Environmental Engineering, University of California at Davis, One Shields Ave., Davis, CA, 95616

[2] Professor, Department of Civil & Environmental Engineering, University of California at Davis, One Shields Ave., Davis, CA, 95616, jdejong@ucdavis.edu

Reference:

Rossiter, A.M. "Use of Reusable Test Pile for Pile Design as Informed by Full Scale Pile Load Tests", M.S.C.E. Thesis, University of California Davis, 2016.

ABSTRACT

Current in-situ testing measurements used in pile design procedures, such as SPT N_{60} and CPT q_t, are prone to elevated measurements caused by the presence of gravels. Measurement uncertainty caused by the influence of gravel on in-situ testing results necessitates the use of increased factors of safety on final pile design to ensure adequate performance of the system. Large factors of safety often lead to overdesigning of pile foundation elements, increasing the cost associated with construction. The Reusable Test Pile system (RTP) is designed to provide reliable penetration resistance measurements in gravelly soils and directly measure the force distribution within a scaled driven pile installed at the site.

This paper presents RTP testing performed adjacent to previously performed full scale pile load tests in the Los Gatos Creek alignment in Coalinga, CA. The pile load test data is interpreted and compared to pile capacity calculations performed using data collected by the RTP. A system overview explains the design and operation of the RTP, as well as the process of data collection and interpretation. Testing performed at this site includes two RTP soundings, each adjacent to a separate full scale pile load test. During each sounding, a total of 6 static pullback tests were performed.

INTRODUCTION

Development of a robust in-situ testing system that is capable of assessing soil strength, as well as site specific pile drivability and performance can reduce uncertainty and increase the efficiency of deep foundation systems. In order to account for uncertainty in design, it is common practice to use a factor of safety of four or greater for SPT based design, and no smaller than two for pile design using static or dynamic pile loading tests according to the Canadian Foundation

Engineering Manual (2006). These large factors of safety ensure acceptable performance from deep foundation systems, however it can also lead to significant overdesign. Reducing the factor of safety required through the use of static pile load tests and detailed dynamic analyses is expensive, and not feasible on smaller projects. The goal of the Reusable Test Pile (RTP) system is to increase the reliability of in-situ measurements and overall pile design in order to reduce the number of change orders during construction.

A regular challenge facing geotechnical engineers is the presence of gravel during site investigation, and the affect it has on the ability to obtained reliable in-situ measurements. Common in-situ testing methods such as the standard penetration test (SPT) and the cone penetration test (CPT) are susceptible to the effect of large particles, making testing difficult and often yielding unreliable results. The RTP system, however, utilizes the closed ended Becker Penetration Test (BPT) platform, which has been shown to produce more repeatable results than SPT and CPT in the presence of gravel due to its 168 mm (6.625 in) outside diameter (DeJong et al., 2016). Increasing reliability in the penetration resistance measurements used for direct methods of pile capacity calculation can reduce the required factor of safety used in design.

Reducing uncertainty in field measurements is beneficial, however there is still uncertainty incorporated within the assumptions and empirical correlations used for pile design, as well as the effects of installation method on pile capacity. The RTP system is designed with the intention of directly measuring shaft friction for a driven pile through the use of tensile pile pullback tests. The total force along the length of the pile can be captured at multiple points, which can be used to calculate average skin friction values for segments between the force measurements. This method of direct shaft friction measurement is intended to decrease the variability associated with design equations using penetration resistance, or other in-situ measurements. By increasing reliability in

the pile design parameters, the designer can choose to use a less conservative, more efficient final design.

BACKGROUND

In the past, instrumented piles have been used to provide insight into the distribution and mobilization of resistance along the pile shaft and base during installation and service loading in order to better predict load distribution and pile behavior. However, most of these piles were installed through the use of jacking or pushing, and focused on implementation in clayey soils. A summary of some instrumented piles is presented in Table 1 (Thurairajah, 2013).

The most commonly used of these instrumented piles is the Cone Penetration Test (CPT). Originally designed for in-situ testing and soil characterization, a range of pile design methods have been created using the CPT because of the similarity in penetration using the CPT to the pile loading and failure mechanisms. Early methods of pile capacity calculation using the CPT are generally based on empirical predictions, including Schmertmann (1978) and the LCPC method (Bustamante and Gianeselli, 1982). Incremental advancements in design methods such as the methods presented in the Canadian Foundation Engineering Manual then the UWA-05 Method have led to a shift toward methods based on fundamental soil properties and load-transfer mechanisms.

Other instrumented piles of differing size and measurement capabilities that were developed include the Piezo Lateral Stress cell (PSL), Grosche & Reese (G&R) Test Pile, Norwegian Geotechnical Institute (NGI) Test Pile, 3” Model Pile, X-Probe, In Situ Model Pile (IMP), Imperial College Pile (ICP), and the Multiple Deployment Model Pile (MDMP). Typical values these instrumented piles measured include axial strain, acceleration, radial strain and pore

pressure. Using these test piles for prediction of driven pile capities is not ideal as all are installed by means of jacking, with the exception of the MDMP. In general, these piles are designed for use in clayey soils, and are not sufficiently robust for peneratation in granular soils, with the exception of the ICP. The ICP was successfully tested in medium dense sands, where it was installed by means of hydraulic jacking. Measurements of radial stress as well as axial stress distributed along the length of the pile were able to provide data supporting the theory of friction fatigue, as well as the relationship of penetration rate to skin friction and formation of shear surfaces caused by pile installation (Bond and Jardine, 1991)

Unlike the previous methods summarized above, the RTP is designed to replicate installation of driven piles while providing reliable data in both granular and clayey soils, without damage to equipment or sensors. The original design of the RTP system included measurement of axial strain, acceleration, pore pressure and radial strain at each module, as well as displacement at the pile head (Thurairajah, 2013). During testing and development of this system, it was found that hard driving conditions would lead to damage in the thin walled section used to measure radial strain. Saturation of the pore pressure transducer was also found to be an issue, so both the pore pressure and radial stress measurements were removed from the system. As described in the following section, this led to a system redesign that focused on axial strain and acceleration measurements.

EQUIPMENT

Design

The RTP system consists of two main sets of instrumentation, above and below ground, as shown in Figure 1. Above ground instrumentation records the bounce chamber pressure (BCP) of

the diesel hammer and vertical displacement of the pile at the head as well as four separate measurements of axial strain and acceleration at the pile head. The BCP and vertical displacement measured using a string potentiometer are continuously recorded, while the strain and acceleration measurements at the head are recorded for each blow. These measurements are recorded through a National Instruments data acquisition system.

The below ground instrumentation consists of instrumented sections, or modules, placed in series through a wired connection. Each module consists of four strain gages, two accelerometers, two thermistors, and a computer module mounted inside a 0.6 m (2 ft) long standard Becker drill pipe. The four strain gages are mounted axially around the center of the pipe and spaced equidistant along the circumference as shown in Figure 2. The strain gages are wired in two pairs, resulting in an average measurement for each pair. Accelerometers are attached to one strain gage in each pair, providing two measurements of motion. The computer system within the module is used to record, package, and transmit data to the above ground DAQ board through the GCM module. It is mounted using an isolation system to protect it from the extreme loads and accelerations of up to 1500 g that occur during pile driving. All sensors conform to or exceed the ASTM standard D4633-10 (ASTM, 2010) and D4945-12 (ASTM, 2012) for dynamic energy measurement for dynamic penetrometers and dynamic testing of deep foundations.

During operation, the sampling frequency and duration of each module are controlled by the user. The modules power the strain gages and accelerometers, measure strain and acceleration analog signals, and conditions the signal with a low pass filter. The signals are digitized at a frequency of 14.4 kHz per channel. For driving measurements, the typical sampling duration is 130 ms, split so that 30 ms is recorded pre-impact, and 100 ms is recorded post-impact. During

static pullback tests, the sampling duration can be decreased to as low as 25 ms, resulting in a much lower sampling frequency.

Due to the time necessary for the computer within the module to package and transmit data, not every blow during driving can be recorded. The time required for each data package to be recorded and transmitted increases with number of modules, cable length, and sampling duration. With two modules, a blow is recorded typically every 5 to 6 seconds (9 to 10 blows). With three modules, this time increases to roughly 7 seconds (11 to 12 blows), and to roughly 9.5 seconds (15 to 16 blows) with four modules.

Additional cable length and number of modules necessitates a decrease in transmission rate for the system to operate reliably. The transmission rate is a manual user input to the system, so the recording frequency does not change continuously with cable length or depth. The length of cable that can be added to the system before the transmission rate must be lowered decreases as more modules are added to the system. Typically, lowering the transmission rate increases the time between data records by 1.5 to 2 seconds (2 to 3 blows).

The modular nature of the RTP system allows it to be placed into a standard Becker drill string using 1.5 or 3 m (5 or 10 ft) drill pipes. The ability to place modules as needed provides flexibility for site investigations, allowing them to be tailored to address specific soil layers using one or more modules.

Operation

The RTP system is designed with the goal of fitting in seamlessly with a standard closed ended Becker test. No modification is required to the standard Becker rig. All instrumentation and cabling is kept inside the standard drill string, with the exception of those cables spanning from

the head of the pile to the DAQ board. Minimal additional steps are needed during operation to ensure that the site investigation will not be delayed.

The RTP system is typically operated with a three person crew, each responsible for one aspect of the system. One crew member is in charge of the physical tasks, such as making and breaking electrical connections and managing cables between the DAQ and instrumentation. Another crew member is in charge of running the DAQ system and communicating with the drill rig operator. The third crew member is able to process data live, and assist with any other tasks necessary.

Installation of the RTP system follows the same procedure as the Becker Penetration test, with some added complexities. During driving for the standard Becker test, the pile is advanced using the diesel hammer until the pile head is approximately 0.75 m (2.5 ft) above ground. The hammer is then removed, and the next pipe section added in a fairly quick process. A standard Becker hoist is used to pick up and position the next section of drill pipe, which is then screwed into place using pipe wrenches. While using the RTP system, however, this process is slowed by the instrumentation and cabling in each pipe section. Each time a new pipe section is added, the head module must be moved from the top of the already installed section to the top of the new pipe, requiring breaking and re-making the cable connection between the head and pipe sections. The head and next section of drill pipe are then lifted in place over the top of the pile, where another cable connection is made before the new pipe is screwed into place. Before driving can commence, the RTP system must be armed in order to collected data from the instrumentation downhole.

The pullback test is conducted by hydraulically lifting the pile at the ground surface and using the downhole instrumentation to measure the force distribution within the pile. Pullback tests

utilize the hydraulic jacks and spider clamps already in place on a standard Becker drill rig. A frame is used to hold two string potentiometers in place, each with a 15 cm (6 in) maximum stroke. The string potentiometers are connected to the pile below the spider clamps using magnets. The pullback tests were conducted with an average displacement rate of 0.25 mm (0.01 in) per second. The pullback speed is manually controlled by a hydraulic valve, so rates varied widely, however conditions suggest fully drained behavior. Through proper planning of module placement along the length of the pile, it is possible to grip the pile just behind the instrumentation on the head module, thus obtaining a direct measurement of the force applied by the hydraulic jack to the pile, with the tip and downhole modules at the desired depth. During pullbacks, the modules downhole will be armed and manually triggered to record the force distribution along the pile length with displacement.

DATA PROCESSING

Binning Process

Data collected during driving is measured either per blow (E_{res}, F_{res}, etc.) or per foot (N_B). In order to combine this data for calculations, measurements taken per blow are binned into per foot increments. The average value for each bin is determined by taking a weighted average in which the desired property is weighted by the residual displacement for that blow. The resulting average value takes into account the percentage of the total foot increment each blow contributes to the final value.

Driving Data

The strain and acceleration measurements at each module are processed using methods developed for use with the Instrumented Becker Penetration Test (iBPT) to calculate force, velocity, displacement, and energy (DeJong et al., 2016). At the tip module, normalized blow counts (N_{B30}) and SPT equivalent N_{60} values (iBPT N_{60}) are calculated in addition to those previous parameters. Example measurements from a single blow recorded at the tip module are shown in Figure 3. The force within the pile is calculated using the measured strain along with the cross-sectional area and Young's modulus of the module section, equal to 95.72 cm^2 and 198 GPa, respectively. For driving records, the force measurement is baselined to the quiet time before the impact wave arrival. This non-zero baseline value is the locked-in residual force (F_{res}) caused by downward shaft friction and elastic rebound of the soil beneath the pile tip.

The acceleration measurements are baselined using the pre-impact quiet time similar to the force measurements. The baselined acceleration measurements are then integrated to produce velocity. During this integration, a residual velocity is often calculated as a result of electronic noise from the accelerometer measurement. The calculated velocity record is then baselined using a half cosine baseline shift for a smooth baseline correction resulting in zero velocity during both pre and post-impact quiet times.

Velocity is then integrated to calculate the displacement record for each blow. As shown in Figure 4, the residual displacement calculated is similar to what is calculated at the pile head, as well as that measured using the string potentiometer at the pile head. Differences between the tip and head displacements are caused by elastic compression within the pile due to locked-in forces.

The energy arriving at each module is calculated by integrating the force multiplied by velocity over the duration of the impact.

$$E\ (\%) = \frac{\int \mathrm{FVdt}}{11.0\ \mathrm{kJ}} \qquad [1]$$

The normalized energy is reported as a percentage of the theoretical ICE 180 hammer energy (11.0 kJ). The energy arriving at each module is also presented as the delivered energy ratio (DER), defined as the ratio of energy at the tip module to the energy at the head for each foot of driving.

Normalized Blow Counts and Equivalent SPT N_{60} Values

Blows per foot are measured by the RTP system using continuously streaming measurement of the bounce chamber pressure (BCP) and string potentiometer. Each blow is indicated by a peak in the BCP, and the blows are broken into per foot increments using the string potentiometer data, resulting in the raw blow count values (N_B).

Historically, two energy values have been examined for the purpose of Becker Penetration testing, the peak energy (E_{max}) and residual energy (E_{res}). In this method, E_{res} is used for blow count normalization as it is more appropriate than E_{max} for normalizing residual displacements. The raw blow counts are normalized to 30% of reference energy, as is the standard of practice for Becker Penetration testing. The energy normalized blow count (N_{B30}) is calculated using the following equation (DeJong et al., 2016).

$$\mathrm{N_{B30}} = \mathrm{N_B}\frac{\mathrm{E_{res}}}{30} \qquad [2]$$

After energy normalization, iBPT N_{60} is found using the following correlation.

$$\mathrm{iBPT\ N_{60}} = 1.8\ \mathrm{N_{B30}} \qquad [3]$$

This linear correlation is robust and does not show bias based on soil type (Ghafghazi et al., 2016).

Equivalent CPT Tip Resistance

Based on current ongoing work by Alex Sturm, Chris Krage, and Kevin Kuei at UC Davis, it is suggested that N_{B30} can be correlated to CPT cone tip resistance through the relationship of plastic work per unit volume needed to advance the penetrometer. By taking the equation for work per unit volume to advance the Becker pile

$$\frac{W_p}{A \times 1ft} = \frac{\frac{E_{res,Tip}(\%)}{100(\%)} \times 11(kJ) \times \frac{N_b}{1ft}}{A(m^2)} = \frac{N_{B30,Tip} \times \frac{30(\%)}{100(\%)} \times 11(kNm)}{0.0222(m^2)}$$

$$\frac{W_p}{A \times 1ft} = 0.149 N_{B30,Tip}\ (MPa) \qquad [4]$$

and combining that with the equation for work per unit volume to advance the CPT probe

$$\frac{W_p}{A \times 1ft} = \int^{1ft} q_c dl = \overline{q_c}(MPa) \times 0.3048(m) \qquad [5]$$

the following correlation based on equal work per unit volume can be developed.

$$\overline{q_c}(MPa) = 0.49 \times N_{B30,Tip} \qquad [6]$$

This correlation serves as the functional form for a useful correlation in predicting CPT q_c values. However, with the complexities involved in the mechanics of pile driving, it is expected that N_{B30} would need to be empirically scaled to correlate with cone penetration resistance. The current (un-finalized) form of the proposed correlation is the following:

$$\overline{q_c}(MPa) = f_S \times f_D \times f_V \times 0.49 \times N_{B30,Tip} \qquad [7]$$

f_S- A size and shape factor to account for differences in tip geometry.

f_D- A dynamic factor to account for the energy lost due to the complexities of the driving mechanism.

f_V- A penetration rate factor to account for the relative drainage condition present during driving.

The shape factor, f_S, was suggested to account for differences between geometry between the Becker's crowd out bit, and the 60° cone tip used in CPT testing. Previous testing using the iBPT and RTP system, however, shows that there is no significant difference in N_{B30} caused by the different tip geometries. Using this logic, it should stand to reason that f_s is equal to 1.0 for the purpose of this correlation.

The dynamic factor, f_D, is intended to resolve the issue of energy loss due to the dynamic nature of pile driving that results in unload-reload loops. By analyzing multiple successive blows, it was shown that a back-bone penetration resistance develops. This penetration resistance agrees with CPT resistance for a value of 0.85.

The penetration rate factor, f_V, accounts for the change in penetration resistance that occurs based on drainage condition from rapid advancement of the probe. The value of f_v is dependent on soil type, as it is largely controlled by the relation between hydraulic conductivity of the soil relative to the rate of loading during an impact and the time between blows (~0.6 seconds) that is available for pore pressure dissipation. Data used to create this correlation suggests that f_V in sand is approximately 2.0. This value is supported by the relationship of N_{60} to q_t (q_c under hydrostatic conditions in sand) based on I_c when used with the iBPT N_{60} values collected. Figure 5 shows data from side by side iBPT and CPT soundings used to create the correlation, and that data is also plotted on the SPT-CPT correlation chart proposed by Robertson (2012).

Soil at the site is mostly sand and gravel and is assumed to behave like sand. For the purpose of this report, f_V equal to 2.0 is used for the entirety of both soundings. Placing the values of each empirical factor into equation [7] yields the following correlation for sand:

$$\overline{q_c}(MPa) = 0.830 \times N_{B30,Tip} \qquad [8]$$

Research is ongoing to improve this correlation.

Temperature Corrections

The process of driving the RTP creates an appreciable amount of heat from shearing of the soil surrounding the pile. The heat created by penetration causes a differential expansion between the steel Becker pipes and the strain gages, mounted on aluminum proving rings. In order to account for this differential thermal expansion, two thermistors are located in each module to module to measure the average temperature. The thermistors are located in the aluminum mounting bracket, directly against the pile wall, as shown in Figure 2. Before testing, baseline force and temperature measurements are obtained with the module disconnected from the drill string. During data processing, a correction factor of 11.94 kN/°F of difference from the baseline value is applied to the force measurements. Application of this correction factor has been verified to correct for uniform temperature changes that occur within the instrumented pipe sections.

During driving, it was found that the axial strain measurements were affected by uneven heating due to a thermal gradient caused by the rapid increase in temperature surrounding the pile. The high gradient caused an uneven heating of the pile, strain gages, and thermistors. The thermistors used provide the temperature of the inside wall of the pile, however this value may not be the same as the temperature of the sensors and throughout the thickness of the pile wall. This difference was found to be significant as this site was very hard driving, with no ground water, which resulted in significant friction induced heating. This process of uneven heating and cooling presented a complex problem that could not be corrected with the measurements obtained, so a simplified correction method was used.

Correction for the effect of the temperature gradient created by driving was done by correcting the baseline force individually for each section of continuous pile driving, or "segment". For each segment, the correction at the beginning of the segment is zero and increases linearly with time until the end of that driving segment. The final correction value for each driving segment is such that the corrected residual force at the end of driving is equal to the residual force at the start of the next driving segment. This start of the next driving segment was chosen as the "anchor point" for force corrections, as it is assumed that the temperature of the pile, axial strain gage, and thermistor have all equilibrated, and it is the true value of force in the pipe. For driving segments followed directly by a pullback test, the anchor point was chosen from a hammer blow that occurred roughly 0.2 m (0.5 ft) into virgin material following the pullback. Previous testing conducted with iBPT at North Haiwee Reservoir showed that full residual force is established after driving only 0.2 m (0.5 ft) into virgin material.

The correction was applied for each module individually throughout the entire sounding. This method, however, could not be used for the final segment of continuous driving, as there was no baseline value to correct to. In the future, it is recommended that the pile be left in place for some period of time to allow for temperature equilibration and collection of a final baseline point (however this was not done for this testing).

Correction of the baseline force also affects the calculated energy of each blow. The energy is corrected by multiplying the force correction calculated above by the total measured displacement for each blow. The corrected energy values were then used to calculate energy dependent data including N_{B30} and iBPT N_{60} values.

This baseline correction is also applied to each module over the duration of every pullback test. This correction assumes the heat generated from the pullback test is negligible. The correction

value and anchor point used is the same as in the driving segment immediately preceding the pullback. However, the time used for each data point is calculated as the time until the beginning of the next drive. This accounts for the pile coming to equilibrium, instead of heating while driving. When this is done, if the pullback were to begin the moment driving finished, the correction value would be the difference between the residual force at the end of driving and the beginning of the next driving segment. The correction value immediately before beginning the next driving segment would be zero, as the residual force would theoretically be the same as measured when driving commences.

The magnitude of the above corrections is illustrated by the following representative example from RTP-15-2 at a depth of 7 m (23 ft). After applying the baseline correction, the change in F_{res} over the 0.3 m (1 ft) interval is a decrease of 34 kN (28%). The resulting change in E_{res} over that interval is 0.76 % of the 11 kJ reference energy (0.084 kJ). This equates to a 4% decrease in E_{res} from the uncorrected value for this interval. The resulting N_{B30} using the baseline corrected energy is also 4% lower (3 blows per foot), as N_{B30} is directly related to E_{res}. The change in F_{res} is more pronounced than the change in E_{res}, because the baseline is only a small portion of the force used in the energy calculation for each blow.

SITE BACKGROUND

The RTP tests discussed in this report consist of two soundings performed in Coalinga, CA. The test site is located within the Los Gatos Creek in Coalinga, shown in Figure 6. Testing was conducted directly adjacent to the existing Los Gatos Creek Overflow bridge located along Highway 33, just north of the town. This site is located within a valley just west of the Diablo Range and north-east of an anticline ridge, in California's central valley. Data from three

geotechnical borings, 00-1, 00-2, and 00-3, performed at this site by Caltrans show that the subsurface conditions consist of silty sand and silt underlain by dense to very dense gravels and cobbles (Figure 7, Caltrans, 2002). The existing bridge is a pre-stressed slab construction supported by six bridge piers located within the Los Gatos Creek. This bridge was constructed in 2003, widening the road to allow for two more lanes of traffic.

Pile Load Tests

In April 2002, two full scale PP 610 X 19 CISS test piles were driven within the Los Gatos Creek, as shown in the site map in Figure 8. Pile driving data was collected during installation to estimate pile capacities and monitor for signs of pile damage. The test pile driven at Bent 6 was halted at a tip elevation of 184.0 m (603.7 ft corresponding to a depth of 17.7 m (58 ft)) due to tip damage indicated by PDA monitoring. The test pile at Bent 3 was halted at a tip elevation of 187.9 m (616.5 ft corresponding to a depth of 14 m (46 ft)). Both piles met requirements for minimum penetration required for soil plugging, scour potential, and lateral resistance. PDA monitoring also indicated that the compressive resistance well exceeded the required 2,200 kN. A total of eight reaction piles, four for each test pile, were installed using PDA measurements to ensure adequate tensile capacity for the load test (Caltrans, 2002).

Static pile load tests were conducted on the two test piles in May 2002, two weeks after installation. The maximum compression test load measured 4,960 kN with 20.5 mm displacement at Bent 3, and 4,340 kN with 14.6 mm displacement at Bent 6. The maximum compressive capacity was not measured for either pile due to yielding in anchor piles. The maximum tensile test load measured 1,540 kN at 28.3 mm upward displacement for Bent 3, and 1,630 kN at 24.9 mm upward

displacement for Bent 6. The load-displacement curves for both tension and compression are shown in Figures 9 and 10 (Caltrans, 2002).

Interpretation of the pile load test produces pile capacities that depend on the failure criteria used for prediction from the load displacement curves. Pile capacity defined by the 1.3 cm (0.5 in) failure criteria commonly used by Caltrans can be determined. The limiting total pile capacity was predicted using the Chin criteria (1970), in which a load-displacement curve is created using an initial stiffness and ultimate capacity. These two parameters are adjusted to make the curve fit with the measured curve from the static pile load test. The Davisson failure criteria (1972) requires a larger displacement than was achieved during the pile load test. Predicted load-displacement curves from the Chin method were used to estimate the capacity corresponding to the Davisson failure criteria, as shown in Figures 11 and 12 and in Table 2.

The total capacity for each pile consists of a shaft and base capacity component. By using the tension test performed, the load supported by the shaft at a given value of displacement could be estimated. The displacement value chosen corresponds to the displacement for each method used in for the total capacity analysis. The tensile shaft capacity from the load test was assumed to be 75% of the compressive shaft capacity (Randolph, 2003). The base capacity component was estimated by subtracting the calculated compression shaft capacity from the total capacity for a given displacement. The base, shaft, and total capacities from the pile load tests are presented in Table 3.

FIELD TESTING

The two RTP soundings discussed herein, RTP-15-2 and RTP-15-3A, extended to depths of 17.7 m (58 ft corresponding to a depth of 183.7 m (602.5 ft)) and 15.5 m (51 ft corresponding

to a depth of 185.8 m (609.5 ft)), respectively. A total of 12 pullback tests were performed, six during each sounding. Four instrumented modules and a separate head module were used in both soundings. However, due to a mechanical failure at 14.6 m (48 ft), the second sounding, RTP-15-3A, was completed with only three modules. For both soundings, the modules were configured into two module pairs separated by 4.6 m (15 ft) of drill pipe. Each 1.8 m (6 ft) module pair consisted of two module sections separated by a 0.6 m (2 ft) spacer pipe in an attempt to better capture shaft friction effects between the modules during driving and pullbacks. The depth at which pullbacks were performed was chosen with the hope of being able to capture possible degradation in shaft friction due to continuous driving by performing pullbacks with the trailing pair located at the same depth as the lead pair in a previous pullback. Figures 13 and 14 show a schematic of the pile and module configuration, along with module depth during each pullback.

The two RTP soundings were located within the Los Gatos Creek, on the east side of the bridge as shown in the site map (Figure 15). The soundings were performed as close to the test piles as possible; however, final location was dictated by limited access caused by the bridge deck, overhead powerlines, and rough terrain within the creek bed (Figure 16). The first sounding, RTP-15-2, was performed 5.0 m (16.5 ft) from the test pile for Bent 6 of the bridge deck. The second sounding, RTP-15-3A, was performed 11.9 m (39 ft) from the test pile used for Bent 3.

RESULTS

Tip Data

Unlike most previous instrumented pile tests, the RTP has the ability to collect pile driving measurements at the tip of the pile during installation. Energy measurements at the tip are used for generating energy normalized blow counts, N_{B30}, as presented in Figures 17 and 18. From the

profiles it is evident that a dense layer around a depth of 9.1 m (30 ft) exists, underlain by a loose layer at 12.2 m (40 ft). By comparing the profile of N_B to N_{B30} in the soft layer for both soundings, a substantial decrease in the energy normalized blow counts compared to the raw blow counts is evident. The dense layer causes a drop in the DER in the soft layer, even when head energy increases as in RTP-15-2, shown in Figures 19 and 20. Without instrumentation at the tip, this drop in energy being delivered to the pile tip would go unnoticed, leading to an elevated blow count measurement, and an unconservative over prediction of the soil penetration resistance.

A comparison of the iBPT N_{60} values to the SPT N_{60} values provided at this site, shown in Figure 21, can be used to see bias in the testing methods. The original boring logs provide raw SPT blow counts, which were corrected using a measured hammer energy efficiency of 80%. The open symbols in Figure 21 were SPTs considered to reach refusal at 100 blows, and terminated without recording final penetration distance. The SPT blow counts are expected to be elevated due to the influence of gravel throughout the soil profile, however, the comparison presented in Figure 21, shows that the iBPT N_{60} values tend be elevated from the SPT values, for both borings. The cause of the increased iBPT N_{60} values is likely spatial variation in the soil deposit, as both RTP soundings and both borings were performed within the creek alignment.

As discussed previously, cone tip resistances were predicted using N_{B30} values in each boring. The correlation remains constant throughout the entirety of the profile, so the $\overline{q_c}$ profile follows the same shape as the N_{B30} profile. The predicted $\overline{q_c}$ profiles for both soundings are presented in Figure 22. CPT testing was not possible at the site, therefore a direct comparison of the iBPT based predicted values could not be made.

Pile Shaft Data

Data collected along the pile shaft can provide valuable measurements during pile driving that can be used to help predict pile capacity. In the future, it is hoped that the wave measurements collected can be used to increase the accuracy of CAPWAP analyses. Figure 23 shows data collected at all modules from two example blows, one during soft driving and one during hard driving. The force and acceleration measurements are plotted over a grid of 2L/c, where L is the pile length, and c is the wave speed within the pile, equal to 5030 m/sec. The difference in wave arrival time for each module can be seen as a horizontal shift of the pulses in Figure 23. Figure 23 also shows that the wave arrival time increases along the pile length to the tip module, where the wave arrives at a time approximately equal L/c.

Energy is measured for each recorded blow along the shaft of the pile at each module location. By looking at Figures 24 and 25, it can be seen that energy measurements agree between the module pairs when plotted against pile tip location. This is to be expected, as the energy arriving at each module in the pair is roughly the same. See figures 13 and 14 for module configuration along pile. When plotting the energy measurements against module depth, however, the energy arriving at a given depth, along with the DER, generally increases as the pile advances, as shown in Figures 26 and 27. The cause of this energy increase is likely friction fatigue along the pile shaft as the pile is driven, resulting in less energy transferred from the pile to the surrounding soil per blow.

Residual force within the pile develops during driving according to the relationship between the magnitude and distribution of shaft friction and resistance at the pile tip. Near the surface, the residual force in each module is controlled by the skin friction mobilized along the pile above that specific module. Low skin friction allows the pile to rebound after each blow,

resulting in little residual force. This behavior can be seen in the near identical trend in residual force for all modules plotted as a function of module depth (Figures 28 and 29), until a dense layer is reached at roughly 6.1 to 7.6 m (20 to 25 ft) below the ground surface. Figure 30 shows that during hard driving at 7.9 m (26 ft) depth there is a large elastic rebound and small residual displacement, because the low shaft friction above the module allows the soil below the tip and the pile to relax, resulting in little residual force. Immediately below a dense layer, the residual force is limited primarily by the tip capacity because the shaft capacity in the dense layer is greater than the tip capacity. The residual force plotted as a function of tip depth in Figures 28 and 29 shows that the residual force in the first two modules below the dense layer at roughly 9.1 to 10.7 m (30 to 35 ft) trace with tip depth, rather than module location.

Pullback Data

Results of all pullback tests for both soundings is shown in Figures 31 and 32. The force measured at each module represents the total force in the pile at the module location. In the results from pullback tests four and five in RTP-15-3A, and test four in RTP-15-2, measurements indicate that the total tensile force at module three is greater than at module four. This is not physically possible as the pile is being lifted from the top, and resisted by friction along the shaft. Force within the shaft should decrease in magnitude along the length of the shaft, to nearly zero at the tip. These errors are likely caused by the temperature correction described previously not properly accounting for the heating and cooling occurring immediately following driving and during pullback tests. Further development of a temperature correction method is suggested. It is also suggested that modules be spaced further apart in future testing to lessen the effects of measurement errors caused by temperature gradients.

The distribution of total tensile force within the pile at 12.7 mm (0.5 in) displacement for each pullback is presented in Figures 33 and 34. In Figure 33, the measurements for modules three and four were removed when large negative forces were present, and an inferred linear trend between module two and the head was introduced. The slope of the line connecting each point along the curve indicates the average shaft resistance acting along that pile segment. As expected, the slope of the line segments tends to be shallower when passing through the dense layer at around 30 ft depth in each pull back. A more direct prediction of average skin friction can be produced by taking the difference in total force between modules, and dividing by the length between the two modules. Figures 35 and 36 show predicted average skin friction following this method.

The predicted average skin friction profile for RTP-15-2, presented in Figure 35, shows a decrease in shaft friction as the pile is driven further. At each depth with multiple measurements of shaft friction, the highest measurement of friction is from the measurement furthest toward the tip of the pile. This is expected as shaft friction tends to degrade with continuous advancement of the pile. Exceptions to this trend occur at roughly 3 and 16.8 m (10 and 55 ft) depth, where the average shaft friction between modules one and two are less than other module pairs. The cause of this drop in average shaft friction is likely due to localized areas of low shaft friction over the depth interval between modules one and two. These localizations are made less apparent in other module pairs because the average is taken over larger depth intervals.

ANALYSIS

Pile Capacity Calculation

Using iBPT N_{60} collected with RTP, SPT N_{60} from previous borings, and iBPT equivalent cone tip resistance, $\overline{q_c}$, pile capacity calculations were performed for each of the two piles used in

the pile load tests at this site. Pile capacities were predicted using N_{60} values following the method provided by Meyerhoff (1976) as suggested in Canadian Foundation Engineering Manual (2006). Capacity using $\overline{q_c}$ was calculated using the method presented in the Canadian Foundation Engineering Manual (2006) and Fugro-05 (Lehane et al., 2005). The resulting pile capacities are given in Table 4.

In general, there is not a good match between the pile design methods used and the pile capacity values inferred from the pile load test in Table 3. The calculated pile capacities are generally higher than the pile capacities found using the 2.5 cm (0.5 in) failure criteria for both pile load tests. All of the design methods used tend to overestimated shaft capacity, while underestimating the base capacity. The two CPT based methods predict the lowest base capacity for both Bent 3 and 6, and the Fugro-05 method wildly overpredicts the shaft capacity. Overall, the best results are from using the SPT N_{60} values to predict pile capacity based on Davisson's criteria.

RTP Design Method

In order to better predict pile capacity in granular soils containing gravel, a new method of pile design which utilizes RTP measurements directly is proposed. The proposed design method follows the same functional form as that suggested for other direct design methods in the Canadian Foundation Engineering Manual (2006):

$$q_b = K_c \times \overline{N_{B30}} \qquad [9]$$

$$q_s = \frac{1}{\alpha} \times N_{B30} \qquad [10]$$

q_b- Base capacity in kPa.

q_s- Unit shaft friction in kPa.

K_c- Bearing capacity factor based on soil type and pile type

α- Friction coefficient.

N_{B30}- Becker penetration resistance normalized to 30% reference energy.

$\overline{N_{B30}}$- Average N_{B30} in the vicinity of the pile tip (1.5 times the pile diameter above and below the pile tip).

Using the data collected in this study, preliminary estimates of the bearing capacity factor and friction coefficient were made for driven steel piles in granular soil. It is noted that a limiting shaft resistance value to limit the q_s value was not determined.

The friction coefficient, α, was determined by linear regression of the average skin friction distribution obtained during the pullback tests, as presented previously in Figures 35 and 36, to the normalized blow count profile. However, before comparing the values, the measurements obtained from the pullback test were divided by a factor of 0.75 to compute the estimated skin friction in compression instead of tension. Only skin friction measurements from module pairs including module one (i.e. 1 - 2, 1 - 3, and 1 - 4) were used for this analysis in order to reduce the effect of friction fatigue on the measurements used. The average N_{B30} value used for each data point is taken as the average of the normalized blow counts over the depth interval between the top and bottom module for each module pair in a given pullback test. A plot of the assumed linear correlation is shown in Figure 37.

An α value of 1.4 is recommended based on regression using the average shaft friction measurements between modules one and two (Mod 1-2). Regression of all points results in an α value of 1.6, however, it is recommended that an α value of 1.4 be used as Mod 1-2 averages values over the smallest depth interval. Another benefit to using Mod 1-2 is that the midpoint of

the module pair is closest to the pile tip, resulting in shaft friction measurements that are less likely to be affected by friction degradation due to continuous soil shearing resulting from pile advancement. Any friction degradation should be accounted for separately and explicitly in final pile design. Friction degradation is apparent in these test results, as the α value tends to increase as the midpoint of the module pair gets further from the pile tip, reaching 1.6 and 1.9 for Mod 1-3 and Mod 1-4, respectively.

A comparison of predicted q_s using this method and the average skin friction measured during pullbacks is presented in Figures 38 and 39. In Figure 39, it can be seen that this method significantly under predicts the shaft friction measured during the pullback test in the dense zone around 9.1 m (30 ft). As stated previously, the results from the pullback test at this depth are to be viewed with some skepticism as the results are not physically possible. The results from this method, using an α value of 1.4 and not accounting for friction degradation, produced a shaft capacity prediction of 2,000 kN and 2,400 kN for Bent 3 and Bent 6 respectively. When compared to the results from the pile load test in Table 2 for the Davisson failure criteria, this method overestimates shaft capacity by about 15% to 20%.

The bearing capacity factor to be used for steel piles in granular soils containing gravel was found using the results from the full scale pile load test. The Davisson failure criteria value of base capacity from Table 2 was used as the design base capacity of the piles installed. The base capacity value was then divided by the average N_{B30} in the vicinity of the pile tip for each of the two soundings. Results from RTP-15-2 and RTP-15-3A both suggest a K_c value of 900 be used for design.

CONCLUSIONS

Pile capacity calculations performed on data collected at this site have shown that the methods used are prone to overestimating shaft capacity, while underestimating base capacity under these conditions. The difference in calculated and interpreted pile capacity was fairly large for every method. The pile load tests were not performed to sufficient displacements to obtain the ultimate capacity defined by Davisson's failure criteria, so the Chin method (1970) was used to estimate pile capacities corresponding to Davisson's criteria.

A new pile design method using RTP data directly was developed to better predict pile capacity in granular soils containing gravel. This new method follows the same functional form as the method presented in the Canadian Foundation Engineering Manual (2006), where base capacity in kPa is directly related to normalized penetration resistance by an empirical constant, K_c. The unit shaft capacity in kPa is related to the penetration resistance by the inverse of an empirical constant, α. The value of the empirical constants were found to be 900 and 1.6 for K_c and α, respectively.

The RTP system was successful in measuring the impact wave arrival through the pile during driving. Individual blow data shows the progression of the impact as the wave travels down the pile, and arrives at the tip at a time of L/c, the pile length divided by wave speed. These measurements can potentially increase the accuracy of CAPWAP models and other signal matching techniques. More even spacing of modules along the pile shaft will likely be successful in better capturing wave propagation within the pile.

Overall, the RTP system performed well at this site, however, some improvements to the implementation of the RTP are recommended. The module spacing along the pile shaft should be

optimized to allow for a significant amount of skin friction to develop between modules, while minimizing the effect of averaging over large depth intervals. The modules in this test were spaced too closely, resulting in the measurements between some modules being almost indistinguishable during certain pullback tests.

REFERENCES

ASTM D4633-10 (2010). Standard test method for energy measurement for dynamic penetrometers. ASTM International, West Conshohocken, PA, USA.

ASTM D4945-12 (2012). Standard test method for high-strain dynamic testing of deep foundations. ASTM International, West Conshohocken, PA, USA.

Bond, A., Jardine, R., and Dalton, J. "Design and Performance of the Imperial College Instrumented Pile," *Geotechnical Testing Journal*, Vol. 14, No. 4, 1991, pp. 413-424, https://doi.org/10.1520/GTJ10210J. ISSN 0149-6115

Bond, A. J. & Jardine, R. J. (1991). Effects of installing displacement piles in a high OCR clay. Geotechnique 41, No. 3, 341-363

Chin F.K. (1970) Estimation of the ultimate load of piles from tests not carried to failure. *Proceedings of the Second Southeast Asian Conference on Soil Engineering*, pp83-91.

Davisson M.T. (1972) High capacity piles. *Proceedings, Lecture Series, Innovations in Foundation Construction,* ASCE, Illinois Section, pp 52.

DeJong, J.T., Ghafghazi, M., Sturm, A.P., Wilson, D.W., den Dulk, J., Armstrong, R.J., Perez, A., and Davis, C.A. “Instrumented Becker Penetration Test, I: Equipment, Operation, and Performance”, *ASCE J. Geotechnical and Geoenvironmental Engineering*, 2017, https://doi.org/10.1061/(ASCE)GT.1943-5606.0001717

Geotechnical Design of Deep Foundations. *Canadian Foundation Engineering Manual.*4th ed. Montreal: Canadian Geotechnical Society, 2006 pp. 262-302.

Ghafghazi M, DeJong JT, Sturm AP, Temple CE. "Instrumented Becker Penetration Test, II: iBPT- SPT correlation for liquefaction assessment in gravelly soils", *ASCE J. Geotechnical and Geoenvironmental Engineering*, 2017, https://doi.org/10.1061/(ASCE)GT.1943-5606.0001718

Meyerhof, G.G. (1976). Bearing Capacity and Settlement of Pile Foundations. *Journal of the Soil Mechanics and Foundations Division*, ASCE, Division, Vol. 85, SM6, pp. 1-29.

Randolph, M. F. (2003). Science and Empiricism in Pile Foundation Design. *Geotechnique* 53.10: 847-875

Robertson, P.K. (2012) The James K. Mitchell Lecture: Interpretation of in-situ tests – some insights. *Geotechnical and Geophysical Site Characterization 4*. Vol. 1,Taylor and Francis, London: 25-42.

Thurairajah, A. (2013) Reusable Instrumented Test Pile for Improved Pile Design in Granular Soils, Doctoral Thesis, University of California Davis.

Table 1. Summary of some instrumented test piles developed in the past (Thurairajah, 2013).

	Cone Penetrator	**PLS**	**G&R Test Pile**	**NGI Test Pile**	**3" Model Pile**	**X – Probe**	**IMP**	**Imperial College Pile**	**MDMP**
Diameter (mm)	35.7	38.4	25.4	153	76.2	43.7	80	102	76.2
Length (cm)	Varies	26.8 + Tip extension	88.9	500.4	1850	143.5	113.5	700	287
Friction Sleeve (cm^2)	150	Area of tip extension (about 2000)	200	NA	1850	200	Variable	Variable	2000 between load cells
Tip type	60^0 Solid cone	60^0 Solid cone	Solid Aluminum plug	Closed ended	Open or closed ended	60^0 Solid cone	Open or closed ended	60^0 Solid cone	60^0 Solid cone or flat nose or open ended

	Cone Penetrator	PLS	G&R Test Pile	NGI Test Pile	3" Model Pile	X – Probe	IMP	Imperial College Pile	MDMP
Load cell locations (Type)	One on tip, one on sleeve	One on top (Strain gauged load cell)	None	One on Top (Vibrating wire strain gauge	Two on sleeve	One on sleeve	Two on sleeve of leading cluster , one on sleeve of following cluster	Three behind tip on sleeve, each on a cluster 1m apart, one at top (High capacity axial load cells)	One behind tip and two on sleeve (Top & middle electric load cell; bottom strain gauge load cell)
Pore pressure transducer location (Type)	At tip, behind tip, above friction sleeve (Piezo cone).	In between PLS cell and tip extension	One at the middle of friction sleeve	Four along the sleeve	One in middle of sleeve (Kistler 4043A)	One on sleeve (Kistler 4043A)	Four on sleeve - Two on each cluster (Druck PDCR-81	One behind tip on sleeve, two on a cluster 1m apart (Druck PDCR-81)	One in the middle of sleeve - Transducer housing (Kistler 4140A20)
Lateral Pressure Transducer Location (Type)	None	Top of tip extension (Piezo Lateral Stress cell)	None	Four along sleeve (Vibrating Wire)	One - Middle of sleeve (Sensotec Model 13)	One - on sleeve (Sensotec Model 14)	Four on sleeve - Two on each cluster	Three behind tip on sleeve, each a cluster 1m apart (Cambridge earth pressure cell)	One, middle of the sleeve - Transducer housing (Electric Strain Gauges)

	Cone Penetrator	PLS	G&R Test Pile	NGI Test Pile	3" Model Pile	X – Probe	IMP	Imperial College Pile	MDMP
Displacement Transducer	None	None	None	One at Top	Slip Joint – DC LVDT between cutting shoe and instrumented portion, Cutting shoe act as anchor during loading	Slip Joint – DC LVDT between cutting shoe and instrumented portion, Cutting shoe act as anchor during loading	None	Three at top	One - behind tip
Accelerometer	None	None	None	None	Four (2 on each load cell)	None	None	None	Four, one at top of rod, one at each load cell
Temperature Sensor	Special cone	One in PLS cell	None	None	None	None	None	Three behind tip on sleeve, each on every surface stress transducer	None

	Cone Penetrator	PLS	G&R Test Pile	NGI Test Pile	3” Model Pile	X – Probe	IMP	Imperial College Pile	MDMP
Slop Sensor	Omni-directional inclinometer – Special cone	None	None	None	None	None	None	None	None
Driving Mechanism	Jacking (20mm/s)	Jacking (20mm/s)	Reversible, variable speed screw jack	Jacking (4 - 15 cm/min)	Driving / Pushing	Pushing	Jacking	Jacking (fast 400-600 mm/min: slow 50-100 mm/min)	Driving with SPT hammer/ Pushing
Pile Type	Probe	Probe	6061 Aluminum tube	Steel Pipe	Steel Pipe	Probe	Steel Pipe	Steel Pipe	Steel Pipe with 3/8” wall thickness

Table 2. Pile Capacity results from interpretation of pile load tests.

	Bent 3		Bent 6	
	Load (kN)	Displacement (mm)	Load (kN)	Displacement (mm)
Compression				
Maximum test load	4,960	21	4,340	15
Measured Capacity at 0.5"	3,700	13	3,850	13
Chin (1970) Maximum Capacity	8,000	Not Achieved	8,300	Not Achieved
Davisson's Criteria (1972)	4,848	19	5,260	23
Tension				
Maximum test load	1,545	28	1,630	25
Measured Capacity at 0.5"	1,070	13	1,470	13
Load Corresponding to Chin Capacity	1,545	28	1,630	25
Load Corresponding to Davisson's	1,230	19	1,580	23

Table 3. Pile capacity values separated into shaft and base capacities.

	Bent 3			Bent 6		
	Q_t (kN)	Q_s (kN)	Q_b (kN)	Q_t (kN)	Q_s (kN)	Q_b (kN)
0.5" Failure Criteria	3,700	1,427	2,273	3,850	1,960	1,890
Chin (1970)	8,000	2,060*	5,940*	8,300	2,173	6,127
Davisson's Criteria	4,848	1,640	3,208	5,260	2,107	3,153

*Displacement level not reached during testing. Maximum value used.

Table 4. Calculated pile capacities using RTP data.

	Bent 3			Bent 6		
	Q_t (kN)	Q_s (kN)	Q_b (kN)	Q_t (kN)	Q_s (kN)	Q_b (kN)
iBPT N60	11,080	8,600	2,490	9,750	7,120	2,635
SPT N60	5,110	3,760	1,350	4,920	3,650	1,269
CPT - CFEM	3,660	2,700	960	4,440	3,630	810
CPT - Fugro-05	5,890	5,420	470	12,450	12,015	430

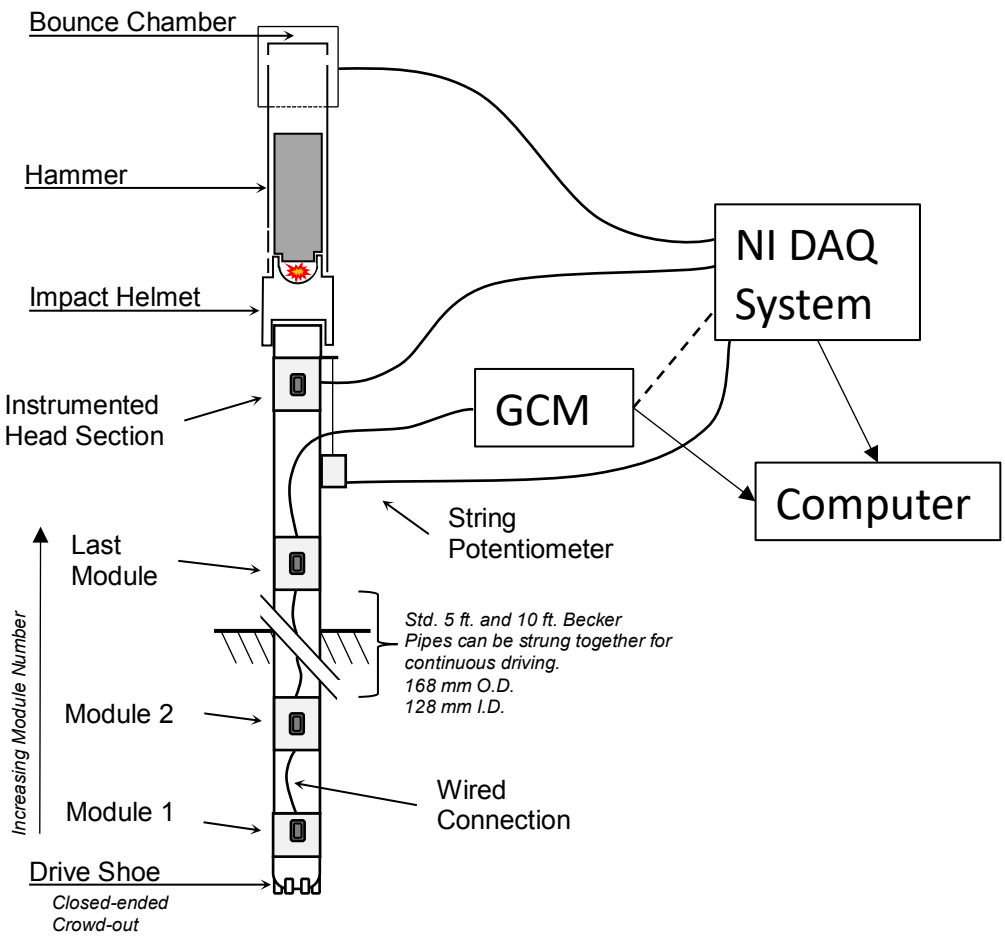

Fig. 1. RTP system schematic. All measurements above ground (BCP, displacement, and head measurements) are collected by the NI DAQ system directly, then passed to the computer. Measurements form below ground modules are received by the GCM unit before entering the computer.

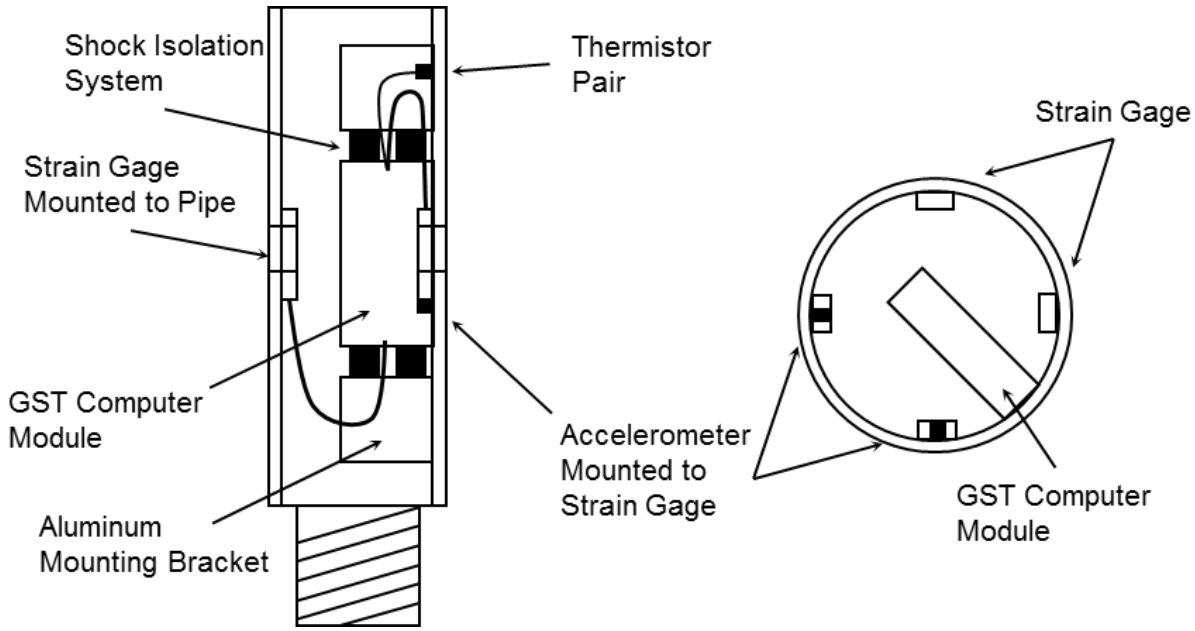

Fig. 2. Schematic of RTP downhole module. Strain gages and aluminum mounting brackets are connected directly to the 0.61 m (2 ft) long Becker pipe with two bolts each. Accelerometers are attached to two of the four strain gages. The GST computer is protected from the harsh vibrations of pile driving through the shock isolating system.

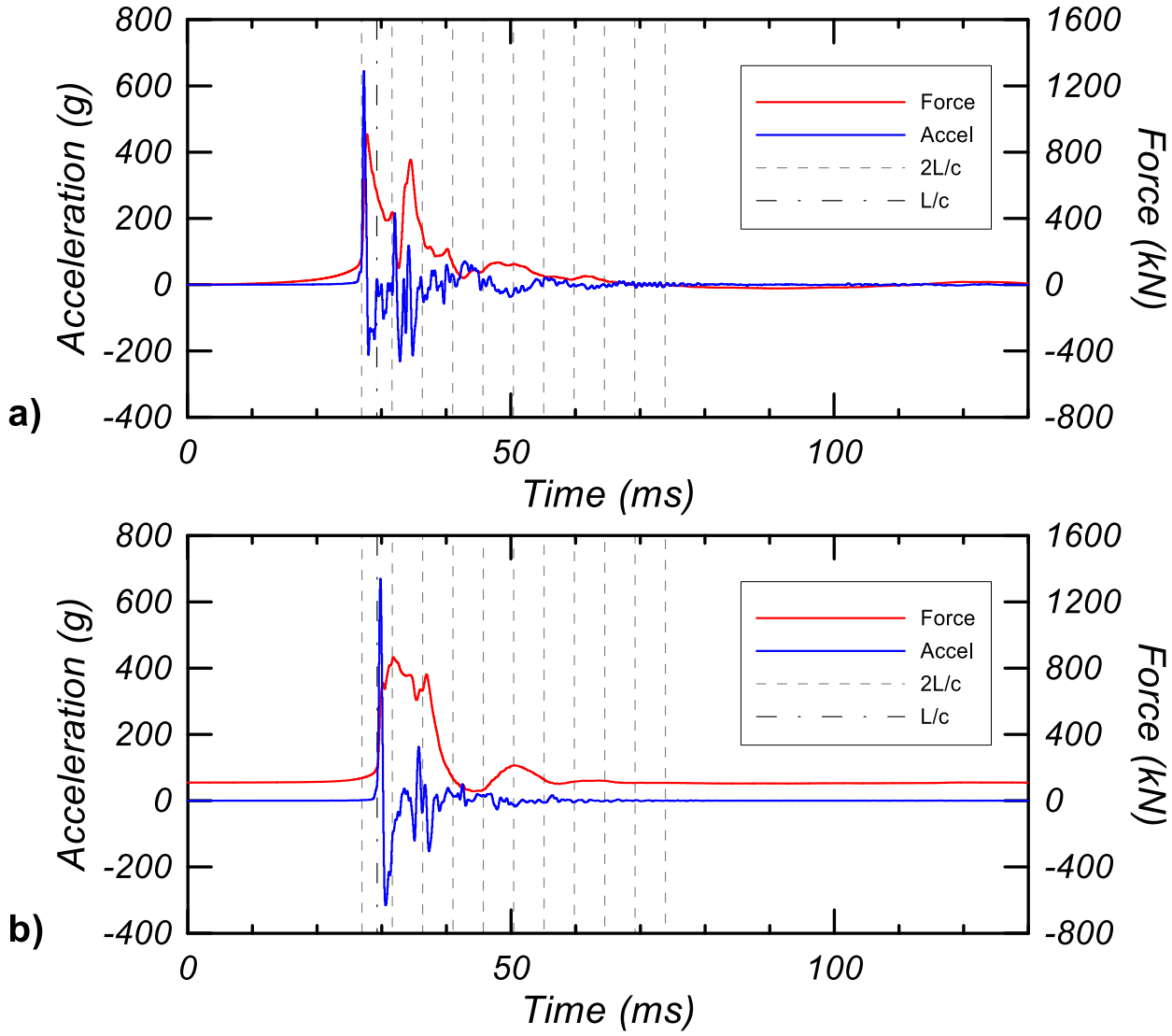

Fig. 3. Example force and acceleration measurements collected at the a) head and b) tip module, displayed over a grid of 2L/c.

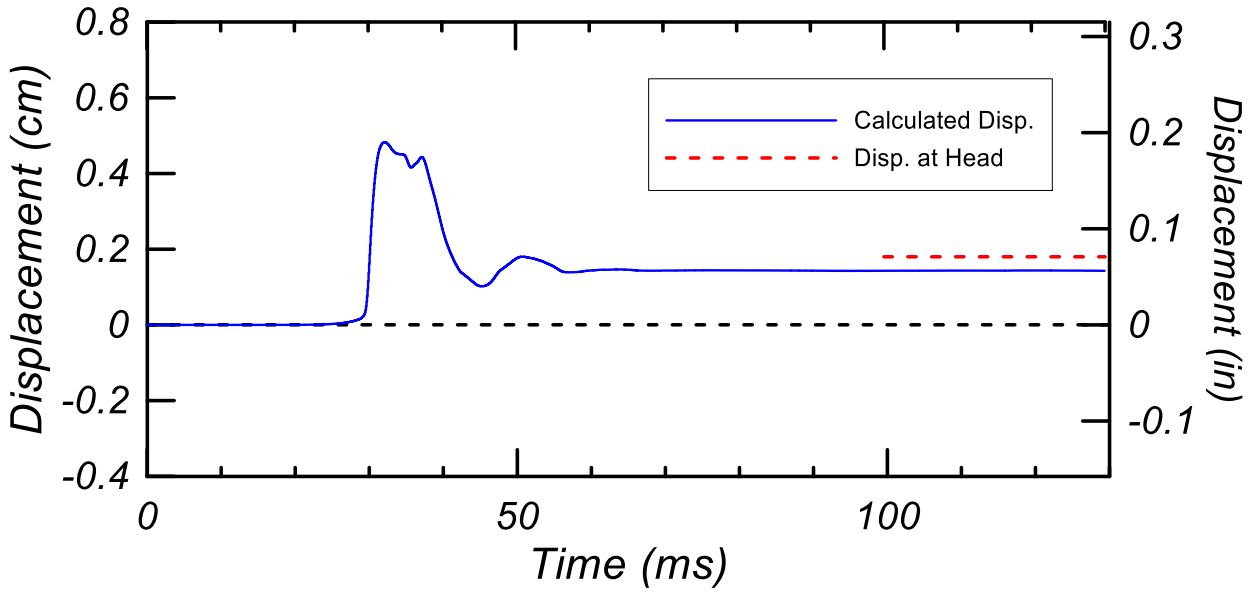

Fig. 4. Example displacement record created from integration of acceleration measurements. Measured displacement at the head is also displayed to show agreement between these two measurements.

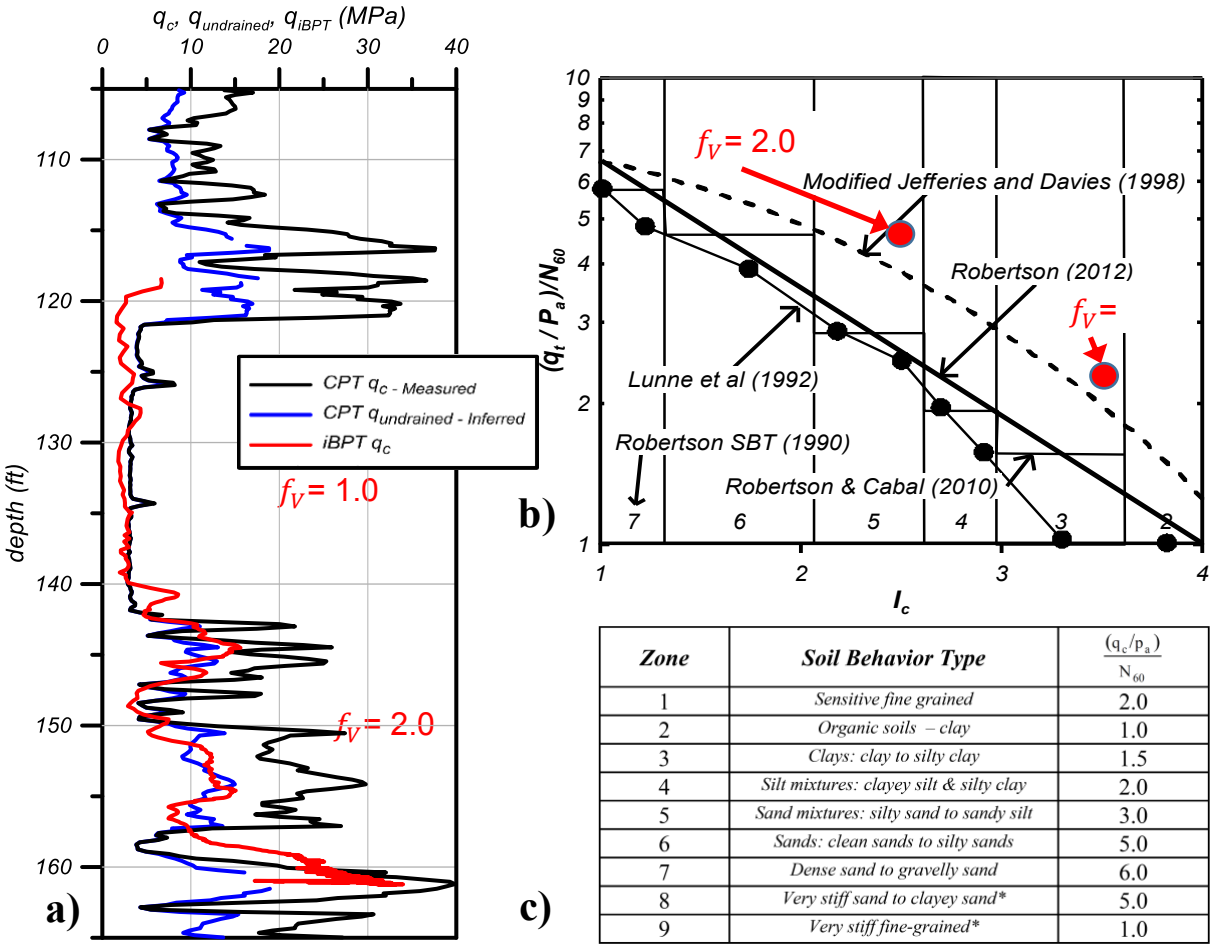

Zone	Soil Behavior Type	$\frac{(q_c/p_a)}{N_{60}}$
1	*Sensitive fine grained*	2.0
2	*Organic soils – clay*	1.0
3	*Clays: clay to silty clay*	1.5
4	*Silt mixtures: clayey silt & silty clay*	2.0
5	*Sand mixtures: silty sand to sandy silt*	3.0
6	*Sands: clean sands to silty sands*	5.0
7	*Dense sand to gravelly sand*	6.0
8	*Very stiff sand to clayey sand**	5.0
9	*Very stiff fine-grained**	1.0

Fig. 5. a) Side by side testing of iBPT and CPT in a profile containing both sand and clay, b) Correlation of SPT to CPT (Robertson 2012), and c) a table of the correlation presented in b). Points plotted in red correspond to data used to create the proposed iBPT-CPT correlation, based on iBPT N_{60} values. The point labeled f_v=2.0 corresponds to sand, while the point labeled f_v=1.0 corresponds to clay.

Fig. 6. Aerial photo of Coalinga showing the location of test site.

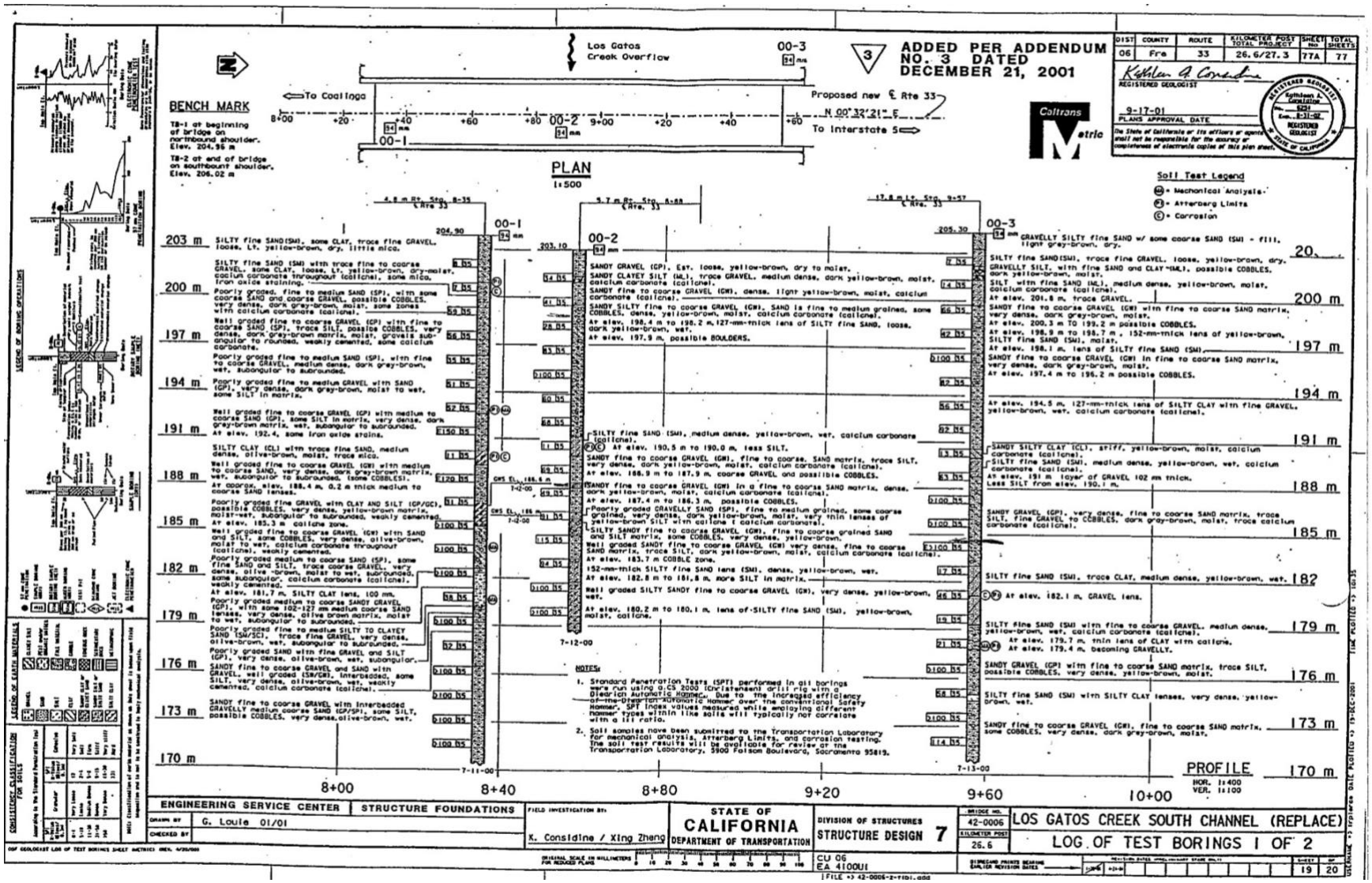

Fig. 7. Boring logs from previous investigation.

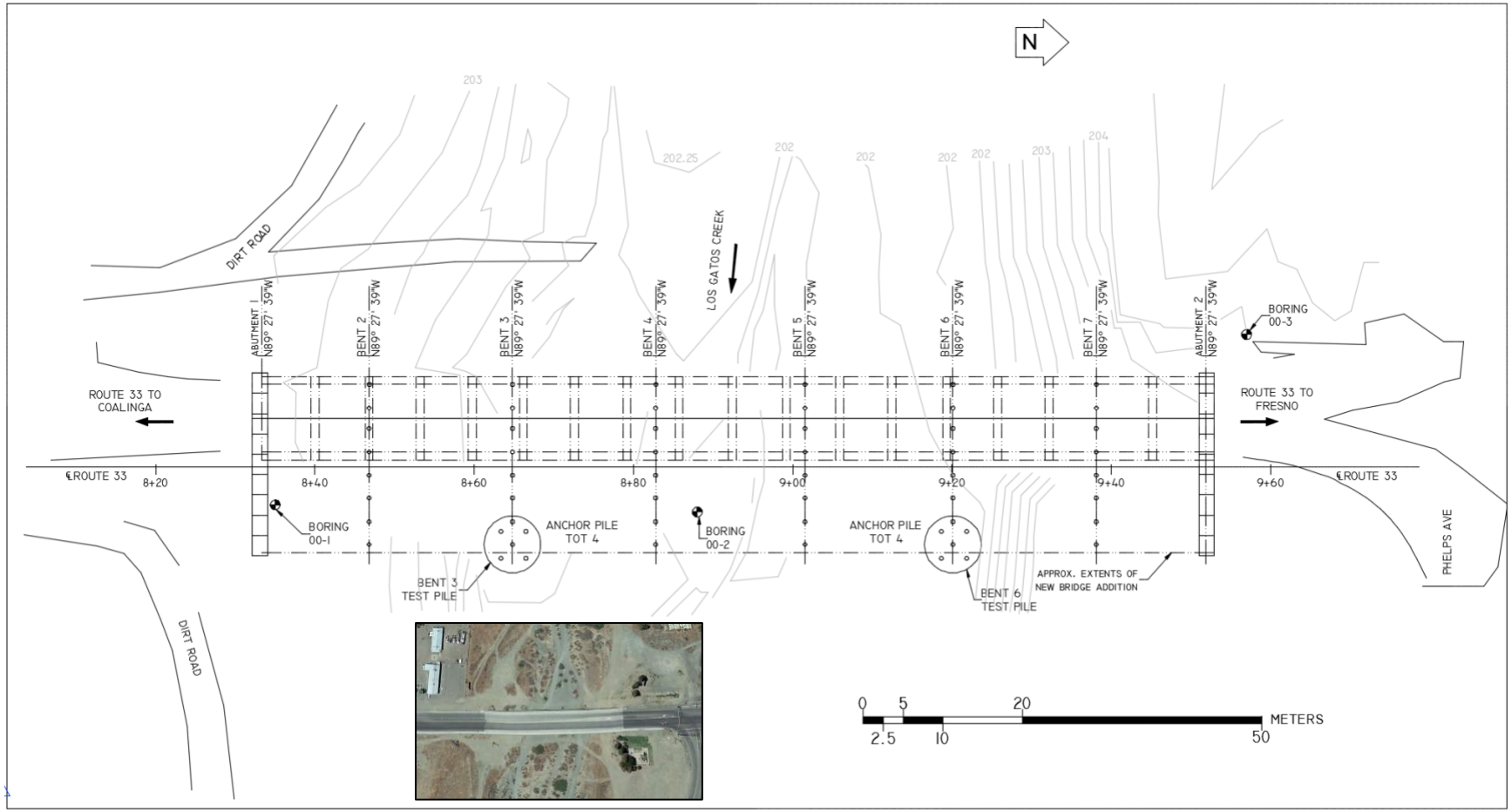

Fig. 8. Site plan showing the location of pile tests located at Bents 3 and 6, as well as historic boring locations.

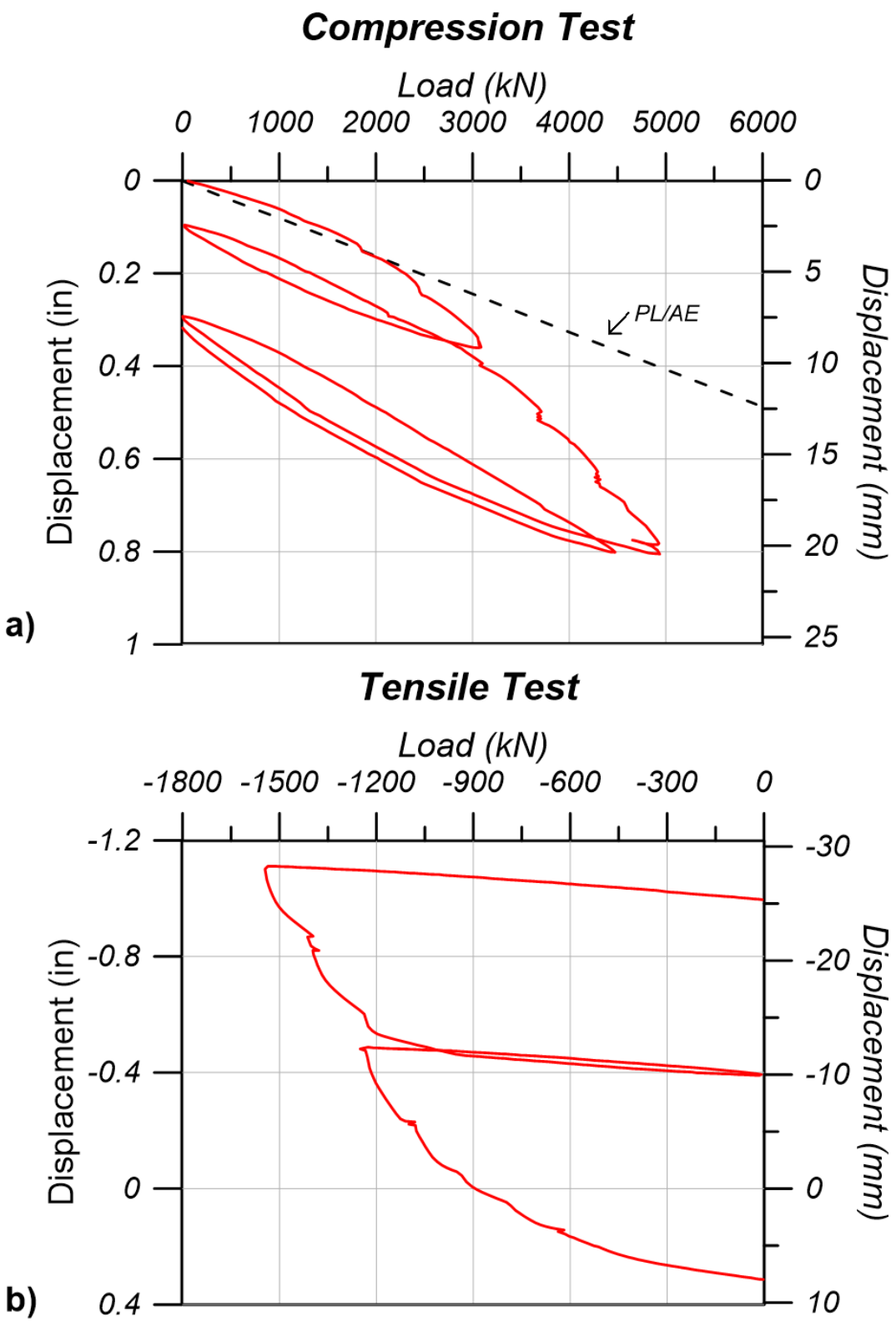

Fig. 9. Bent 3 a) compression and b) tension pile load test results.

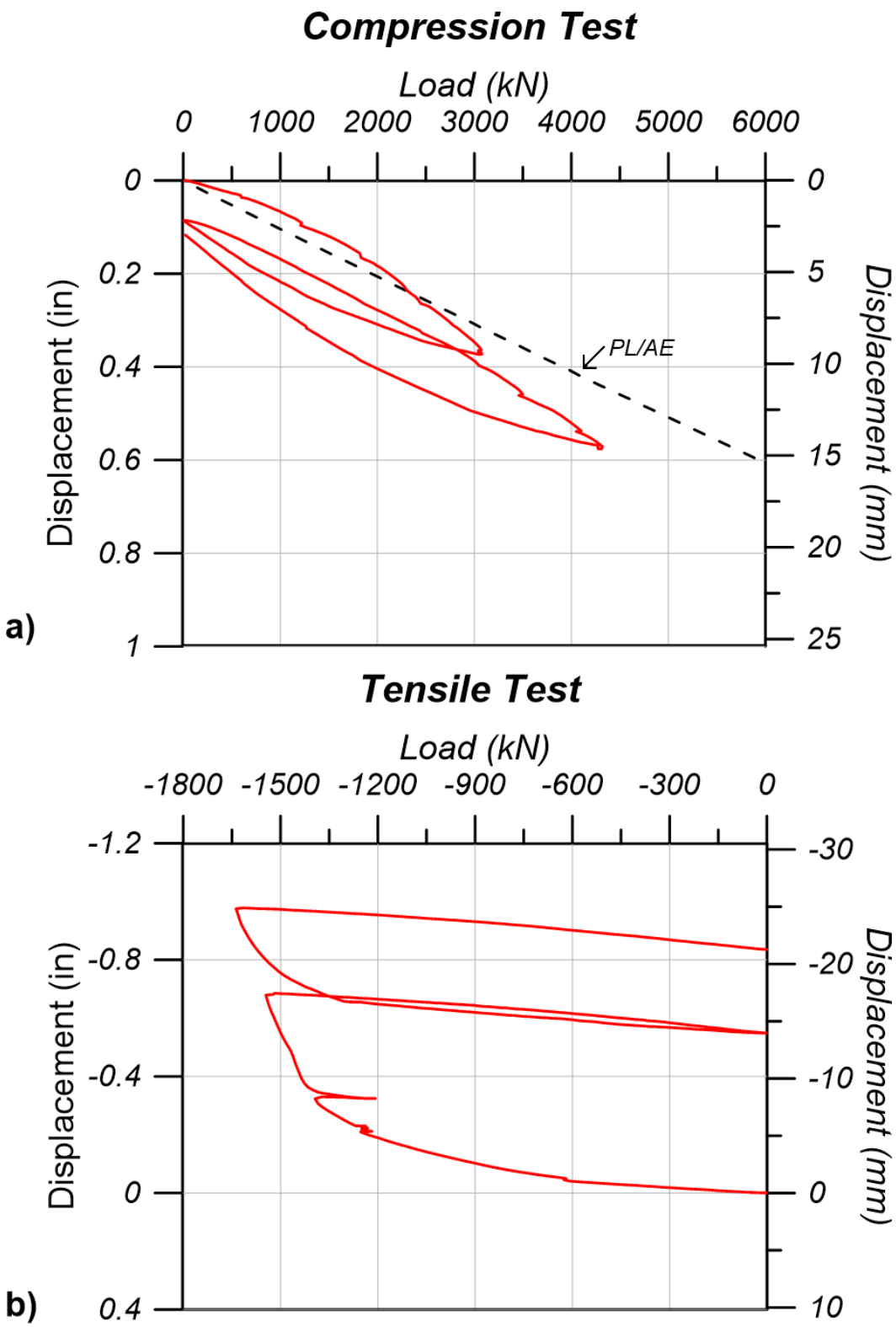

Fig. 10. Bent 6 a) compression and b) tension pile load test results.

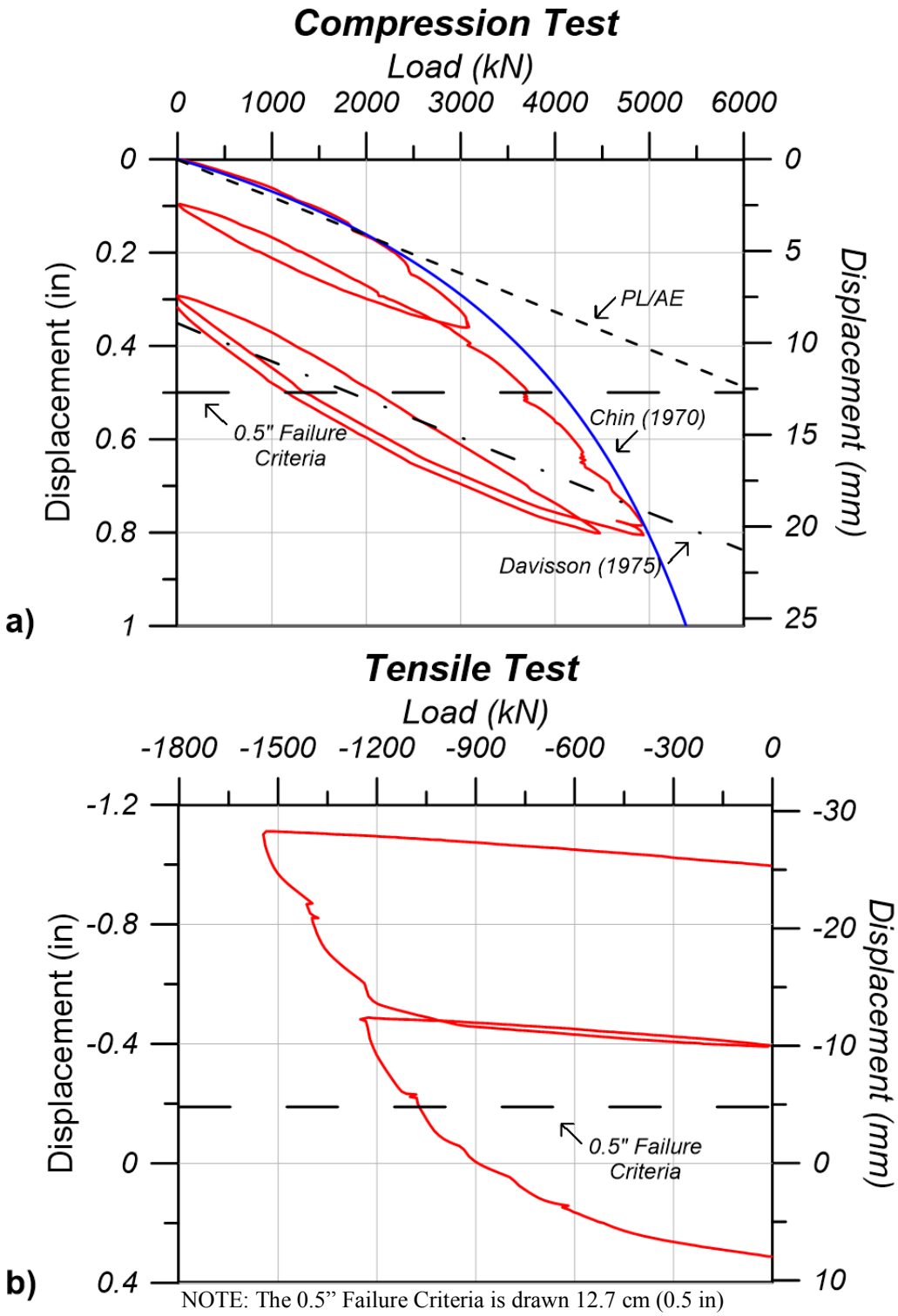

Fig. 11. Bent 3 a) compression load test curve with failure criteria and b) tension load test curve with failure criteria.

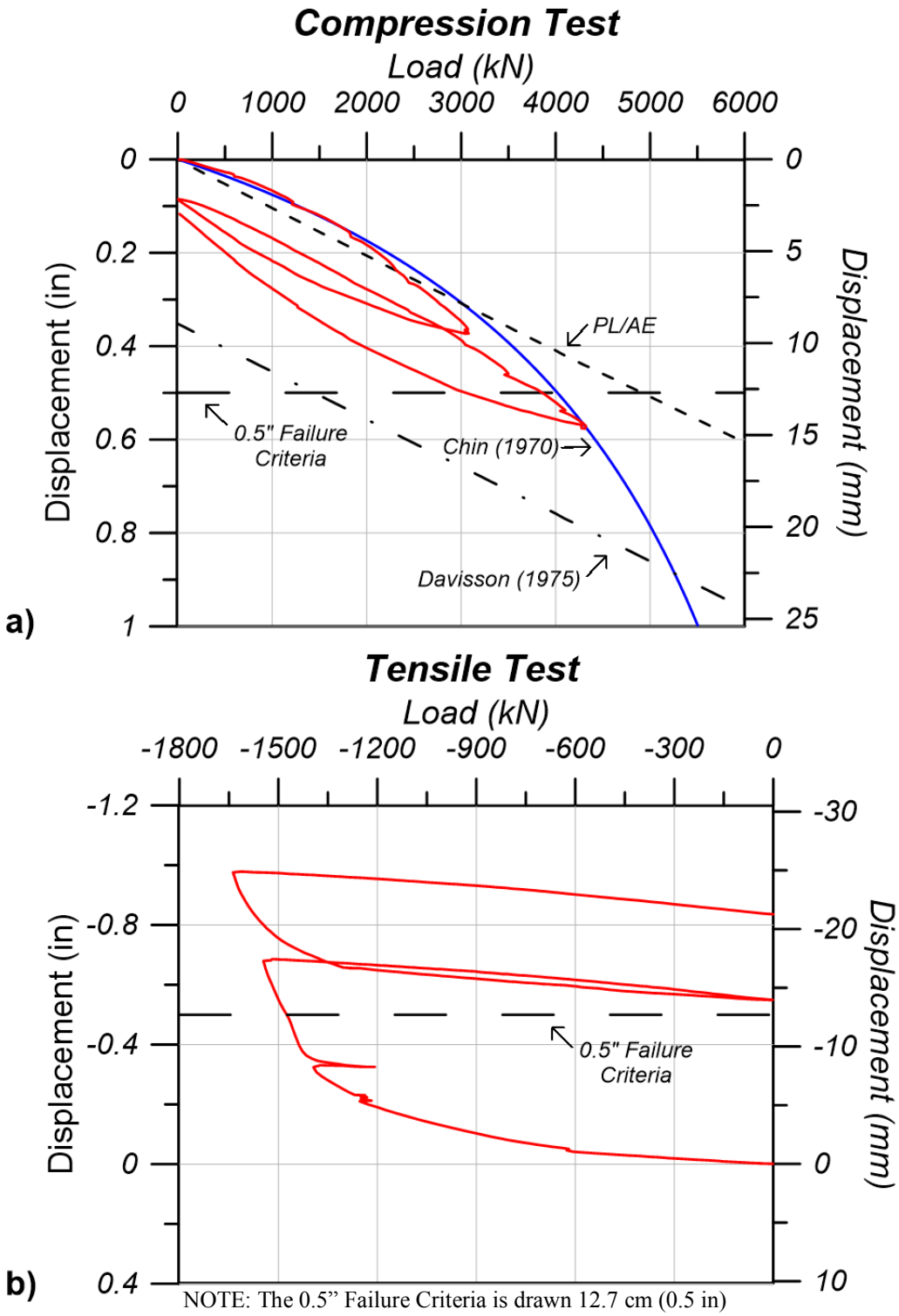

Fig. 12. Bent 6 a) compression load test curve with failure criteria and b) tension load test curve with failure criteria.

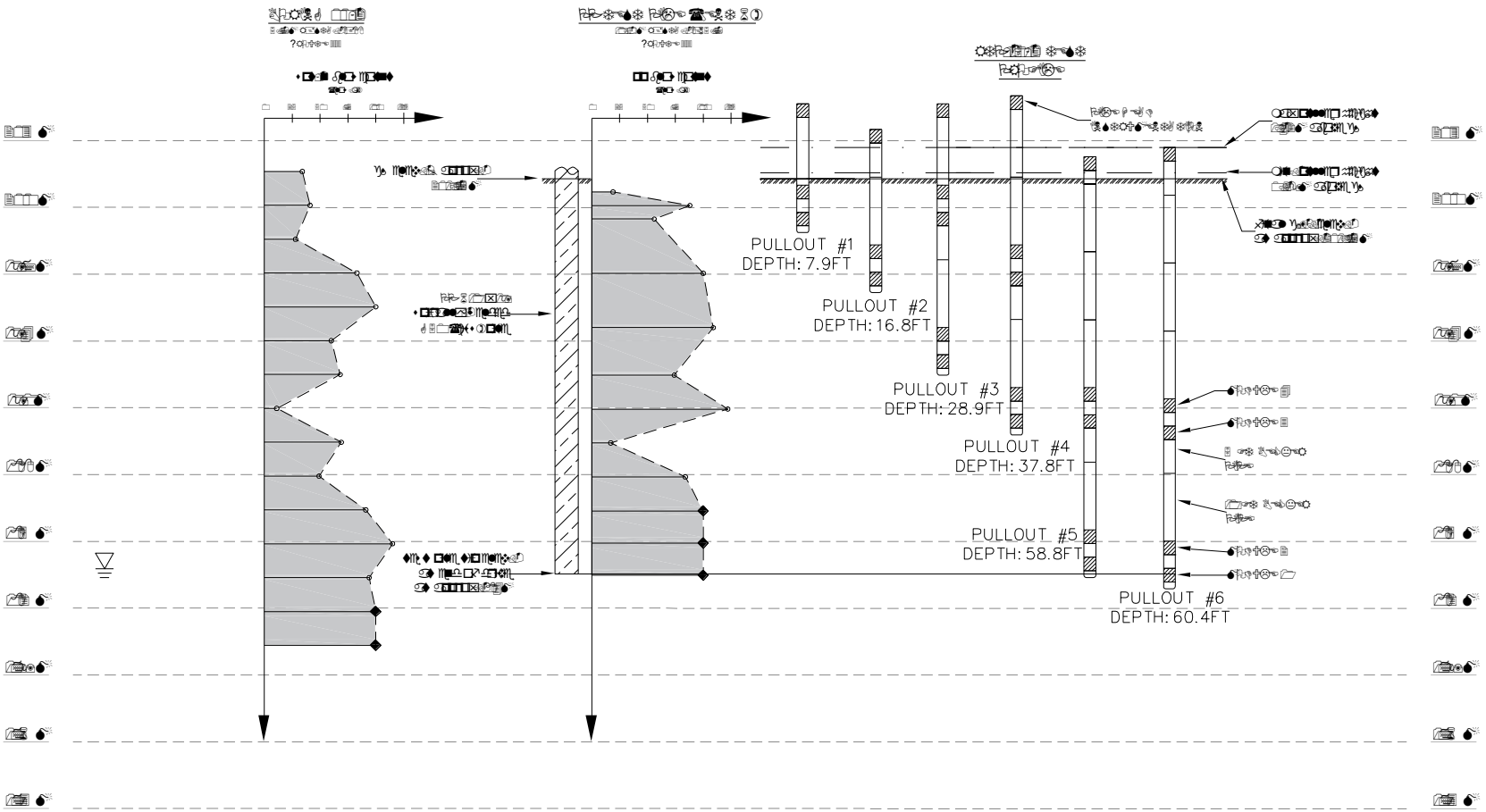

Fig. 13. Pile module configuration and module location during pullback testing in sounding RTP-15-2.

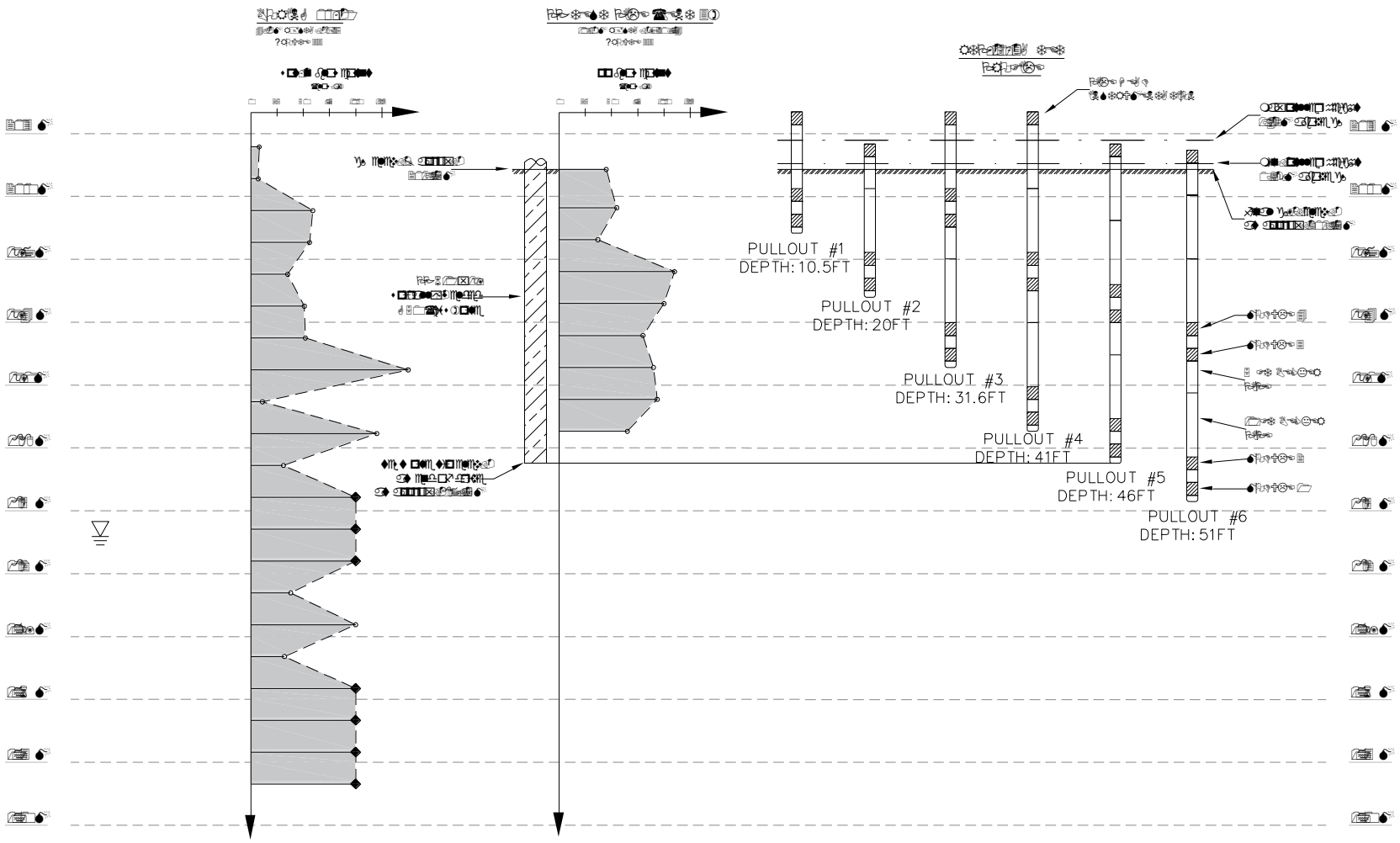

Fig. 14. Pile module configuration and module location during pullback testing in sounding RTP-15-3A.

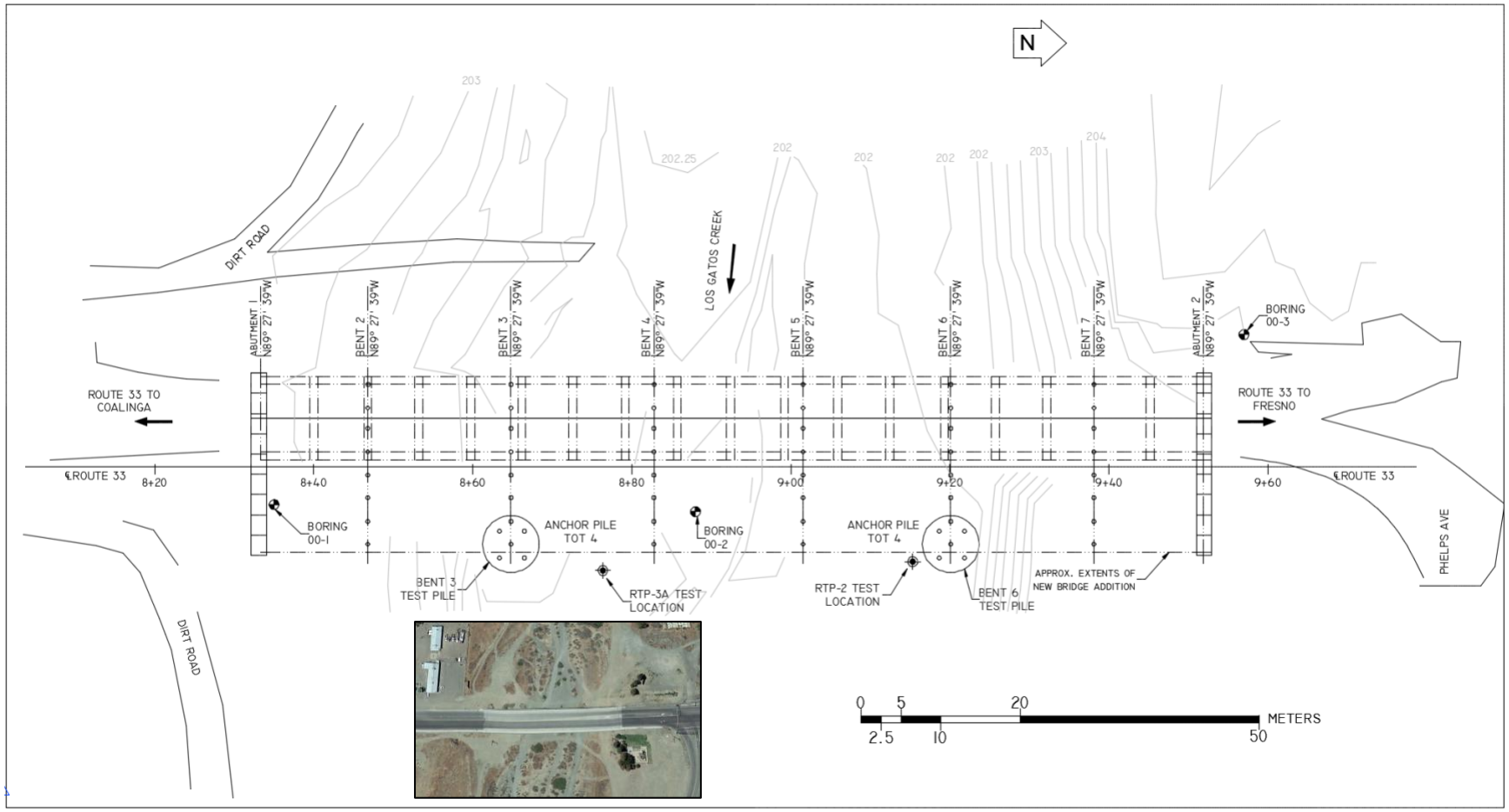

Fig. 15. Site plan showing the location of RTP soundings. Soundings were located as to pile load tests as site access would allow.

Fig. 16. Testing location for RTP-15-3A. Final testing location controlled by overhead powerlines, and uneven ground within the Los Gatos Creek bed.

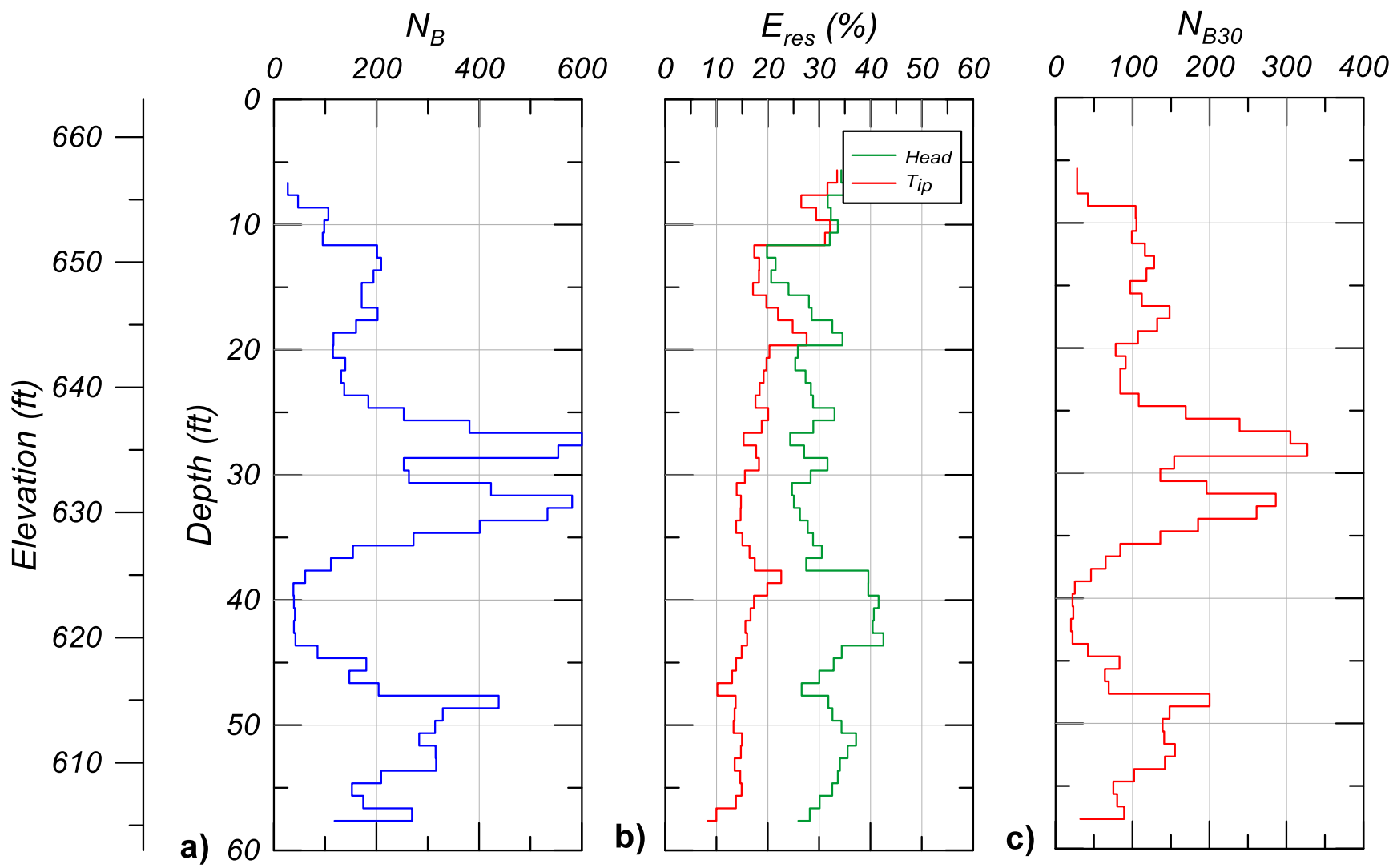

Fig. 17. – Energy normalization of RTP-15-2 showing a) raw blow counts, b) residual energy measured at the head and tip, and c) energy normalized blow counts using residual energy (E_{res}) measured at the tip.

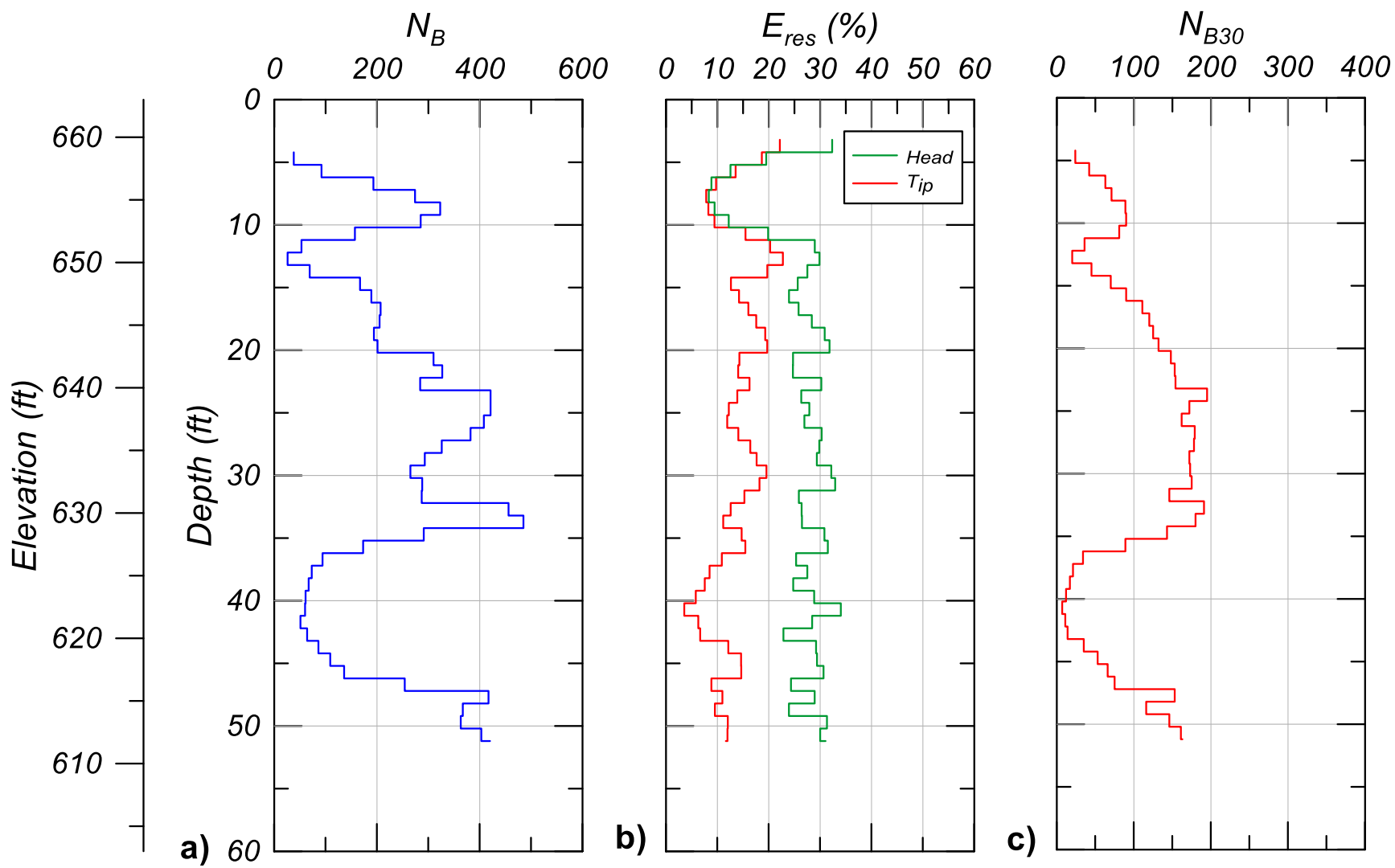

Fig. 18. Energy normalization of RTP-15-3A showing a) raw blow counts, b) residual energy measured at the head and tip, and c) energy normalized blow counts using residual energy (E_{res}) measured at the tip.

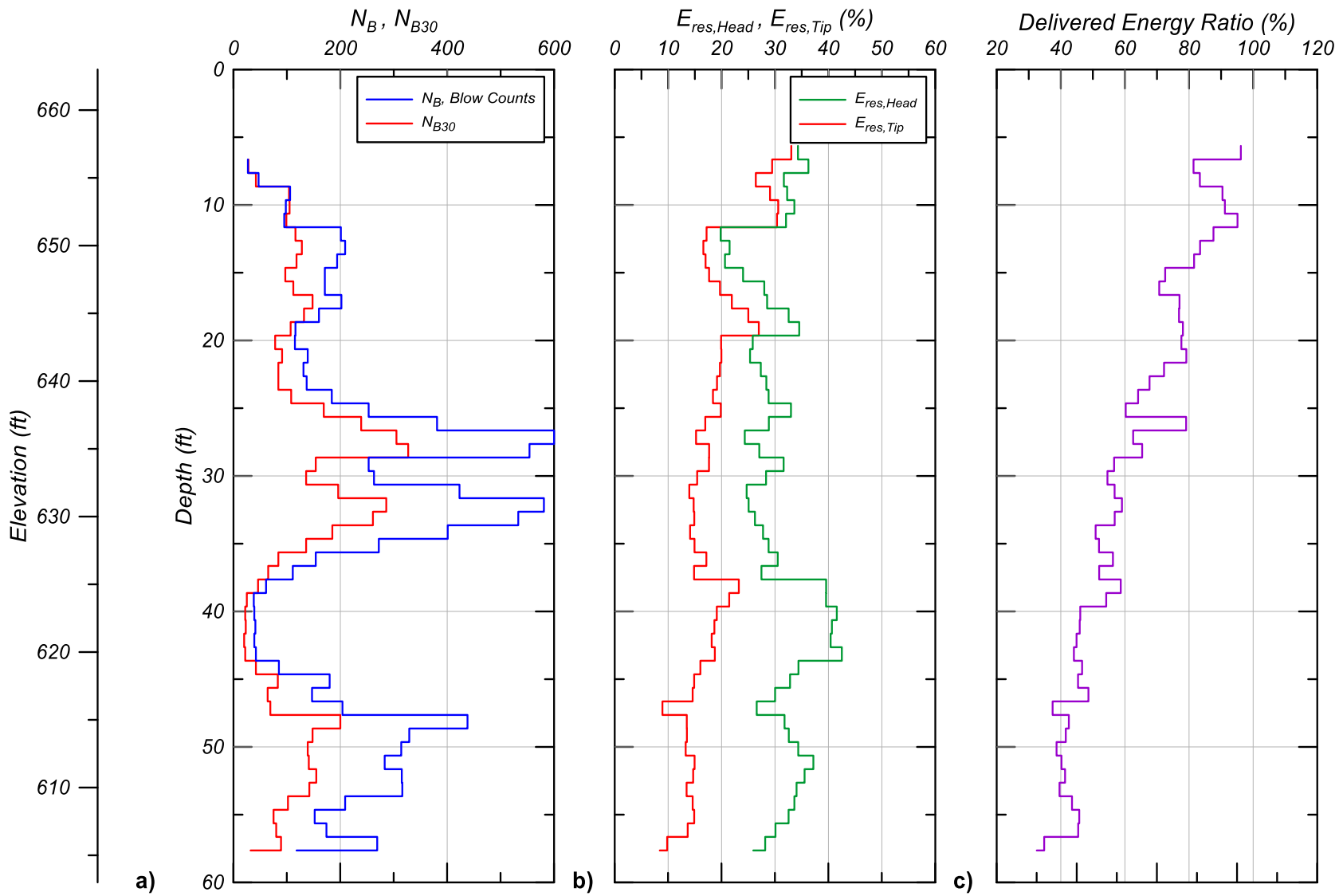

Fig. 19. Delivered Energy Ratio with depth in RTP-15-2.

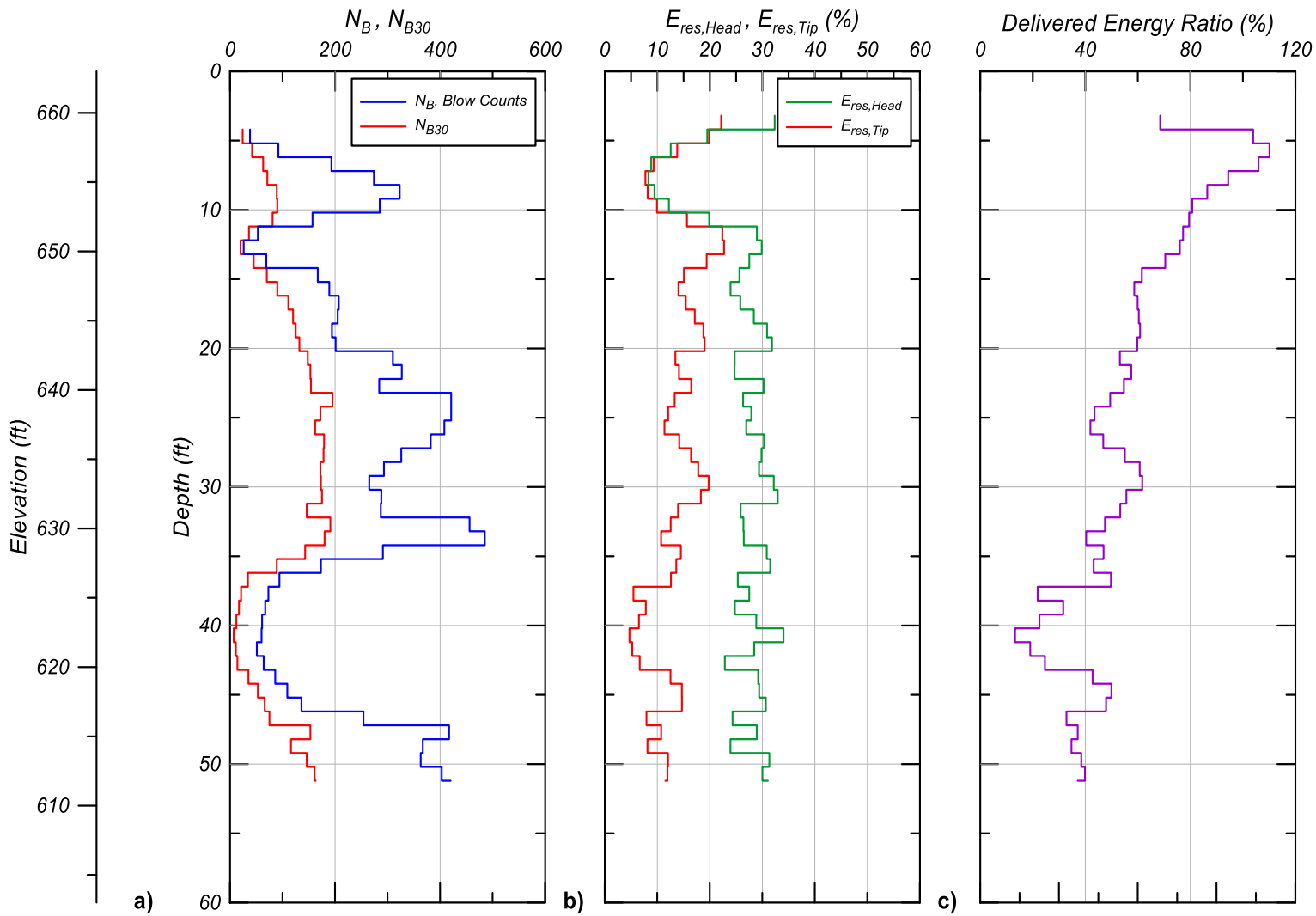

Fig. 20. Delivered Energy Ratio with depth in RTP-15-3A.

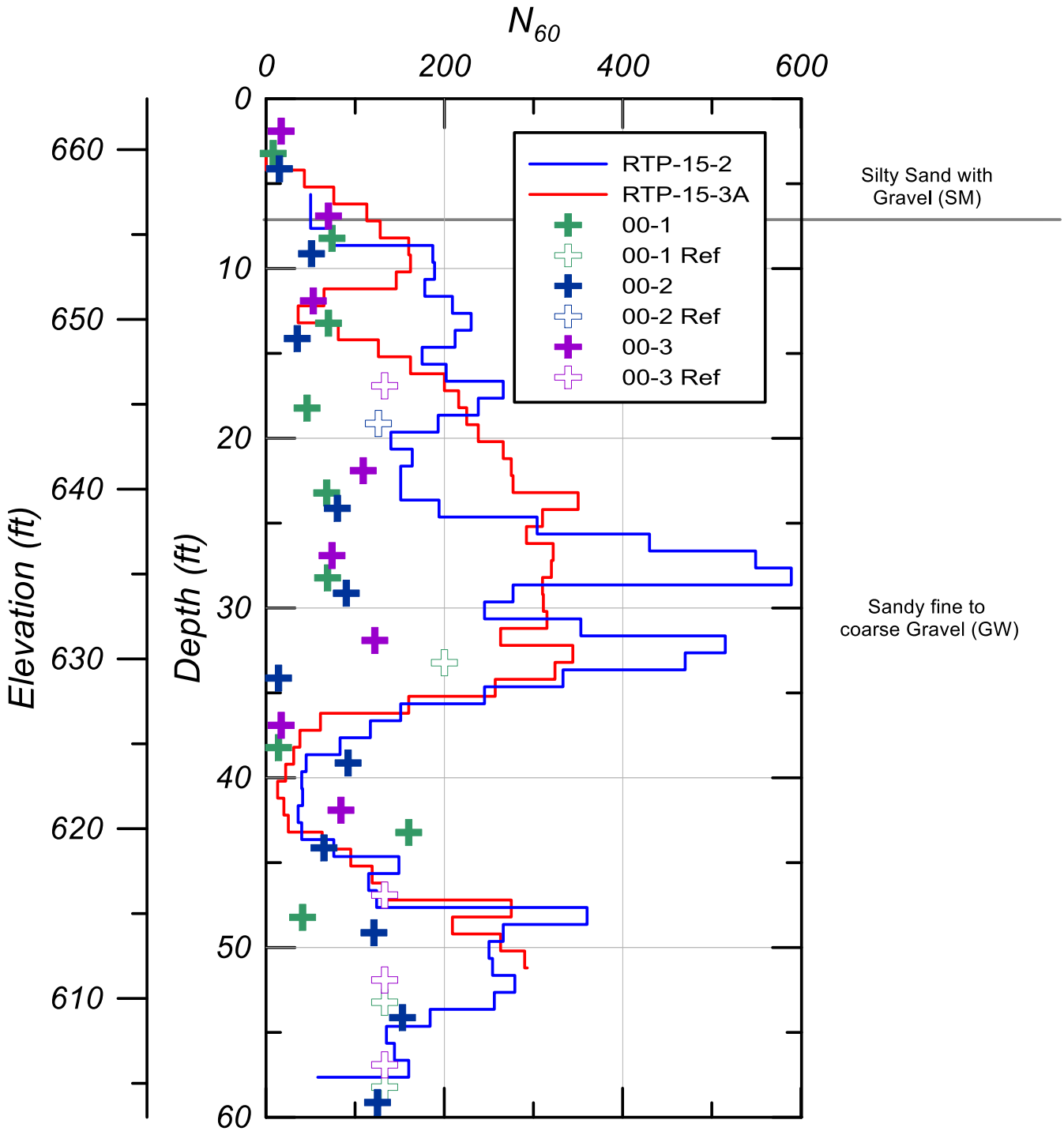

Fig. 21. N_{60} profile comparison of all penetration resistance tests at the site. Open crosses represent highest blow count before refusal was called for that test.

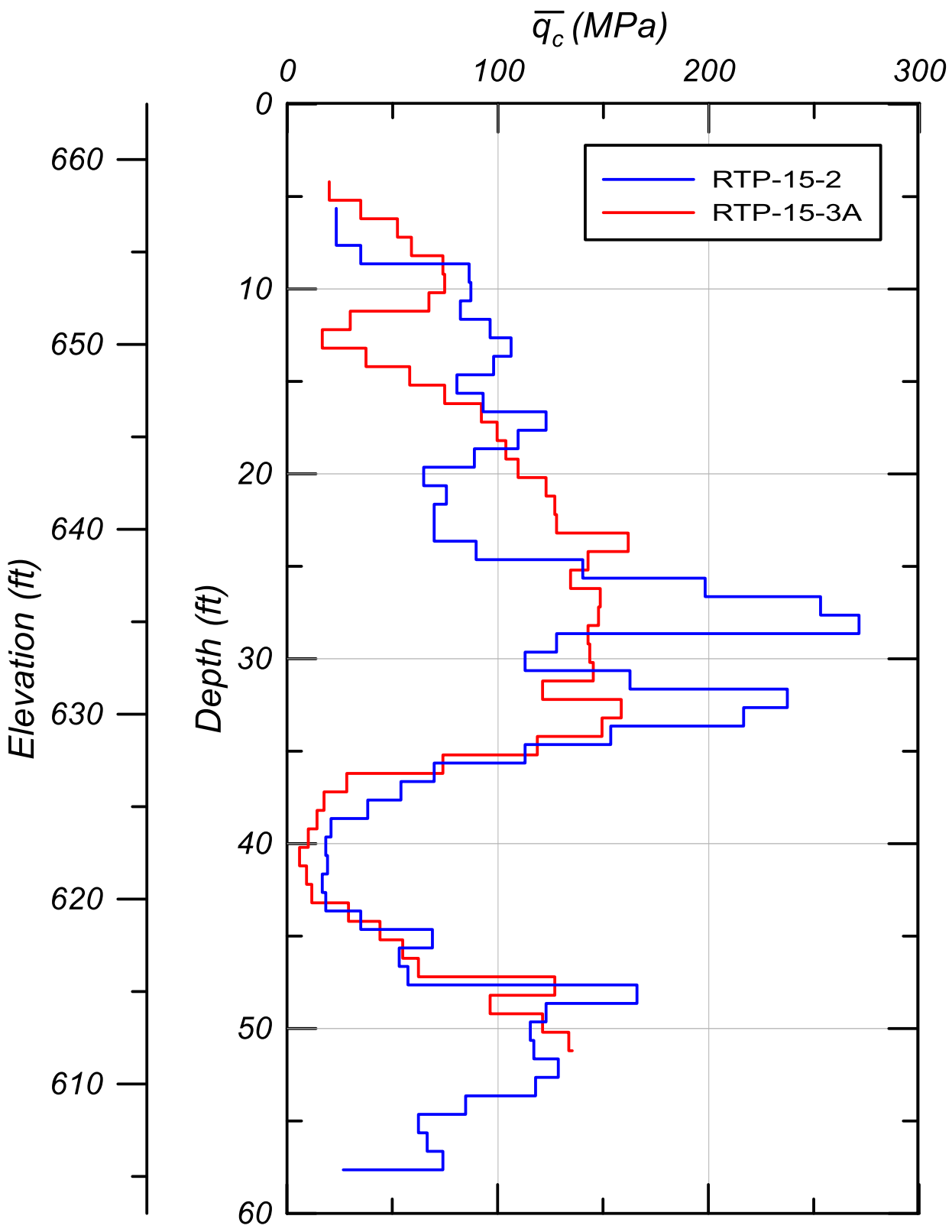

Fig. 22. iBPT equivalent CPT tip resistance.

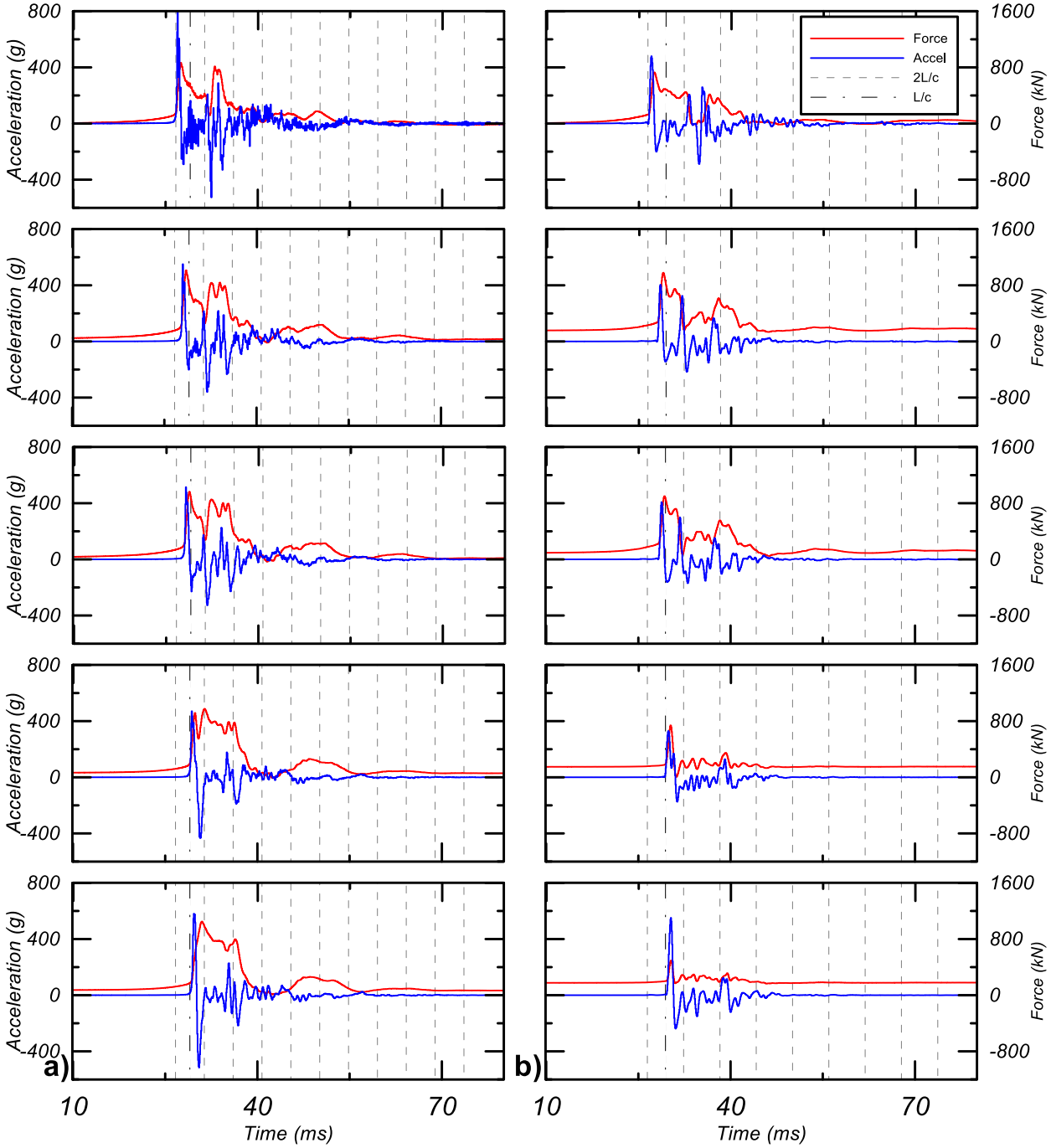

Fig. 23. Example data collected at all modules from a) hard driving (RTP-15-2 at 26 ft) and b) soft driving (RTP-15-2 at 40 ft).

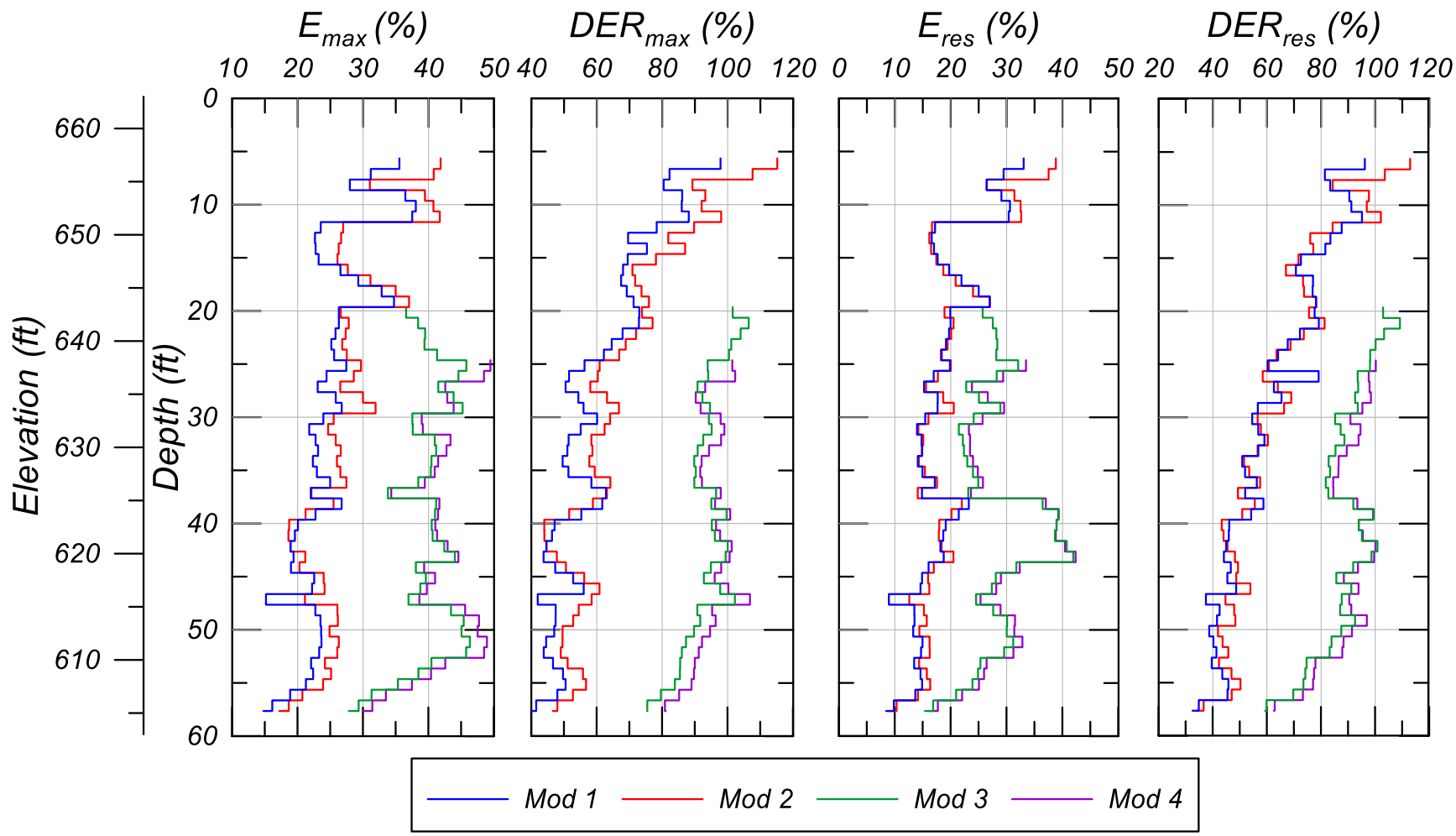

Fig. 24. Energy measurements along pile as a function of tip depth in RTP-15-2. See Figure 13 for module location on pile.

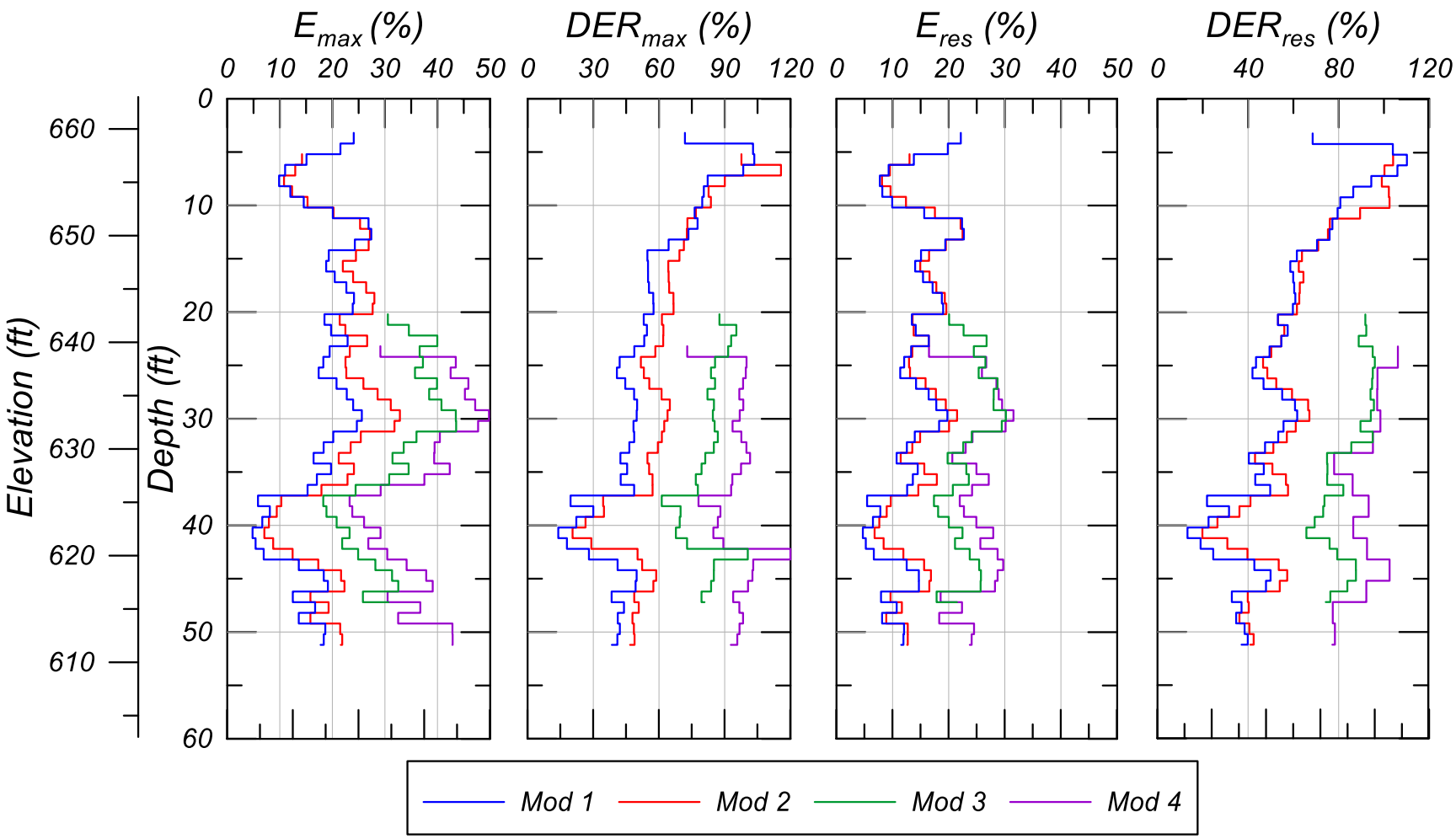

Fig. 25. Energy measurements along pile as a function of tip depth in RTP-15-3A. See Figure 14 for module location on pile.

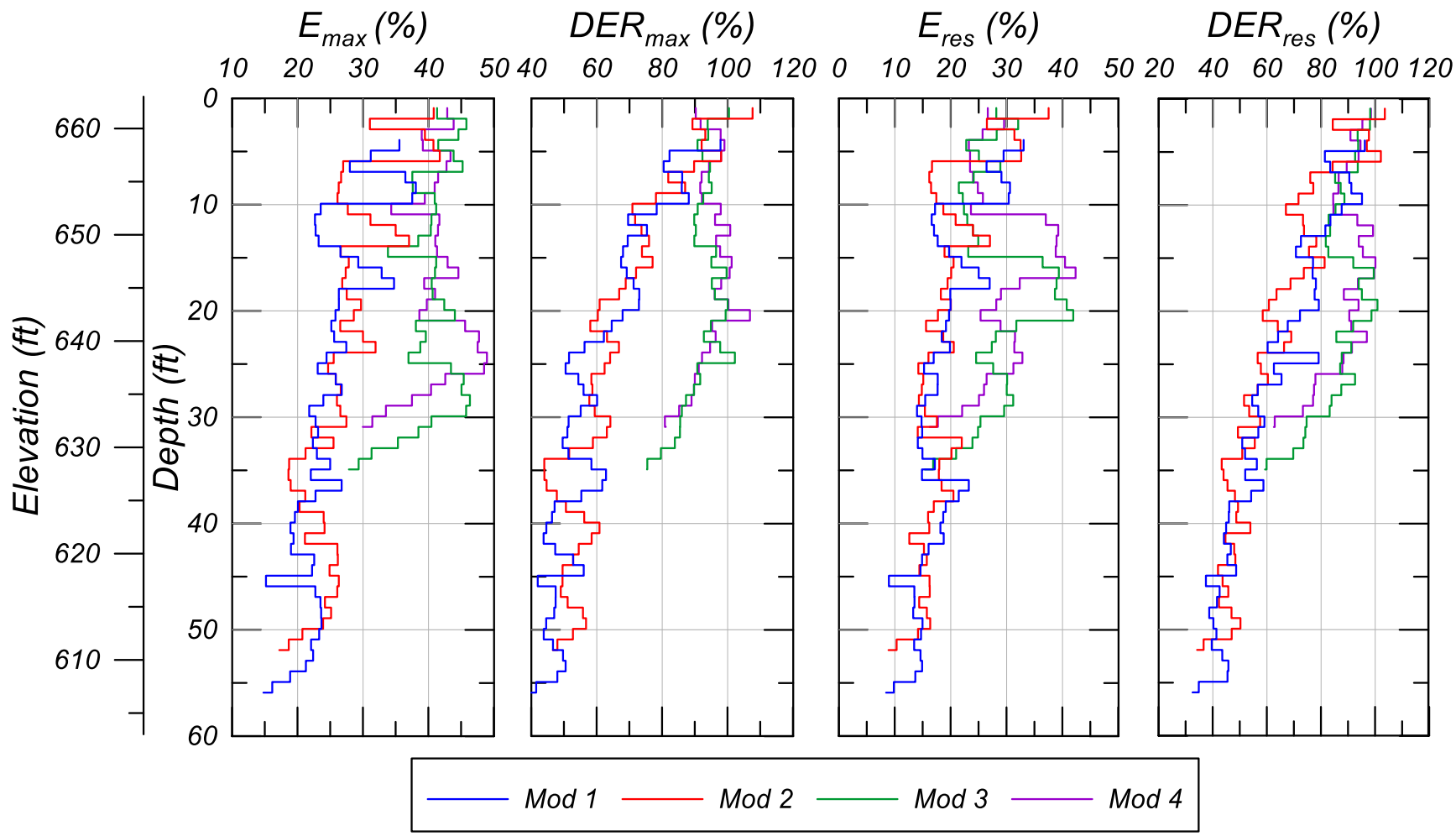

Fig. 26. Energy measurements along pile as a function of module depth in RTP-15-2.

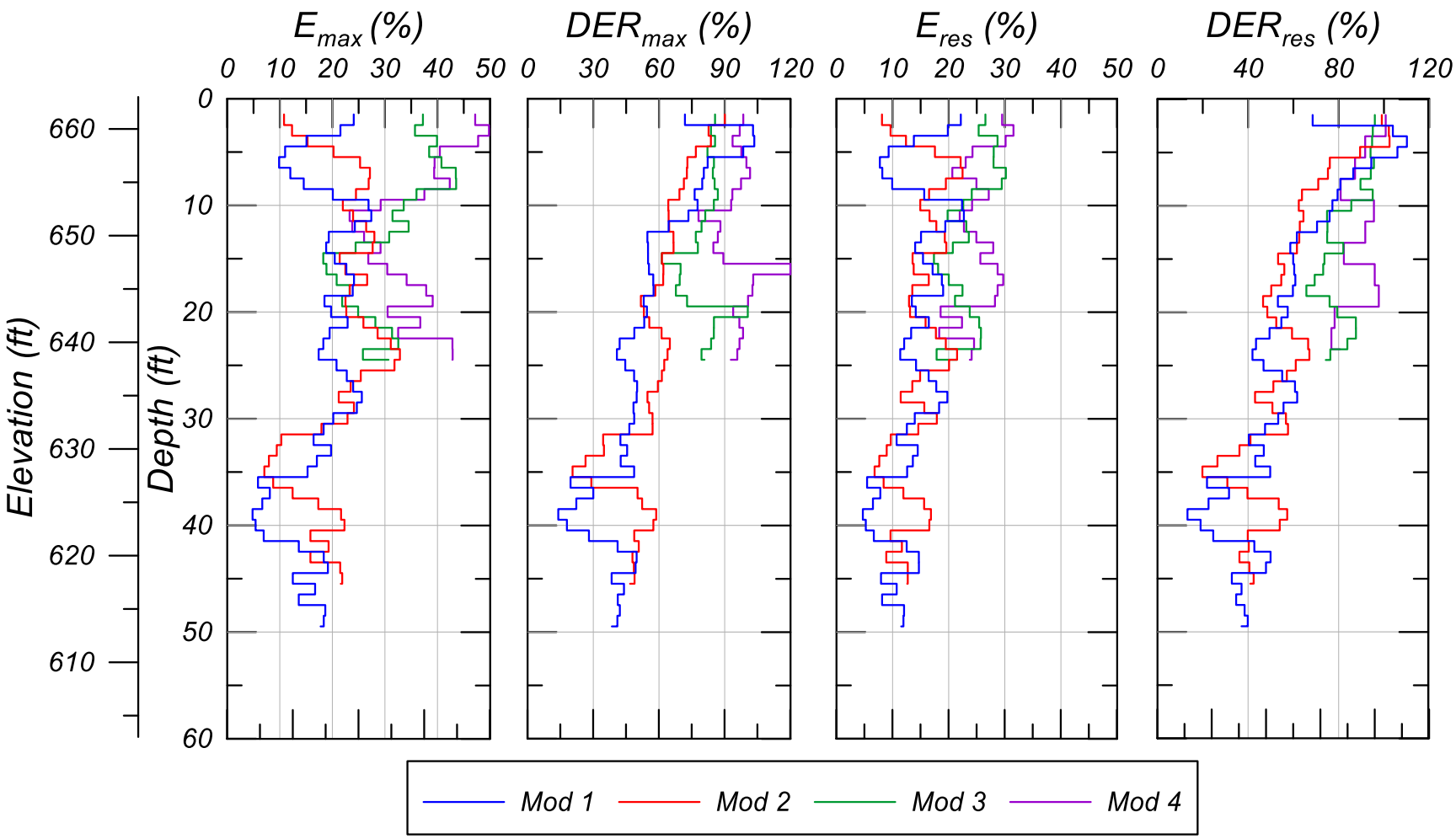

Fig. 27. Energy measurements along pile as a function of module depth in RTP-15-3A.

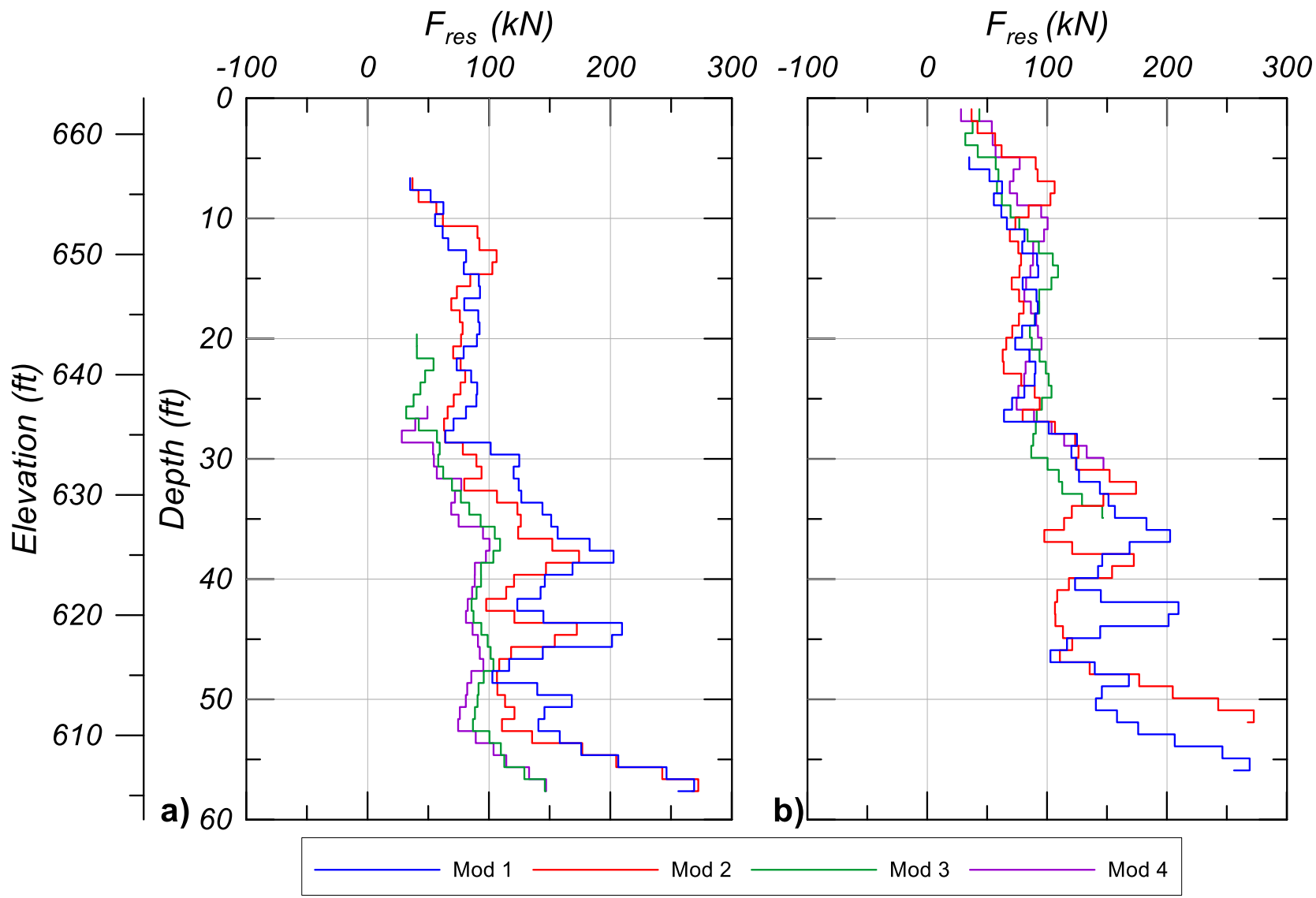

Fig. 28. Residual force of all modules in RTP-15-2 plotted against a) tip depth and b) module depth.

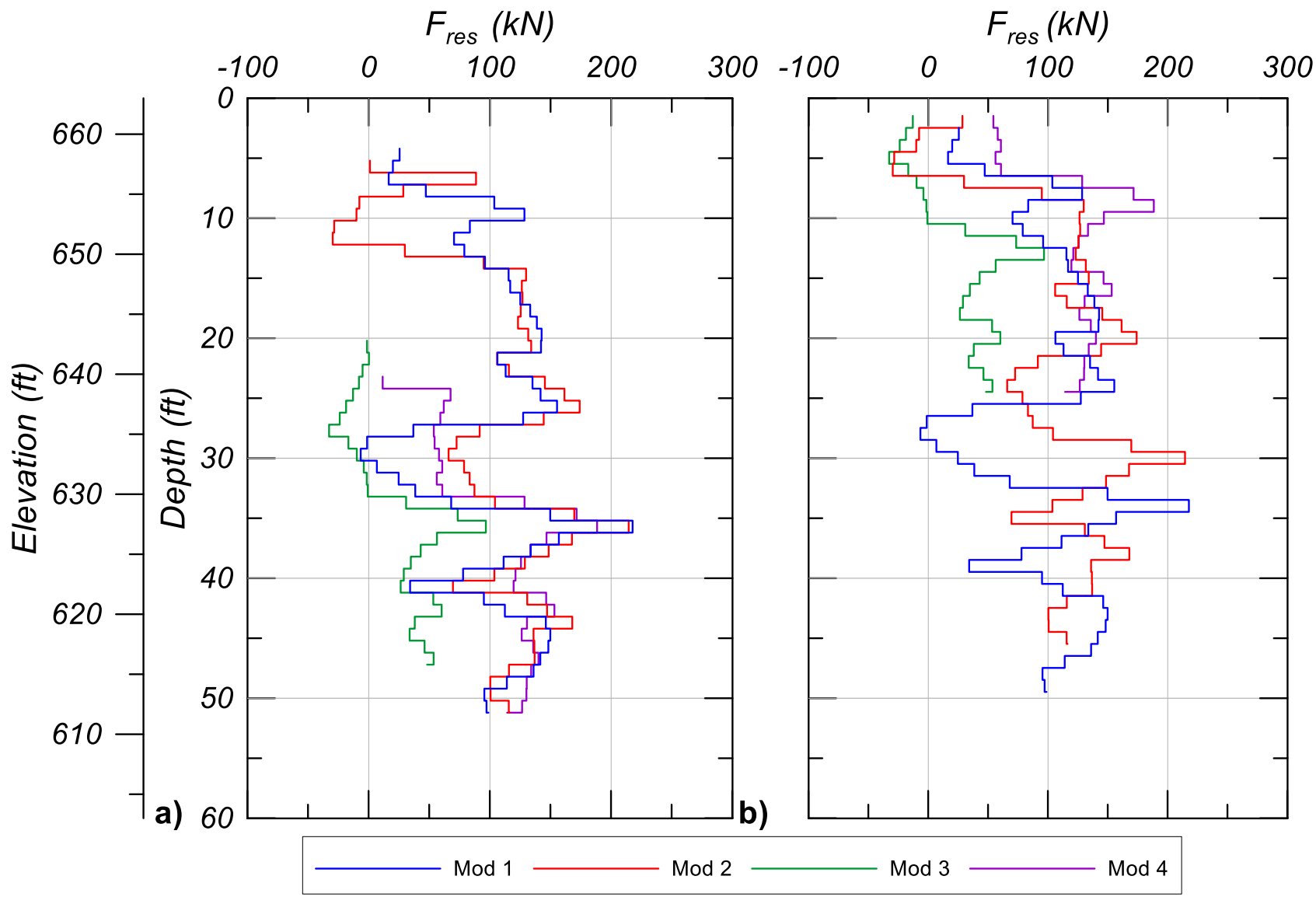

Fig. 29. Residual force of all modules in RTP-15-3A plotted against a) tip depth and b) module depth.

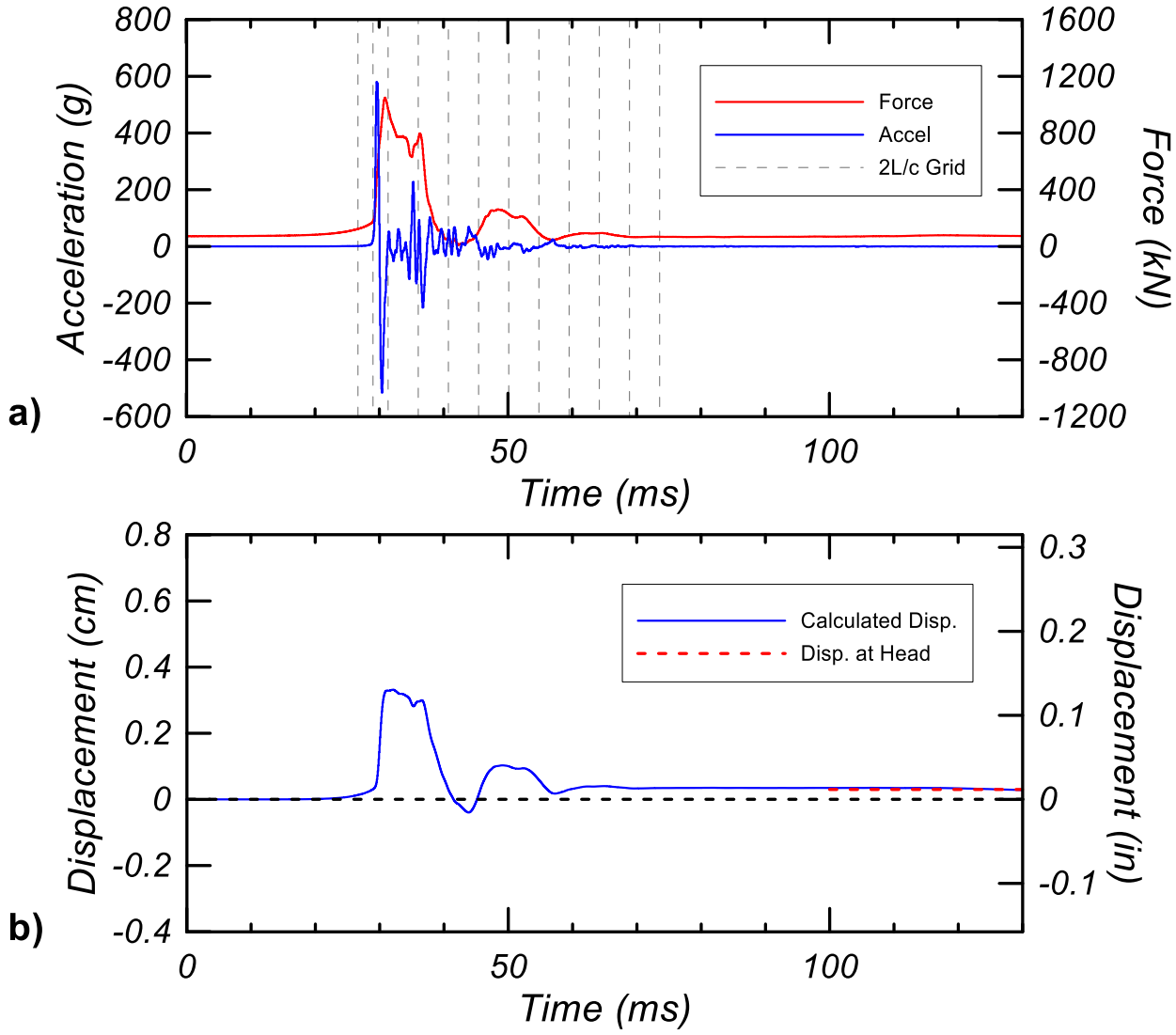

Fig. 30. Example tip data from hard driving in RTP-15-2, at a depth of 7.9 m (26 ft). Notice a) the low residual force, and b) the large elastic rebound, with small residual displacement.

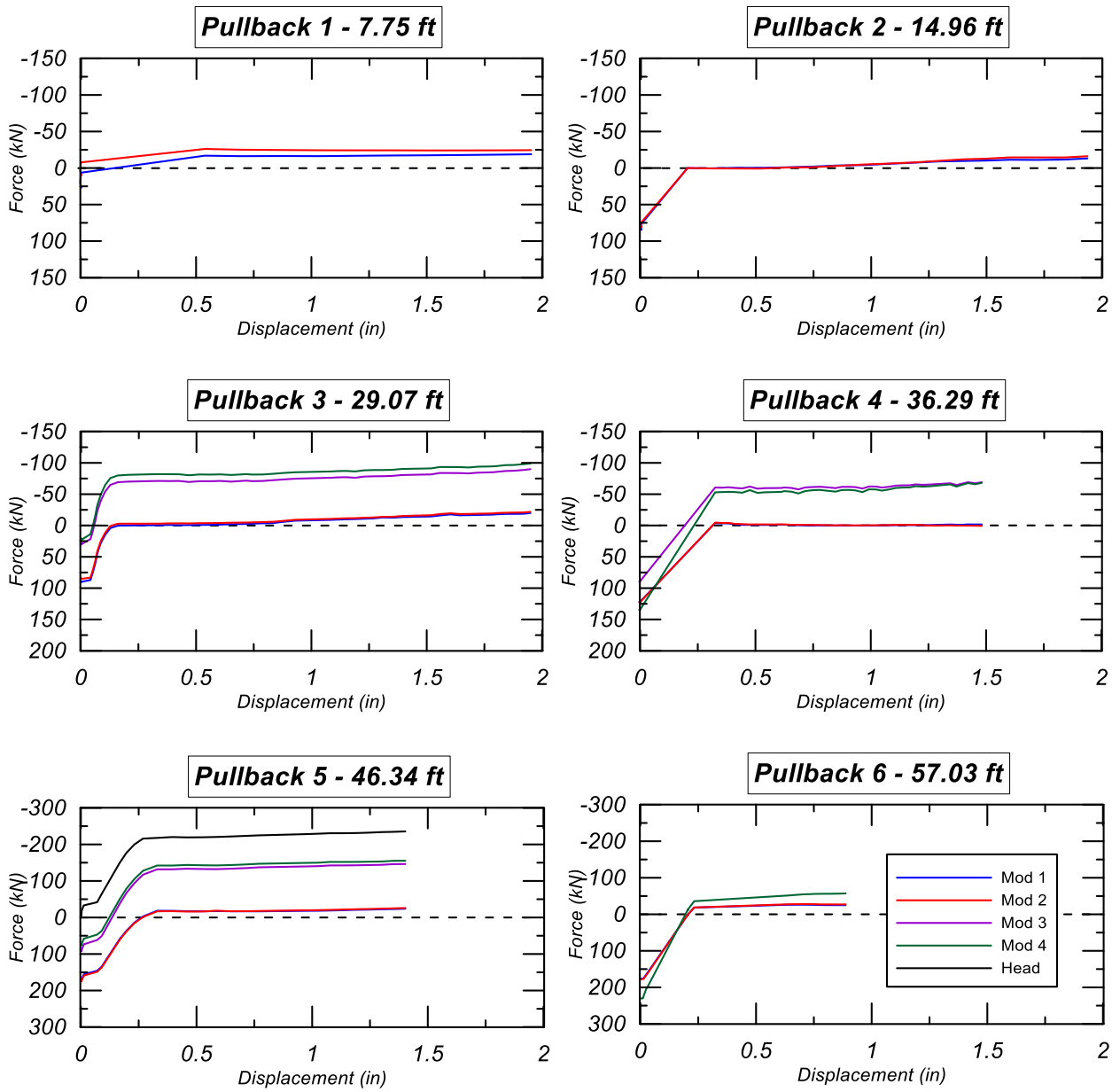

Fig. 31. Load-displacement data for all pullbacks performed in RTP-15-2.

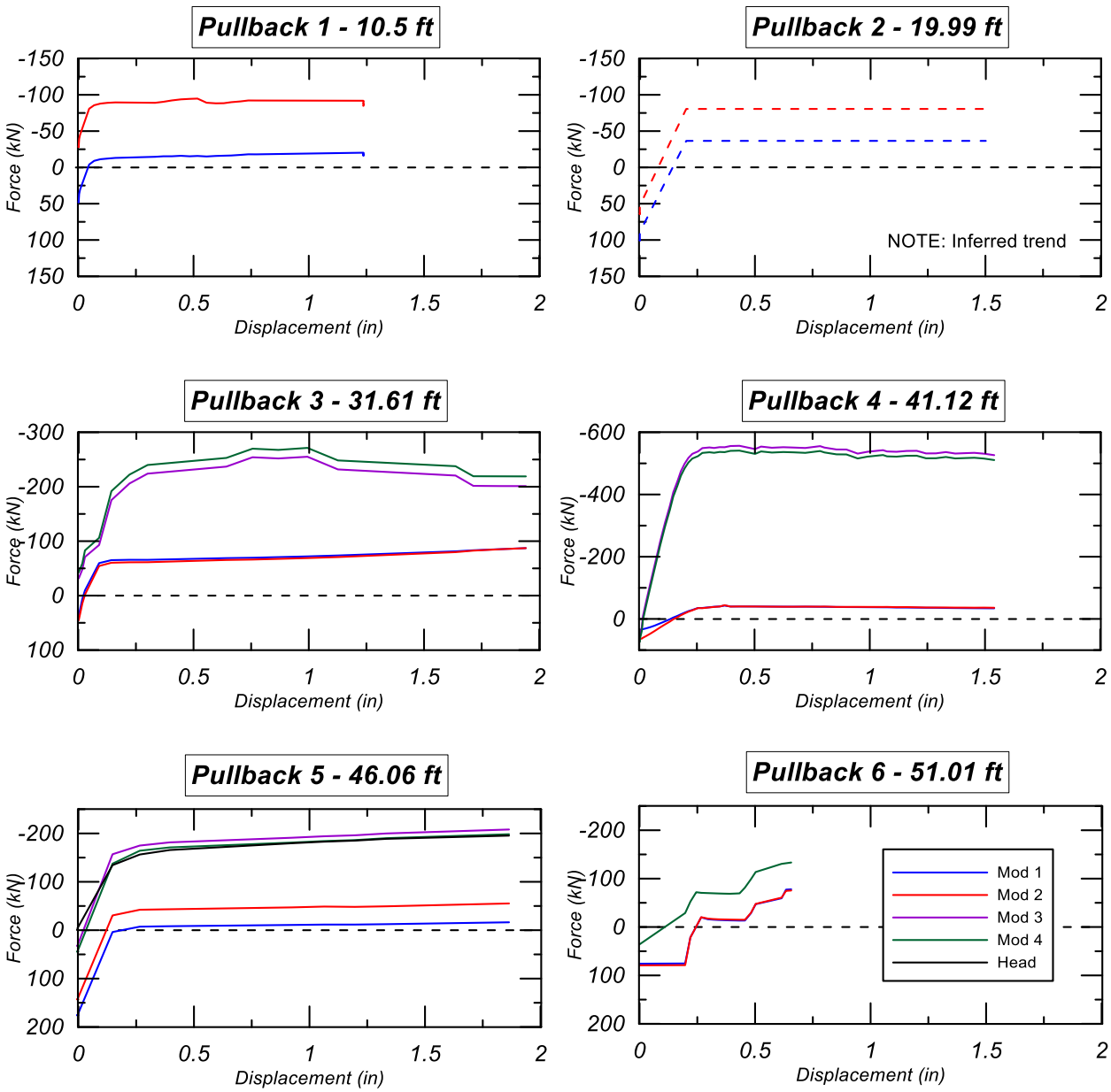

Fig. 32. Load-displacement data for all pullbacks performed in RTP-15-3A.

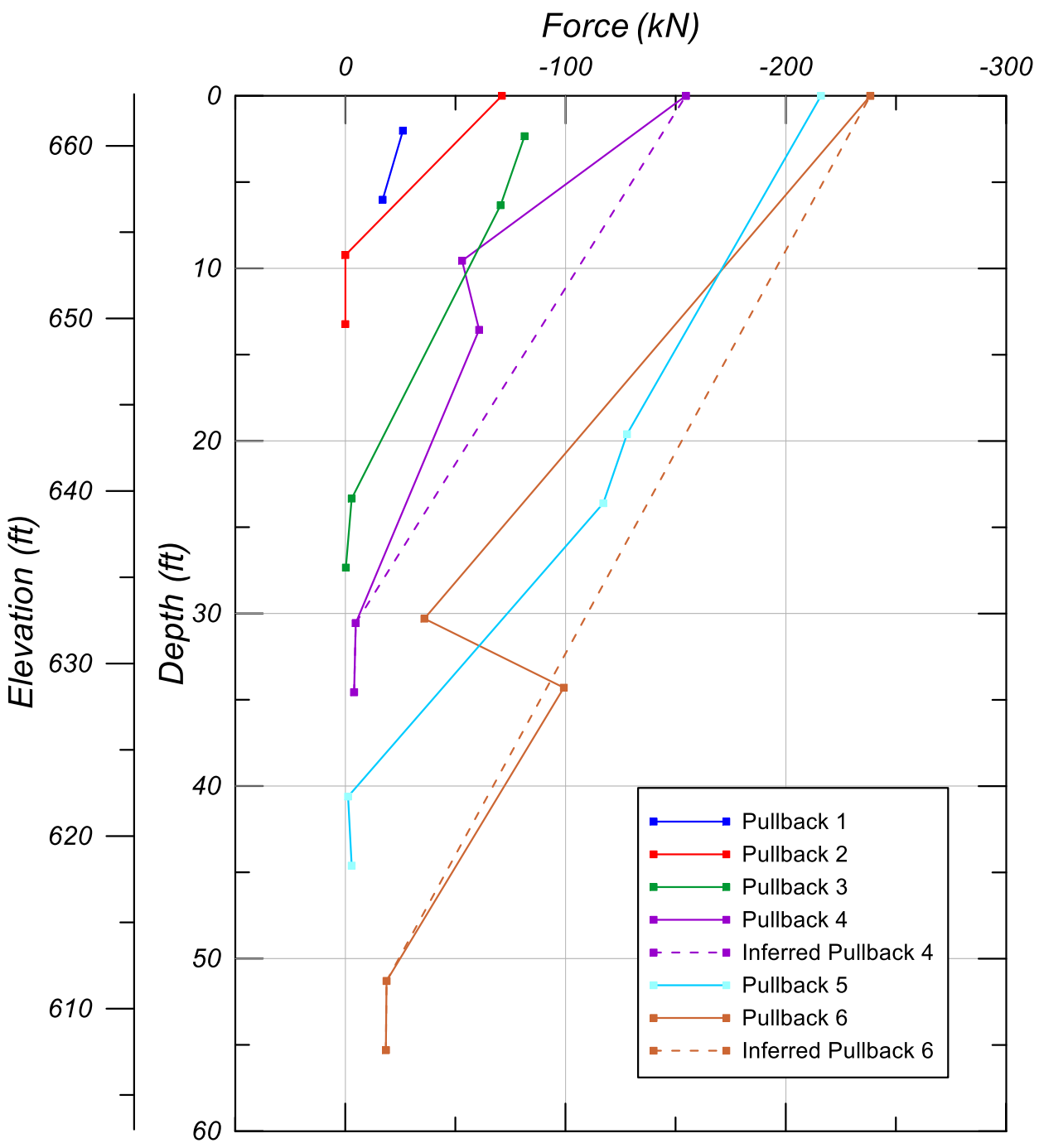

Fig. 33. Total force measurements during pullback testing along pile in RTP-15-2.

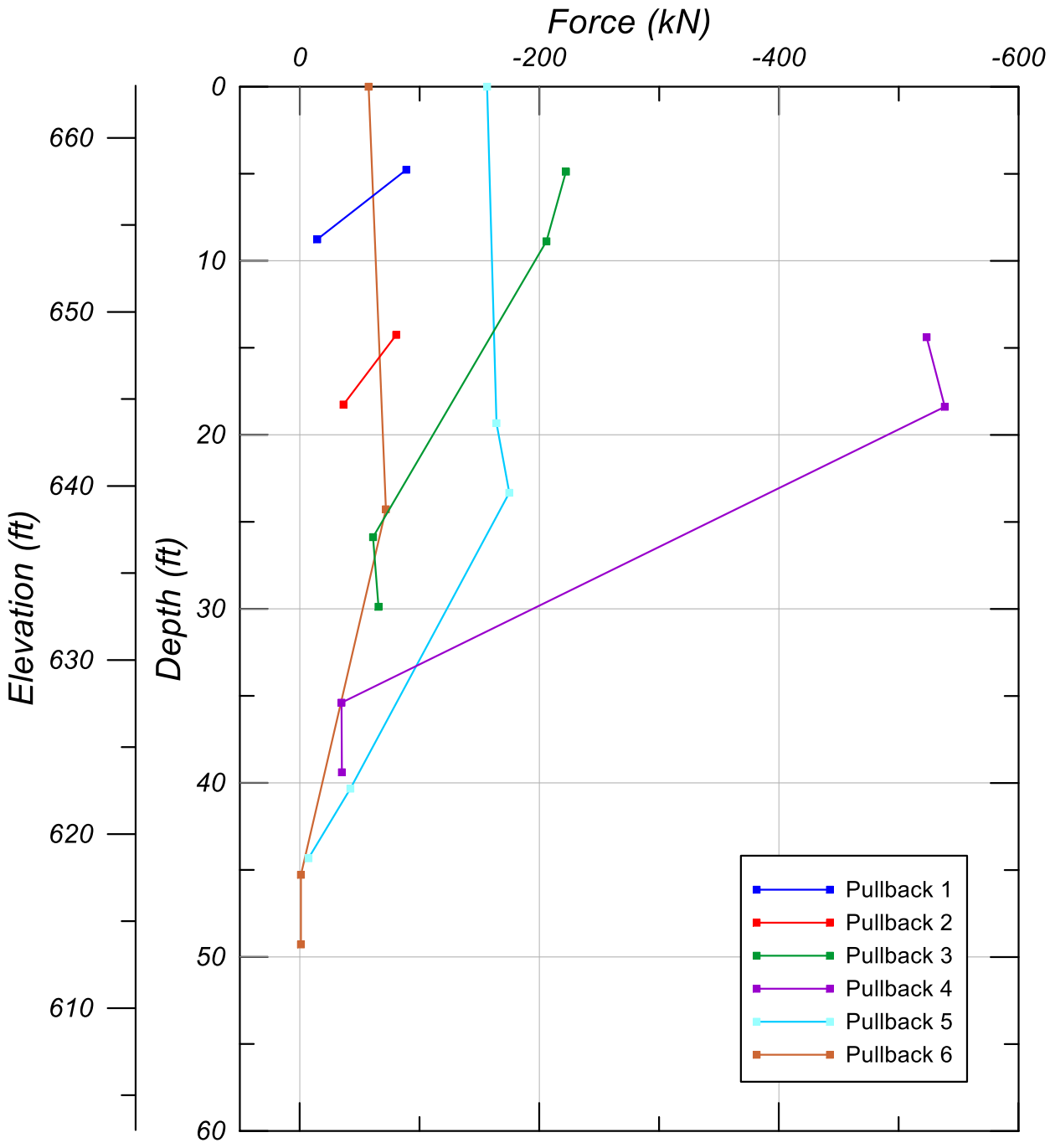

Fig. 34. Total force measurements during pullback testing along pile in RTP-15-3A.

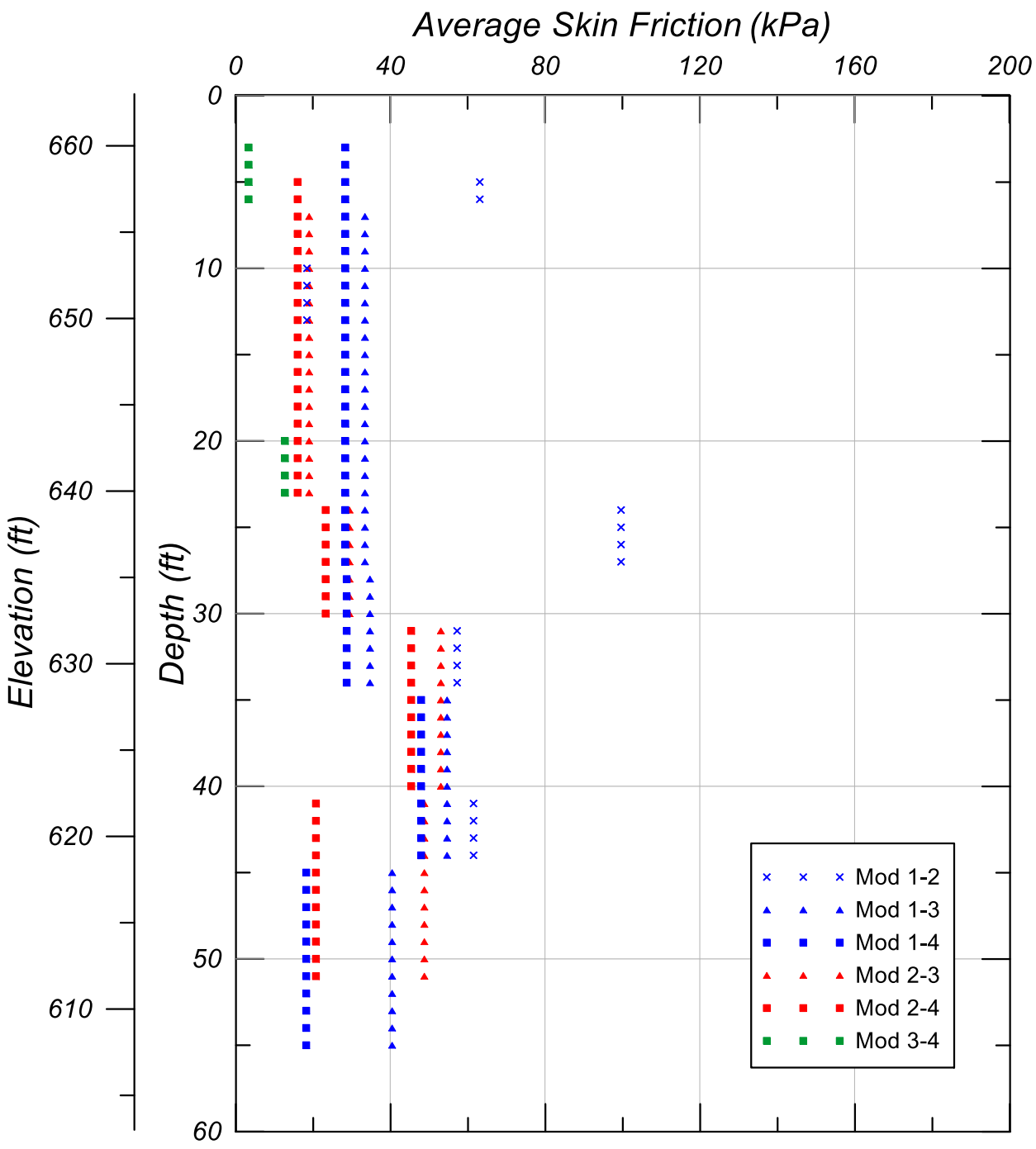

Fig. 35. Average skin friction calculated between modules during pullback tests in RTP-15-2.

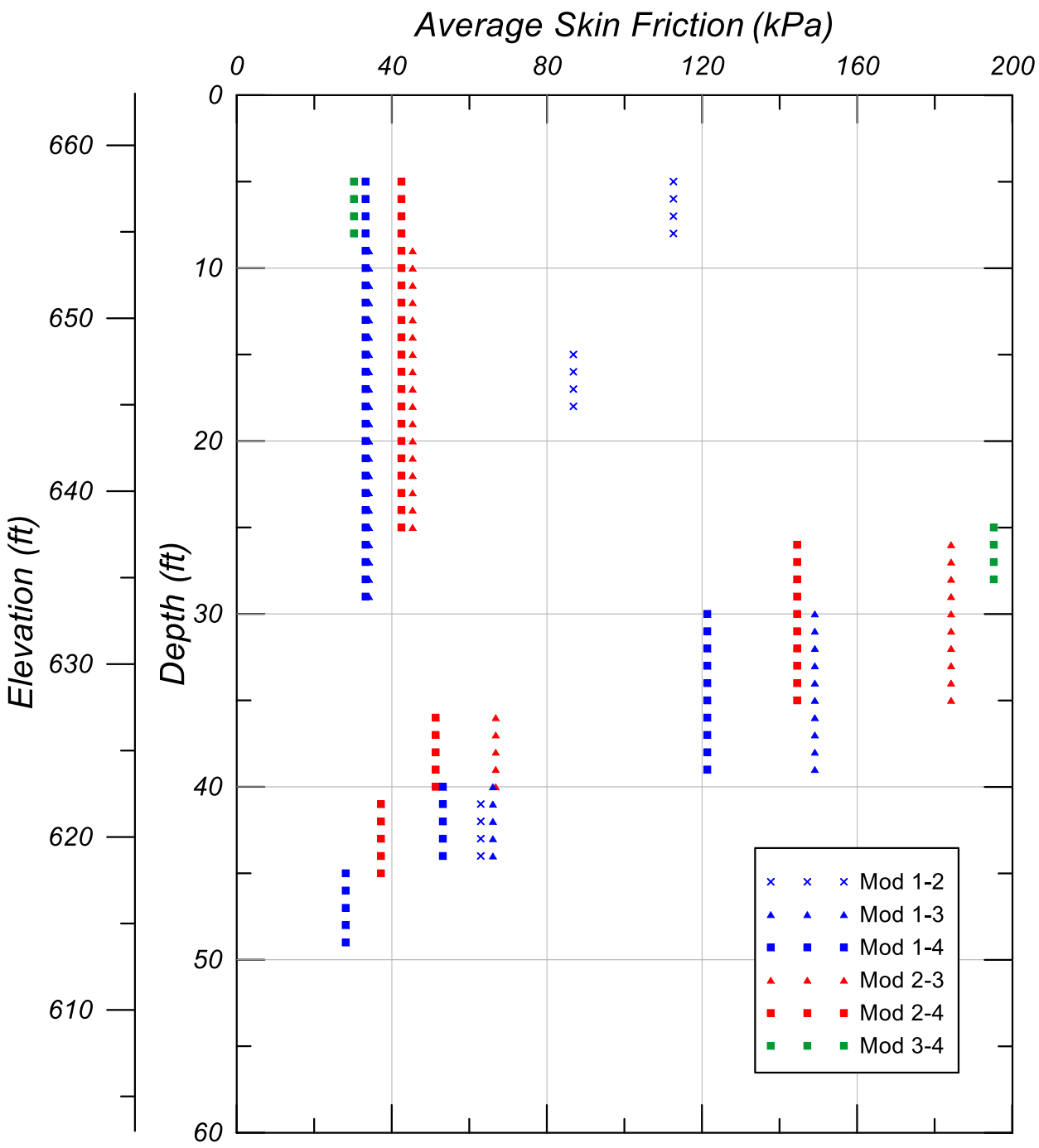

Fig. 36. Average skin friction calculated between modules during pullback tests in RTP-15-3A.

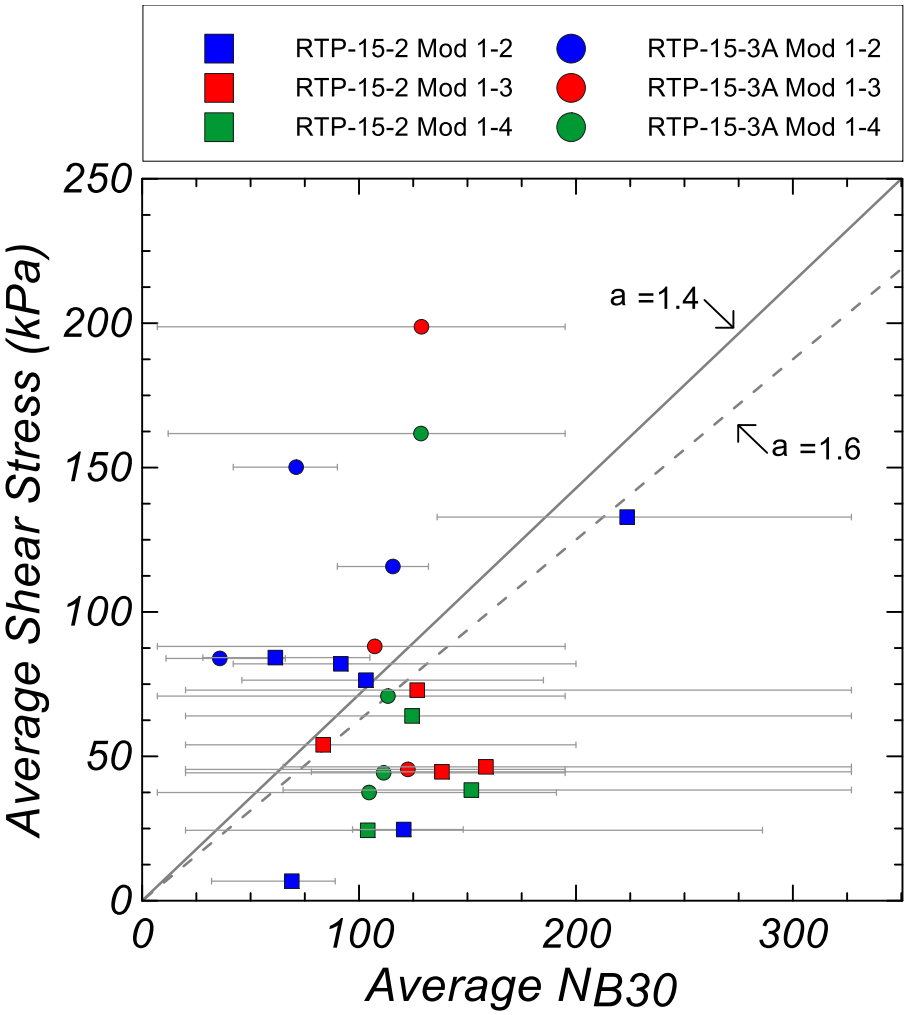

Fig. 37. Proposed α value for shaft capacity prediction found using linear regression of average N_{B30} versus average sheer stress from pull back tests.

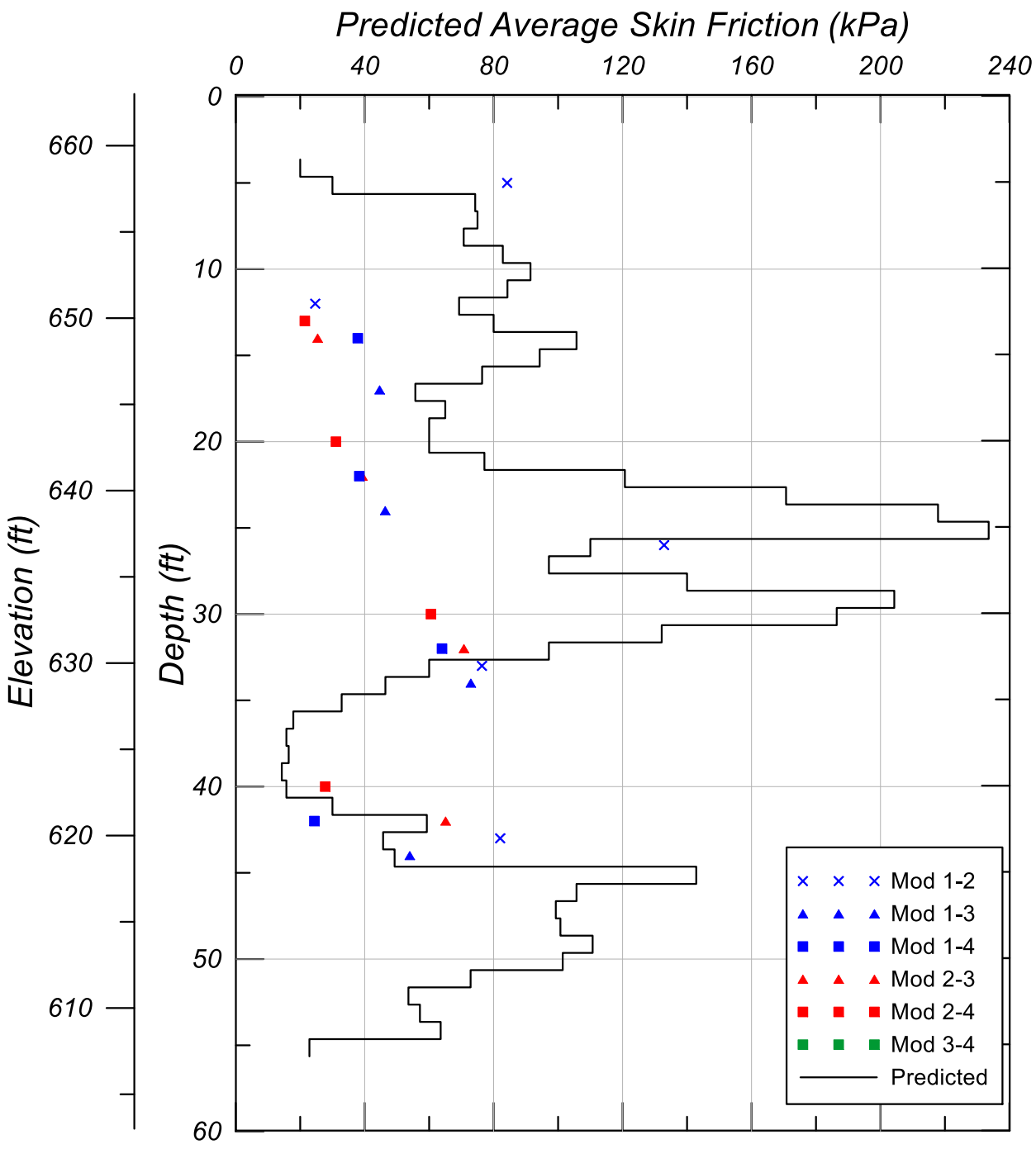

Fig. 38. Average skin friction calculated between modules during pullback tests plotted at the midpoint between the two modules, compared to the predicted skin friction value predicted using the RTP design method in RTP-15-2.

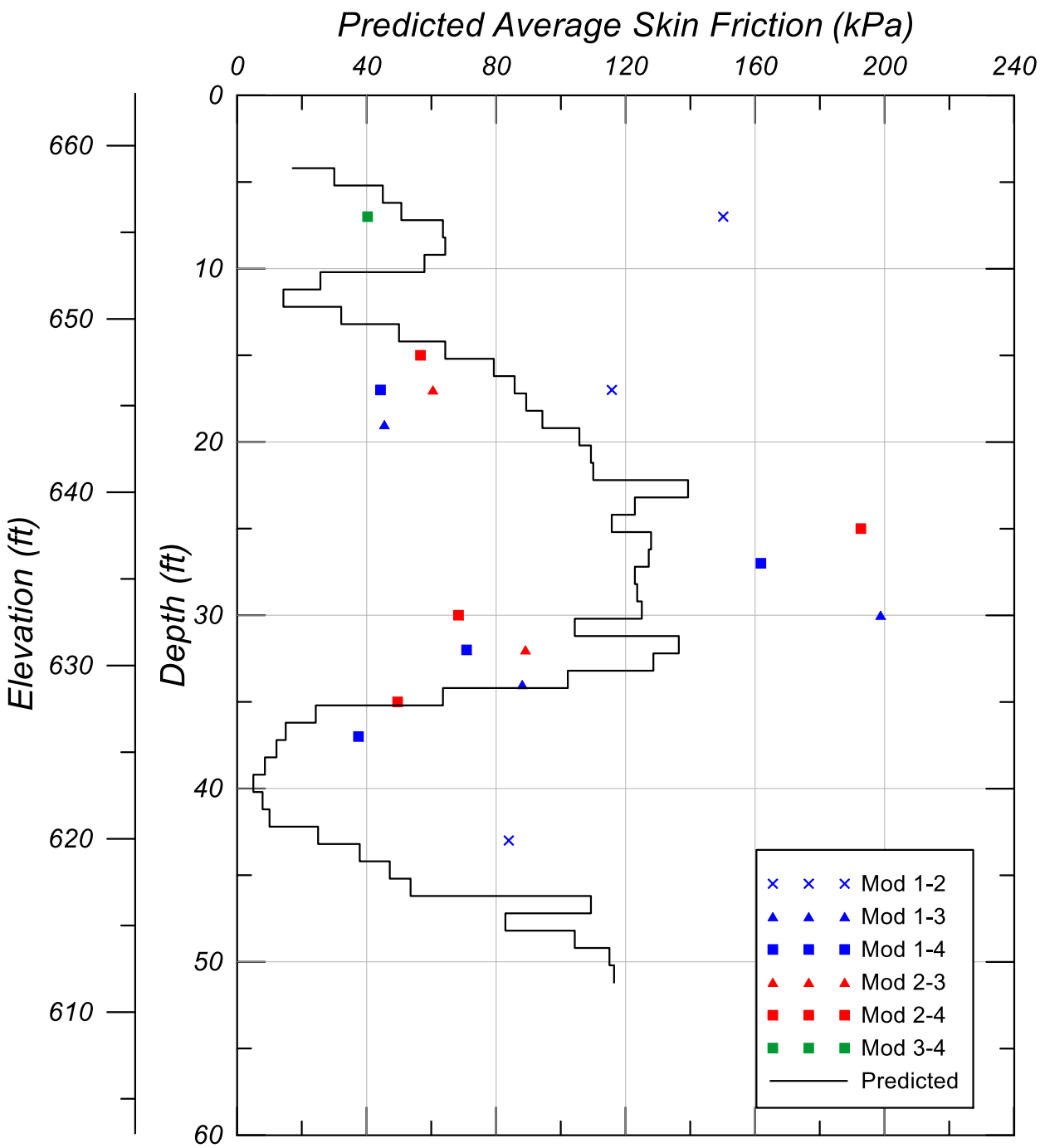

Fig. 39. Average skin friction calculated between modules during pullback tests plotted at the midpoint between the two modules, compared to the predicted skin friction value predicted using the RTP design method in RTP-15-3A.

CHAPTER 4

Pile Driving Mechanics at the Base as Informed by Direct Measurements

Kevin C. Kuei, S.M.ASCE[1], Mason Ghafghazi, M.ASCE[2], Jason T. DeJong, M.ASCE[3]

[1] Graduate Student, Department of Civil & Environmental Engineering, University of California at Davis, One Shields Ave., Davis, CA, 95616, kckuei@ucdavis.edu

[2] Assistant Professor, Department of Civil Engineering, University of Toronto, 35 St. George St., Toronto, ON, Canada M5S 1A4, mason.ghafghazi@utoronto.ca

[3] Professor, Department of Civil & Environmental Engineering, University of California at Davis, One Shields Ave., Davis, CA, 95616, jdejong@ucdavis.edu

Paper Reference:

Kuei, K.C., Ghafghazi, M., and DeJong, J.T. "Pile Driving Mechanics at the Base as Informed by Direct Measurements", *ASCE J. Geotechnical and Geoenvironmental Engineering*, 2017, https://doi.org/10.1061/(ASCE)GT.1943-5606.0001746

ABSTRACT

Determination of the base contribution to total pile capacity is an important aspect in the design of end-bearing piles. For driven piles, dynamic load testing and signal matching are the predominant approach for estimating total pile capacity. This includes separating the base and shaft resistance, and differentiating between static and dynamic contributions. Despite its widespread usage, the approach is susceptible to uncertainty and non-uniqueness of solutions. The new instrumented Becker Penetration Test (iBPT) configured as a Reusable Test Pile (RTP) is capable of directly measuring the dynamic pile response at the base and along the shaft during driving. In this paper, RTP measurements at the base are presented and used to guide the selection of models and parameters available in signal matching methods. The direct measurements at the base show pile driving as a steady penetration process with unload-reload cycles, and consistency of locked-in residual force between subsequent blows. The results show that when fundamental mechanical constraints are satisfied, simple existing models are adequate for capturing the measured response, and uncertainty and non-uniqueness at the base is curbed.

INTRODUCTION

Piles derive their bearing capacity through mobilization of soil resistance acting along the pile shaft and base. For piles founded on firm strata, i.e. end-bearing piles, reliable assessment of the base contribution is an important aspect in design. Several methods are available for estimating the capacity of driven piles based on fundamental soil properties or correlations to in-situ tests. Most large projects are initially designed using such methods and correlations before site-specific confirmation is obtained via static or dynamic tests.

Verification of pile capacity by signal matching to dynamic waves recorded above ground during pile driving is common practice. The method is used to estimate the distribution of

resistance along the pile shaft and base, and to obtain the pile load-settlement response. This is done by performing wave equation analyses with force and velocity measurements from individual blows obtained during pile installation or restrike. A basic underlying assumption is that static and dynamic contributions to total soil resistance can be effectively separated during the signal matching process. In practice, the pile is modeled as an elastic continuum, and interface soil resistance is modelled using discrete simplified spring-dashpot elements. Soil model parameters are then adjusted until a match between the measured pile head response with the computed response is obtained (e.g. Rausche et al., 2010; Middendorp, 2004).

The soil models used in the analysis of piles generally consist of a spring and a dashpot in parallel, with the spring representing the static response, and the dashpot representing the dynamic effects. Occasionally a mass is also included to capture inertial effects, especially for plugging of open-ended piles. Soils can demonstrate different stress-strain characteristics during unload-reload or cyclic loading in what is generally referred to as hysteretic behavior. The spring-dashpot concept has been used to capture this behavior in earthquake engineering (e.g. Kramer, 1996), foundation vibration applications (Lysmer, 1965), and modeling of piles (Smith, 1960). Figure 1a illustrates an example of hysteretic soil response and Figure 1b shows how a linear spring-viscous dashpot model, known also as the Kelvin-Voigt model (Kramer, 1996), captures the hysteretic behavior. In pile driving applications, where large deformations and high straining of soil is expected, the spring has been modified to undergo yielding (e.g. linear or piecewise linear elastic-perfectly plastic, hyperbolic, etc.), rendering the dashpot redundant for capturing the hysteretic behavior. The mass and dashpot have remained parts of the system in a pursuit to curve-fit the measurements or to capture other types of damping.

Some soils such as clays demonstrate higher resistance when loaded at high rates, a

phenomenon often referred to as rate effects (e.g. Taylor, 1948; Dayal and Allen, 1975). A viscous dashpot can capture this effect by increasing the total resistance as a function of the loading velocity. Energy is also lost when waves leave the geometric boundaries of the system in what is known as radiation, or geometric damping. A combination of the viscous dashpot and the mass can capture radiation damping and rate-sensitive behavior to an acceptable degree.

Several modifications and alternatives to Smith's original formulation for pile driving analysis have been proposed over time based on laboratory experiments (e.g. Coyle and Gibson, 1970; Hereema, 1979), and signal matching using aboveground measurements (e.g. Rausche et. al, 2010). In practice, the modifications have led to several damping model variants and inclusion of additional static parameters for capturing the element response. These modifications have generally led to more complicated models that may not necessarily conform to mechanical principles of pile driving or be compatible with the simplified framework for which the analysis was originally developed. These modifications have also led to the inclusion of additional static parameters and damping options to conventional signal matching tools. There is a need to identify what is necessary and what is redundant to reduce the dependence of signal matching results to the choices software operators make.

Some researchers have attempted to connect the spring-dashpot framework to a more theoretical basis to express its parameters in terms of fundamental soil properties in an attempt to better differentiate various phenomena contributing to damping (Randolph and Deeks, 1992; Nguyen et al., 1988). Others have attempted more sophisticated means of analysis such as finite element or boundary element models (e.g. Masouleh and Fakharian, 2008; Loukidis et al., 2008). While the more sophisticated and theoretical approaches are necessary for understanding mechanisms, they are generally underutilized outside of research applications and may require

additional validation.

Signal matching analyses have been shown to yield non-unique solutions, leading to uncertainty in the predictions of resistance distributed along the pile, and the inferred static pile response (Fellenius, 1998; Middendorp and van Weele, 1986; Middendorp and van Zandwijk, 1985). In the study by Fellenius (1998) which considered variations in signal matching amongst various operators, it is shown that relatively good agreement could be achieved in the computed total static resistance. However, the results also demonstrated that the resistance distribution along the pile, and particularly predictions of base resistance could show considerable variation among operators. In a more recent study, Ghafghazi et al. (2017) present similar findings, showing variations of shaft resistances estimated from signal matching between different operators. There has generally been a lack of experimental data to evaluate the ability of signal matching techniques in adequately capturing the distribution of the total resistance between the pile shaft and the base.

The observed non-uniqueness in conventional signal matching applications exist at two levels: within a given soil element for separation of static and dynamic components, and on a system level for the distribution of resistance (static plus dynamic) along the pile. One source for this non-uniqueness arises from the governing equation for the total element response, which following the functional form of the dynamic equation of motion, assumes the separation of displacement-, velocity-, and acceleration-dependent force contributions to the total response. A consequence of the latter is that more than one set of soil behavior parameters may be generated to satisfy the governing equation (i.e. a non-unique solution). The relatively large number of unknowns to be estimated from limited measurements, choice of models, and search algorithms, among other subjective choices which must be made by the operators further convolute the issue.

One obvious means to address the non-uniqueness at the system level for the distribution

of resistance along the pile is to utilize supplementary observation points in addition to the pile head. Moreover, if the total response between the pile shaft and base can be differentiated, the separation of static and dynamic contributions at the element level can be studied in more detail.

The earliest use of dynamic below ground measurements during pile driving was by Glanville et al. (1938) in studying stress waves in concrete test piles which were instrumented at the head, middle and base. More recently, Tran et. al (2012) used embedded sacrificial sensors near the pile base to estimate the static base resistance of full scale driven precast concrete piles from dynamic measurements. Their approach was to model the pile base using a nonlinear single degree of freedom system to satisfy force and energy equilibrium by accounting for an inertial force (mass), viscous damping, and nonlinear static resistance. Using dynamic base measurements, they resolved the static response at the pile base, and compared the prediction to the measured base response from static pile load tests performed on the instrumented precast piles. Their measurements and analyses did not explicitly account for residual stresses. More importantly, their rigorous analysis algorithms are only applicable where base measurements are available, which rarely occurs in practice.

An instrumented Becker Penetration Test (iBPT) configured as a Reusable Test Pile (RTP) capable of measuring the dynamic response and accumulation of residual stresses at the base and along the pile shaft is introduced (see Figure 2a). The RTP is a field scale pile that is fully retrievable and reusable after driving (sensors and equipment are not sacrificial). In this paper, direct base measurements are used to analyze the dynamic base response, without the additional uncertainty associated with the distribution of resistance along the pile length. The problem is effectively reduced to separation of static and dynamic contributions to total measured resistance at the base soil element level. Recognizing that such direct measurements are, and will likely

remain limited to research endeavors, the understanding obtained from reviewing thousands of records of dynamic base response in a variety of materials is used to produce general recommendations for wave equation analyses performed on aboveground head measurements in practice. Data from five representative sets of base measurements are presented. The soil response at the base is analyzed as steady state penetration with unload-reload cycles. The simple static and damping models discussed earlier are shown to adequately capture the response. Fundamental mechanics of penetration are utilized to inform the interpretation of static resistance and unload and reload stiffnesses. It is suggested that the uncertainty of wave equation analyses in separating static and dynamic components of soil response at the base can be reduced if these models are used with consideration of the mechanics of pile driving at the base. The inferred static behavior, non-uniqueness aspects, and practical considerations are subsequently discussed.

REUSEABLE TEST PILE (RTP) SYSTEM AND MEASUREMENTS

The instrumented Becker Penetration Test (iBPT) configured as a Reusable Test Pile (RTP) provides a new tool for assessing pile drivability and improving pile design. During pile driving, the dynamic pile response and accumulation of residual forces are directly measured near the base and at discrete locations along the shaft. Pull-back (tension load) tests can also be performed to measure the distribution of static shaft resistance. Measurements are made by multiple instrumented modules (610 mm long, 168 mm O.D., 127 mm I.D.) that are assembled and driven in series with the standard closed-ended Becker drill string consisting of standard Becker pipe segments with similar diameters and lengths of 0.6 m, 1.5 m, or 3.0 m. The basic RTP system configuration during normal field operation consists of instrumented modules located immediately at the pile head and pile base. The distance between sensor centerlines of the tip module to the pile

base is 437 mm (2.6 pile diameters). In addition, up to four additional intermediate modules can be positioned along the drill string for measuring wave propagation and estimating the distribution of the resistance along the shaft. Blows per foot are counted automatically by monitoring bounce chamber pressure, and penetration depth is tracked continuously by means of an aboveground string potentiometer. Figure 2a depicts the RTP system equipped with tip, head, and two intermediate modules interspaced within the Becker drill string, along with typical dynamic force and velocity measurements recorded at each module.

Each module is equipped with four strain gauges and two accelerometers. Thermistors are also installed within the pipe sections to monitor temperature changes during pile driving. The pipe sections house data acquisition modules, which provide power to sensors, record analog output, and perform signal conditioning, digitization, and data transmission. One cable runs through the entire system, powering and controlling different modules, and transmitting the data. Sampling is performed simultaneously across tip and intermediate modules (independent of the head module). The head module records blows continuously while below ground modules, due to digitization and transmission time delays, typically record every 4th blow (approximately every 3 seconds) when operated with two modules (head and tip) and about every 20th blow (approximately every 12 seconds) when operated with six modules (head, tip, and four intermediates).

The Becker drill system on which the RTP system is implemented was originally developed in the late 1950s as a geotechnical investigation tool for coarse grained granular soils. Testing is performed by driving specially designed closed-ended steel pile with an outer diameter of 168 mm into the ground using an ICE Model 180 double-acting diesel pile driving hammer attached to the Becker rig. The hammer operates at 90 to 95 blows per minute and has a nominal energy rating of 10.85 kJ per blow, with hammer efficiencies typically ranging from 30 to 50% of the nominal

value during field operation. At the end of driving, the drill string is extracted by a hydraulic jacking system. The drill string diameter being large enough to reduce scale effects is one way in which the platform provides realistic pile driving conditions. Further, the pile is robust for harsh driving conditions, and capable of withstanding penetration through boulders and weak rock formations.

The RTP is a variant of the instrumented Becker Penetration Test (iBPT) that was developed for liquefaction assessment in a variety of soils including those with significant gravel content. The RTP system has been field tested at seven sites consisting of hydraulic fill, compacted fill, and alluvial, colluvial, and marine deposits, with materials ranging from clays to sandy gravels. To date, the system has been driven more than 1200 linear meters in 53 soundings to depths ranging from 12 to 60 m with over 250,000 individual hammer impact time-histories recorded. DeJong et al. (2017) present a complete overview of the equipment, and its operation and performance.

System Measurements

Forces are calculated from strain gauges based on cross sectional area (A) and Young's modulus (E_s). To ensure accuracy of strain measurements and prevent zero shifts over long periods of driving, strain sensors were designed for full curvature contact with the pile wall. Any meaningful assay of residual forces during pile driving requires a means to account for temperature fluctuations during pile driving. Temperature is measured at each module and a linear correction scheme is applied to account for the differential thermal straining of the steel pile and aluminum strain gauges (10.2 $\mu\varepsilon$/°C). This correction is essential for measuring residual forces locked-in during pile driving. Displacement and velocity time-histories are obtained through integration of acceleration time histories. Integrated displacements are then compared to those directly measured

above ground to confirm the accuracy of computed values.

Example measurements obtained at head and tip module sensor locations over a single blow are presented in Figure 3. The figure shows force and velocity (v) multiplied by section impedance ($Z = E_sA/c$), displacement, and energy as obtained through integration of corresponding force and velocity time-histories. A compressive locked-in residual force (F_R) is recorded at the tip module due to an opposing downward force along the shaft caused by the elastic rebound of the pile and soil. Direct measurement of final pile penetration by means of the aboveground linear potentiometer is also shown, confirming the integrated displacements at the end of the blow.

The record presented in Figure 3 was recorded during pile driving through a poorly graded sand with gravel at a depth of 26.4 m with average per foot BPT blow counts (N_B) of 52. Force and velocity ($v \cdot Z$) arrive at the tip module at approximately 6 ms (L/c) after the hammer impact, and again at the head module at 12 ms ($2L/c$) after impact when reflections from the initial wave front reach the pile top. L is the distance between the head module centerline and the pile base (30 m for this case), and c is the wave speed in the pile (5028 m/s). The observed disproportionality between force and velocity occurring early on in the pile head record is expected due to the reflections caused by shaft resistance and the discontinuities at the threaded joints causing impedance contrasts. The effect of multiple impedance contrasts would influence the stress waves reflected along the pile and subsequently would have an important bearing on signal matching with head measurements which requires modeling the entirety of the pile. When signal matching with the tip, as the present work is concerned with, the significance of the impedance contrasts is expected to be minimal.

The measured head and tip module displacement time histories are characterized by elastic rebound following maximum displacement (u_{max}) resulting in similar final, or residual sets (u_{res}).

The calculated energies at head and tip modules also exhibit a peak followed by a reduction to a plateau. The delivered energy to the tip module is lower due to energy losses caused by shaft resistance during wave transmission. The measured residual tip energy ($E_{res,Tip}$) associated with the plastic work to advance the pile base is expressed as a percentage of the rated hammer energy (10.85 kJ) and used to normalize the blow counts N_B to obtain energy normalized blow counts N_{B30} (DeJong et al., 2017). N_{B30} can be used to estimate equivalent SPT N_{60} values to characterize the denseness of the materials at the base (Ghafghazi et al., 2017). It is noted that N_{B30} is defined here using the residual energy measured directly at the tip module whereas Sy and Campanella (1994) had originally defined it in terms of the maximum energy measured at the pile head.

The force response and motion immediately at the pile base is obtained by transferring the measurements from the tip module sensor location. The transfer is performed by using closed-form transfer functions derived in frequency domain as defined in Eq. 1 to Eq. 4. The transferred force (f_M), displacement (u_M), velocity (v_M), and acceleration (a_M) immediately at the pile base are obtained from measured force (f_S) and acceleration (a_S) at the tip module sensor locations, also in frequency domain. d is the transfer distance (437 mm) shown in Figure 2a, Z is the pile impedance ($Z = E_sA/c$), and k is the wave number ($k = 2\pi h/c$), where h is the frequency. In deriving the transfer functions, the shaft resistance between the pile base and sensor location is assumed to be negligible. This is a reasonable assumption given that shaft resistance over this short length is in most cases negligible compared to the base resistance for competent materials, and the eight crowd-out teeth of the driving shoe (see Figure 2) are expected to further reduce the shaft resistance immediately behind the base.

$$f_M = \frac{e^{ikd}+e^{-ikd}}{2} f_S - \frac{(e^{ikd}-e^{-ikd})Z}{2ikc} a_S \quad [1]$$

$$u_M = \frac{e^{ikd}-e^{-ikd}}{2ikcZ} f_S - \frac{e^{ikd}+e^{-ikd}}{2k^2c^2} a_S \quad [2]$$

$$v_M = \frac{e^{ikd} - e^{-ikd}}{2Z} f_S + \frac{e^{ikd} + e^{-ikd}}{2ikc} a_S \quad [3]$$

$$a_M = \frac{(e^{ikd} - e^{-ikd})ikc}{2Z} f_S + \frac{e^{ikd} + e^{-ikd}}{2} a_S \quad [4]$$

Figure 4 illustrates the application of the transfer to the tip module measurements introduced in Figure 3b**.** F_M is the transferred force in time domain, and F_S is the measured forced at the sensor location also in time domain. The effect of the transfer is a smoothing of the response and reduction in the peak force, essentially removing the inertial effect induced by the mass of the pile below the sensors (35.4 kg) from the force record as well as a short (0.087 ms) lag. The transfer has no considerable effect on the velocity, except for inducing the same lag as the wave travels between the sensors and the base. For the remainder of this paper, the transferred forces (referred to as measured force, F_M) and motions are presented and used.

OBSERVATIONS ON PILE BASE RESPONSE

Tip force versus displacements over four consecutively recorded blows are shown in Figure 5a. The measurements demonstrate that relatively simple mechanics appear to occur at the base. On impact wave arrival, the soil is rapidly loaded from an initial locked-in residual force until onset of yield or plastic-flow-like behavior. Following maximum pile penetration, elastic rebound occurs to a final residual force, resulting in some amount of permanent set at the pile base.

The observed locked-in residual force has been recognized in pile driving analysis (Hunter and Davisson, 1969; Briaud and Tucker, 1984), and is related to the degree of shaft resistance, pile compressibility, and end-bearing soil characteristics. Physically, the compressive end-bearing force remaining at the end of a blow, and thus at the start of the subsequent blow is in equilibration with the downward shear forces developed along the pile shaft during decompression of the pile base from maximum displacement. The presence of the locked-in residual force means that the

base soil rests at a stress state closer to the limit resistance, and a smaller additional force is required to yield the soil in the subsequent impact. Thus, the apparent displacement to mobilize full resistance of an otherwise idealized linear-elastic, perfectly plastic soil for a given residual force is less than that for a soil beginning at a zero stress state.

Measurements obtained over an entire sounding are presented in Figure 5b, 5c and 5d. The figure shows profiles for blow counts per foot (N_B), energy normalized blow counts (N_{B30}), tip locked-in residual force (F_R), and the incremental change in the locked-in residual force per blow (ΔF_R / blow) for 3,371 recorded blows over 34 m of pile driving in a highly variable alluvial deposit. At this site, the ground water table was recorded at 11m. Recorded temperatures within the tip module during pile driving ranged from 5°C to 10°C. The locked-in residual force is zero at grade and generally accumulates with depth as shaft resistance accumulates. Local instances of reduction and re-accumulation are also observed with penetration into different layers. It is generally higher for denser materials and lower for looser materials, as denser materials can sustain larger residual forces due to their higher stiffness and resistance. In this sounding, residual forces reach a maximum of 300 kN (or 13.6 MPa when normalized by the pile closed-ended area), and increase rapidly with depth (Figure 5c), generally consistent with the observed reduction in energy dissipated at the tip as reflected by the divergence of N_B and N_{B30} (Figure 5b). While the measurements show that tip residual forces can vary substantially over depth, the incremental change in locked-in residual force within a single blow is relatively small (Figure 5d) meaning that locked-in residual forces are 'consistent' between the start and end of individual blows. The increment of locked-in residual force per blow is adequately captured within ± two standard deviations, or ± 8 kN (± 0.4 MPa) in Figure 5d.

The observed residual force at the base has important implications for the performance of

driven piles. Residual stresses directly influence the reflected stress waves from the pile-soil interaction, thus changing the distribution of energy. If ignored, the effect may be unrealistically compensated elsewhere, which would impact the parameters estimated from signal matching. In performing wave equation analysis of piles, residual forces are often incorrectly assumed to begin from a zero stress state at the start of the blow. To more accurately account for its effect, residual stress analysis (RSA) is sometimes performed (e.g. Holloway et al., 1979; and Rausche et al., 2010). Beginning from a zero stress state, the blow is iterated, with the static resistance at the end of the previous iteration becoming the starting static resistance of the next, until convergence of start and end blow is achieved. This type of analysis is analogous in concept to the observed consistency condition on the start and end locked-in residual force at the pile base presented in Figure 5. These observations reiterate the importance of including residual stresses in wave equation analyses.

Additional insight into the mechanics of pile driving can be gained by considering multiple recorded events in direct succession. Figure 6 shows the transferred force and $v{\cdot}Z$ of five records selected to represent typical responses observed in the entire database, and Figure 7 illustrates their force-displacement responses. Records 1 and 2 (Figure 7a and 7b) were obtained in granular materials, whereas records 3H, 3L, and 4 (Figure 7c, 7d, and 7e) were obtained in cohesive materials. The hysteretic plots are constructed using two sequentially recorded blows (every 4th blow), with the first recorded blow plotted three additional times (i.e. as 2nd, 3rd, and 4th consecutive blows) to infill before the next recorded blow. It is assumed that the blows not recorded are similar to those immediately before or after. The figure portrays pile driving as a steady penetration process with a backbone resistance and multiple unload-reload cycles when driving through one material (i.e. a quasi-steady state condition). The back-to-back presentation of blows indicates self-

similarity, with the initial loading of one blow directly following the unloading of the prior blow.

The penetration process depicted in Figure 7 is not fundamentally different from what occurs in static processes that include unload-reload cycles. Figure 8 shows static cyclic pile load test data from a bored bottom-instrumented pile that was tipped at a transition into a dense stratum (Osterberg, 1988). The penetration has not reached a steady level; nevertheless, the formation of a penetration backbone resistance asymptotically approaching a steady value is evident. The unload-reload cycles are very similar to those in Figure 7. The main difference between Figures 7 and 8 (apart from the transition influence in Figure 8) is the presence of dynamic components, generally manifested by a pronounced oscillation during the loading (reloading) phase where velocities and accelerations are higher. As expected, the dynamic effects are generally more pronounced in blows obtained in cohesive soils (Figures 7c, 7d, and 7e) and less pronounced in those obtained in granular materials (Figures 7a and 7b).

Given the expectation of a single steady penetration backbone for a given soil, it is not unrealistic to expect that the backbone resistance value may change at a layer transition between two materials as shown in the static measurements of Figure 8. Figure 9 shows dynamic RTP tip measurements made during penetration across layer transitions. The force-displacement response during transition from a soft clay to a dense silty sand, followed by the exit transition back to a soft clay, is illustrated in Figure 9a, and 9b respectively. Recorded blows are plotted back-to-back instead of filling in the gaps by repeating recorded blows (as in Figure 7) in order to present how the records change across the transition. The similarity between the observed unload-reload behavior and backbone resistance formation of Figure 9 and Figure 8 is evident.

The formation of a steady penetration resistance when driving through one material is conditional on the displacement being sufficient to mobilize full plastic yielding of the soil (i.e.

mobilize the "quake"). As a general rule of thumb for driven piles, quake is mobilized at approximately 1/120 the pile diameter (Goble and Rausche, 1976). In the case of the Becker pile (O.D. = 168 mm) displacements less than 1.4 mm or blow counts (N_B) in excess of 220 will be problematic. Figure 10a presents the soil hysteresis for a case where quake is not fully mobilized (N_B = 240) and hence the steady penetration condition is not achieved, while Figure 10b illustrates a case of complete refusal. In both cases, the pile tip advances through 'ratcheting' (gradual accumulation of small permanent deformations from repetitive loading) as opposed to large deformation, plastic yielding of the soil. Within individual blows, a defined plateau is not identifiable.

SIGNAL MATCHING USING DIRECT MEASUREMENTS

Representative Records for Signal Matching

The records presented in Figures 6 and 7 are a subset from a larger database that was used for signal matching analyses in order to investigate the adequacy of the spring-dashpot-mass models for capturing the overall base response. The presented blows represent driving in cohesive and non-cohesive materials of varying densities. For the selected records, N_{B30} values range between 10 to 70 (equivalent N_{60} values between 18 and 126), and the residual energy delivered to the tip ($E_{res,Tip}$) ranges from about 5 to 20 percent of the rated hammer energy. Records 3L (low energy) and 3H (high energy) were selected in adjacent soundings at the same depth but with different shaft resistance and tip energy values (achieved by pre-drilling in 3H) to investigate the influence of different dynamic conditions.

Signal Matching Methodology

To model the pile-soil interaction at the base, an idealized single degree of freedom model was adopted consistent with current practices. The model consists of a non-linear spring in parallel with a viscous dashpot, and an inertial mass, as illustrated in Figure 2b. The nonlinear spring captures the static loading, yielding, and unloading, and the viscous dashpot represents the dynamics contributions due to radiation damping and rate effects. The mass accounts for additional inertial effects due to radiation, and/or soil mass (plug) moving with the pile base. The computed force response at a given time can be resolved into static and dynamic components as expressed by

$$F_c(t) = R_u(t) + R_v(t) + R_a(t) \qquad [5]$$

where R_u is the displacement dependent static component, R_v is the velocity dependent dynamic component, R_a is the acceleration dependent dynamic component, and t is the time.

Figure 11 presents two static models (i.e. non-linear springs) including an elastic-plastic (EP) model (e.g. Rausche et al. 2010) and a hyperbolic model. The static models are generally defined by three parameters: the initial loading stiffness (K_b), limit resistance (R_{bL}), and unloading stiffness (K_{bu}). For the hyperbolic model, a load-settlement relationship given by Eq. 6 is used.

$$R_u(t) = \frac{R_{rev} + K(u(t) - u_{rev})}{1 + |u(t) - u_{rev}|\left(\frac{K}{R_{bL}}\right)} \qquad [6]$$

In Eq. 6, u_{rev} and R_{rev} are the displacement and static resistance at the last force reversal point, respectively. The quantity K is the stiffness which is taken equal to K_b for initial 'virgin' loading, and K_{bu} for subsequent unloading and reloading. In the hyperbolic model, R_{bL} is asymptotically approached at large displacements. For practical purposes, where quake is mobilized, the difference between the mobilized static resistance at maximum displacement and R_{bL} is negligible (see Figure 11b). The locked-in residual force, F_R, is an additional static parameter

that must satisfy the consistency condition described earlier. The dynamic components are calculated using Eq. 7 and 8. Following the conventions of wave equation analyses, damping is quantified using the parameter, j_b, where the product of j_b and R_{bL} represent viscous damping (Rausche et al., 2010). The inertial mass, M_b, produces the inertial resistance force when multiplied by the acceleration at the base.

$$R_v(t) = j_b R_{bL} v(t) \quad [7]$$

$$R_a(t) = M_b a(t) \quad [8]$$

Measured displacement, velocity, and acceleration are used directly in the model, with the parameters K_b, K_{bu}, R_{bL}, j_b, and M_b adjusted to minimize the weighted mean-squared error (*wMSE*) between the measured and computed force response (Eq. 5). The weighting function, is defined to be constant from impact arrival to the point of maximum displacement, and linearly decreasing to the end of the blow. By virtue of the direct measurements with which the computed response is matched, consistency of locked-in residual force is enforced in the analysis.

Non-uniqueness of Inferred Static and Dynamic Components

Non-uniqueness at the element level arises due to uncertainty in the relative contributions of static and dynamic components to the total response. As noted previously, this is a consequence of the governing equation (see Eq. 5). This non-uniqueness is illustrated with examples of different solutions from signal matching analyses using the hyperbolic model on record 2 as presented in Figure 12a, 12b, and 12c, respectively. The figure shows the measured force (F_M), computed force (F_C), and computed static (R_u) and dynamic (R_v and R_a) contributions. The three fits in Figure 12 show nearly identical matches between F_C and F_M despite significantly different static loading stiffnesses. A softer static response can be balanced by higher dynamic contributions (damping)

early in the record, and vice-versa. It is shown that while the measured dynamic base soil response can be adequately captured using the simple model formulation selected, the estimated contributions are not necessarily unique, even when direct measurements eliminate the uncertainty associated with the distribution of the total response along the pile. Further, the results illustrate the uncertainty associated with signal matching and the possible deviations in the estimated static response that may arise when match quality is used as the sole selection criteria. It is therefore of interest to distinguish regions of higher and lower uncertainty, and to further constrain the solution where more uncertainty exists.

Generally, the greatest uncertainty occurs during initial loading where velocity and acceleration are the highest. As shown in Figure 12 (load-displacement plots), both velocity and acceleration significantly decrease as the displacements approach their peak values, and remain relatively small during the rebound portion of the record. Accordingly, all the fits essentially attain the same computed maximum mobilized static resistance ($R_{bL,m}$) by the time of peak displacement because velocity is zero and acceleration is small at this point. Further, the unload response is forced to be compatible with the final residual force, which can only be satisfied by the displacement-based static component (R_u). The consequence of the distribution of uncertainty over the blow is that the limit resistance and unloading stiffness (R_{bL} and K_{bu}) do not change appreciably amongst different solutions in Figure 12. Instead, it is the loading stiffness, K_b, and accordingly the dynamic components and particularly the damping factor, j_b, that are most uncertain.

While the uncertainty in estimating the static loading stiffness cannot be eliminated, a lower bound can be identified for a typical blow in the case of the steady penetration process depicted in Figure 7 (a sustainable condition). The constraint is based upon the reasoning that energy cannot be created by an unload-reload cycle. This condition is similar to Drucker's stability

postulate (Drucker, 1959) that ensures energy is not generated when a system is loaded and unloaded to the same stress level. In Figure 13, the area A_1 highlighted under the force-displacement unload-reload curves represents the energy dissipated in the static process. In order for the unload-reload loop not to generate energy, the area A_1 must be greater than or equal to area A_2. This leads to a practical constraint that the residual energy of the computed static response must be greater than or equal to the product of the maximum mobilized static resistance value, $R_{bL,m}$, and the residual set, u_{res} (Eq. 5).

$$E_{res,static} \geq R_{bL,m} \times u_{res} \qquad [9]$$

$E_{res,static}$ is the area under the static force-displacement curve for one impact, including the locked-in residual force. Since the limit resistance and unloading can be computed with higher certainty, Eq. 9 essentially applies a lower limit on the loading stiffness, K_b, favoring a stiffer loading response. In the case of the EP model (with no gap opening in unloading), the condition forced on loading stiffness through Eq. 9 simply translates to $K_b \geq K_{bu}$. The lower bound condition on the loading stiffness translates into an upper bound for the damping factors and inertial masses that would produce acceptable matches to the measured total response. It is possible to imagine temporary cases where an abrupt transition from a stiff material to a soft one may create a stiffer unloading curve than reloading. From an energy perspective, energy stored in other parts of the system (surrounding soil, or compressed pile) is temporarily added to the unload-reload cycle. Such rare cases are not of concern to the current work which is dealing with typical steady state blows that are used for pile driving analyses.

The three non-unique responses previously presented in Figure 12 can now be reconsidered. According to Eq. 9, with u_{res} = 5.8 mm and $R_{bL,m}$ = 320 kN, the minimum allowable $E_{res,static}$ would be 1.86 kJ. The solutions shown in Figures 12a, 12b and 12c have $E_{res,static}$ values of 2.12 kJ, 1.81

kJ, and 1.59 kJ accordingly. Hence only the solution with the stiffest loading response shown (12a) is allowed when limiting the loading stiffness K_b by Eq. 9.

Signal Matching Results

The elastic-perfectly-plastic (EP) and hyperbolic static models along with the viscous damping and inertial component described by Eq. 7 and 8 were fit to the five representative blows shown in Figure 6 and 7. Consistency of locked-in residual force and the loading stiffness condition described by Eq. 9 were applied in all analyses. Figure 14 shows the results in force-time, and force-displacement spaces, with both the measured force (F_M) and the computed force (F_C) plotted for comparison. The figure also shows the static, viscous damping, and inertial force contributions. Model parameters estimated from the analyses are summarized in Table 1.

The results demonstrate that the measured base soil response can be adequately captured using the simple spring-dashpot-mass models. Table 1 shows that for both static model formulations damping factors are generally lower (0.04 to 0.06 s/m) in records 1 and 2, which were obtained in granular materials, than for records 3H, 3L, and 4 (0.15 to 0.18 s/m) which were obtained in more clayey materials. These results appear consistent with expectations that granular materials exhibit minimal rate effects compared to cohesive soils.

The damping factors obtained from direct dynamic measurements at the tip suggests a lower range than typically used in the industry: minimum of 0.04 s/m (Rausche, 2005) and average of 0.5 s/m (GRL, 1997). The lower damping values obtained is a direct consequence of the condition imposed by Eq. 9 resulting in a lower bound on the loading stiffness, hence limiting the damping factors. The damping factors shown in Table 1 for the EP model can also be converted to the Case damping factor ($j_c = j_b \cdot R_{bL}/Z$) equivalent for which recommendations exist. Dividing

the computed $j_b \cdot R_{bL}$ by the pile impedance, Z (376 kN·s/m) yields $\underline{j_c}$ values ranging from 0.04 to 0.08 for all records. These are also lower than the conventionally assumed in CAPWAP of 0.05 to 0.20 for sands, 0.60 to 1.10 for clays, and 0.15 to 0.70 for their mixtures (Rausche et al., 1985).

Inertial mass terms range from 0 to 351 kg and 0 to 197 kg for the EP and hyperbolic models, respectively. The inertial mass values do not appear unreasonable for a soil wedge or plug at the base of the Becker pile. As an example, for record 4, assuming a three quarter volumetric sphere and unit weight of 2000 kg/m^3 for the soil, the implied radius of the soil mass would be 0.22 to 0.25 m; a reasonable zone of soil around the 0.168 m diameter closed-ended pile tip. The peak force captured by the inertial mass term may depend on the strength of the soil, plasticity, and layer transitioning effects amongst other driving factors.

The estimated stiffnesses and limit resistances for the records tend to increase with N_{B30} (or penetration resistance in general). The computed limit resistances of records 3H (high energy) and 3L (low energy) from adjacent soundings in the same materials agree well, with values within 10% of one another. However, the stiffness value in 3L is higher compared to 3H (Table 1). Record 3H is a special case where Eq. 9 is satisfied without resulting in stiffer loading than unloading. Inspection of the signal matching results for Record 3H in Figure 14a shows that the force response is adequately captured (within model limitations), and that the initial loading stiffness cannot be increased any further. In the force-displacement curves of this record (Figure 7d), the force goes to zero upon unloading, and remains close to zero as the pile rebounds to its final residual set (i.e. a temporary gap is formed). The gap formation at the end of the blow in 3H, and unloading of the soil to a zero stress state may explain a softer reloading response at the start of the following blow. Nevertheless, the condition set by Eq. 9 is applicable and has been used to constrain the loading stiffness.

The limit resistance in both models is close to the unload point at maximum penetration where dynamic effects are negligible. The unload point demarcates the major loading and unloading regions. At this point, velocity is zero and acceleration is generally small, resulting in the total resistance being instantaneously comparable to the maximum mobilized static resistance, $R_{bL,m}$. Provided sufficient displacement is attained, this would be also comparable to the limit static resistance, R_{bL}, regardless of the dynamic parameters. The inferred unloading stiffness is not sensitive to the choice of the dynamic parameters either. This is because the velocity and acceleration remain small, rendering the total response nearly static from the unload point forward.

The existing modeling framework has been shown to work adequately for capturing the measured base response if the mechanical aspects of pile driving at the base are properly accounted for. The difference between EP and hyperbolic static models appears to be marginal, with the hyperbolic model better capturing the transition from loading to steady penetration, and the unloading nonlinearity.

IMPLICATIONS FOR WAVE EQUATION ANALYSES

The observations and arguments presented were made possible by the direct dynamic measurements at the pile base using the instrumented reusable test pile (RTP). However, the wave equation analyses commonly used by industry for signal matching to above ground dynamic measurements can benefit from these findings.

- Simple model formulations such as linear-elastic-perfectly-plastic or hyperbolic static models, viscous damping, and constant mass inertial contribution appear to be sufficient for capturing the dynamic response at pile base.
- Each individual blow should be viewed as an event amongst a series of essentially identical

blows. The loading portion should be viewed as reload that is occurring after the unload portion (of a prior blow), and should, in general, be stiffer than the unloading portion to avoid impossible energy generation. For the unusual case of gap formation, particularly in low resistance soils, a softer initial loading response may be justifiable, but must be constrained using Eq. 9.

- Consistency of locked-in residual force is an important aspect of the analysis that becomes evident by viewing each individual blow as one in a series of identical ones. The locked-in residual force consistency has been recognized in pile driving analysis (e.g. Holloway et al. 1979; and Rausche et al., 2010) in what is more commonly referred to as residual stress analysis (RSA).
- At the moment rebound from maximum displacements starts, the velocity at the contact between pile base and soil is zero and the acceleration is small. The total force at this point is very close to the static limit resistance, given that the soil has reached yielding (quake is mobilized).
- Implementing the recommendations made regarding residual force consistency and energy constraint on static load/unload stiffnesses can help reduce the non-uniqueness aspect of signal matching in separating static and dynamic components. The non-uniqueness of computed distribution of the total response along the pile still persists and requires further investigation.

CONCLUSIONS

A new tool capable of capturing the dynamic base response and residual stresses at the pile tip during driving was introduced. A number of mechanistic constraints supported by the

measurements were proposed. Recognizing that such direct measurements are, and will likely remain limited to research endeavors, a number of general recommendations were offered for wave equation analyses performed on aboveground measurements in practice.

Presented measurements show that simple mechanics govern the dynamic measurements during pile driving. The soil is loaded from an initial locked-in residual force, yields, reaches a maximum displacement, and then rebounds to a final residual set and locked-in residual force. Consideration of consecutive blows shows consistency of the locked-in residual force over a given blow, as well as self-similarity between blows. Direct measurements illustrate the formation of a back-bone limit resistance during pile driving. During penetration through one material, it is consistent with a quasi-steady-state penetration process.

Non-uniqueness of signal matching solutions in separating static and dynamic contributions was demonstrated with models when match quality was used as the sole selection criterion. More uncertainty exists in initial static loading due to the presence of high dynamic contributions. The estimated limit resistance and unloading stiffness can be determined with more certainty due to diminished dynamic contributions following peak displacement. Practically, the static limit resistance is equal to the total response near the unloading point at maximum displacement where dynamics are small.

An important energy conservation constraint is proposed for the inferred static response for the typical case of steady penetration conditions. The constraint sets a lower limit on the loading stiffness, resulting in an upper bound for damping coefficients. As a result, soft loading stiffnesses produced by analyses that solely rely on signal match quality are not permissible.

Signal matching results for representative blows performed with adherence to the residual force consistency and fundamental energy conservation principles shows that the existing simple

spring-dashpot-mass models are adequate for capturing the base soil response. Ockham's razor favors using these simple models over more complicated ones, which may be redundant, or produce erroneous results depending on their formulation.

ACKNOWLEDGEMENTS

The authors would like to acknowledge the funding provided by California Department of Transportation (Caltrans) under contract No. 201222670. The funding and collaboration of California Department of Water and Los Angeles Department of Water and Power in developing the equipment and obtaining the data are also greatly appreciated. The help and input from Tom Schantz of Caltrans, Jim Benson of Great West Drilling, and finally of Dan Wilson, Bill Sluis, Daret Kehlet, Alex Sturm, and Chase Temple of University of California Davis are also greatly appreciated.

REFERENCES

Briaud, J.L., and Tucker, A.M. (1984). "Piles in sand: a method including residual stresses". ASCE J. Geotech Eng., 110(11), 1666-1680.

Dayal, U., and Allen, J.H. (1975). "The effect of penetration rate on the strength of remolded clay and sand samples." Can. Geotech. J., 12(3), 336-348.

DeJong, J.T., Ghafghazi M., Sturm A.P., Wilson D.W., den Dulk J., Armstrong R.J., Perez A., and Davis C.A. (2017). "Instrumented Becker Penetration Test: equipment, operation, and performance". ASCE J. Geotech. and GeoEnv. Eng., under review.

Ghafghazi, M., DeJong, J.T., Sturm, A.P., and Temple, C.E. (2017). "Instrumented Becker Penetration Test: The application of SPT and iBPT for liquefaction assessment in gravelly

soils". ASCE J. Geotech. and GeoEnv. Eng., under review.

Ghafghazi, M., DeJong J.T., and Wilson, D.W. (2017). "Evaluation of Becker Penetration Test Interpretation Methods for Liquefaction Assessment in Gravelly Soils". Can. Geotech. J., under review.

Glanville, W.H., Grime, G., Fox, E.N., and Davies, W.W. (1938). "An investigation of the stresses in reinforced concrete piles during driving". Department of Scientific and Industrial Research, British Building Research Board, London, England.

Fellenius, B.H. (1998). "Variation of CAPWAP results as a function of the operator". Proc., 3rd Int. Conf. on the Application of Stress-Wave Theory to Piles, Ottawa, May 25-27, 1988, 814-825.

Coyle, H.M., and Gibson, G.C. (1970). "Empirical damping constants for sands and clays". ASCE J. Soil Mech. Found. 96(3), 949-965.

Goble, G.G., and Rausche, F. (1976). "Wave equation analysis of pile driving, WEAP program". U.S. Dept. of Transportation, Federal Highway Administration, Washington, DC. Report FHWA-IP-76-13 (4 Vols.).

Goble Rausche Likins and Associates, Inc. (GRL). (1997). "Wave equation analysis of pile driving: GRLWEAP background, procedures and modeling".

Hereema, E.P. (1979). "Relationships between wall friction, displacement, velocity, and horizontal stress in clay and in sand, for pile drivability analysis". Ground Engineering, 12(1), 55-65.

Holloway, D.M., Cloug, G.W., and Vesic, A.S. (1979). "A rational procedure for evaluating the behavior of impact-driven piles". Behavior of Deep Foundations, ASTM STP 670, American Society for Testing and Materials, 335-357.

Hunter, A.H., and Davisson, M.T. (1969). "Measurement of pile load transfer". Performance of

Deep Foundations, ASTM STP 444, American Society for Testing and Material, 106-117.

Kramer, S.L. (1996). Geotech. Earthquake Eng., Prentice Hall, Upper Saddle River, New Jersey.

Loukidis, D., Salgado, R., and Abou-Jaoude, G. (2008). "Assessment of axially-loaded pile dynamic design methods and review of INDOT axially-loaded pile design procedure". U.S. Dept. of Transportation, Federal Highway Administration, Washington, D.C. Report FHWA/IN/JTRP-2008/6.

Lysmer, J. (1965). "Vertical motion of rigid footings". Report No. 3-115, U.S. Army Engineer Waterway Experiment Station, Corps of Engineers, Vicksburg, Mississippi.

Masouleh, S.F., and Fakharian, K. (2008). "Verification of signal matching analysis of pile driving using finite difference based continuum numerical method". Int. J. of Civil Eng., 6(3), 174-183.

Middendorp, P., and van Zandwijk, C. (1985). "Accuracy and reliability of dynamic pile testing techniques." Proceedings 4th International Conference on Behavior of offshore structures (BOSS), Delft, Netherlands.

Middendorp, P., and van Weele, A.F. (1986). "Application of characteristics stress wave method in offshore practice." Proceedings of 3rd International Conference on Numerical Methods in Offshore Piling, Nantes, Supplement, 6-18

Middendorp, P. (2004). "Thirty years of experience with the wave equation solution based on the method of characteristics". Proc., 7th Int. Conf. on the Application of Stress Wave Theory to Piles, Kuala Lumur, Malaysia.

Osterberg, J.O. (1988). "The Osterberg load test method for bored and driven piles - the first ten years". Proc., 7th International Conference and Exhibition on Piling and Deep Foundations, Deep Foundations Institute, Vienna, Austria.

Randolph, M.F., and Deeks, A.J. (1992). “Dynamic and static soil models for axial pile response”. Proc., 4th Int. Conf. on the Application of Stress-Wave Theory to Piles, Balkema, Rotterdam, p. 3-14.

Rausche, F., Goble, G.G., and Likins, G.E. (1985). “Dynamic determination of pile capacity” ASCE J. Geotech. and GeoEnv. Eng., 111, 367-83.

Rausche, F., Likins, G., Liang, L., and Hussein, M. (2010). “Static and dynamic models for CAPWAP signal matching”. Art of Foundation Engineering Practice, 534-553.

Rausche, F., Goble, G.G., and Likins, G. (1992). “Investigation of dynamic soil resistances on piles using GRWEAP”. Application of Stress-Wave Theory to Piles, Balkema, Rotterdam.

Smith, E.A.L. (1960). “Pile-driving analysis by the wave equation”. ASCE J. Soil Mech. Found. 86(4), 35-61.

Taylor, D.W. (1948). Fundamental of Soil Mechanics, John Wiley and Sons, New York, New York.

Tran, K.T., McVay, M., Herrera, R., and Lai, P. (2012). “Estimating static tip resistance of driven piles with bottom pile instrumentation”. Canadian Geotech. J., 49(4), 381-393.

Table 1. Summary of estimated parameters from signal matching

Record ID	F_R[a] (kN)	Elastic-Plastic Static Model					Hyperbolic Static Model				
		K_b (kN/mm)	K_{bu} (kN/mm)	R_{bL} (kN)	j_b (s/m)	M_b (kg)	K_b (kN/mm)	K_{bu} (kN/mm)	R_{bL} (kN)	j_b (s/m)	M_b (kg)
1	109	210	189	521	0.06	54	689	358	670	0.04	20
2	71	140	130	308	0.06	103	510	234	350	0.05	79
3L	54	243	201	157	0.16	0	733	333	169	0.18	0
3H	35	77	104	170	0.13	1	170	317	185	0.14	42
4	0	107	104	87	0.17	351	202	211	88	0.12	197

[a] The locked-in residual force is prescribed in the analysis here. It would be an additional model parameter in general wave equation analysis, determined through an iterative process.

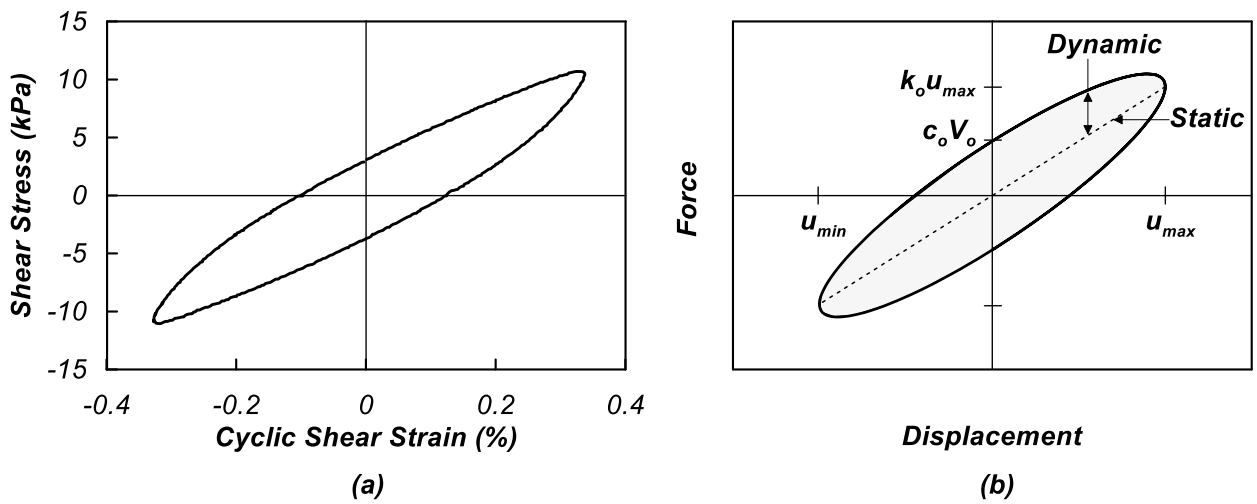

Fig. 1. a) Soil hysteretic behavior from an undrained cyclic direct-simple-shear test (after Lanzo et al., 2009); b) Hysteretic material damping modeled with a linear elastic spring (static) and viscous dashpot (dynamic).

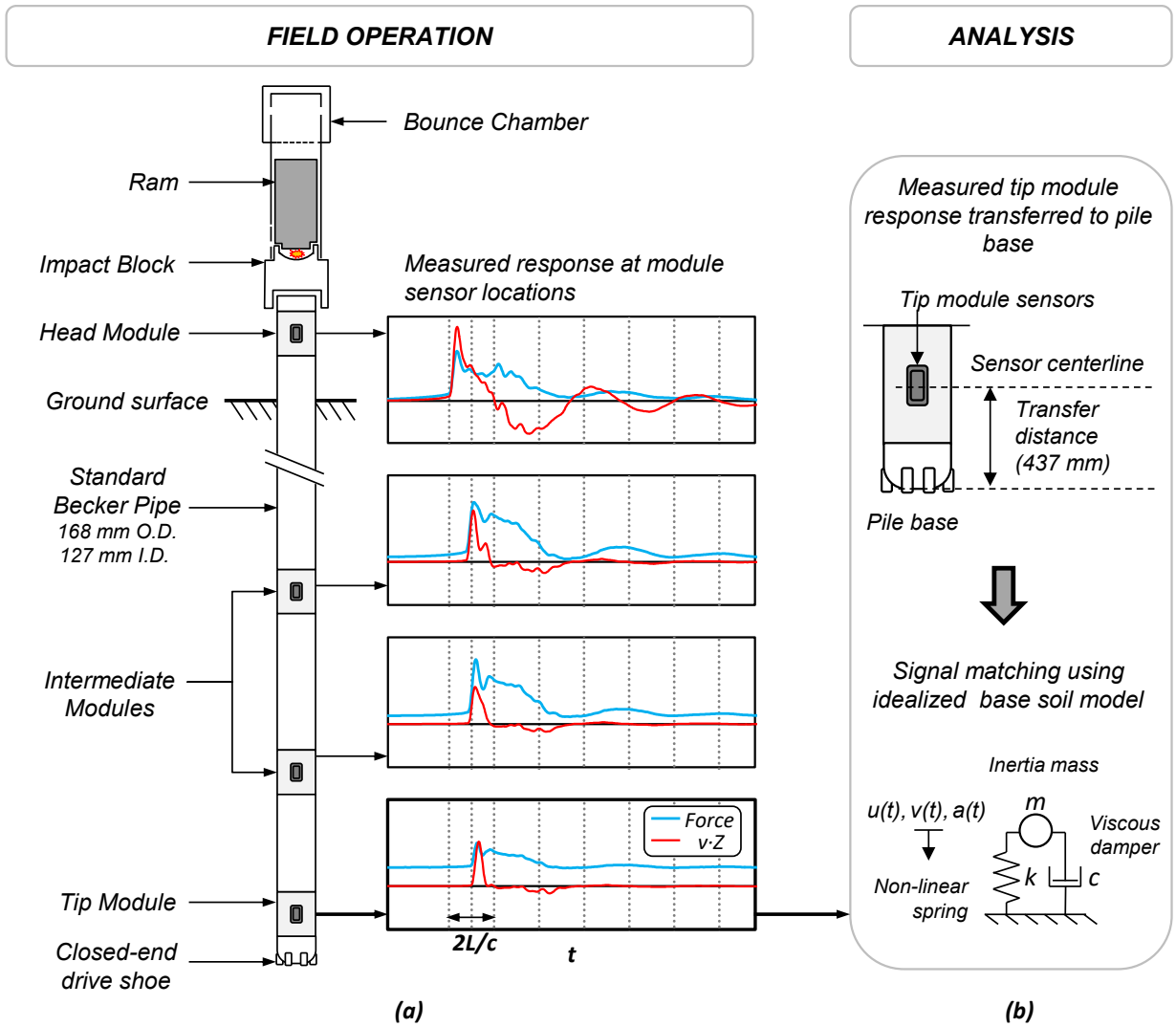

Fig. 2. a) Schematic of RTP system setup during typical field operation, showing hammer system, instrumented modules, and dynamic measurements; b) Use of dynamic tip module measurements for analysis of the pile base.

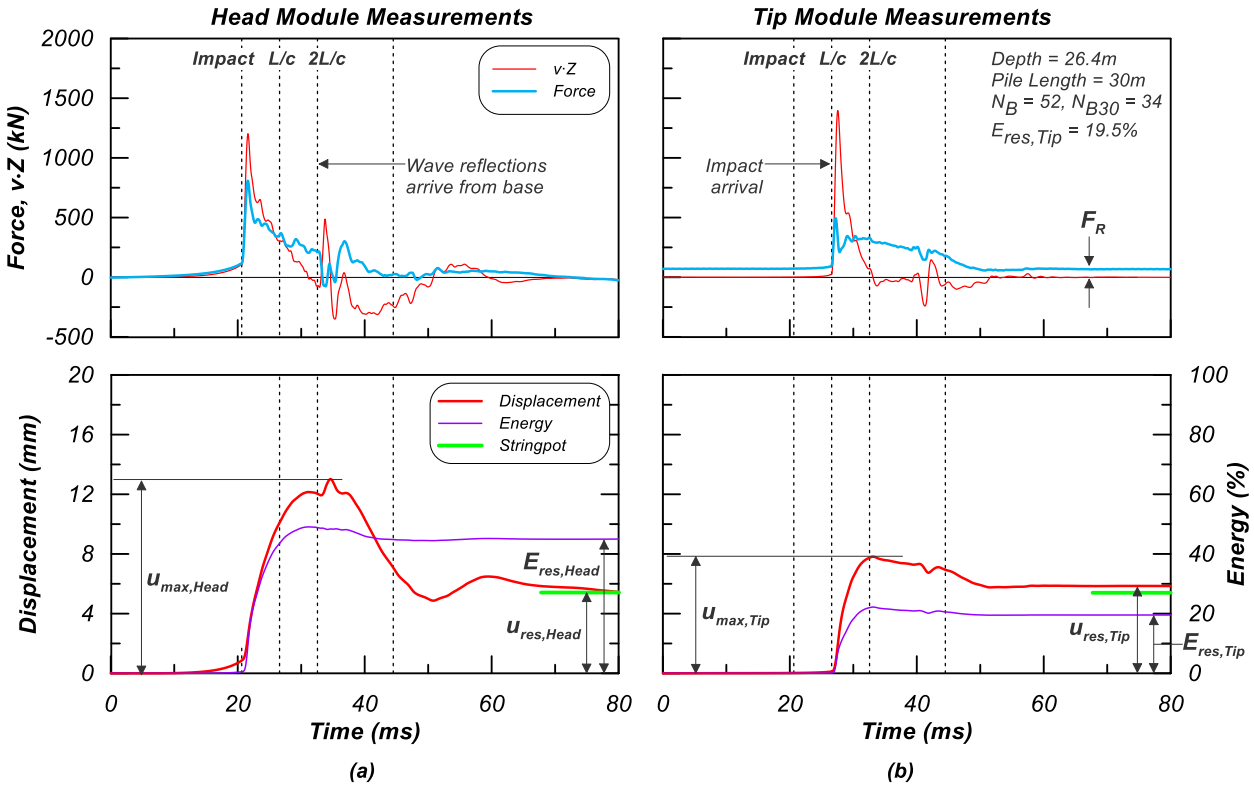

Fig. 3. Example RTP dynamic measurements recorded over a single blow; a) Head module; b) Tip module sensor locations. The top row shows force and *v·Z*, and the bottom row shows displacement and energy during pile driving at a depth of 26.4 m.

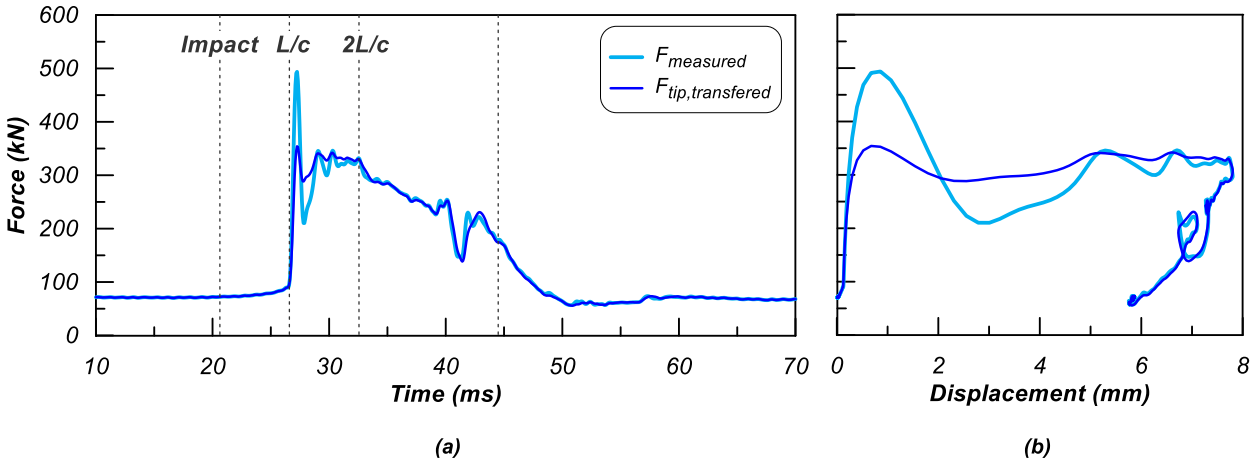

Fig. 4. Application of wave transfer at the tip; a) Force vs. time; b) Force vs. displacement.

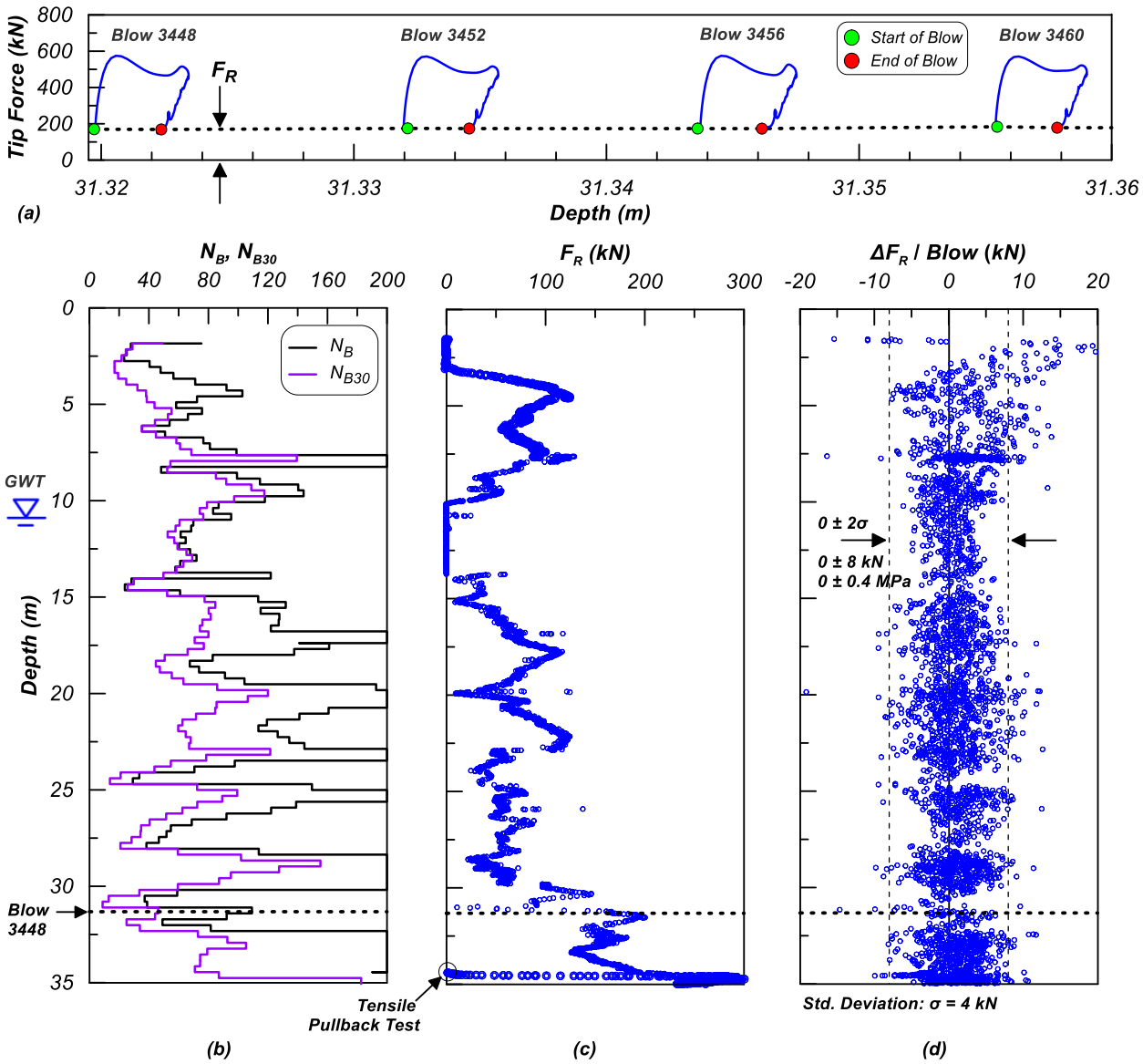

Fig. 5. RTP data for one sounding; a) RTP tip force vs. displacement (depth) as recorded over four blows during pile driving; b) Raw blow counts (N_B) and normalized blow counts (N_{B30}); c) Locked-in residual force (F_R); d) Change in locked-in residual force (ΔF_R) per recorded blow.

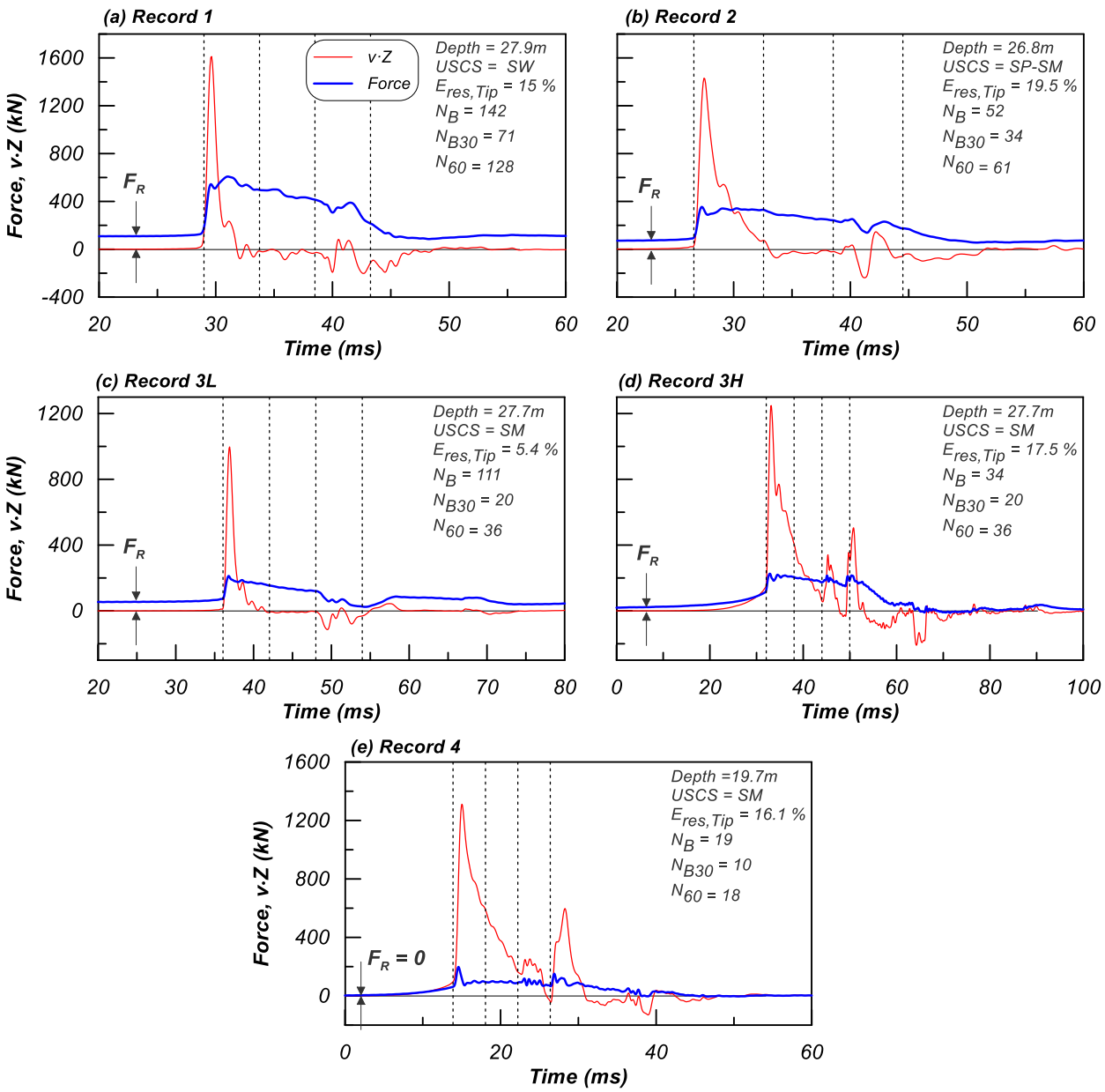

Fig. 6. Representative blows (transferred) for signal matching analyses. Records represent driving in cohesive and non-cohesive materials with different densities; a) Record 1; b) Record 2; c) Record 3L; d) Record 3H; e) Record 4.

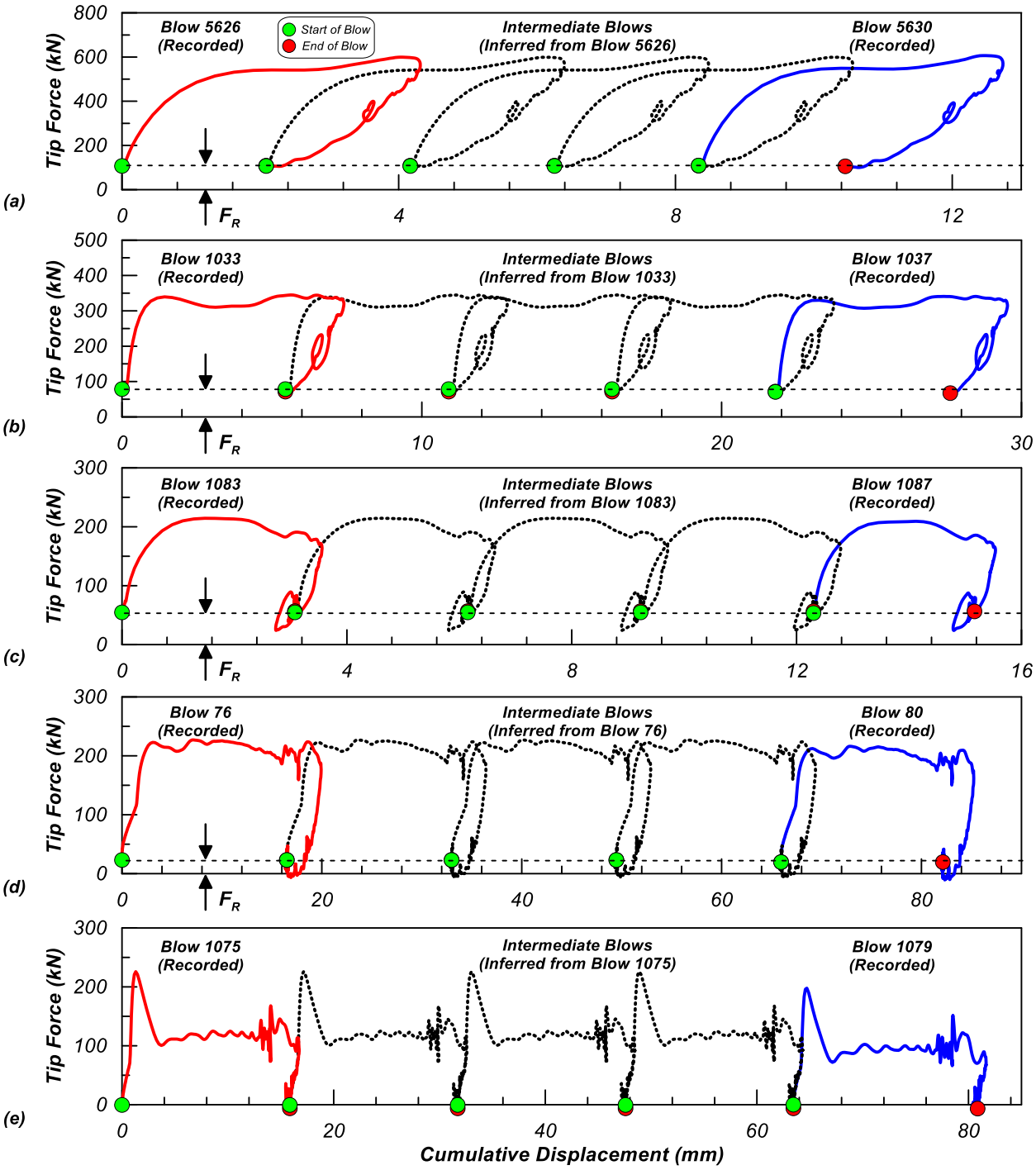

Fig. 7. Measured force vs. displacement for representative records presented in actual sequence; a) Record 1; b) Record 2; c) Record 3L; d) Record 3H; e) Record 4. The continuous response is constructed from two sequentially recorded blows by reproducing the unrecorded blows in between from the first recorded one.

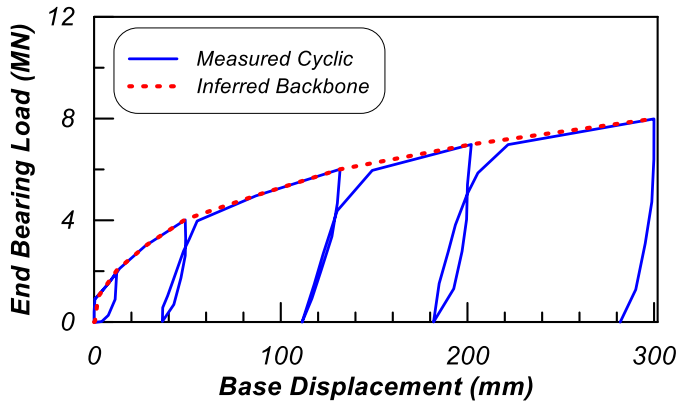

Fig. 8. Static load/unload test from a bottom-instrumented bored pile tipped in dense silty sand transition and inferred monotonic (backbone) curve (after Osterberg, 1998).

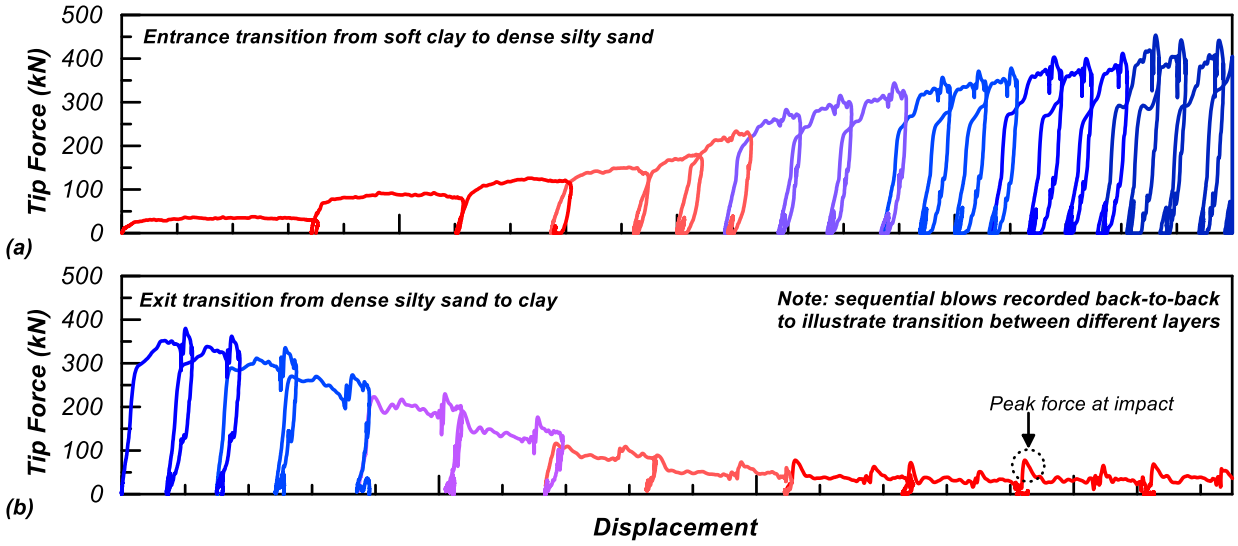

Fig 9. Measured force vs. displacement presented in sequence of recorded displacements illustrating formation of a penetration backbone resistance; a) Transition from soft clay to dense silty sand; b) Transition from dense silty sand to clay.

.

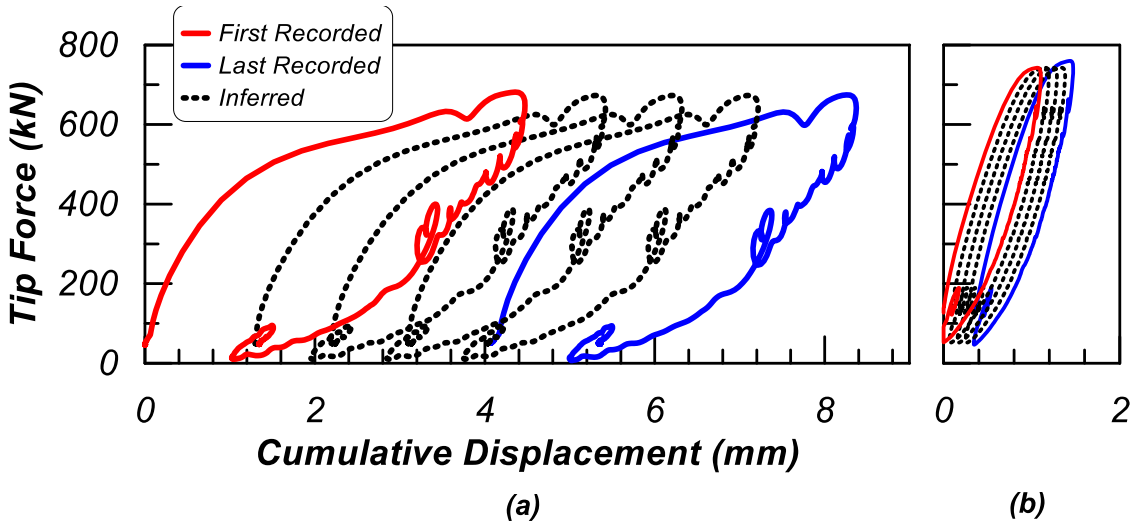

Fig. 10. Example RTP measurements showing a) hard driving with N_B = 240, and b) practical refusal conditions, illustrating a representative case where quake is not fully mobilized.

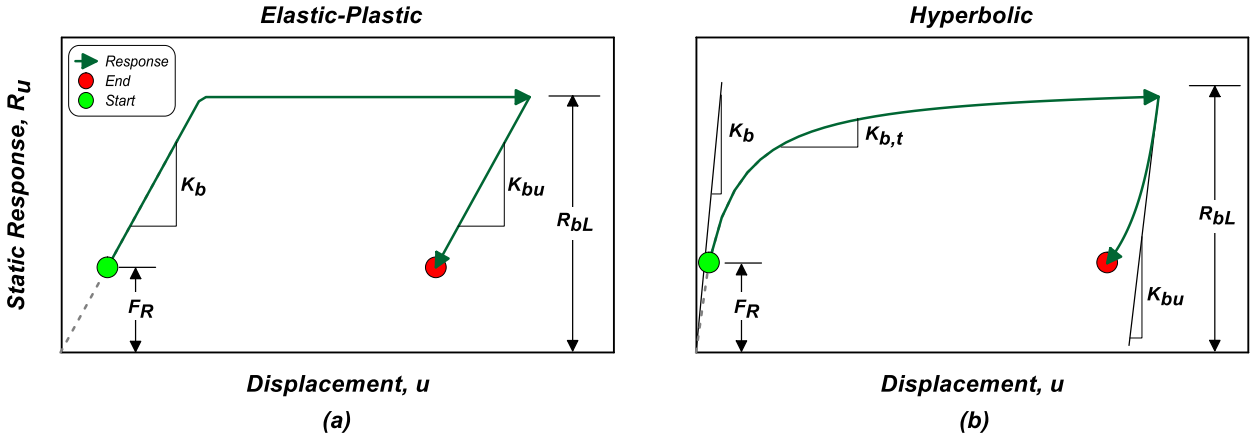

Fig. 11. Static force-displacement models used for signal matching; a) elastic-plastic model; b) hyperbolic model.

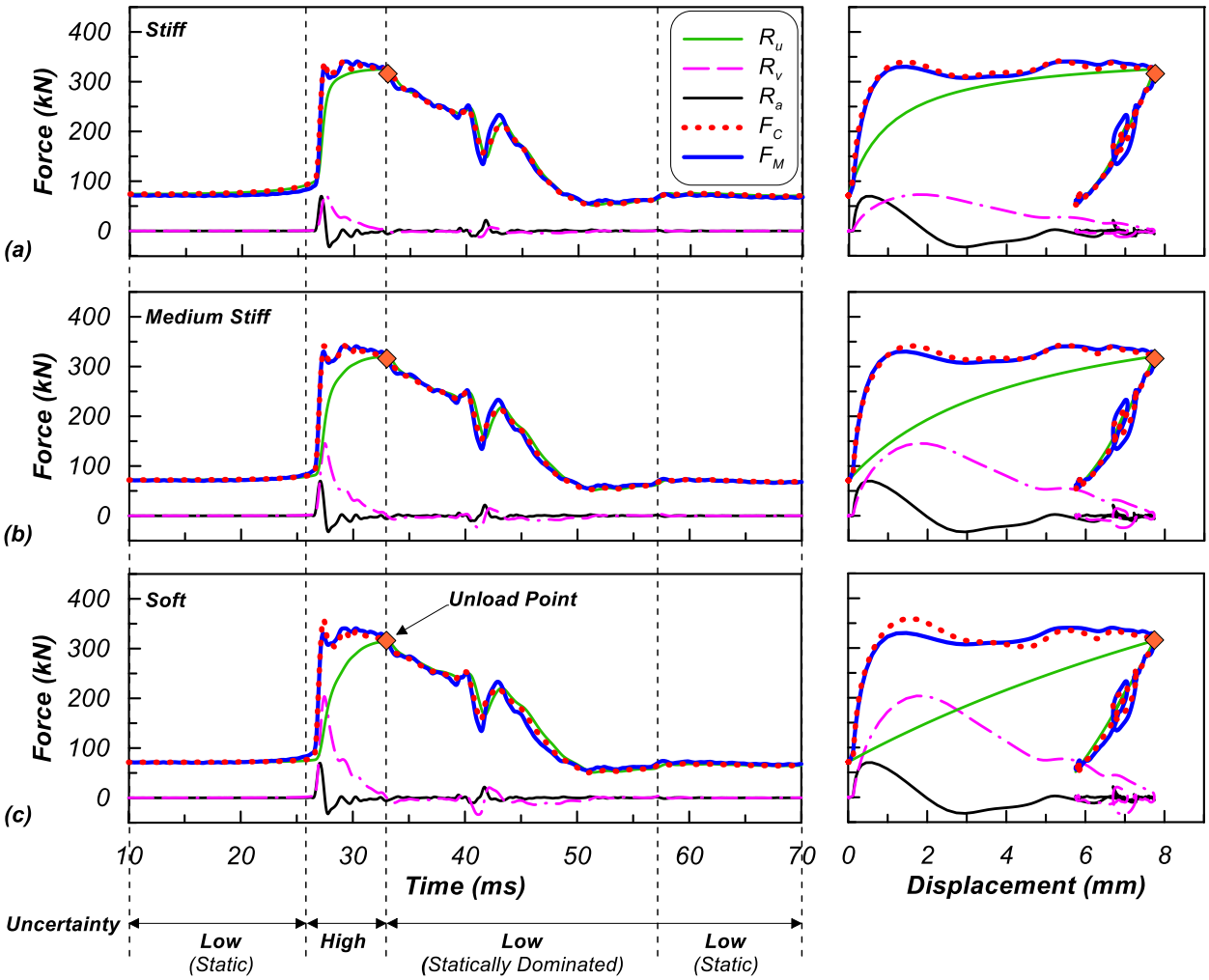

Fig. 12. Non-uniqueness of signal matching results with variable static loading stiffness; a) Stiff initial loading response; b) Medium initial loading response; c) Soft initial loading response. R_u is the displacement-dependent static component, R_v is the velocity-dependent viscous damping component, R_a is the acceleration-dependent inertia component, F_c is the total computed response, and F_m is the measured response.

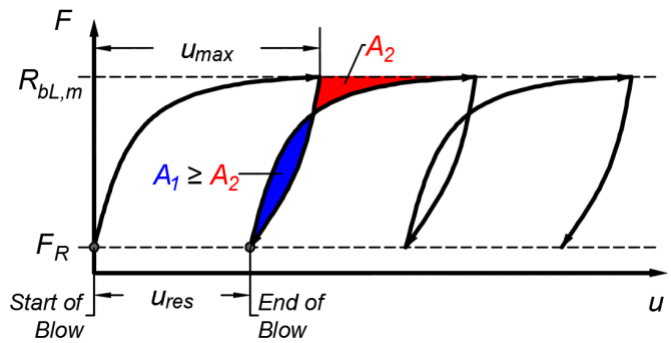

Fig. 13. Schematic showing the condition on unload-reload cycles to satisfy energy loss in unload-reload compared to steady penetration.

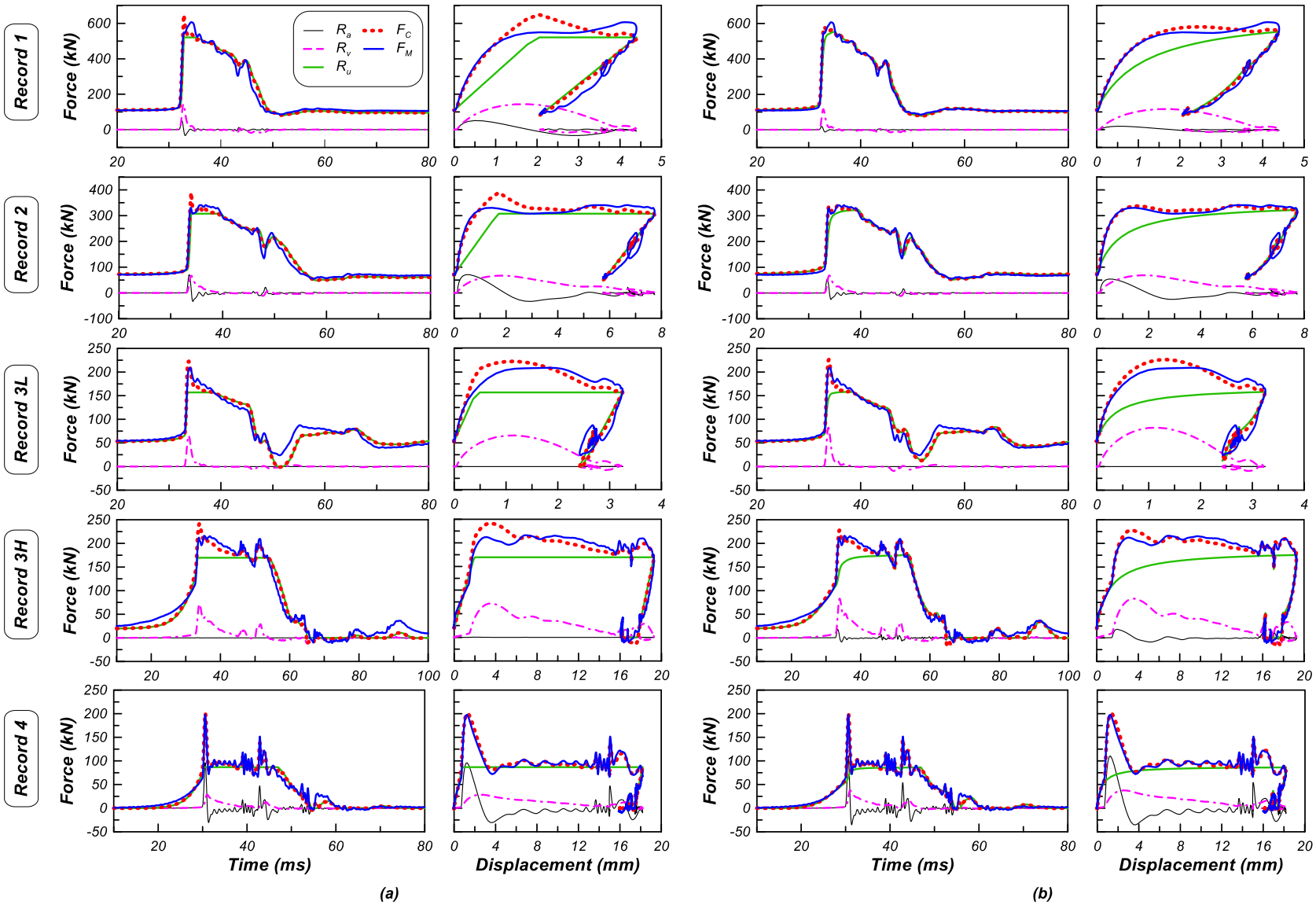

Fig. 14. Signal matching results for representative records; a) Elastic-plastic static model; b) Hyperbolic static model. R_u is the static component, R_v the viscous damping, and R_a the inertia component. F_c is the total computed response, and F_m is the measured response

CHAPTER 5

Prediction, Performance, and Uncertainty in Dynamic Load Testing and Signal Matching Applications as Informed by Direct Measurements from an Instrumented Becker Penetration Test

Kuei K.C., S.M. ASCE[1], Ghafghazi M., M. ASCE[2], DeJong J.T., M. ASCE[3]

[1] Graduate Student, Department of Civil & Environmental Engineering, University of California at Davis, One Shields Ave., Davis, CA, USA 95616, +1 (510) 449 – 4305, kckuei@ucdavis.edu

[2] Assistant Professor, Department of Civil Engineering, University of Toronto, 35 St. George St., Toronto, ON, Canada M5S 1A4, +1 (416) 978 – 5972, mason.ghafghazi@utoronto.ca

[3] Professor, Department of Civil & Environmental Engineering, University of California at Davis, One Shields Ave., Davis, CA, USA 95616, +1 (530) 754 – 8995, jdejong@ucdavis.edu

Paper Reference:

Kuei, K.C., Ghafghazi, M., and DeJong, J.T. "Prediction, Performance, and Uncertainty in Dynamic Load Testing and Signal Matching Applications as Informed by Direct Measurements from an Instrumented Becker Penetration Test", *ASCE J. Geotechnical and Geoenvironmental Engineering*, 2018 (to be submitted)

ABSTRACT

Dynamic load testing and signal matching is commonplace for verification of pile capacity but can be subject to non-uniqueness and thus uncertainty of solutions. Improved predictions with these methods could potentially reduce conservatism in design, but relatively little work has been expressed in this area. The recently developed Instrumented Becker Penetration Test (iBPT) when configured as a reusable test pile provides direct static and dynamic measurements at the base and along the pile shaft. These measurements collectively provide a means for prediction and self-validation of the distributed resistance, and thus represents an ideal vehicle for investigating these aspects. In this study, iBPT measurements collected at three project sites in California where pile indicator test programs were previously conducted are presented. The collective iBPT measurements are used to demonstrate a new multistage signal matching approach. To evaluate the robustness and sensitivity of results obtained from signal matching techniques, and to assess potential improvements from the additional measurements, several alternative solution procedures incorporating iBPT measurements to varying degrees are also considered. In addition, feasibility of the iBPT system for prediction of full-scale pile capacity is examined to a limited extent through comparisons of analysis results with available historic data. Results from this study indicate that predictions of ultimate capacity from signal matching to be generally robust and insensitive to selection of solution procedure and rheological parameters, provided that an adequate match is obtained. The distribution of resistance is however, shown to be relatively more sensitive. The sensitivity is largely due to the possible interchange of dynamic and static components to total resistance, and the influence of parameters on timing of resistance activation, which is a methodological limitation. Through consideration of the different solution schemes, non-uniqueness of signal matching solutions is also demonstrated. Although the additional

measurements are not shown to be significantly advantageous in the signal matching applications undertaken, several new measurements are shown to have immediate and objective value. Comparison with historic static and dynamic load testing results indicate somewhat reasonable agreement with historic bounds, and establish some basis for further development of a direct iBPT-pile-design methodology. However, pile setup effects would likely limit the applicability of the system to more granular soils. With additional data and continued work, the direct measurements provided by the iBPT could eventually be used to develop a direct prediction methodology for pile capacity.

INTRODUCTION

Accuracy in forecasting pile capacity is an important aspect in design. Several approaches can be used to estimate pile capacity including in-direct methods based on in-situ tests, or by more direct means including full-scale static, or dynamic load testing and signal matching. In practice, most large projects are initially designed using in-direct approaches prior to direct confirmation via the latter.

Dynamic load testing and signal matching is often the preferred method for verification of pile capacity. Through an iterative approach, strain and acceleration measurements recorded at the pile head during installation or restrike are used as boundary conditions in a pile-soil interaction model to predict the resistance distributed along the pile, and total ultimate capacity. However, the method is known to be subject to non-uniqueness of results as is common of inverse problems, resulting in uncertainty of the solution (Ghafghazi et al. 2017b; Fellenius, 1998; Middendorp and Zandwijk, 1985).

The uncertainty associated with dynamic load testing and signal matching presents an avenue for pursuing methodological improvements. More accurate predictions resulting from such improvements could justify using lower factors of safety and reducing conservatism in design, which can have significant implications when scaled to large piling projects. At the minimum, work in this area can result in understanding methodological limitations, and inform where to concentrate future research efforts.

The observed non-uniqueness from signal matching solutions can broadly be attributed to several sources including the many unknown parameters to be estimated from limited measurements, search algorithm, the nature of separation of static and dynamic components at the element constitutive level, and on a global, distributed level for total resistance. These aspects may be further complicated by other subjective choices which must be made by the operator. The various sources also represent directional forks, from which past and future research may attempt to address and improve upon limitations of existing methods.

A large majority of research efforts have been concerned with improving the modelling of the pile-soil interaction. These efforts have largely focused on improving the realism or representation of the physical mechanics of the models, while also generally increasing their complexity. For example, Salgado et al. (2015) provides a state of the art one-dimensional pile driving analysis model which distinguishes between an interface zone, near-field, and far-field with well constrained relationships tied to soil properties or indices. Masouleh and Fakharian (2008) performed signal matching analysis using a continuum model which may provide higher fidelity in capturing vertical coupling and wave mechanics of the problem. While useful, these newer models, and even their simpler variants may lack sufficient validation. Furthermore, these

efforts do not explicitly consider the potential benefits which may come about simply from incorporation of additional measurements.

As technology and instrumentation reliability has improved, the use of additional measurements besides conventional pile head measurements have gained traction. For example, Tran et al. (2012a, 2012b, 2017) have begun using pile top and sacrificial bottom embedded sensors in conjunction with new methodological procedures to predict end-bearing capacity and skin-friction of full-scale precast and voided piles. While clearly useful as a direct prediction method for full-scale pile capacity, their work does not provide a baseline from which to quantify and assess the benefits of such measurements over conventional approaches. In general, there has a been a lack of experimental studies and data in evaluating aspects of non-uniqueness, and whether improvements in accuracy and reductions in uncertainty can be achieved with conventional models with the inclusion of additional measurements or alternative solution procedures.

The Instrumented Becker Penetration Test (iBPT) configured as a reusable test pile is a new field-scale, fully retrievable test pile. The system was originally conceived in collaboration with the California Department of Transportation (Caltrans) along with other funding agencies with the intent of eventually creating an in-house design tool with pile design capabilities that could be mobilized during the site investigation phase. The basic system provides direct measurements of dynamic strain and acceleration at select locations along the drill string during pile driving installation. In addition, the distributed resistance from static shaft friction in tension can be measured by performing pullback tests at select depth intervals, thus providing a means of direct self-validation of dynamic predictions of shaft friction at a field-scale level. Such measurements provide an ideal vehicle for systematically evaluating the potential benefit of

additional measurements, performance, uncertainty, and limitations in dynamic load testing and signal matching applications.

The primary purpose of this work is to evaluate different dynamic load testing and signal matching solution procedures and to understand their implication on pile capacity forecasting. The perspective of this study is driven principally by the static and dynamic measurements made available from the iBPT configured as a reusable test pile. Specifically, this study addresses the following aspects: how new measurements from the iBPT may be incorporated for dynamic signal matching applications; how iBPT dynamic predictions compare with static measurements; how solutions are sensitive to different signal matching procedures; and finally, on a limited basis, how iBPT field-scale predictions may potentially scale to full-scale pile predictions. For the study profile, this work adopts the simpler, traditional models as is typical of industry (e.g. Rausche et al., 2010; Middendorp, 2004), and omits more complex rheologic models from the scope. This work attempts to provide a transparent portrayal of the analysis treatment in addition to providing some focus for future research.

The paper is organized as follows: first, the iBPT configured as a reusable test pile system is introduced. An overview three project sites where iBPT static and dynamic measurements were obtained is presented. Representative pile driving analysis (PDA) data and site investigation data obtained from the system is presented for each site, along with static and dynamic results for select depths. A new multistage signal matching approach incorporating any number of observation points is demonstrated using the iBPT data. A sensitivity analysis is then performed with respect to different signal matching solution procedures. Finally, a limited comparison of predictions between iBPT field-scale results to full-scale historic indicator piles is performed.

SYSTEM AND MEASUREMENTS

The iBPT was originally developed for liquefaction assessment of gravelly soils (DeJong et al. 2017; Ghafghazi et al., 2017a). However, when configured as a reusable test pile, the system provides additional static and dynamic measurements amenable to pile design applications.

System

The principal component to the iBPT system is an instrumented module (610 mm long, 168 mm O.D., 127 mm I.D.) which sits directly behind the penetrometer tip. The module houses four strain gauges, two accelerometers, two temperature sensors, and a data acquisition computer mounted on a shock absorption system. When operating as a reusable test pile, up to four additional modules of identical configuration can be sequentially positioned and embedded along the drill string. One cable runs through the entire system to power and control different modules, and transmit data. A head module of similar configuration is also mounted at the pile top during driving, and is temporarily disengaged and remounted whenever additional pile is added. A separate aboveground data acquisition system exists for trigger detection, recording head module measurements, monitoring bounce chamber pressure for automatic blow counting, and tracking penetration depth and final set after each blow to confirm integrated displacements.

Modules are installed and driven in series with standard Becker spacer pipes (available in 0.61, 1.5, and 3 m lengths, 127 mm O.D.) using the closed-ended configuration. The drill string system is advanced by a Becker drill rig equipped with an ICE Model 180 double-acting diesel pile driving hammer. The hammer operates at 90 to 95 blows per minutes and has a nominal energy rating of 10.85 kJ per blow. Typical hammer efficiency ranges from 30 to 50 percent of the nominal

energy rating during field operation. Drill string extraction and static pull-back tests and performed by means of a hydraulic jacking system.

Forces are calculated from strain using the stiffness computed from Young's Modulus and the pile cross-sectional area. For embedded modules, a temperature correction is also made to account for the differential thermal straining between the aluminum gauges and the steel pipe wall, which is necessary to account for residual forces (F_R) which can accumulate during driving. To mitigate eccentric loading effects, cross-pairs of force and acceleration are averaged. Displacement and velocity is obtained through time integration of acceleration, and energy is obtained through time integration of derived force and velocity.

The system can principally be operated in two modes. During pile driving installation, the dynamic force and motion response associated with a given blow is recorded at each observation point, or module location. Static pullback tests can also be performed to obtain load versus pile top displacement plots (in tension) at a specific depth. Figure 1a shows the iBPT system with instrumented modules, pile driving hammer, and typical dynamic force, and velocity multiplied by section impedance (Z) time histories as collected during field driving. Example load versus pile top displacement plots obtained from static pullback tension tests are shortly presented in the following sections.

PROJECT SITES AND TEST PROGRAM

This section provides an overview of the project sites, test program, and data presented in this paper. The iBPT system was deployed to three Caltrans project sites in California where infrastructure projects had already been established, of which two sites were located in Oakland,

and the final in Coalinga. Test sites were selected based primarily on the availability of historic static and dynamic pile load test data, which in conjunction with the iBPT data, was intended to assist in eventually developing an iBPT-specific pile design methodology for Caltrans. In addition, the project sites were selected to encompass a wide range of soils, ranging from more conventional, clayey and sandy soils, to more challenging gravelly deposits.

In general, the testing program consisted of driving the iBPT system with multiple modules to target depths consistent with previously installed piles. During pile installation, dynamic time histories were recorded at each module to facilitate PDA-type profiling and capacity forecasting via signal matching. At target depths, static pullback tests were performed to measure the distribution of static shaft friction in tension. The positioning of modules generally reflected intentions to capture average measurements across stratigraphic layers, investigate degradation effects, or investigate the shaft response at the element level.

At the time of testing, the iBPT configured as a reusable test pile system with multiple modules was still in the development phase. Due to some equipment challenges and unexpected driving conditions, not all data was ultimately of usable quality. Subsequently, the data presented herein subjectively reflects the best quality data obtained.

Oakland Project Sites

The first two project sites, herein referred to as Site 1, and Site 2 are located in Oakland, California. Site 1 is located within a vacant lot between Crush and Castro Street, and Sixth and Seventh Street, adjacent to the I-880 and I-980 south connector overpass. Site 2 is located within the Southern Pacific Railroad Desert Yard, adjacent to the I-880 alignment. Both sites had previously served as one of several historic locations in Oakland for indicator pile test programs

that Caltrans was conducting around 1994 to better understand potential challenges with design and construction of structure foundations using large diameter steel pipe piles. A total of 22 indicator test piles had previously been installed at Site 1 to depths of up to 10 m (8.8 m median). The primary geologic units identified at Site 1 generally consist of compact to very dense fine sands, silty fine sands, and clayey fine sands of the Merritt Sand Formation. Site 2 consisted of a similar indicator program to depths of up to 13.1 m (12.2 m median), with primary geologic units including Young Bay Mud, Merritt Sand, and Old Bay Mud. All historic indicator piles consist of PP24X0.750 cold rolled, straight seamed, double-submerged arc welded line pipe piles of open or closed configuration.

Two iBPT soundings were performed at each site, of which representative data from one sounding from each pair will be presented. One static pullback tests measured at end of installation from Site 1, and three static pullback tests at two intermediate depths and end of installation from Site 2 are presented. It is noted that modules were sequenced to be consistent with stratigraphic layering and final target installation depths.

Coalinga Project Site

The final project site is located in Coalinga, California, adjacent to the Los Gatos Creek overflow bridge along Highway 33 which is supported on driven piles. A complete static and dynamic pile load testing program had previously been performed adjacent to two of the bridge bents. Subsurface conditions at the site consist of silt and silty sands, underlain by thicker deposits of dense to very dense gravels and cobbles. Historic indicator piles consist of PP24X0.750 cold rolled, straight seamed, double-submerged arc welded line pipe piles of open configuration.

In total, four iBPT soundings were performed at the site, of which representative data from two of the soundings will be presented. Each of the soundings was performed near one of the bridge bents where historic load tests had been performed. iBPT soundings at the site reached depths of up to 18 m, which were targeted to match either historic pile target or final refusal depths of the installed piles. In addition, a total of six pull-back tests were also performed in the sounding to ascertain static shaft friction distributions, of which three of the tests will be presented. It is noted that modules were sequenced partly on the basis of collecting data for examining degradation effects at a given horizon, and for investigating the element shaft response.

TYPICAL RESULTS

This section presents typical results from the iBPT configured as a reusable test pile obtained during pile driving and static pullback operation. The measurements presented here are intended to demonstrate some of the utility of the iBPT system in addition to providing context for some of the measurements used subsequently in signal matching analyses.

iBPT and Dynamic Measurements

The iBPT can be used to delineate stratigraphic variations and provide continuous profiles of iBPT equivalent SPT through an energy normalization framework and iBPT-SPT N_{60} correlation as established by DeJong et al. (2017), and Ghafghazi et al. (2017a). The iBPT-based site characterization profiles for Oakland Site 1, Site 2, and Coalinga are shown in Figures 2, 3, and 4, respectively. The figures show the raw blow count (N_B), energy normalized blow count (N_{B30}), residual energy measured at the head ($E_{res,Head}$), and tip ($E_{res,Tip}$), delivered energy ratio

(DER), iBPT equivalent SPT N_{60}, historic SPT N_{60}, site stratigraphy, and iBPT configuration at end of drive and each pullback test depth presented in this work.

The measurements provide direct delineation of competent end-bearing layers. In addition, the ability to predict equivalent SPT N_{60} values can facilitate in-direct estimation of pile capacity through the use of SPT-based design correlations, where applicable. It is evident that iBPT equivalent and historic SPT N_{60} values generally agree well at the Oakland project sites, but have higher disagreement at the Coalinga site. This discrepancy could potentially be related to higher influence of gravel particles on the SPT measurements obtained. It is noted that for the Coalinga site, the overlay of both soundings generally indicates similar end-bearing trends (Figure 4a), but some discrepancies in energy dissipation, thus potentially real differences in shaft resistance (Figure 4b and 4c).

Kuei et al. (2017a, 2017b) showed that the iBPT-specific maximum mobilized static base resistance could be estimated from tip measurements using an unload point approach (ULP) based on maximum displacement (a zero-velocity point). Similarly, the maximum reaction resulting from total shaft and base resistance with dynamics included (RMX) as estimated from head measurements can also be applied to the iBPT (Rausche et al., 1985). These values and their variants can be used directly to estimate driving resistance due to side friction.

Quantification of end-bearing and shaft resistance values is depicted for Oakland Site 1, Site 2, and Coalinga in Figures 5, 6, and 7, respectively. As an example, Figure 5a depicts the max reaction measured at the head (RMX), unload point resistance at the tip (ULP), head max force (H FMX), and tip max force (T FMX); Figure 5b depicts the differences of some combinations of the head and tip quantities to quantify possible bounds for total shaft friction. The differences in the pairs shown in Figure 5b thus represent different assumptions in the inclusion or exclusion of

dynamic effects. In addition, Figure 5b also shows the total shaft friction as estimated from static pullback tests as presented in this work.

With exception to Oakland Site 1, the results generally indicate that the measured point static shaft friction (cumulative at a depth) trends with and agrees with shaft resistance profiles estimated from iBPT dynamic measurements. Some scatter in the estimates exist which are likely due to simplifying assumption of the methods and uncertainties of dynamic contributions. These measurements can provide immediate and continuous profiling of both end-bearing and shaft friction in units of load from an iBPT context. Although not the primary emphasis of this current work, such quantities could potentially be normalized to stress and scaled for estimating capacity of true production piles.

Extrema profiles as measured during the pile driving installation process for Oakland Site 1, Site 2, and the two soundings from Coalinga are shown in Figures 8 to 11. The figures show the evolution of the extrema profiles during pile driving installation on a per foot basis. Each trace is constructed from averaging individual module measurements collected over the foot of driving, and linearly interpolating between the observation points. The traces provide envelopes of minimum and maximum stresses, displacements, energies, etc. that can be expected during installation. In addition, these measurements, and in particular the energy dissipation traces are indicative of energy transmission losses along the pile due to shaft resistance, thus provide some basis for inferring the distributed resistance along the pile. It is further noted that in normal applications, obtaining extrema profiles or estimating minimum or maximum stresses in piles must normally be estimated from performing signal matching analyses for an individual blow. With the iBPT configured as a reusable test pile, it is demonstrated that such measurements are trivial and can be obtained for each foot of driving, or to provide extrema envelopes for the entire sounding.

Inferred Shaft Resistance Distribution

Figure 12 shows for each blow to be subsequently analyzed, the corresponding normalized distributions for the inferred shaft resistance distribution from iBPT dynamic measurements. Figure 12a corresponds to Site 1, Figure 12b to 12d to Site 2, and Figure 12e to 12g to Coalinga. Each figure shows a possible shaft resistance distribution shape deduced from computing gradients of individual extrema profile traces using either residual energy (ERS), max energy (EMX), point max resistance (RMX), or the average (AVG) of the three. A uniform trend is assumed between modules, and each trace is normalized by the maximal value. The gradients are thus indicative of areas of higher shaft resistance contribution. The average response is subsequently enforced in one of the analysis methods to be discussed. The inferred shape provides a more objective basis for the distribution of resistance as they are derived purely from PDA measurements. However, it is also noted that the representativeness of the distribution shapes is generally dependent on the resolution (spacing) of modules in addition to the actual stratigraphy and relative contribution of shaft resistance.

iBPT Static Measurements

Static pullback measurements relevant to the analyses to be run are presented in Figure 13. Figure 13a corresponds to Oakland Site 1, Figure 13b to 13d to Site 2, and Figure 13e to 13g to Coalinga. Figure 13 generally shows the pile to be locked in compression (positive) initially, and that this compression is relieved during pullback tests to a tensile (negative) value. The value at the base module at failure should be theoretically zero, but some shaft friction can exist over the

short distance between the actual sensor centerline to the pile base. Theoretically, higher modules should always measure a larger load than those below due to load transference along the shaft. In some cases, it is observed that some modules violate this by a small amount, primarily in the case of very closely spaced modules pairs at Coalinga where shaft resistance is also small. Such cases are considered within measurement resolution error, and for subsequent analyses, negative differentials are simple interpreted as zero for practical purposes.

The load versus pile top displacement plots are used to construct known distributions of average shaft resistance for cross-validation of side friction, and direct assignment in one of the signal matching analysis methods. The average shaft resistance acting across a segment between two consecutive modules is computed as the differential of the module force response at failure. Failure is defined somewhat subjectively as the best fit straight-line average following the predominantly elastic unloading response. In most cases, this is representative of the ultimate expected shaft resistance for the majority of tests, with exception to one case.

Figure 13a shows that soil resistance was not actually fully mobilized in failure (in tension). It is evident that significant residual stresses are still locked in the tip module. Computed differentials thus represent maximum mobilized shaft resistance values in this case. Furthermore, it is noted that for Figure 13e, the head module was positioned above hydraulic jacks, and therefore not engaged during the pullback test. Therefore, shaft resistance could only be estimated for module 4 and below.

ANALYSIS

Signal Matching Approach

A cross comparison of five different solution procedures was performed to assess their efficacy, and to evaluate variations in predictions for static capacity estimated through dynamic load testing and signal matching applications.

This section provides a descriptive overview of the general modelling approach, solution procedure, basic assumptions, differences in the signal matching method variants, and explicitly demonstrates a new multistage signal matching approach for one set of complete iBPT measurements. Finally, results from the collective analyses are summarized and discussed.

General Solution Procedure, Pile-Soil Modelling, and Assumptions

To facilitate analyses, a solution procedure based on the method of characteristics was adopted for ease of implementation and consistency with industry practice for one-dimensional pile analysis. In this approach, the pile is divided into segments of equal wave travel time, and continuous soil friction is approximated at discrete points located along the pile. Subsequently, at each time step, downward and upward travelling waves are modified and propagated at segment internal boundaries to account for impedance contrasts and interface soil friction based on force equilibrium and pile displacement compatibility. The initial wave front is initiated by the down-force boundary condition (obtained from measured force, velocity, and section impedance), and the analysis is carried to the end of the down-force time history. Additional mathematical relationships and details are provided in Middendorp (2004), and Rausche (1983).

To model the interface soil element response, standard industry spring-dashpot elements were used for simulating the soil hysteretic behavior and dynamic effects (e.g. Rausche et al., 2010; Middendorp, 2004). In this case, an elastic-plastic spring in parallel with a viscous (Figure 1b) were selected to capture soil hysteretic behavior, and additive dynamic contributions due to

rate effects and radiation, respectively. The elastic-plastic spring generally conforms with the soil model described by Rausche et al. (2010) with the ability to define both the initial loading stiffness, unload stiffness, and limiting resistance in both compression and tension; for the base element, a no tension limit is enforced. In practice, the stiffness is controlled through prescribing a loading and unloading quake (elastic displacement range), collectively with loading and unloading limit resistances, where unloading parameters are usually defined as a percentage of their loading counterparts.

Impedance contrasts within the pile due to changes in cross-sectional area or other jointing phenomena are accounted for explicitly in the initial discretization of the pile model, or implicitly through specification of a relative impedance change as an unknown parameter during the matching process. At onset of pile creation, impedance profiles are initialized to reflect known differences between cross-sectional areas between iBPT instrumented sections and 0.61m spacer sections (377 kN/m/s) relative to standard Becker pipe sections (300 kN/m/s). During the matching process, additional impedance relative changes are applied to the baseline profile to account for other jointing phenomena which can cause reflections. Such assignments, if used, are constrained to locations coincident with or adjacent to real physical pile joints where sudden discontinuities exist. The magnitude of assignments can range up to 50% based on previous industry analyses of the iBPT system. In reality, the interaction at the joints is complex, and an impedance contrast may be a simplification of the actual behavior, but is justified in this work based on its treatment in past industry analysis. In general, it is observed that these assignments have a relatively small effect for the range of values considered, and are used sparingly for analyses.

Residual stresses are accounted for through the locked-in residual force (F_R) directly measured at each module, and by performing a minimum of five iterations of residual stress

analysis (RSA) or until convergence is achieved. No internal pile damping is used, and for all analyses, a pile modulus of 198 GPa, density of 7830 kg/m^3, and resulting wave speed of 5028 m/s is assumed, with an average analysis time step of 0.0151 ms. Before analysis, input measurements are filtered to 2000 Hz, and undergo typical iBPT baselining and integration procedures; the resulting down-force and up-force time histories are resampled at the analysis time step value.

Soil and pile parameters are adjusted manually for every analysis (and analysis stage) to minimize the observed error by the operator between the measured and computed force (e.g. up-force, force) and motion (e.g. velocity, displacement). A match quality value was initially defined in terms of computed and measured up-force for optimization applications, and is subsequently reported in the results. However, these values did not have any direct bearing on analyses and are provided only for reference.

Multistage Signal Matching Analysis Approach

A new multistage signal matching approach is demonstrated using representative iBPT dynamic measurements obtained from individual modules. The multistage approach builds upon conventional signal matching techniques, with the distinction being that additional measurements along the drill-string (knowns) are introduced in stages such that modeling of the entire pile-soil system is performed incrementally piece-wise from the bottom-up. In addition, any number of measurements along the drill-string can be incorporated in this fashion, essentially converting a single problem with many unknowns into a subset of smaller problems with fewer unknowns.

The basic analysis sequence is depicted in Figure 1b. Beginning from the tip module, an increment of pile and associated soil elements is modelled, and parameters estimated. At the next stage of analysis, the pile increment is increased, and new pile top boundary conditions are applied,

but the current pile increment includes redundant regions. Accordingly, previously solved pile and soil parameters from the preceding stage is remapped to the current stage using a tributary approach such that the average response is preserved assuming an analysis time step equal or greater than the previous. The process is repeated until all modules have been accounted for, or until the depths of interest have been analyzed.

The signal matching results for each stage are presented in Figure 14 for the set of measurements obtained from the Coalinga project site, in sounding iBPT-15-3A at a depth of 46 ft. Stage 1 corresponds with module 1 (M1 in Figure 4e), and so forth. The figure shows the discrete and cumulative resistance profiles determined at each stage, as well as the matching of computed (Cpt) with measured (Msd) motions and forces. F is the force, V is the velocity, U is the displacement, and t denotes time. F_D and F_U are the respective down-force and up-force. The results show that the module measured responses can be adequately matched using the proposed multistage analysis framework, and that the total pile capacity and distribution of resistance at the base and along the shaft can be determined.

In this analysis, a total ultimate resistance (R_U) of 821 kN was estimated from the multistage approach. This ultimate resistance falls within the previously reported RMX value of 1014 kN estimated from the blow, which includes dynamic effects. The end-bearing resistance (R_B) was estimated to be 590 kN, which agrees within five percent of the initial estimate for the static end-bearing of 613 kN based on the ULP approach (Figure 3a). Secondary parameters such as quake, unload quake, unload resistance, damping, etc. were generally found to be within reasonable ranges.

Signal Matching Analysis Variants

Using the same set of iBPT dynamic blow measurements where accompanying confirmatory static measurements were also available, analyses were performed using (1) the aforementioned multistage approach, (2) a two-stage head and tip approach, (3) a conventional single-stage head approach, (4) an "enforced" static measurement approach, and (5) a "hybrid" dynamic signal matching approach. The multistage approach is an extension of existing methods, thus the second and third approach can be considered derivatives of the first. When head measurements are used, the multistage approach simplifies to a conventional single-stage head approach; where tip and head measurements are used, the analysis can be considered a two-stage head and tip approach. For the remainder of this work, "multistage" herein implies the use of all module measurements obtained.

The first three approaches fundamentally represent one category of solution procedures which attempts to quantify the benefit of additional measurements (or multiple levels of analyses) through consideration of all module measurements, industry practice of head measurements, or head and tip measurements in estimating parameters. In contrast, the next two methodological variations (enforced static and hybrid) are based on the conventional single-stage head approach requiring only one level of analysis, but with the inclusion of additional assignment rules for the distributed resistance based on direct-measurements from all modules.

In the enforced static approach, the average static shaft friction as measured directly during pullback tests (Figure 13) are directly assigned to the distributed shaft resistance parameters while the base and associated shaft secondary stiffness and damping parameters are adjusted to obtain a match. In the hybrid approach, the general shape of distributed resistance based on dynamic measurements is enforced, but with no constraint on magnitude. A generic normalized shape

function based on the average of energy and RMX gradients is used (Figure 12). Thus, the overall shape of distributed resistance is enforced, but the total shaft resistance is iterated as a singular parameter, unlike in the static enforced analysis.

RESULTS AND DISCUSSION

The results and discussion section are organized into five main topical areas as follows. First, the signal matching results are presented in terms of the matched response, and estimated distributions. Predictions for ultimate capacity are then compared across the different signal matching approaches; contributions of base and total shaft friction, and direct versus dynamic predictions for total shaft friction are assessed. Non-uniqueness and uncertainty of parameters as informed by the signal matching results is discussed. Advantages and disadvantages of different analysis methods is summarized. Finally, a preliminary comparison is made between iBPT and historic pile load test to evaluate its use-case for full-scale prediction.

Matched Responses and Distributions

The results of the signal matching analyses are presented in the form of condensed summary plates in Figures 9 through 12. For brevity, only the final stage of results corresponding to the pile top is presented in the case of analysis types requiring more than one stage of analysis. Each plate shows (a) predictions of the distributed resistance normalized to stress, measured and computed (b) up-force and down-force, (c) force, (d) velocity, and (e) displacement for each signal matching approach. In addition, results for the distributions of resistance from historic CAPWAP analyses of adjacent piles performed at the same or similar installation depths is plotted for comparison with iBPT trends.

The results show that adequate matches of the measured force and motion responses can be obtained from any one of the signal matching solution procedures. In general differences amongst the matches appear to be only marginal. Inspection of element resistance distributions suggest that the distributions are somewhat sensitive to rheological parameters (e.g. quake, damping, etc.) prescribed in the analyses, with small adjustments shifting static distributions up or down without significantly changing the match itself. While distributions of shaft resistance from the different approaches show variation, the general trends are mostly consistent internally, as well as with the initial site characterization. With respect to historic CAPWAP predictions, more disagreement exists, but zones of larger concentrations of shaft resistance, particularly at depth, are also observed to coincide with iBPT predictions. Discrepancies can be due to analysis uncertainty or other real differences in scaling mechanisms, aging effects, pile setup, or other unaccounted driving conditions at the time of data collection.

Predictions for Capacity

Figure 22 compares the ultimate capacity (R_U) predicted from the collective iBPT analyses using the different signal matching procedures. The relative contribution of total shaft friction (R_s) and base resistance (R_B) to ultimate capacity is also shown for each analysis. As noted earlier, the static enforced approach applies the actual measured iBPT static shaft friction in the analysis, thus shaft predictions from this analysis variant is hatched to make this distinction and establish it as a reference when comparing it to the alternative approaches. PDA-type values such as RMX, and the ULP resistance corresponding to each blow are also denoted as symbols in Figure 22 for comparison of simpler PDA-type results against the more sophisticated analyses. A computed metric of match quality between measured and computed up-force is shown for reference.

The end-bearing component is observed to be a significant contributor to ultimate capacity for the majority of blows analyzed. This is with exception to Blow F, which was tipped in a looser zone with moderate levels of shaft friction (see Figure 4 and Figure 13f). In general, the results indicate relatively good agreement for predictions of ultimate resistance across the different analysis methods, with one major exception to Blow A. Total measured static shaft friction shows good agreement across methods in some cases, but also exhibits a wider range of values collectively across all project sites; notable exceptions include Blow A and Blow C. In general, predictions of R_U fall within about 10% of the average group composite, while the proportion of R_B and R_S generally fall within 30-40%, and 30-50% of the average group composite, respectively. When comparing to the PDA-type quantities, the base resistance estimated from the more sophisticated signal matching analyses is shown to be reasonably approximated by the simplified ULP approach. As expected, RMX values tend to be higher than predicted ultimate resistance values due to the contribution of dynamic effects, but appear to still trend and correlate with R_U.

Blow A in Figure 22 shows that the predictions of R_S were in general overly conservative compared with the static enforced approach; this also translates to conservative predictions for R_U. This discrepancy can be attributed to insufficient driving energy to fully mobilize or activate all soil resistance forces to failure. As shown in Figure 2a for Blow A, the exceedingly high blow counts near end of installation are indicative of extremely hard driving conditions. Moreover, as shown in Figure 15a and Figure 22, the maximum static resistance mobilized in the "enforced" analysis shows a mobilization level much closer to the other companion analyses. In fact, the prescribed R_s in the enforced analysis represents only a minimum bound considering that shaft friction exceeded the pullback capacity of the system for this particular blow (Figure 13a).

The discrepancy for total shaft friction for Blow C in Figure 22 can be attributed to difficulty with differentiating the fraction of side-friction versus base resistance immediately at the vicinity of the toe as wave reflections arriving to the observation point, or pile head would essentially be coincident.

Non-Uniqueness and Uncertainty of Parameters

The results shown in Figure 22 indicate that predictions for R_U are relatively robust and insensitive to selection of rheological parameters and solution procedure barring unusually hard driving conditions which may prevent full mobilization to failure. Where resistances are not fully mobilized, it is shown that extrapolations for ultimate capacity can be arbitrarily made while obtaining an adequate signal match. This is due to the fact that the stiffness rather than the failure condition is being paired, and extrapolated resistances need not necessarily be mobilized in the analysis. This limitation with estimating ultimate capacity when displacements are small has long been recognized in pile driving analyses and is why rule of thumbs for estimating fully mobilized conditions, such as the permanent set exceeding 1/120 the pile diameter exist (Goble and Rausche, 1976).

In contrast, predictions of R_S and R_B appear to be more sensitive to the selection of rheological parameters and solution procedure as indicated by the range of variation within analysis composite groups. Under certain driving conditions where a meaningful level of shaft friction may be present near the vicinity of the toe, predictions of the relative proportion of base to shaft friction to ultimate capacity may be less reliable. This difficulty with differentiation is a known limitation in practice. The consistency of R_U and similar levels of variation between R_S and R_B support this observation. It is noted that correlations or procedures dependent on such

differentiated quantities (e.g. either R_S, or R_B where end-bearing is not the dominant contributor) could be subject to the same uncertainty, and less reliable as a result. The observations of R_U generally being reliable, and the differentiation of R_S and R_B showing more uncertainty is generally consistent with results from past studies by Fellenius (1998) and Ghafghazi et al. (2017b).

Figure 23 provides a summary comparison of average parameters from the collective iBPT analyses. Values are also summarized in Table 1. Average quake, unload level, tension resistance, and damping for the shaft elements are denoted as QS, QSU, RSN, and JS, respectively; quake, unload level, and damping for the base element is denoted as QB, QBU, and JB, respectively. Of the parameters made available in the analysis, it is observed that RSN, and QBU were largely not utilized for the majority of analyses, and can be considered largely secondary parameters.

The results illustrate the sensitivity of parameters to solution approach, and demonstrate the uncertainty of results associated with signal matching applications. The variation in parameters lies predominantly in the selection of quake and damping values. This variation reflects some uncertainty in the interchange between static and dynamic contributions to the total element response and highlights the separation uncertainty which is potentially a framework limitation. Variations in quake values (e.g. QS, QB) would naturally change the timing in activation of element static resistance forces, which would essentially explain some of the observed variations in predicted static distributed resistances. This also explains the comparable signal matches between methods since the timing of the total element response (sum of components) would be similar since damping (e.g. JS, JB) could offset or compensate for changes in quake.

Signal Matching Variants and Value Proposition

The predominant value of dynamic load testing and signal matching is derived from estimating pile ultimate capacity. In addition, the distribution of resistance along with secondary quake and damping parameters can also be useful for forecasting additional pile drivability studies. Based on the predominant use-case and results of this work, there does not seem to be a clear or immediate advantage of additional measurements, or of any one analysis method over the other. Such distinction depends on the value criteria, and may become more of a philosophical evaluation.

While the enforced approach provides a direct measurement of shaft friction, such measurements render signal matching analyses for prediction of static capacity redundant when such measurements can be obtained directly. Furthermore, a goal of this work was to evaluate potential improvements to signal matching applications from added measurements or observation points.

The multistage, head and tip, and conventional head analysis variants represent a category of procedures which differs in the number of observation points used. The primary advantage of additional observation points is that the problem is simplified by reducing the number of unknowns for a given analysis stage. However, in the process, more subsets of analyses are created with each observation point, resulting in a similar volume of work performed. Such analysis simplification perhaps does not warrant the cost of additional instrumentation. Considering that in many cases, the end-bearing response is a significant contributor to ultimate capacity, a head and tip approach may be preferable if a more expedient, and concrete evaluation of end-bearing capacity is desired, especially if capacity derived from the shaft friction is not to be relied upon for design due to code restrictions.

A common critique of signal matching is that solutions are susceptible to subjective choices made by the operator (e.g. differentiation of quake and damping). If reducing subjectivity is valued, the hybrid approach may provide a less subjective alternative since the approach becomes independent of interpretation of stratigraphy effects while still being informed by actual stratigraphy through dynamic PDA measurements (e.g. energy dissipation, RMX gradient). Since the hybrid approach appears to yield comparable results to other solution approaches while reducing the number of unknowns for the operator to select, it can thus be considered objectively better. It is noted however that the performance of the hybrid approach would depend on the arrangement of modules relative to installation stratigraphy, and would likely suffer the more that an assumed average uniform distribution between two modules deviates from complex conditions.

Comparison with Historic Results

Comparison of iBPT estimated shaft friction distributions and estimates with static load test and dynamic load test results (Figure 15 to Figure 21) show both agreement and disagreement in terms of distributions of shaft resistance, and their magnitudes. Overall, iBPT predictions agree with intervals of higher concentrations of shaft resistance when compared with dynamic load testing results, but the magnitudes can be noticeably different. Figures 24 and 25 provide further comparisons of iBPT predictions against historic estimates of full-scale piles for single-value shaft friction, and end-bearing capacity, respectively. To make the comparison, some simplifying assumptions were required to account for the use of different pile sizes, loads, and end conditions (i.e. open or closed-ended).

Shaft comparisons were made based on an equivalent uniform shaft friction distribution, computed as the total load acting along the pile shaft, divided by side area (embedded pile length

multiplied by the pile perimeter). This assumes further that potential effects of displacement level from end condition on side-friction have a secondary effect. As seen in Figure 24, when the predicted shaft distributions are converted to equivalent uniform distributions, iBPT values generally fall within the range of historic dynamic and static load test results. In general, the equivalent shaft values agree well for the Coalinga project site, Blows E and G, which correspond more closely with the depths of the dynamic and static load test. Blow F shows higher values as expected as it corresponds with a shallower depth with higher side-friction conditions thus load test results are not directly comparable. In addition, the close agreement between historic and dynamic load test results suggest negligible setup or aging effects as expected for the granular materials present at the site. Blows A through D from the Oakland project sites show agreement with historic results, but with larger ranges and differences between historic static and dynamic results. This may reflect slightly more complex stratigraphy at the Oakland sites compared to Coalinga coupled with deficiencies with the simplifying assumptions, or highlight other importance aspects of scaling effects, influence zones, aging, or pile setup. These preliminary results collectively suggest that the iBPT system may be more suitable for estimating shaft friction for granular soils.

Base comparisons were made by normalizing end-bearing resistances with the projection of the end-bearing area (i.e. assuming plugged conditions for open-ended piles). The results show that end-bearing stresses are significantly higher as predicted from iBPT measurements compared to historic static and dynamic results, particularly for Blows E and G for the Coalinga project site. As with the shaft comparison, the zone of influence below the tip is likely a key factor when attempting to make comparisons, especially for very hard driving where small differences in elevation could potentially translate to large differences in stress.

In general, it is difficult to make a meaningful assay with the current data set. Differences may be generally attributed to spatial variability, pile set-up, aging, scaling-effects, or other unaccounted differences in driving factors. More case-specific data is required to further examine or develop an iBPT-specific pile design methodology for prediction of full-scale pile capacity.

SUMMARY AND CONCLUSIONS

The iBPT configured as a reusable test pile is a new system with pile design applications. The system can measure the static shaft friction in tension and dynamic response along the drill-string during pile driving at a field-scale level. The system was deployed to three project sites in California where full-scale piles had previously been installed. Typical iBPT measurements and representative PDA-type results were presented from the system to demonstrate its potential utility and use-case. Direct dynamic and static measurements were subsequently used to evaluate uncertainty, non-uniqueness, and possible improvements to predictions which utilize dynamic load testing and signal matching by evaluating different signal matching procedures. Finally a preliminary comparison of iBPT predictions with full scale historic data was performed. The following key findings can be summarized from this work:

- The iBPT configured as a RTP is a recently developed tool which provides direct measurements along the drill string of the dynamic response during pile driving, and the static shaft friction distribution in tension during pullback testing.
- A new multistage signal matching approach using iBPT dynamic measurements was demonstrated. The results show that the force and motion response can be adequately captured using a bottom-up approach that builds on conventional signal matching analysis techniques to infer the distribution of resistance and secondary stiffness and damping parameters.

- The collective analyses by the different signal matching solution procedures show that predictions for ultimate pile capacity are relatively insensitive to the selection of solution approach, and rheological parameters (e.g. quake, damping etc.). The solutions for the elemental distribution of resistance are found to be generally less robust and more sensitive to these choices.
- Despite the relative sensitivity of determining the elemental distribution, it is found that dynamic predictions of the iBPT static shaft resistance total magnitude (sum of elements) agree reasonably well with direct measurements of iBPT static shaft resistance total magnitude as measured in pullback tension tests.
- Variations of iBPT equivalent uniform unit shaft friction values between different solution procedures generally reflect the sensitivity of determining the elemental resistance distributions in dynamic signal matching applications. Despite the variance, the iBPT equivalent unit shaft friction values generally agree with, and fall within the range of available historic static and dynamic load test data.
- This study suggests that trying to address improvements for predictions of pile capacity in the domain of pile dynamic analyses using additional dynamic measurements may be of limited, or marginal value at best, which can be partially attributed to the inherent limitations of the framework of solution. However, the direct measurements of static shaft friction obtained from the iBPT is still of value. While static base resistance is not directly measured, indirect estimates can be reasonably identified with minor assumptions. With additional work, the shaft and base estimates in conjunction with historic data could eventually be used for prediction of full-scale pile capacity. The limiting factors of the iBPT system is the pullback capacity and

hammer energy, which may not fully mobilize failure conditions during driving and tension load testing conditions, respectively.

ACKNOWLEDGEMENTS

The authors appreciate the funding and support provided by the California Department of Transportation (Caltrans), and the Division of Safety of Dams (DSOD) of the California Department of Water Resources. The support and collaboration of Tom Shantz of Caltrans, and Jim Benson of Great West Drilling is also appreciated. The assistance of Alex Sturm and Anthony Rossiter for their help in collecting the data is also greatly appreciated.

REFERENCES

California Department of Transportation (Caltrans). (1994). "Site 1 Summary Report for Caltrans Indicator Pile Test Program on the I-880 Replacement Project". Service Contract No. 59V149.

California Department of Transportation (Caltrans). (1995). "Site 2 Summary Report for Caltrans Indicator Pile Test Program on the I-880 Replacement Project". Service Contract No. 59V149.

DeJong, J.T., Ghafghazi M., Sturm A.P., Wilson D.W., den Dulk J., Armstrong R.J., Perez A., and Davis C.A. (2017). "Instrumented Becker Penetration Test: equipment, operation, and performance". ASCE Journal of Geotechnical and Geoenvironmental Engineering, 10.1061/(ASCE)GT.1943-5606.0001717, 04017062.

Fellenius, B.H. (1998). “Variation of CAPWAP results as a function of the operator”. Proc., 3rd Int. Conf. on the Application of Stress-Wave Theory to Piles, Ottawa, May 25-27, 1988, 814-825.

Ghafghazi M., DeJong J.T., Sturm A.P., and Temple C.E. (2017a). “Instrumented Becker Penetration Test: The application of SPT and iBPT for liquefaction assessment in gravelly soils”. ASCE Journal of Geotechnical and Geoenvironmental Engineering, 10.1061/(ASCE)GT.1943-5606.0001718, 04017063.

Ghafghazi M., DeJong J.T., and Wilson D.W. (2017b). “Evaluation of Becker penetration test interpretation methods for liquefaction assessment in gravelly soils”. Canadian Geotechnical Journal, dx.doi.org/10.1139/cgj-2016-0413.

Goble, G.G., and Rausche, F. (1976). “Wave equation analysis of pile driving, WEAP program”. U.S. Dept. of Transportation, Federal Highway Administration, Washington, DC. Report FHWA-IP-76-13 (4 Vols.).

Kuei C.K., Ghafghazi M., DeJong J.T. (2017a). “Pile Driving Mechanics at the Tip as Informed by Direct Measurements”. ASCE Journal of Geotechnical and Geoenvironmental Engineering, 10.1061/ (ASCE)GT.1943-5606.0001746, 04017064.

Kuei C.K., Rossiter A.M., Sturm A.P., DeJong, J.T., Wilson D.W., Ghafghazi M., (2017b). “An Instrumented Becker Penetration Test for Estimation of Soil Penetration Resistance and Pile Capacity in Gravelly Soils”. Geotechnical Frontiers 2017, Orlando, Florida.

Masouleh, S.F., and Fakharian, K. (2008). “Verification of signal matching analysis of pile driving using finite difference based continuum numerical method”. Int. J. of Civil Eng., 6(3), 174-183.

Middendorp, P., and van Zandwijk, C. (1985). "Accuracy and reliability of dynamic pile testing techniques." Proceedings 4th International Conference on Behavior of offshore structures (BOSS), Delft, Netherlands.

Middendorp, P. (2004). "Thirty years of experience with the wave equation solution based on the method of characteristics". Proc., 7th Int. Conf. on the Application of Stress Wave Theory to Piles, Kuala Lumpur, Malaysia.

Rausche, F., Likins, G., Liang, L., and Hussein, M. (2010). "Static and dynamic models for CAPWAP signal matching". Art of Foundation Engineering Practice, GSP 198, ASCE, Reston, Virginia: 534-553.

Rausche, F., Goble, G.G., Likins, E. (1985). "Dynamic Determination of Pile Capacity." ASCE Journal of Geotechnical and Geoenvironmental Engineering, 111(3): 367-383.

Rausche, F. (1983). "CAPWAP Analysis Using the Characteristics Approach." User's Day, Philadelphia, PA.

Salgado, R., Loukidis, D., Abou-Jaoude, G., and Zhang, Y. (2015). "The role of soil stiffness non-linearity in 1D pile driving simulations". Géotechnique, 10.1680/geot.13.P.124.

Sturm, A., Kuei, K., Rossiter, M., DeJong, J., Thurairajah, A., Olivera, R. (2016). "Characterization of Gravelly Soils in Vancouver B.C. Using the instrumented Becker Penetration Test". 69th Canadian Geotechnical Conference, Vancouver, B.C.

Sturm, A., Kuei, K., DeJong, J., Thurairajah, A., Olivera, R., Ghafghazi, M. (2017). "Comparison of Becker Penetration Test Interpretation Methods in Characterization of Gravelly Soils". 3rd International Conference on Performance-based Design in Earthquake Geotechnical Engineering (PBD-III), Vancouver, B.C.

Tran, K.T., McVay, M., Herrera, R., and Lai, P. (2012a). “Estimating static tip resistance of driven piles with bottom pile instrumentation”. Canadian Geotech. J., 49(4), 381-393.

Tran, K.T., McVay, M., Herrera, R., and Lai, P. (2012b). “Estimation of nonlinear static skin friction on multiple pile segments using the measured hammer impact response at the top and bottom of the pile”. Computers and Geotechnics, 10.1016/j.compgeo.2011.11.004.

Tran, K.T., Wasman, S.J., McVay, M., and Herrera, R. (2017). “Capacity evaluation of voided driven piles using embedded data collectors”. Canadian Geotech. J., 10.1139/cgj-2017-0008.

Table 1. Summary of primary and secondary soil parameters estimated from signal matching

Blow/ Sounding/ Rec Info	Solution Procedure	RS (kN)	RB (kN)	RU (kN)	QS (mm)	QSU (%)	RSN (%)	JS (s/m)	QB (mm)	QBU (%)	JB (s/m)	MQ
Blow A Oakland Site 1 RTP-15-S1B Blow 2304, 30ft	1 (Staged)	428	550	978	0.88	100	100	0.17	2.5	100	0.12	75
	2 (Tip/Pile top)	461	560	1021	0.73	100	100	0.13	3.5	100	0.12	103
	3 (Pile top)	542	450	992	2.39	222	150	0.10	4	250	0.25	110
	4 (Enforced)	1165	500	1665	5	50	50	0.02	0.5	100	0.35	103
	5 (Hybrid)	455	575	1030	1.2	200	100	0.15	0.35	100	0.15	35
	(RMX-ULP)	869	614	1483	--	--	--	--	--	--	--	--
Blow B Oakland Site 2 RTP-15-S2A Blow 673, 30ft	1 (Staged)	113	280	393	2	100	100	0.15	4	100	0.08	172
	2 (Tip/Pile top)	105	270	375	2.86	100	100	0.24	4	100	0.1	174
	3 (Pile top)	80	300	380	2.5	10	30	0.15	4	80	0.1	134
	4 (Enforced)	138	235	373	2.7	117	100	0.15	2.5	30	0.1	108
	5 (Hybrid)	150	230	380	1.5	200	100	0.12	1.5	100	0.08	137
	(RMX-ULP)	289	294	583	--	--	--	--	--	--	--	--
Blow C Oakland Site 2 RTP-15-S2A Blow 1059, 41ft	1 (Staged)	--	--	--	--	--	--	--	--	--	--	--
	2 (Tip/Pile top)	222	285	507	0.65	100	100	0.48	3	100	0.05	126
	3 (Pile top)	130	400	530	2.5	5	100	0.15	4	80	0.15	108
	4 (Enforced)	493	20	513	6	60	100	0.30	5	100	0.1	164
	5 (Hybrid)	250	250	500	2.5	100	100	0.12	0.5	100	0.08	138
	(RMX-ULP)	397	374	771	--	--	--	--	--	--	--	--
Blow D Oakland Site 2 RTP-15-S2A Blow 1874, 45ft	1 (Staged)	--	--	--	--	--	--	--	--	--	--	--
	2 (Tip/Pile top)	370	415	785	0.52	100	100	0.47	2.75	100	0.12	83
	3 (Pile top)	274	600	874	2	20	100	0.15	4	100	0.15	78
	4 (Enforced)	696	350	1046	6	100	100	0.24	7	100	0.08	125
	5 (Hybrid)	420	400	820	2.5	150	100	0.12	1.5	100	0.08	130
	(RMX-ULP)	626	579	1205	--	--	--	--	--	--	--	--
Blow E Coalinga RTP-15-2 Blow 9088, 47ft	1 (Staged)	175	680	855	0.25	100	100	0.15	4	100	0.15	128
	2 (Tip/Pile top)	150	680	830	0.31	100	100	0.15	4	100	0.15	134
	3 (Pile top)	118.4	650	768	1.5	30	100	0.25	4	100	0.15	41
	4 (Enforced)	259	620	879	2.5	50	100	0.15	3	150	0.05	55
	5 (Hybrid)	150	600	750	0.5	100	100	0.15	3.5	100	0.15	153
	(RMX-ULP)	262	775	1037	--	--	--	--	--	--	--	--
Blow F Coalinga RTP-15-3A Blow 6536, 41ft	1 (Staged)	537	40	577	0.72	100	100	0.08	0.5	100	0.05	126
	2 (Tip/Pile top)	443	80	523	1.52	100	100	0.10	0.75	100	0.05	164
	3 (Pile top)	348	150	498	0.15	25	100	0.15	0.25	100	0.4	23
	4 (Enforced)	486	50	536	1	100	100	0.10	0.25	100	0.25	38
	5 (Hybrid)	475	100	575	0.25	100	100	0.10	0.25	100	0.1	122
	(RMX-ULP)	996	35	1031	--	--	--	--	--	--	--	--

Table 1. Summary of primary and secondary soil parameters estimated from signal matching (cont'

Blow/ Sounding/ Rec Info	Solution Procedure	RS (kN)	RB (kN)	RU (kN)	QS (mm)	QSU (%)	RSN (%)	JS (s/m)	QB (mm)	QBU (%)	JB (s/m)	MQ
Blow G Coalinga RTP-15-3A Blow 7103, 46ft	1 (Staged)	231	590	821	0.5	100	100	0.06	2.2	100	0.04	98
	2 (Tip/Pile top)	213	600	813	0.5	100	100	0.08	2.2	100	0.04	98
	3 (Pile top)	245	450	695	1.42	5	10	0.20	0.25	100	0.12	20
	4 (Enforced)	222	590	812	0.25	100	100	0.06	2.2	100	0.04	31
	5 (Hybrid)	215	525	740	2	100	20	0.10	0.25	100	0.05	128
	(RMX-ULP)	401	613	1014	--	--	--	--	--	--	--	--

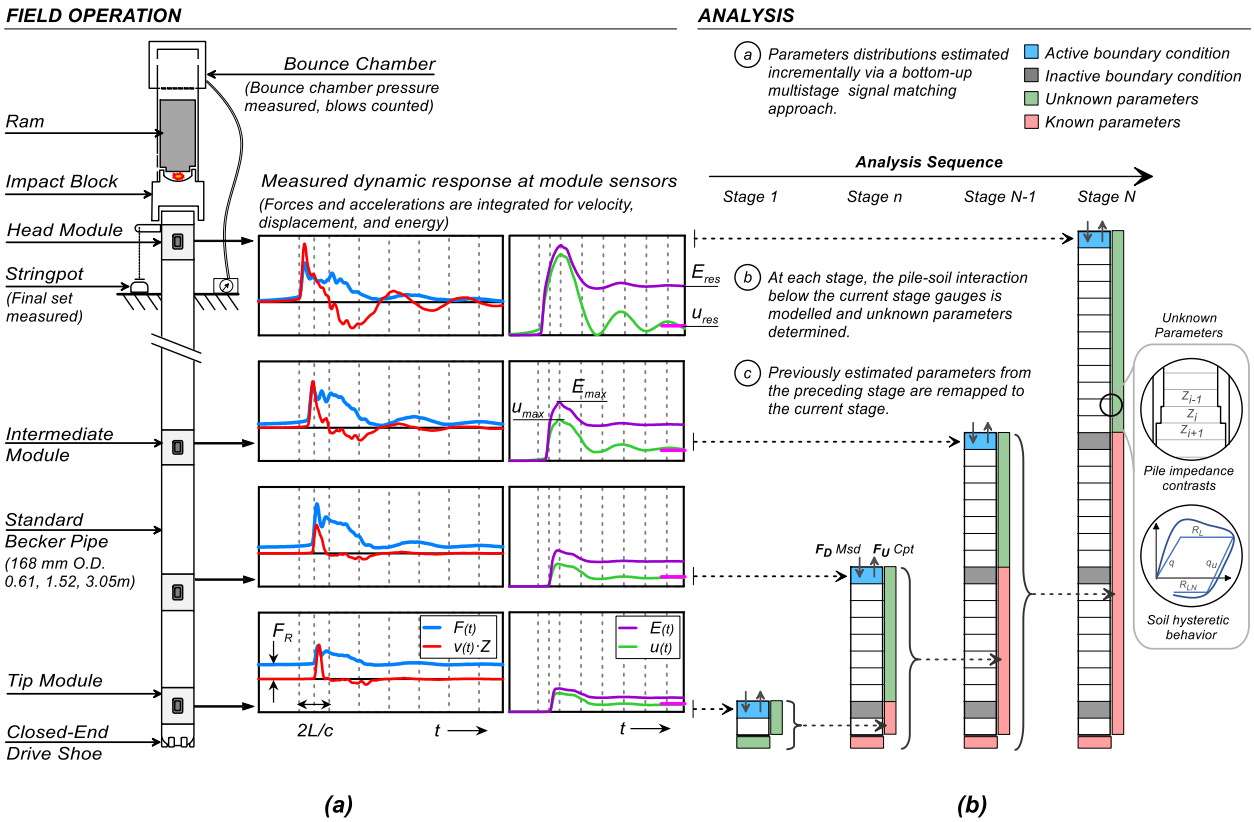

Figure 1. (a) Schematic of iBPT system (configured as RTP) components and typical dynamic measurements recorded at instrumented module locations during field driving, (b) bottom-up, multistage signal matching approach.

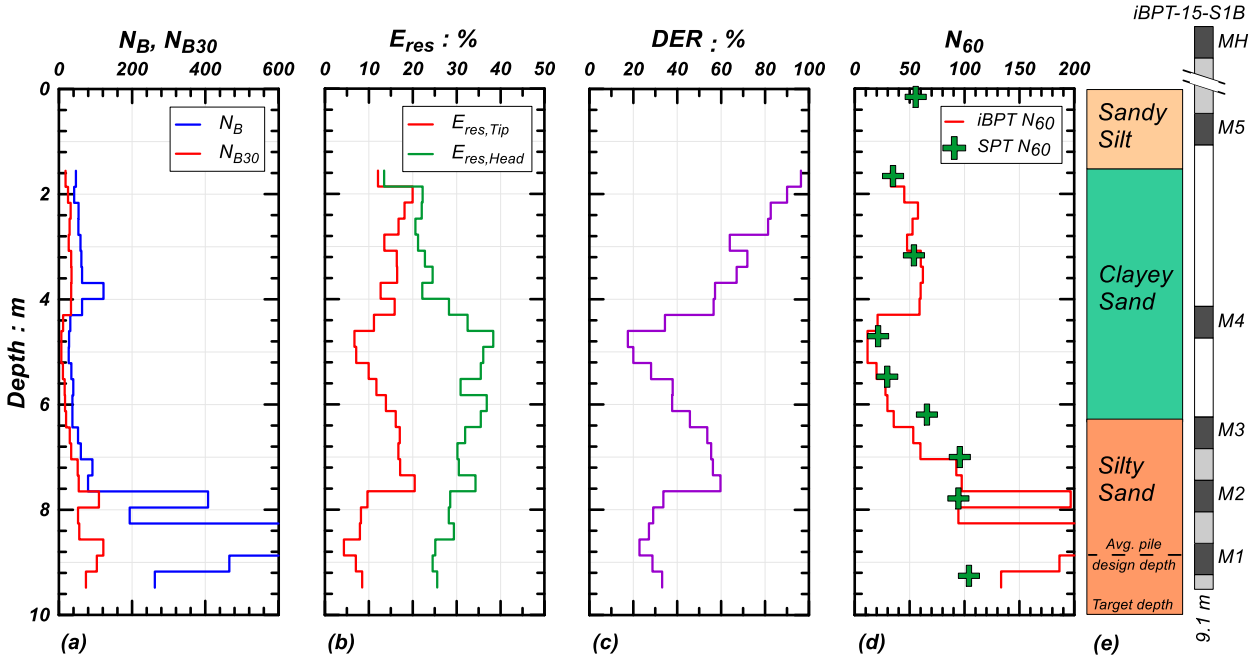

Figure 2. Oakland, Site 1 - iBPT equivalent N_{60} estimation: (a) N_B, N_{B30}, (b) E_{res}, (c) DER, (d) iBPT equivalent N_{60}, (e) site profile and iBPT pullback test depth.

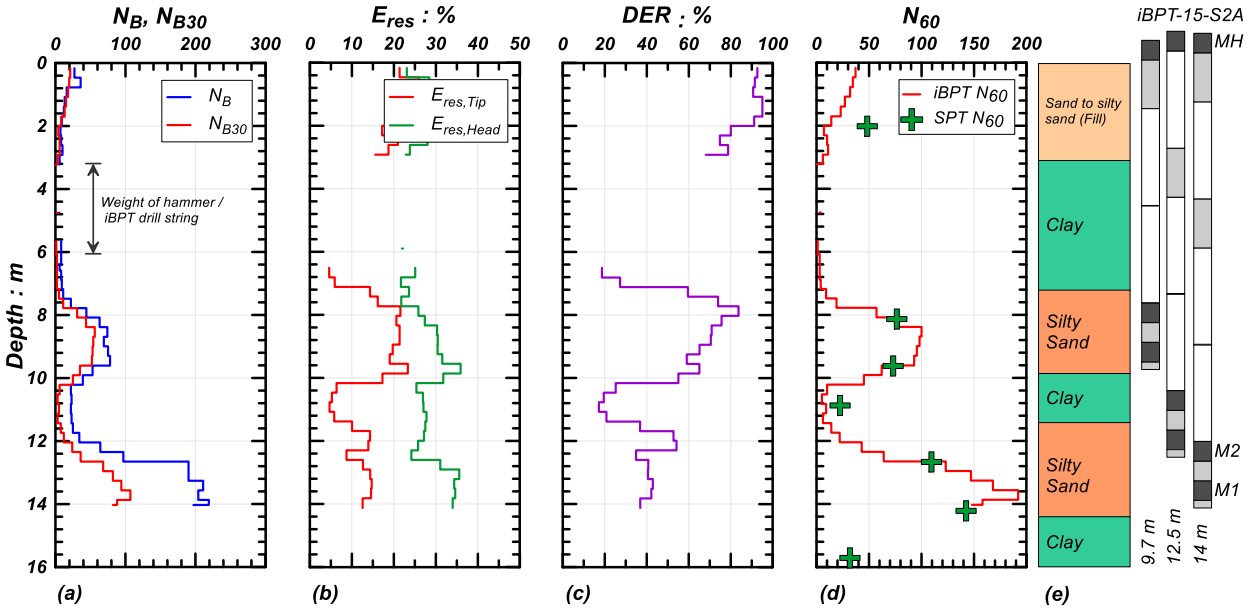

Figure 3. Oakland, Site 2, - iBPT equivalent N_{60} estimation: (a) N_B, N_{B30}, (b) E_{res}, (c) DER, (d) iBPT equivalent N_{60}, (e) site profile and iBPT pullback test depth.

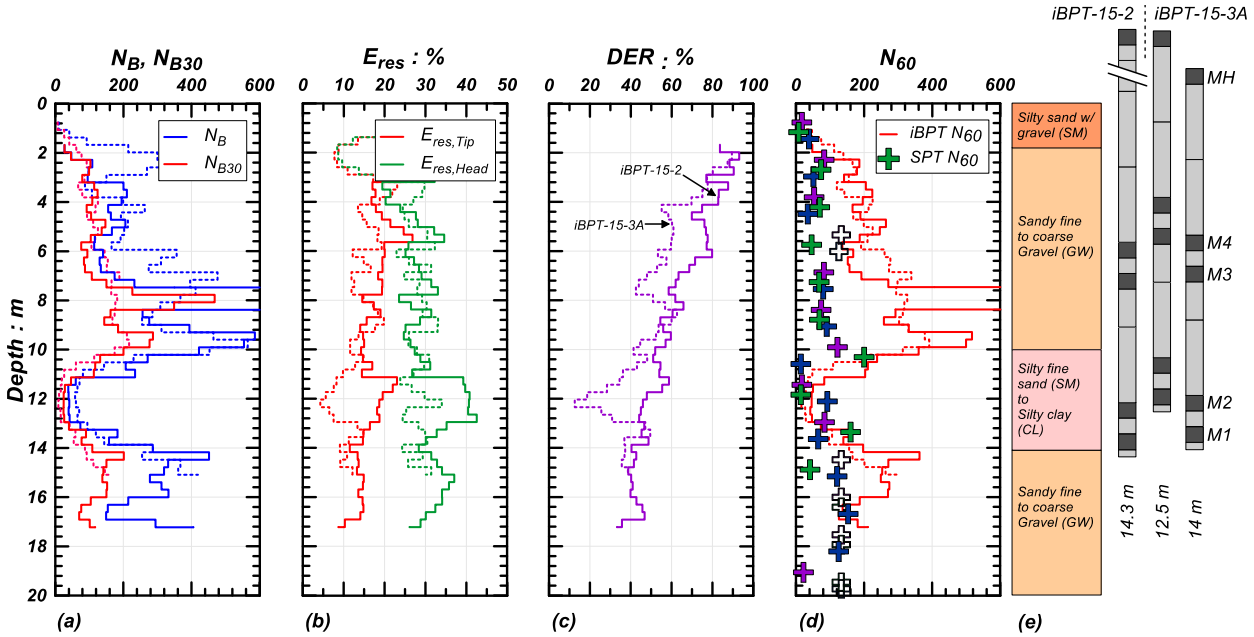

Figure 4. Coalinga - iBPT equivalent N_{60} estimation: (a) N_B, N_{B30}, (b) E_{res}, (c) DER, (d) iBPT equivalent N_{60}, (e) site profile and iBPT pullback test depth.

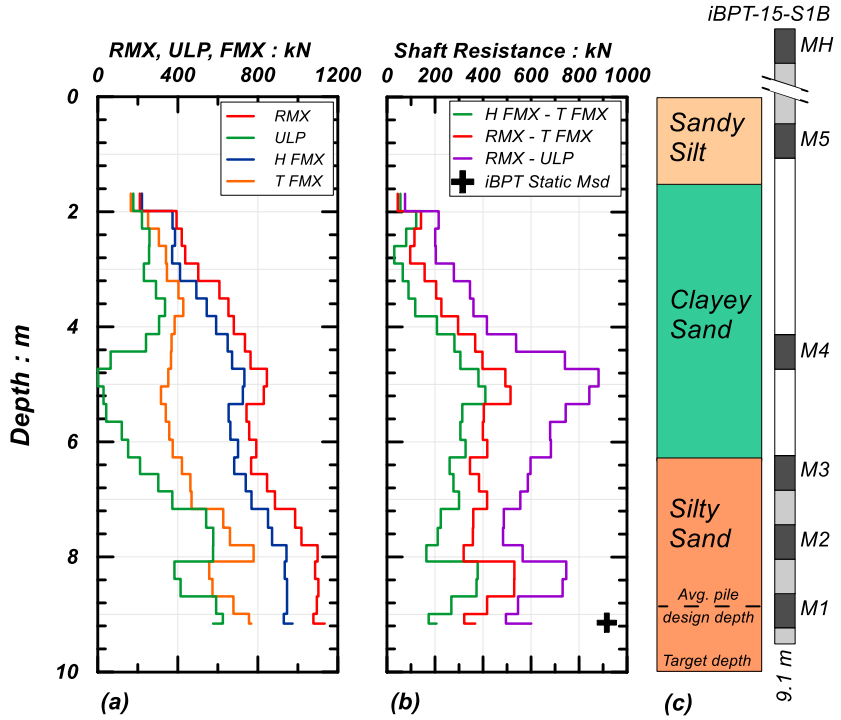

Figure 5. Oakland, Site 1 - iBPT typical pile driving analysis (PDA) results from head and tip modules: (a) head max penetration to resistance (RMX), tip unload point resistance (ULP), head max force (H FMX), tip max force (T FMX), (b) shaft resistance estimates, (c) site profile and iBPT final install depth.

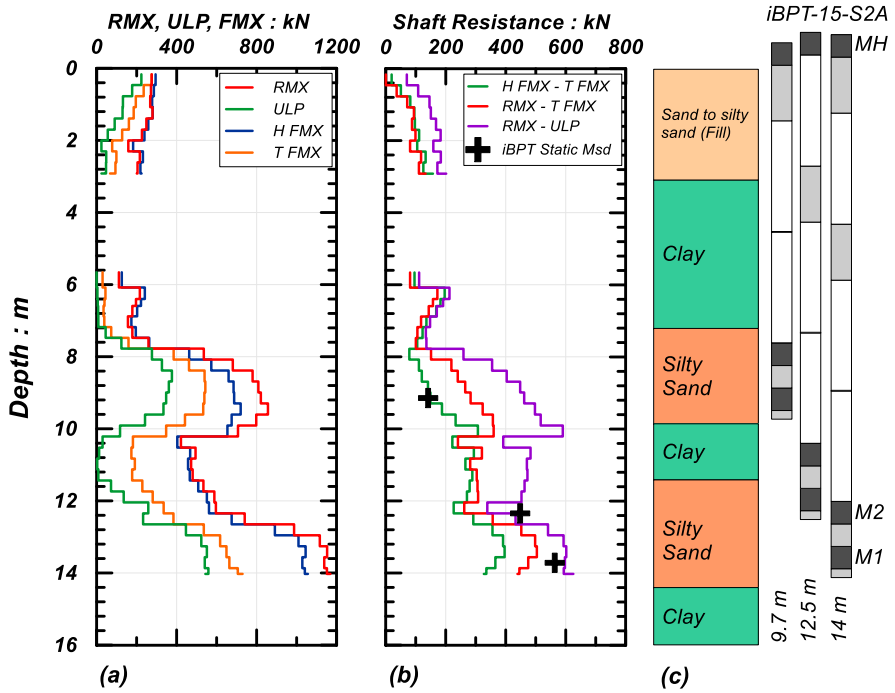

Figure 6. Oakland, Site 2 - iBPT typical pile driving analysis (PDA) results from head and tip modules: (a) head max penetration to resistance (RMX), tip unload point resistance (ULP), head max force (H FMX), tip max force (T FMX), (b) shaft resistance estimates, (c) site profile and iBPT final install depth.

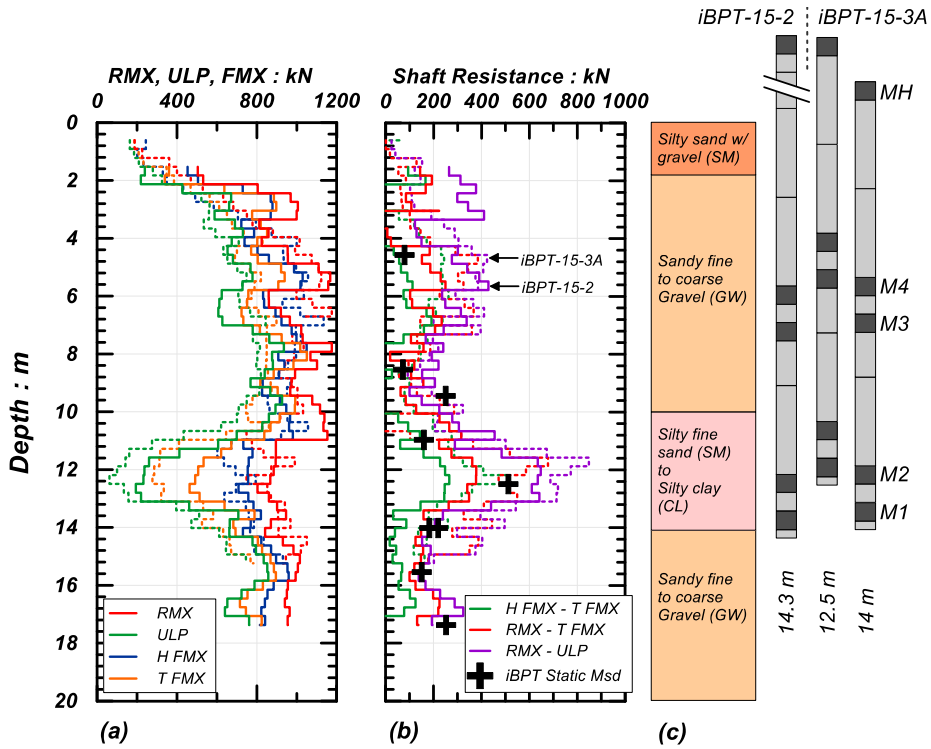

Figure 7. Coalinga - iBPT typical pile driving analysis (PDA) results from head and tip modules: (a) head max penetration to resistance (RMX), tip unload point resistance (ULP), head max force (H FMX), tip max force (T FMX), (b) shaft resistance estimates, (c) site profile and iBPT final install depth.

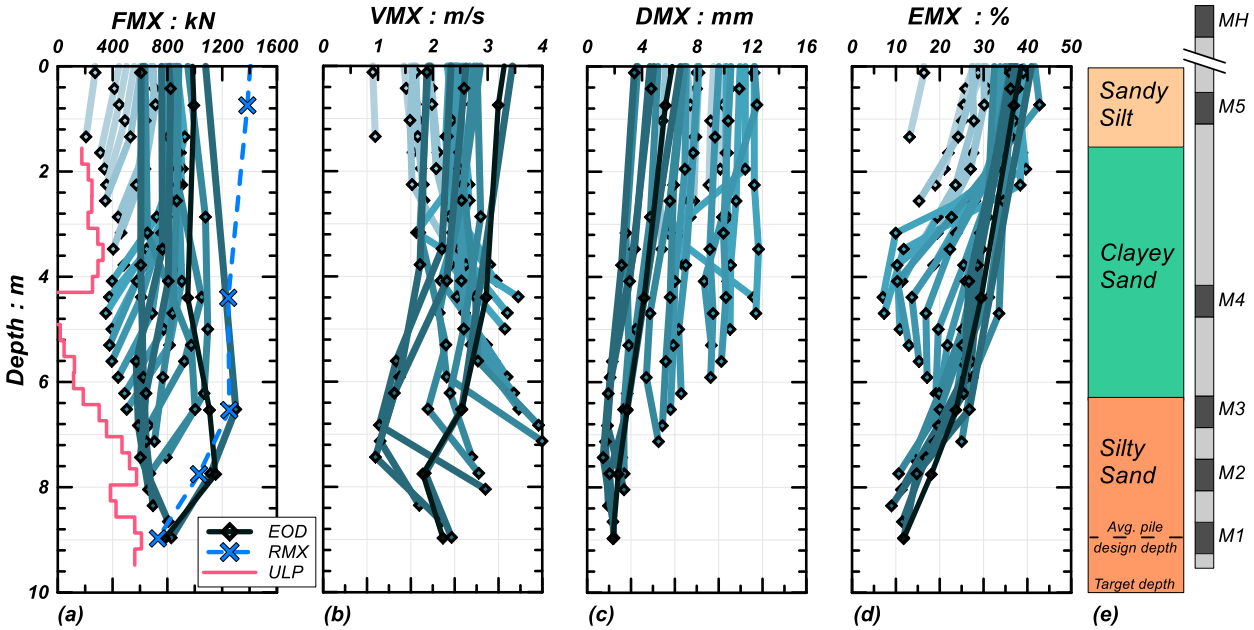

Figure 8. Oakland, Site 1 - iBPT typical pile driving analysis (PDA) results from multiple modules: (a) FMX, (b) VMX, (c) UMX, (d) EMX, (e) site profile and iBPT final install depth.

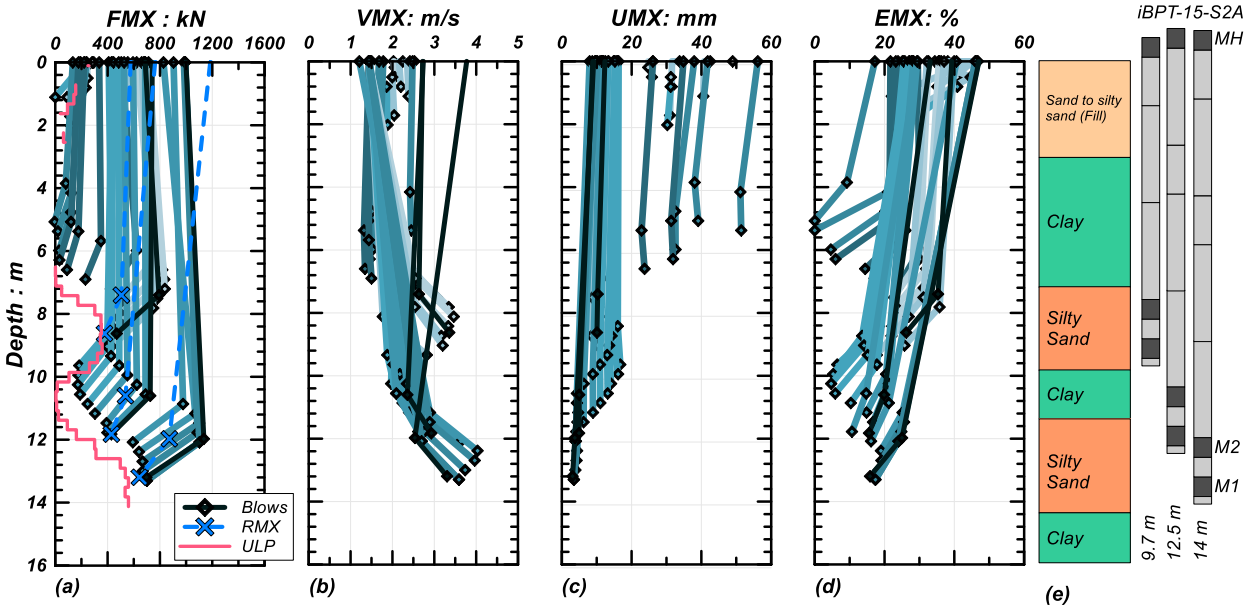

Figure 9. Oakland, Site 2 - iBPT typical pile driving analysis (PDA) results from multiple modules: (a) FMX, (b) VMX, (c) UMX, (d) EMX, (e) site profile and iBPT final install depth.

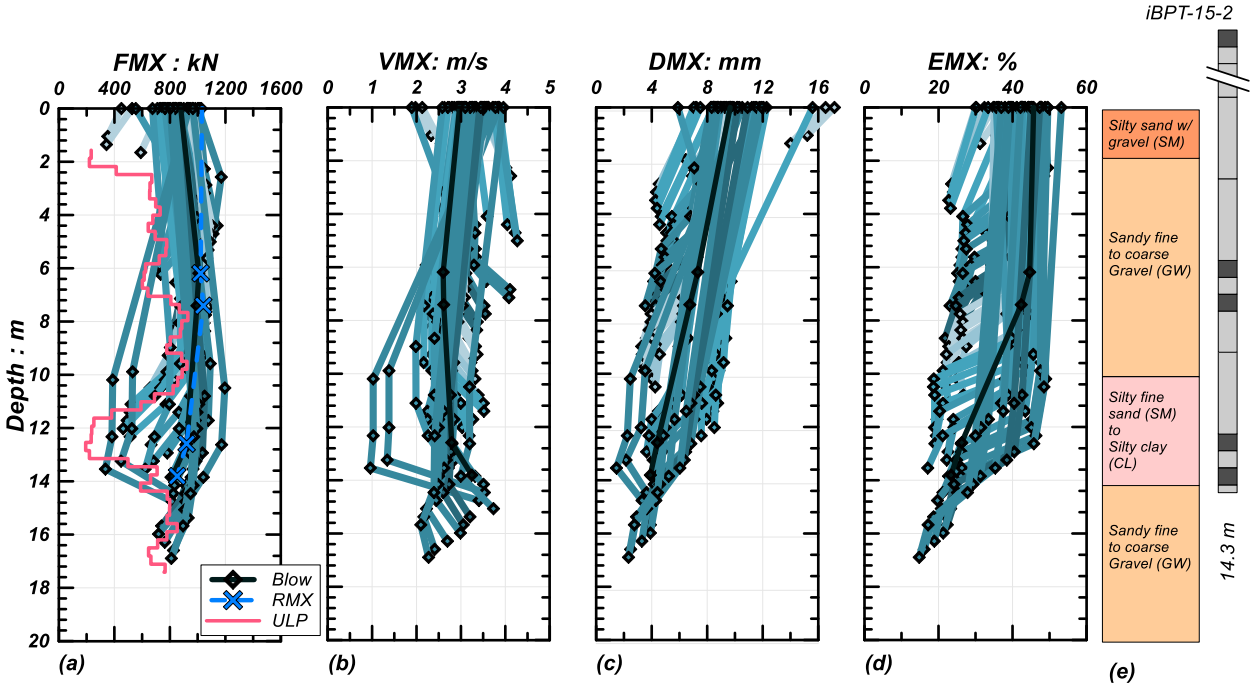

Figure 10. Coalinga, 15-2 - iBPT typical pile driving analysis (PDA) results from multiple modules: (a) FMX, (b) VMX, (c) UMX, (d) EMX, (e) site profile and iBPT final install depth.

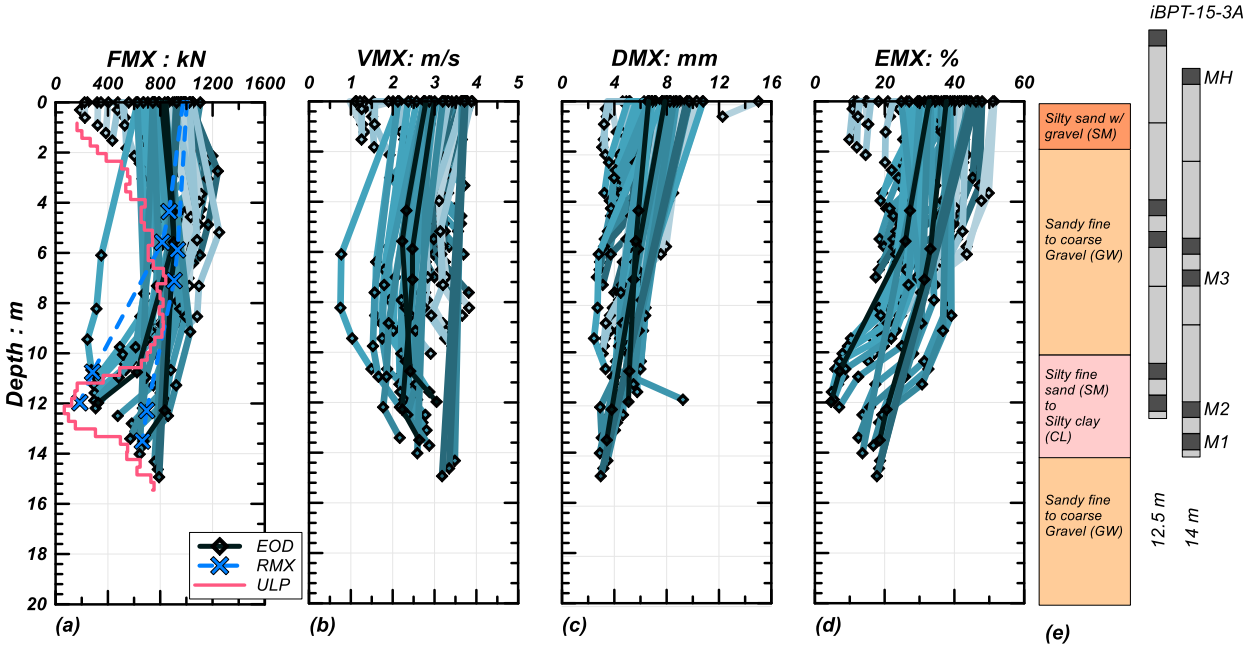

Figure 11. Coalinga, 15-3A - iBPT typical pile driving analysis (PDA) results from multiple modules: (a) FMX, (b) VMX, (c) UMX, (d) EMX, (e) site profile and iBPT final install depth.

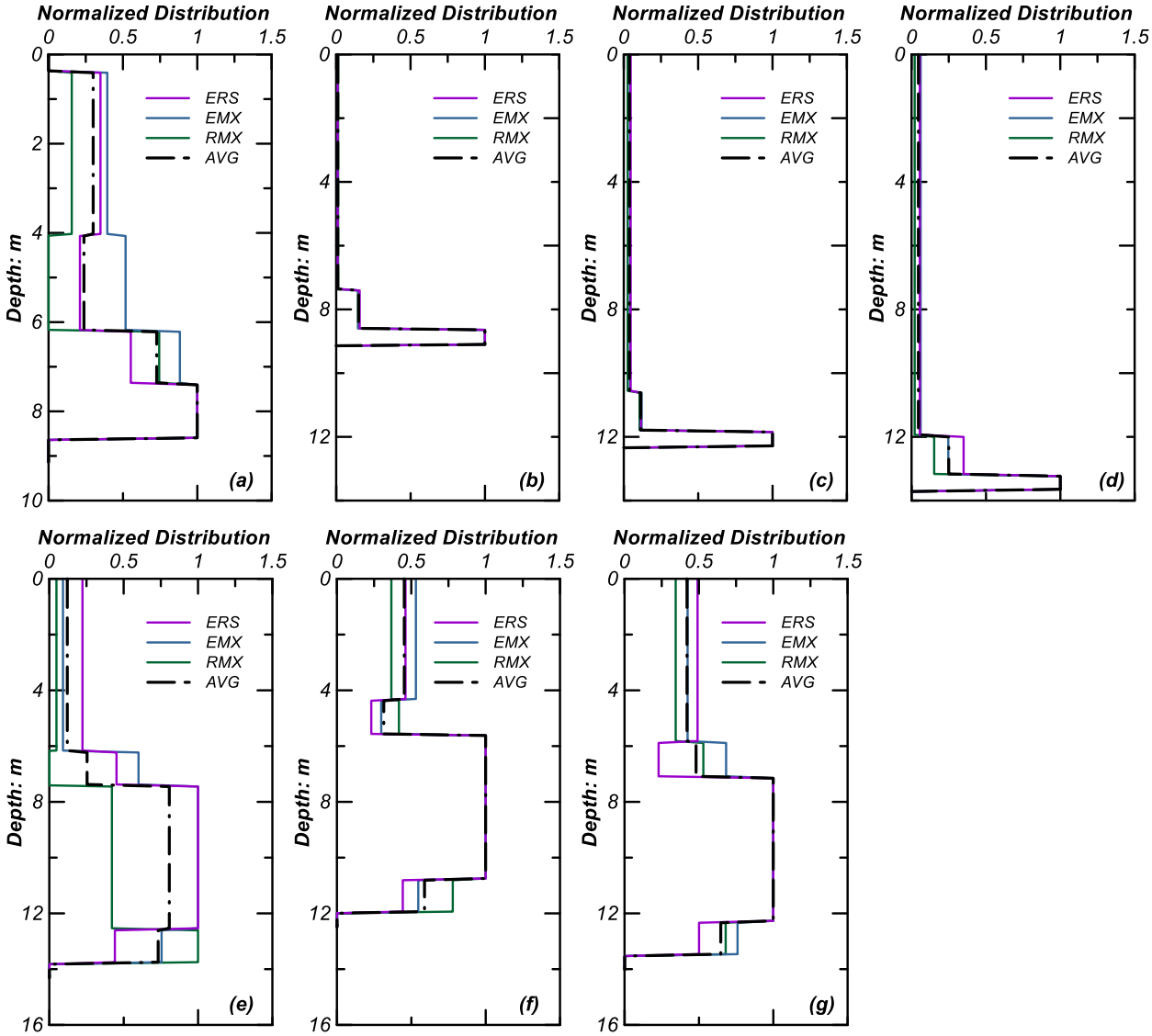

Figure 12. Normalized distributions inferred from iBPT dynamic driving measurements using the gradient of the residual energy (ERS), max energy (EMX), max reaction (RMX), and the average (AVG) of the three: Oakland: a) Site 1, 30ft, b) Site 2, 30ft, c) Site 2, 40.5ft, d) Site 2, 45ft; Coalinga: e) 15-2, 47ft, f) 15-3A, 41ft and g) 15-3A, 46ft.

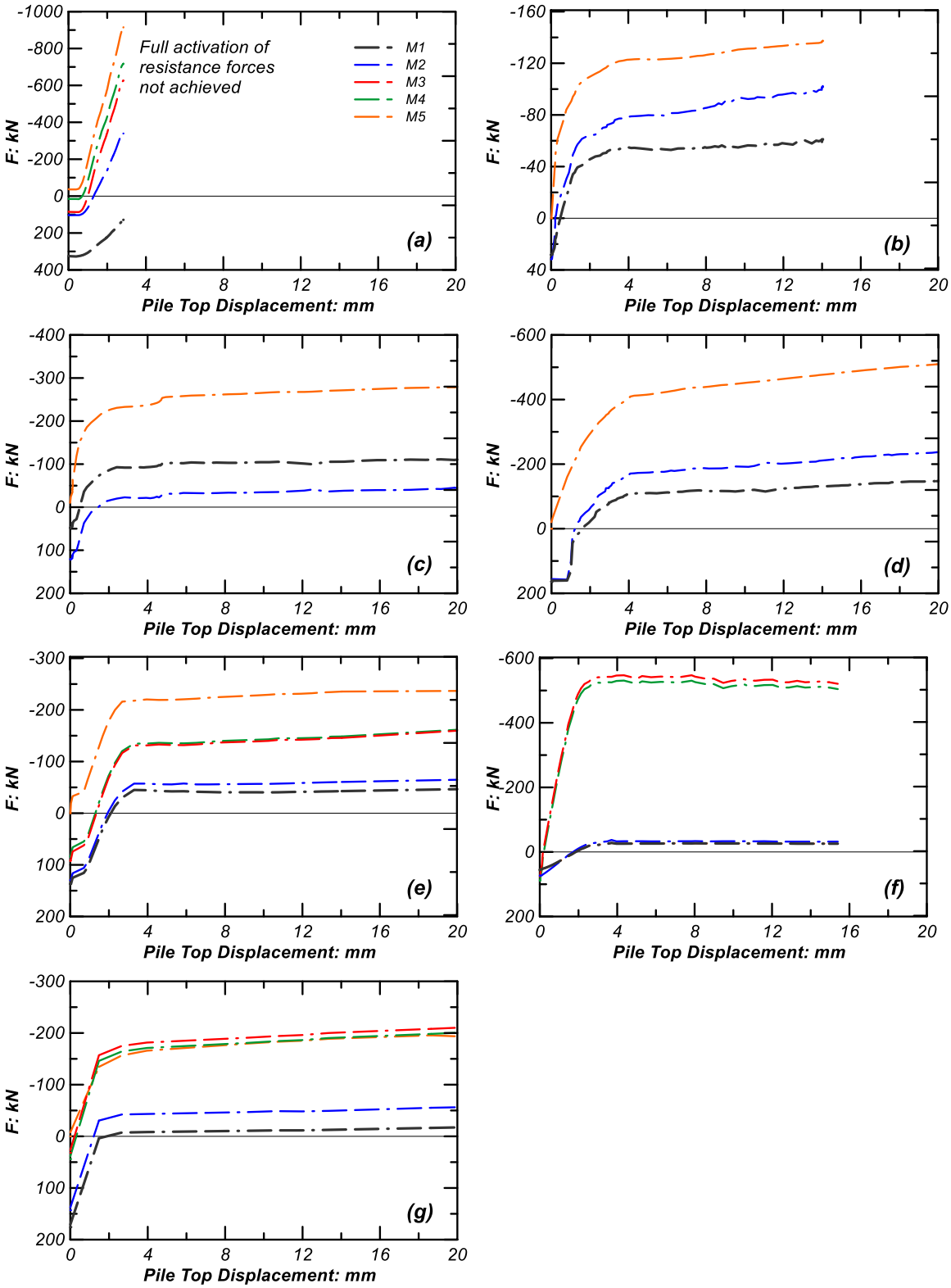

Figure 13. iBPT static pullback (tension) test measurements: Oakland: a) Site 1, 30ft, b) Site 2, 30ft, c) Site 2, 40.5ft, d) Site 2, 45ft; Coalinga: e) 15-2, 47ft, f) 15-3A, 41ft and g) 15-3A, 46ft.

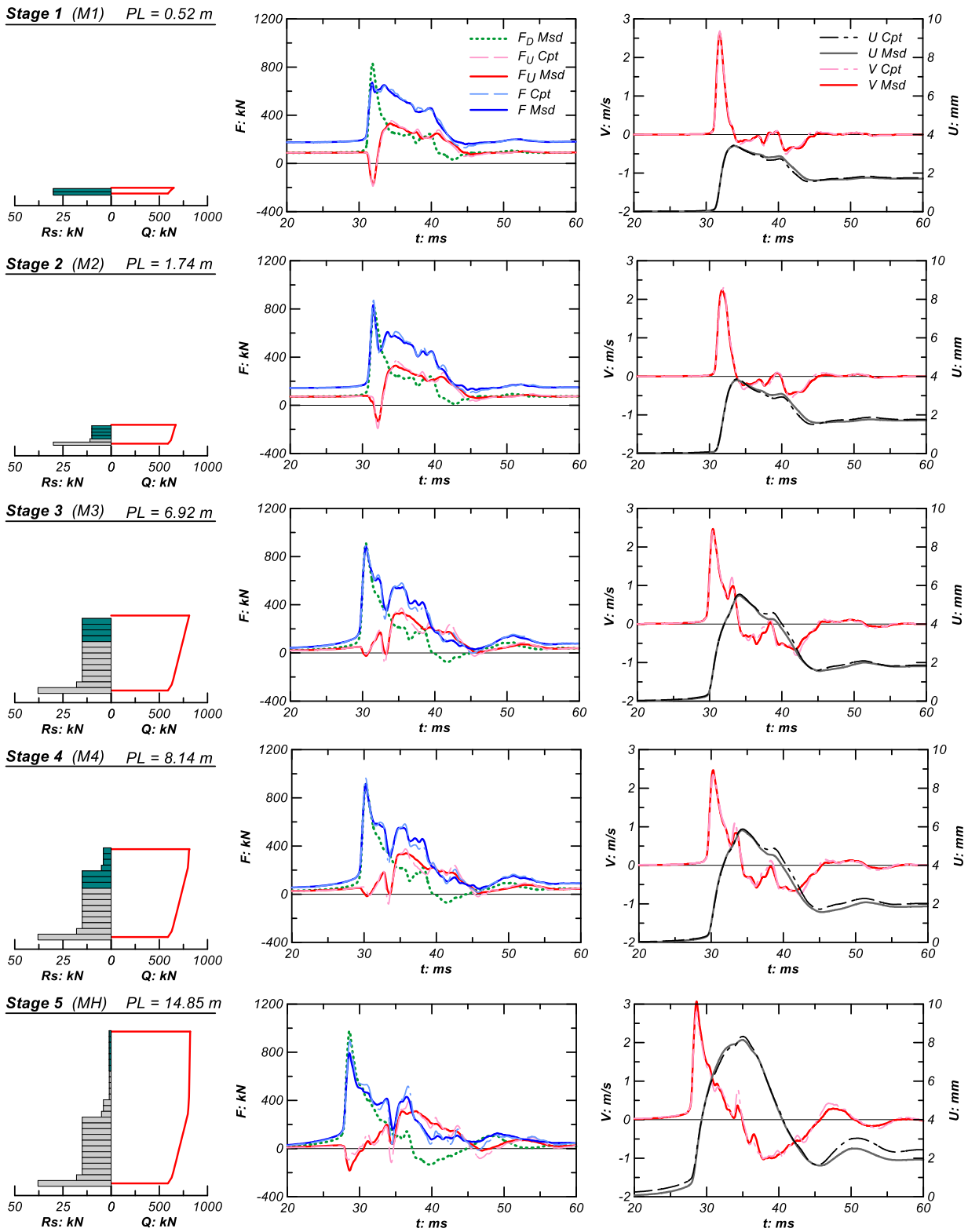

Figure 14. Example bottom-up, multistage signal matching analyses using EOD iBPT blow measurements from the multiple modules (Coalinga, RTP-15-3A, 46 ft).

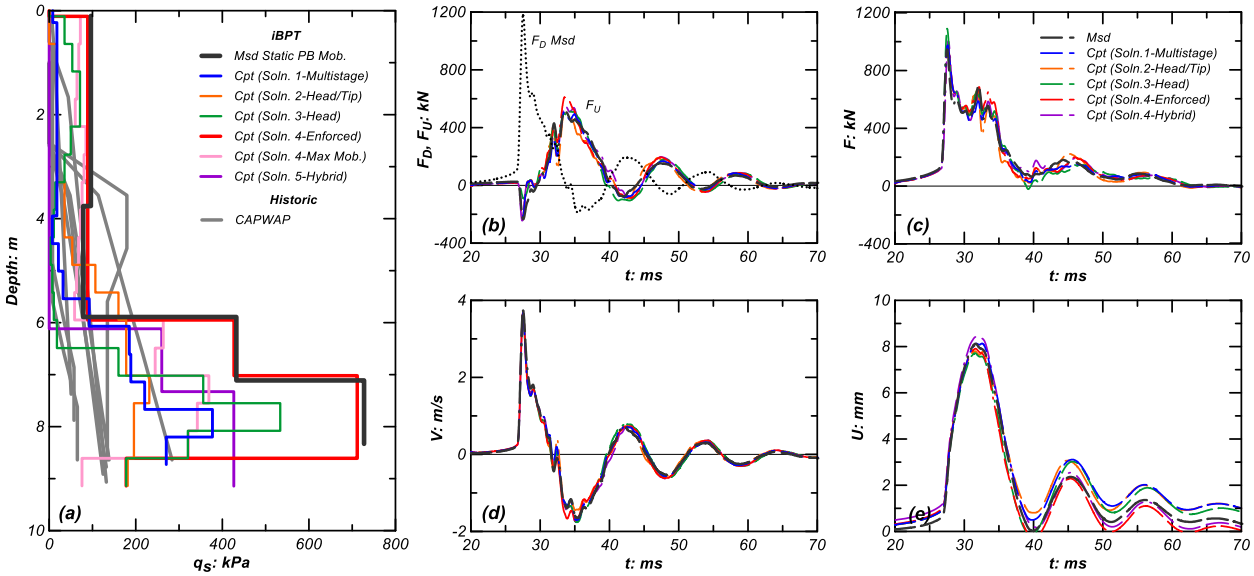

Figure 15. Oakland, Site 1, 30ft - non-uniqueness of signal matching solutions: (a) historic DLT distributions, and distributions of shaft resistances obtained using different signal matching procedures on iBPT measurements, (b) force down and up matching, (c) force matching, (d) velocity matching, (e) displacement matching.

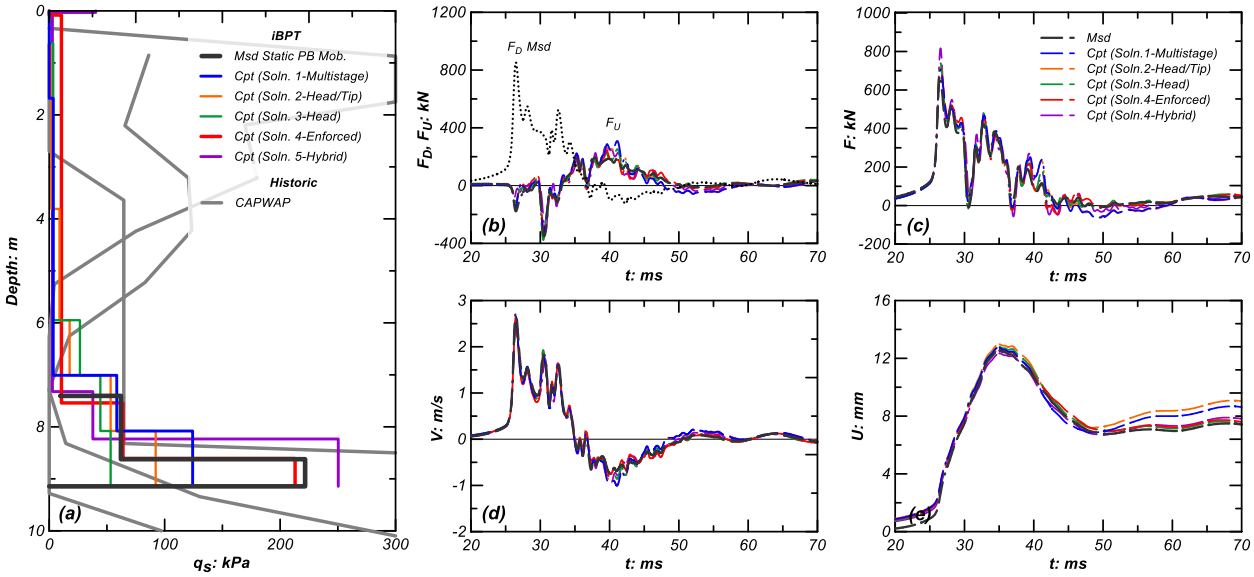

Figure 16. Oakland, Site 2, 30ft - non-uniqueness of signal matching solutions: (a) historic DLT distributions, and distributions of shaft resistances obtained using different signal matching procedures on iBPT measurements, (b) force down and up matching, (c) force matching, (d) velocity matching, (e) displacement matching.

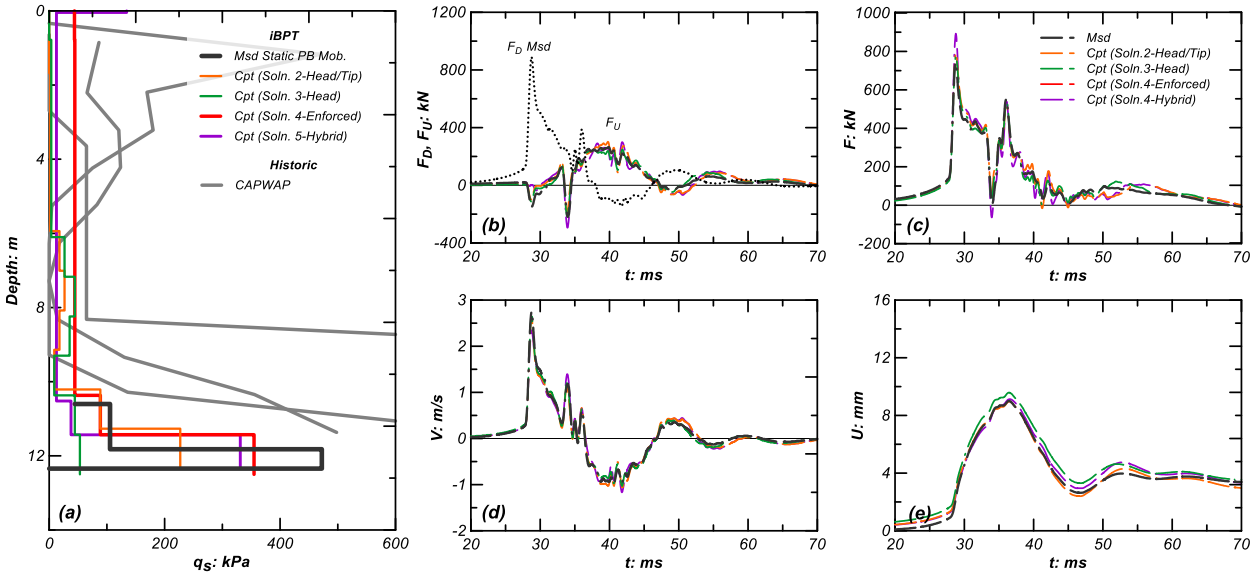

Figure 17. Oakland, Site 2, 41ft - non-uniqueness of signal matching solutions: (a) historic DLT distributions, and distributions of shaft resistances obtained using different signal matching procedures on iBPT measurements, (b) force down and up matching, (c) force matching, (d) velocity matching, (e) displacement matching.

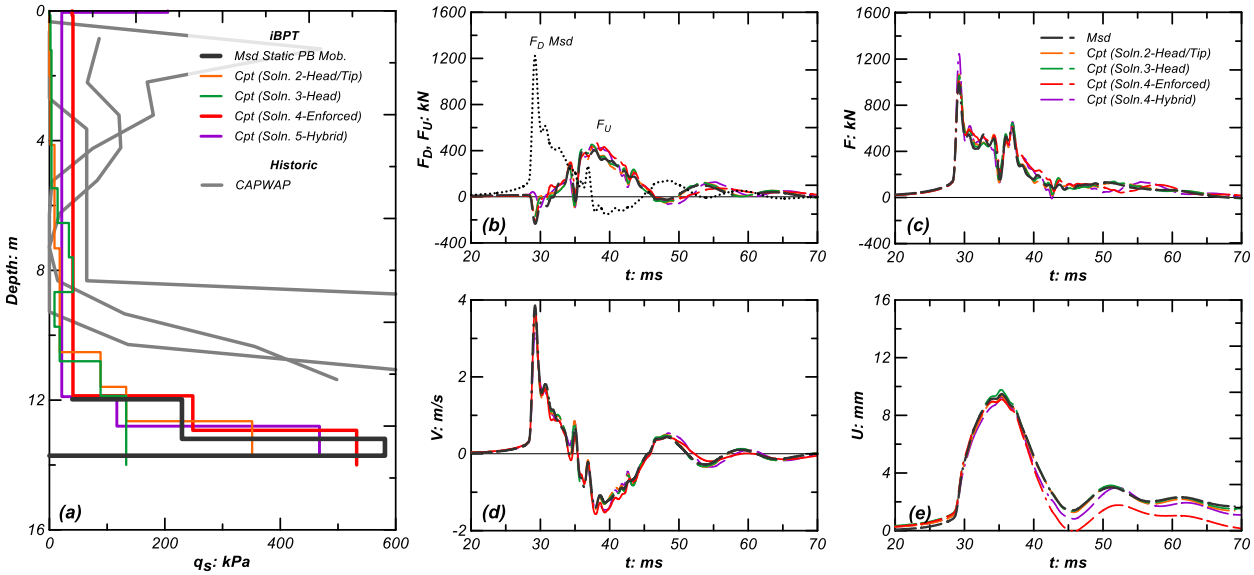

Figure 18. Oakland, Site 2, 45ft - non-uniqueness of signal matching solutions: (a) historic DLT distributions, and distributions of shaft resistances obtained using different signal matching procedures on iBPT measurements, (b) force down and up matching, (c) force matching, (d) velocity matching, (e) displacement matching.

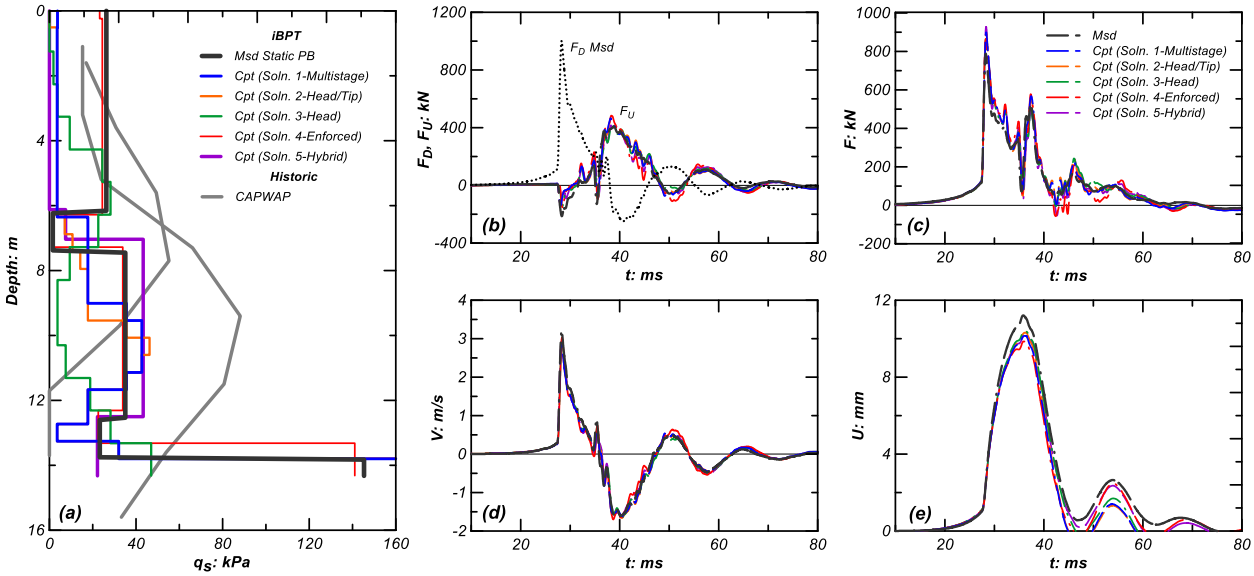

Figure 19. Coalinga 15-2, 47ft - non-uniqueness of signal matching solutions: (a) historic DLT distributions, and distributions of shaft resistances obtained using different signal matching procedures on iBPT measurements, (b) force down and up matching, (c) force matching, (d) velocity matching, (e) displacement matching.

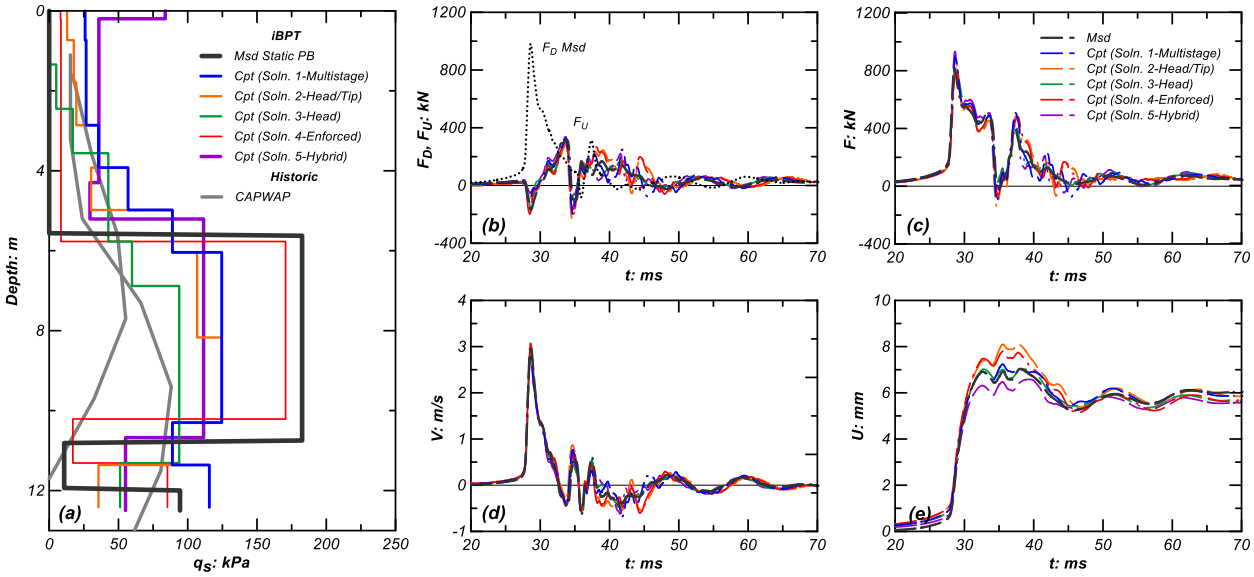

Figure 20. Coalinga 15-3A, 41ft - non-uniqueness of signal matching solutions: (a) historic DLT distributions, and distributions of shaft resistances obtained using different signal matching procedures on iBPT measurements, (b) force down and up matching, (c) force matching, (d) velocity matching, (e) displacement matching.

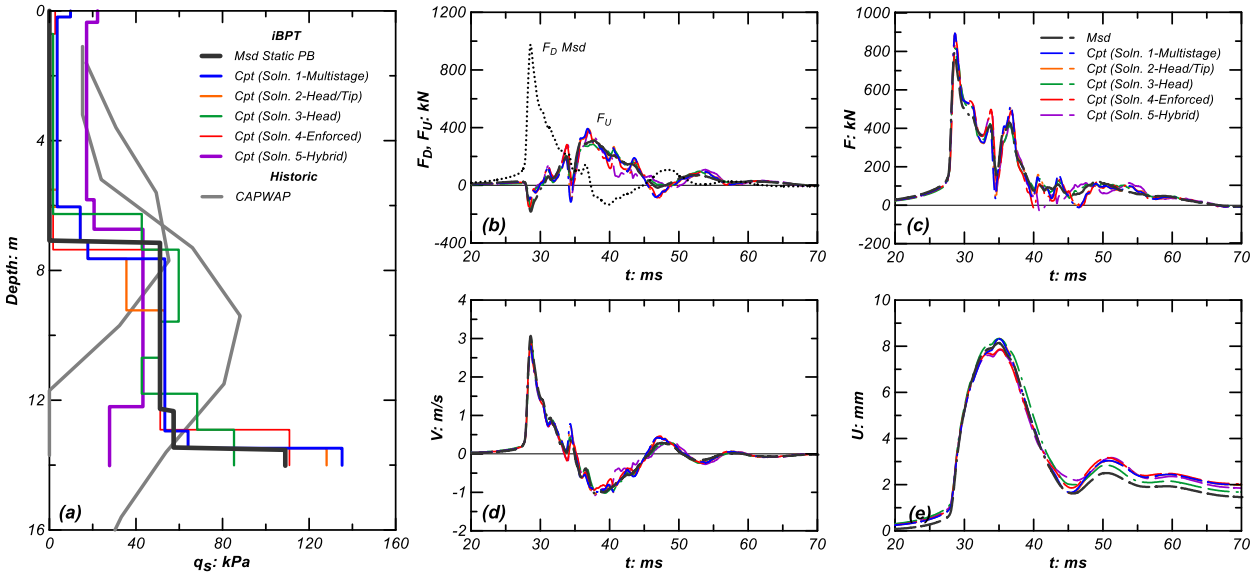

Figure 21. Coalinga 15-3A, 46ft - non-uniqueness of signal matching solutions: (a) historic DLT distributions, and distributions of shaft resistances obtained using different signal matching procedures on iBPT measurements, (b) force down and up matching, (c) force matching, (d) velocity matching, (e) displacement matching.

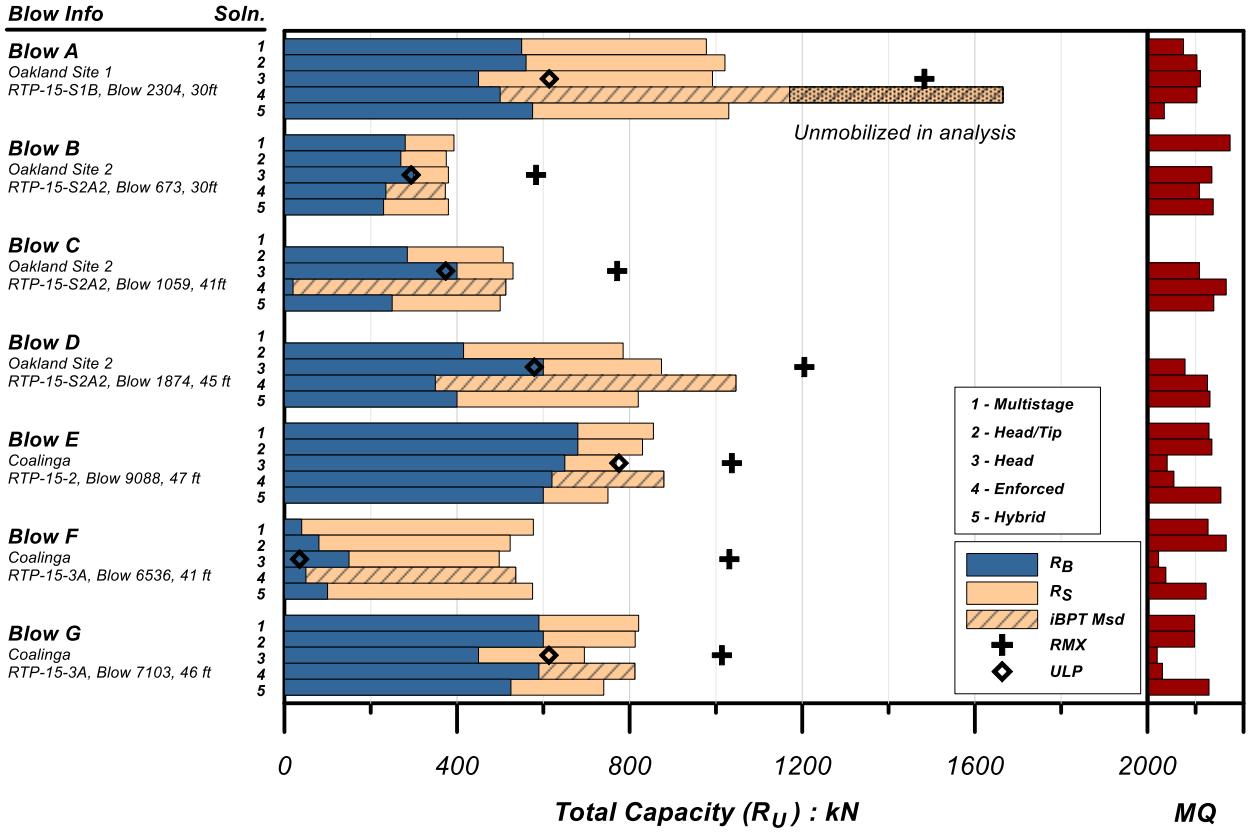

Figure 22. Comparison of ultimate capacity, shaft and base resistances estimates using different signal matching procedures on iBPT measurements.

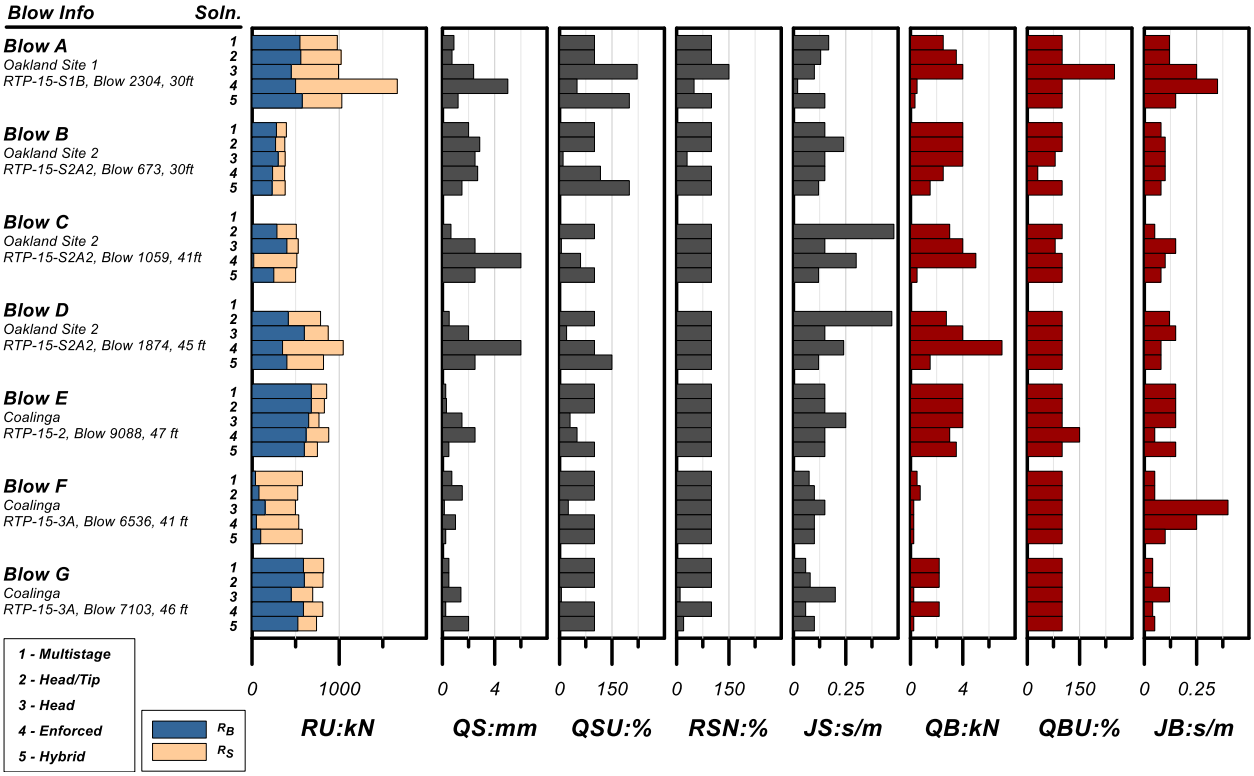

Figure 23. Comparison of signal matching results and average parameter values using different signal matching procedures on iBPT measurements.

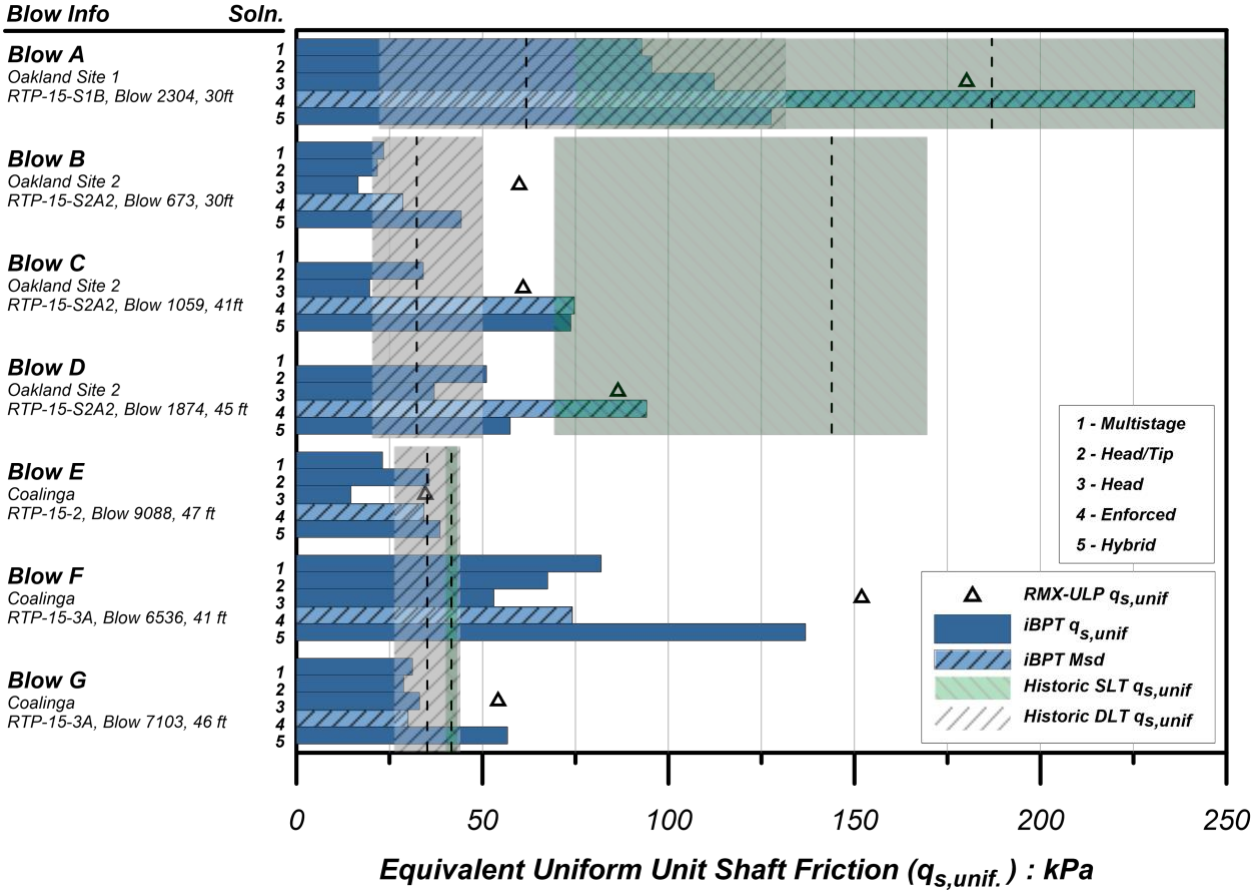

Figure 24. Comparison of equivalent uniform unit shaft friction estimates using different signal matching procedures on iBPT measurements with site-specific historic static and dynamic load testing results.

Appendix

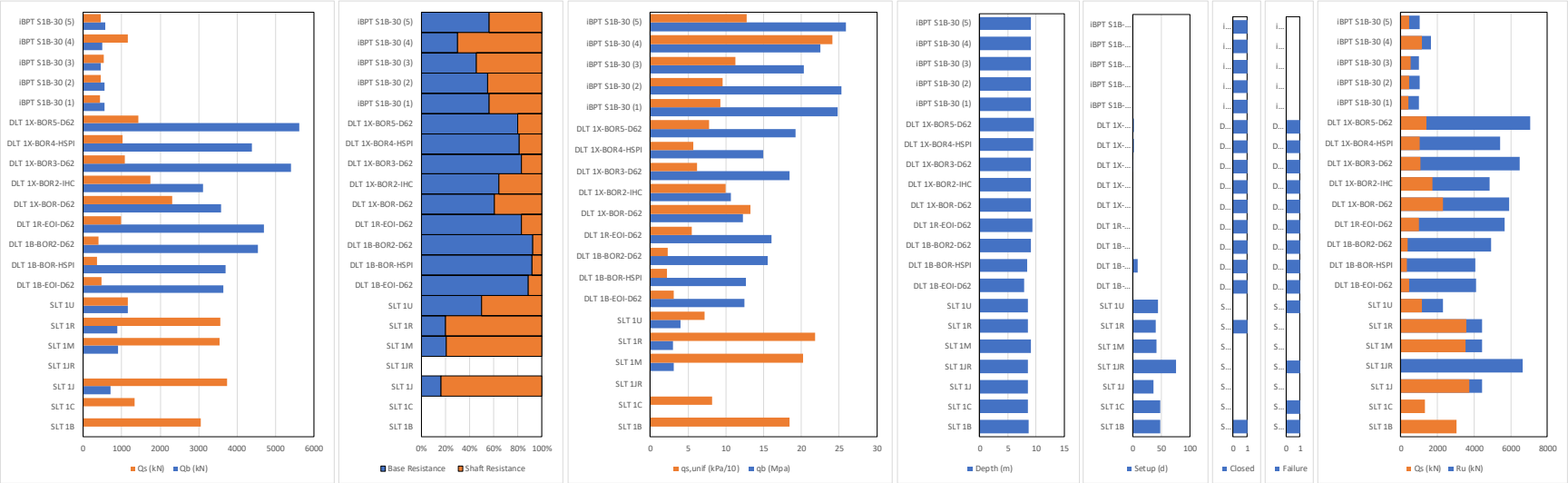

Figure A1. Oakland Site 1 summary plots. Comparison of historic load test database (SLT, DLT) and iBPT analysis results: Qs, Qb, Proportion, qb, qs,unif, embedment depth, setup, closed/open-ended pile, failure criterion achieved, Ru.

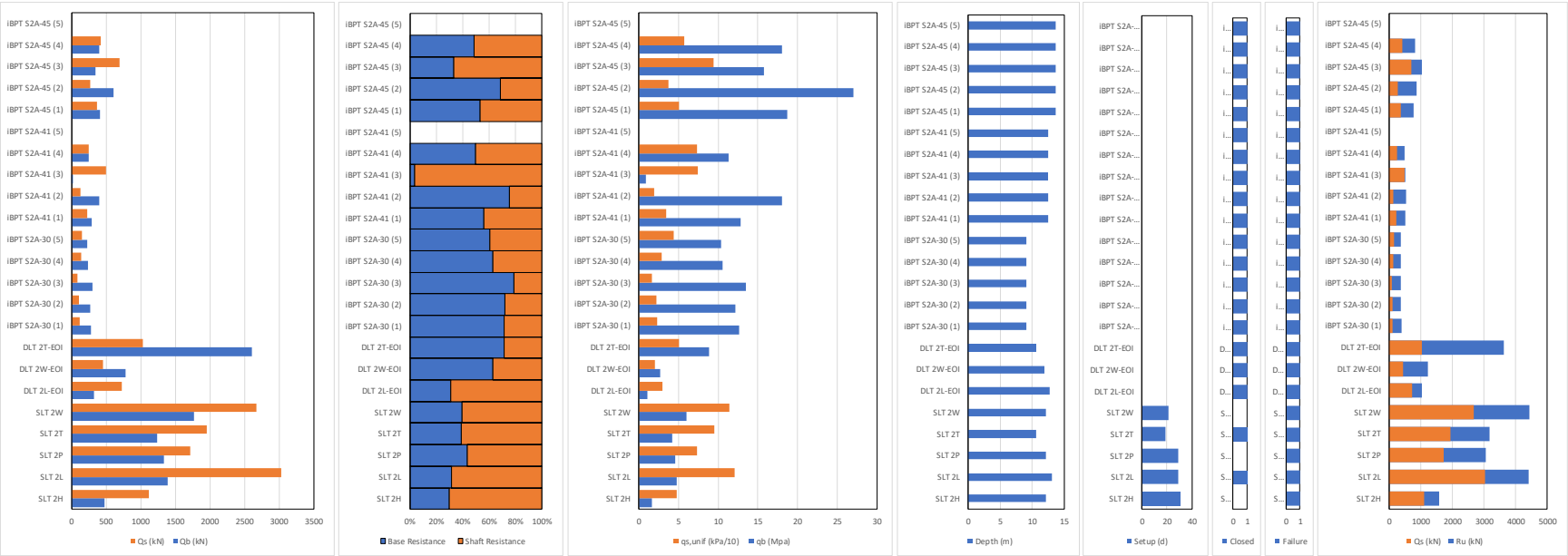

Figure A2. Oakland Site 2 summary plots. Comparison of historic load test database (SLT, DLT) and iBPT analysis results: Qs, Qb, Proportion, qb, qs,unif, embedment depth, setup, closed/open-ended pile, failure criterion achieved, Ru.

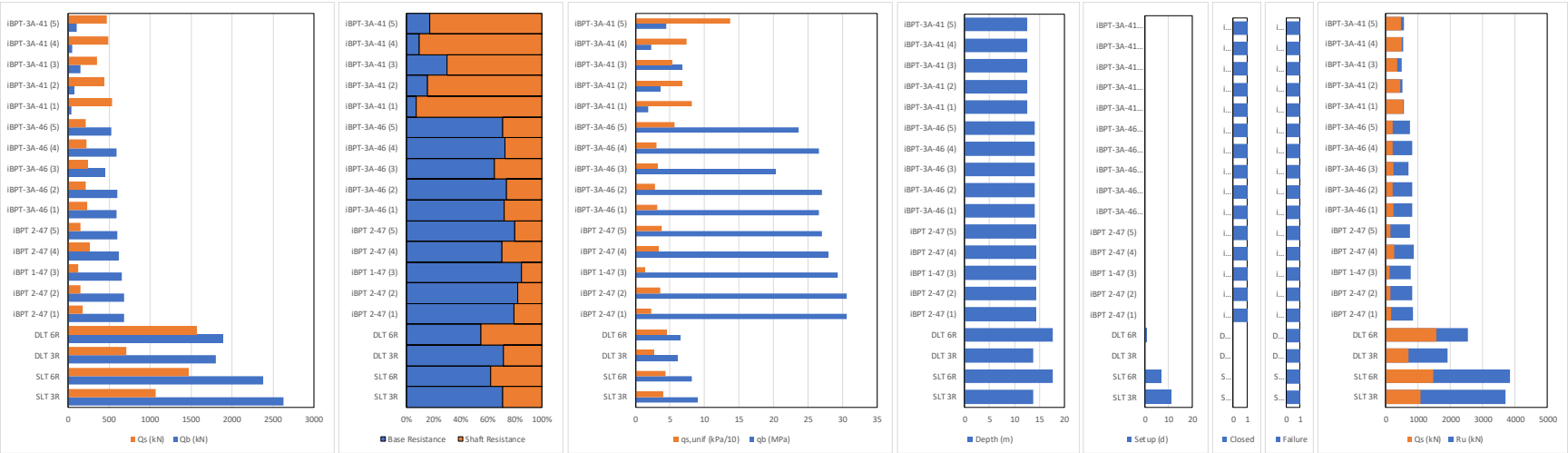

Figure A3. Coalinga summary plots. Comparison of historic load test database (SLT, DLT) and iBPT analysis results: Qs, Qb, Proportion, qb, qs,unif, embedment depth, setup, closed/open-ended pile, failure criterion achieved, Ru.